The Use of Germanium to Control the Properties of Glass Ionomer Cements

by

Brett Dickey

Submitted in partial fulfillment of the requirements
for the degree of Doctor of Philosophy

at

Dalhousie University
Halifax, Nova Scotia

August 2016

For:

Elisha,
Your support has gotten me to this point.

Mom and Dad,
Thank you for encouraging me to pursue my dreams, and supporting me as I do
...even if I take awhile to get there.

Table of Contents

List of Tables

List of Figures

Abstract

Vertebral body fractures (VBFs) are the most common type of osteoporotic fracture, affecting over one million individuals worldwide each year. VBFs can be severely debilitating and may lead to life-threatening complications, associated with intractable pain in the most at-risk patients. Fortunately for these patients, minimally invasive vertebral body augmentation (VBA) procedures provide immediate and lasting pain relief, by stabilizing the fracture via transpedicular injection of a bone cement. However, the state-of-the-art bone cements are prevented from optimizing patient outcome due to deficiencies in biocompatibility, handling characteristics, and/or mechanical durability.

The excellent biocompatibility and appropriate mechanical properties of aluminum-free glass ionomer cements (GICs) have motivated the research and development of GICs based on zinc silicate glass chemistries for use in VBA. However, the clinical potential of zinc silicate GICs is inhibited by the inability to achieve practical handling characteristics, without diminishing the strength of the cement.

The research presented herein examines a novel approach of controlling GIC properties, whereby the silicon content in the glass chemistry is replaced by germanium. Three broad investigations explore the impact of this substitution on the performance of zinc silicate GICs. An initial screening demonstrated that the complete replacement of silicon by germanium significantly improved the handling characteristics of zinc silicate GICs, whilst maintaining the strength necessary for VBA. To determine the mechanistic basis of these behaviors, thorough investigations of the influence of germanium on the GIC setting reaction and mechanical properties were conducted. From these investigations, it was revealed that germanium delays, but does not hinder the GIC setting reaction. This allows the handling characteristics of the cements to be decoupled from their mechanical properties. However, in order for the extended GIC setting reaction to yield mechanically durable cements, the zinc silicate glasses must contain both silicon and germanium in equal quantities.

This research demonstrates that replacing silicon with germanium in the glass chemistry successfully controls GIC properties. Ultimately, this approach identified the necessary compositional changes to produce aluminum-free GICs that balance appropriate handling characteristics with sufficient mechanical properties. In conclusion, Ge-containing GICs are clinically viable as injectable bone cements for use in VBA.

List of Abbreviations and Symbols Used

β_{ijk}	Coefficients of DoM regression models
γ	Strain rate
τ	Shear stress
%	Percentage
%wt	Weight percent
˚C	Degree celsius
θ	Theta
μ	Coefficient of viscosity
μA	Microamp
μm	Micrometer
Ø	Diameter
3Q MAS NMR	Triple quantum magical angle spinning nuclear magnetic resonance
a	Distance between cation and oxygen anion
a	Surface area
Å	Angstrom
Al	Aluminum
ANOVA	analysis of variance
aq	Aqueous
ATR-FTIR	Attenuated total reflectance Fourier transform infrared spectroscopy
Ba	Barium
BFM	Biaxial flexural modulus
BFS	Biaxial flexural strength
BO	Bridging oxygen
C	Carbon
c.	circa
Ca	Calcium
cm	Centimeter
COO–	Carboxylate
COOH	Carboxyl
CS	Compression strength
Cu	Copper
d	Days
dfE	Degree of freedom of overall error of DoM regression model
dfM	Degree of freedom of DoM regression model
DoM	Design of Mixtures
DT	Double torsion
e	Residual of DoM regression model
E_C	Compression modulus
F	Fluorine

F_R	F-ratio
f	Applied force
F_S	Field strength
FTIR	Fourier transform infrared spectroscopy
g	Gram
G	Gauge
Ga	Gallium
Ge	Germanium
GIC	Glass ionomer cement
GPC	Glass polyalkenoate cement
H	Hydrogen
h	Hour
h_t	Spatial gap between chain and hypothetical tube
H^+	Proton
Hz	Hertz
ICP-OES	Inductively coupled plasma optical emissions spectroscopy
K_{IC}	Fracture toughness
kcal	Kilcalories
kHz	Kilohertz
kN	Kilonewton
KP	Kyphoplasty
kV	Kilovolt
l_c	Critical chain length
L_i	Lower bound contraint in DoM regression model
l_t	Contour length of entanglement tube
L_z	Sum of all lower bound constraints of DoM regression model
m	Total number of segments crossing a unit area of the fracture plane
M	Molar mass
M_e	Minimum molar mass for polymer chain entanglements to form.
mA	Milliamp
MAS	Magical angle spinning
mg	Milligram
MHz	Megahertz
min	Minutes
mL	Millilitres
mm	Millimeter
mol	Mole
mol%	Mole percent
MPa	Megapascal
MRI	Magnetic resonance imaging
MSS	Model summation of squares
M_w	Molecular weight
M^{z+}	Metal cation

N	Newton
n	Power law index
n	Number of samples
N_c	Network connectivity
Na	Sodium
NBO	Non-bridging oxygen
NEJM	New England Journal of Medicine
NMR	Nuclear magnetic resonance
NSAIDs	Non-steroidal anti-inflammatory drugs
O	Oxygen
P	Phosphorus
P_c	Load at fracture in K_{IC} testing
Pa	Pascal
PAA	Polyacrylic acid
PMMA	Polymethyl methacrylate
ppm	Parts per million
PVP	Percutaneous vertebroplasty
Q^n	Q-specication of Si glasses
r	Radius
RSS	Residual summation of squares
SD	Standard deviation
sec	Seconds
Si	Silicon
Sr	Strontium
S_t	Setting time
t	thickness
T_g	Glass transition temperature
t_n	Thickness of K_{IC} sample in groove
Ti	Titanium
TSC	Trisodium citrate
v	Poisson's ratio
v	Rate of chain removal
VBF	Vertebral body fractures
vs.	Versus
W	Width
W_m	Moment arm K_{IC} testing
W_t	Working time
x_i	Orignial component proportion DoM regression model
X_{ijk}	Compositional factor of DoM regression model
Y_Q	Working time response
Z_c	Valency
z_i	Pseudo-component proportions DoM regression model
Zn	Zinc

ZnGIC	Zinc-based glass ionomer cement
Zr	Zirconium
μ	Coefficient of viscosity
μA	Microamp
μm	Micrometer

Acknowledgements

First and foremost, I must express my sincere gratitude to my supervisor, Dr. Daniel Boyd. Thank you for your patience, mentorship, and support in all aspects of this work. Your persistence in challenging me to perform my best is greatly appreciated, in retrospect. As I pursue future professional, and personal endeavors, I hope to do so with at least a fraction of the enthusiasm and integrity that you display everyday.

To my committee members, Dr. Mark Filiaggi, and Dr. Darrel Doman: Thank you for your continuous support over the years. I believe your tough questions, constructive criticisms, and encouragement to think critically, has made me a better scientist and engineer (in equal proportions).

To present and past members of the Boyd Lab group: Dr. Sharon Kehoe, Dr. Nancy Kilcup, Dr. Xiao Zhang, Victoria Dickinson, Lauren Kiri, Kat MacDonald, Susan Batchilder, Dr. Katie O'Connell, and Dr. Caitlin Pierlot; thank you for your help in the lab, the thoughtful discussions, and for the overall experience of working with great people.

No acknowledgment section in SBME should be complete without saying a massive thank you to Gordie Hall. Gordie, your expertise in practical skills was an incredible asset to this work, and I am very appreciative of all your support over the years.

To members of the Filiaggi lab group: Dr. Arash Momeni, Dr. Esther Valliant, and Dr. Patricia Comeau; your assistance in the lab, as well as the thought provoking conversations, are very much appreciated.

To the School of Biomedical Engineering, thank you for your support, both in front and behind the scenes. Eleanor, thank you for your assistance in navigating through the CREATE program. Sandra, thank you for your help, whether it was booking or a room, or processing a travel claim, not having to worry about these things makes life as a graduate student much more manageable.

For those who have provided technical assistance along the way: Dr. Bob Abraham, Dr. Allan Paulson, Dr. Ulrike Werner-Zwanziger, Michael Johnson, Matthew Harding, Robbie Sanderson, Patricia Scallion; thank you for your assistance in the various aspects of this work.

I would like to thank the Atlantic Innovation Fund of the Atlantic Canadian Opportunity Agency, and the NSERC: CREATE BioMedic program for the financial support of this work over the years.

Finally, to my family and friends; I am done school now. The document has finally come. Thank you for *always* asking when I would be finished.

Chapter 1: Introduction

Vertebral body fractures (VBFs) are the most common type of osteoporotic fracture, with combined total of over 1 million VBFs occurring each year in North America and Europe [1-3]. Specifically in Canada, VBFs are more common than heart attacks, strokes, or breast cancer [3]. The pain associated with VBFs can be severely debilitating and persist for months or even years for >30% of patients [4, 5]. Predominantly, treatment options are palliative in nature, aimed at relieving symptoms while allowing the fracture to heal naturally over time [6, 7]. Unfortunately, for 10 % of patients, this conservative approach is contraindicated or ineffective. In fact, this conservative approach may be associated with considerable risk (*e.g.* increased bone fragility, increased risk of subsequent fracture, muscle atrophy, gastrointestinal complications, pulmonary dysfunction), particularly for elderly patients who already suffer from reduced bone quality [8-10].

To avoid such risks, or when pain cannot be adequately controlled, percutaneous vertebroplasty (PVP) or kyphoplasty (KP) may be indicated. These procedures involve the injection of bone cement through cannulae into the fractured vertebral body to stabilize the fracture upon setting, providing immediate and lasting pain relief for the patient whilst restoring local mechanical integrity [10]. PVP and KP have been clinically proven to provide superior outcomes over conservative therapies for the treatment of VBFs [11-15]. Despite the clinical evidence, the use of PVP has been decreasing compared to that of KP in recent years [16]. This reduction is associated with the publication of two placebo controlled trials in the New England Journal of Medicine in 2009, which stated sham interventions were equally as effective as PVP in relieving the pain associated with VBFs [17, 18]; however these trials have significant deficiencies on

the basis of design, execution, and data interpretation. Accordingly, they have been widely criticized and are now regarded as poor quality evidence in the debate relating to VBF management [19-25]. Since 2009, new evidence has emerged confirming that PVP provides significantly faster and greater pain relief than conservative therapy [26-28]. However, despite the enhanced PVP evidence, the most recent trends indicate that clinicians are switching from PVP to KP [16], even though KP and PVP have been clinically proven to be equally effective [13, 29, 30]. This is an important consideration in the design of new materials for such interventions, as it indicates that these materials should provide efficacy in both procedures, from the perspectives of clinical deployment and patient safety.

In this regard, the ideal bone cement for PVP and KP applications is described as having excellent biocompatibility, comprising a non-toxic composition that is injectable for a minimum up to 10 minutes, with lasting mechanical properties matched to healthy vertebral bone (generally accepted to be *c.*30 MPa in compression) [31-33]. The current standard of care is polymethyl methacrylate (PMMA) bone cement [34, 35]. However, this cement may cause necrosis to surrounding tissue due to its chemistry, eliciting a host response that commonly results in fibrous encapsulation of the implant, thus jeopardizing its stability [36-40]. The limitations associated with PMMA have motivated the research and development of alternative cements for PVP and KP. However, impractical handling characteristics and / or insufficient mechanical durability have prevented the widespread clinical adoption of these alternatives [31, 32, 41-44].

Glass ionomer cements (GICs), which comprise an acid degradable aluminosilicate glass mixed with an aqueous solution of polyalkenoic acid, have

demonstrated excellent biocompatibility in dental applications and have sufficient mechanical properties for wider skeletal use [45]. However, the aluminosilicate glasses used in conventional GICs exhibit a critical limitation that prevents their use cements in orthopaedic applications; aluminum leached from the cement mantel of alumniosilicate GIC subsequent otoneurological surgeries has been attributed to at least four fatal cases of encephalopathy [46]. Furthermore, impaired bone remodeling subsequent to the use of aluminosilicate GICs in total hip replacements was also attributed to the release of aluminum from conventional GICs [47]. These results led to the contraindication of aluminosilicate GICs for skeletal applications [46-48]. Accordingly, aluminum-free GICs, based on glasses such as zinc silicates, have been developed for orthopaedic applications [49-51]. The use of aluminum-free GICs has been considered in PVP and KP, but crucially these materials set too quickly to be injectable under clinical conditions [52-55]. A considerable amount of research has been conducted to modify or augment the setting reaction of aluminum-free GICs in order to overcome their handling deficiencies. The conventional approach used to manipulate such properties is based on controlling the modifier or intermediate content of the glass chemistry in an attempt to control the quantity and type of ions released from the glass [49, 52, 53, 56-59]. However, this approach continuously generates the same inverse relationship: increasing GIC setting time while concurrently having a deleterious effect on strength; conversely, increasing strength has a detrimental effect on handling characteristics [49, 52, 53, 56-59]. The thesis of this work is based on a different philosophical approach, one that explores alternative glass formers as opposed to augmenting the modifier content of ionomer glasses. This approach is hypothesized to modulate glass reactivity, thus controlling

cement handling without limiting ion release; the latter being a critical factor to GIC strength. Further, this philosophical approach will be in the context of developing an injectable aluminum-free GIC for use in PVP/KP.

To rationalize the clinical need for the development of a new bone cement for PVP/KP, Chapter 2 discusses the epidemiology, etiology, and pathophysiology associated with VBFs. Chapter 3 provides a comprehensive overview of the PVP and KP procedures, including an assessment of the state-of-the-art bone cements used in these procedures. Due to the controversy surrounding PVP arising from the 2009 New England Journal of Medicine articles [17, 18], Chapter 3 includes a critical review of the level of evidence regarding the clinical efficacy of PVP and KP. Furthermore, Chapter 3 argues the validity of PVP and KP as the best treatment modalities to address the clinical burden of VBFs outlined in Chapter 2.

Chapter 4 describes GICs in detail so as to provide a basis for understanding their composition-structure-property relationships. This chapter, by necessity, places particular emphasis on the role that glass chemistry plays in GIC handling and mechanical properties. Additionally, the relevant literature regarding the clinical use of GICs in orthopaedic applications is summarized, reviewed, and discussed in terms of the necessity to develop aluminum-free GICs. Following this, Chapter 5 elaborates on the topic of aluminum-free GICs, and discusses the practical limitations that inhibit their clinical use. Additionally, further arguments are made regarding restrictions of the current approach used to modulate glass composition as a means to control the handling and mechanical properties of GICs. At this point an alternative philosophical approach to ionomer glass design is introduced in particular, the use to germanium and zirconium as

potential network formers with intrinsic characteristics hypothesized to redress the dichotomous nature between the handling and mechanical properties of zinc silicate GICs.

Chapters 6, 7, and 8 are standalone papers, all of which have been published, or accepted pending corrections, in relevant journals. Each paper is preceded by a brief rationale to contextualize its place in the overall body of work. Chapter 6: *Novel Adaptations to Zinc Silicate Glass Ionomer Cements – The Unexpected Influence of Germanium Based Glasses on Handling Characteristics and Mechanical Properties* [60], is published in the Journal of the Mechanical Behavior of Biomedical Materials. This chapter investigates the practicality of replacing silicon with germanium and zirconium as network former components in zinc silicate glass chemistry. Evaluation of GIC handling and mechanical properties were used to assess the impacts of these replacements. The results of this investigation are discussed in the context of the clinical viability of zinc silicate GICs for PVP and KP.

Findings from Chapter 6 influenced the research questions of the subsequent chapters. Chapter 7: *Evidence of a Complex Species Controlling the Setting Reaction of Glass Ionomer Cements* [61], is published in Dental Materials. This chapter provides an in-depth examination of the GIC setting reaction as a function of germanium substitutions for silicon in zinc silicate GICs. This investigation is designed to elucidate the mechanisms associated with the changes in GIC handling characteristics that were discovered in Chapter 6. Chapter 8: *Exploring the Unexpected Influence of the Si:Ge Ratio on the Molecular Architectures and Mechanical Properties of Al-free GICs,* is currently accepted pending corrections (May 2016) by the Journal of Biomaterials

Applications. This investigation compares mechanical properties in relation to various structural changes. The objective of this chapter is to elucidate the mechanisms associated with the time-dependent mechanical changes of germanium based GICs observed in Chapter 6. Limitations of Chapters 6, 7, and 8 are presented in their respective chapters, while Chapter 9 provides a concluding discussion of this work as a whole, and presents potential future research directions.

Chapter 2: Vertebral Body Fractures: Epidemiology, Etiology, and Pathophysiology

Vertebral body fractures (VBFs) are induced by trauma-related events, which occur when the vertebral column is subjected to loads that exceed the strength of the vertebral bodies (Figure 1) [62]. However, the prevalence of VBFs are greatly exacerbated by osteoporosis and metastatic bone disease, which increase the fragility of vertebral bodies by reducing bone quality [63-66]. VBFs profoundly impact the quality of life of patients. In some instances, the pain associated with these fractures can be acute, only lasting until the fracture heals (usually, within a matter of weeks) [4]. However, in other instances pain can become chronic, lasting several months, with one third of patients reporting persistent back pain due to VBFs [4, 5]. The pain associated with VBFs can be severely debilitating for patients. Clinical studies have found that the average number of days of limited activity attributed to lumbar and thoracic VBFs are 158 and 74 days respectively [4]. In comparison, hip fractures have an average of 101 days of limited activity [67]. In addition, the range of complications associated with VBFs is vast. The physical symptoms patients experience include height loss, kyphosis of the spine (*i.e.* excessive curvature), an elevated risk of muscle atrophy, and bone loss due to long-term bed rest [68]. Medical consequences of VBFs include: reduced pulmonary function, higher rates of gastroesophagel reflux disease, and significantly increased risk to subsequent fracture [4]. Consequently, patients with VBFs are 4-times more susceptible to additional VBFs, 2-times more likely to have a hip fracture, and 1.5-times more likely to fracture another skeletal site [4]. Cumulatively, VBFs along with the aforementioned co-morbidities have been correlated to an increased risk of patient mortality [4].

Figure 1: Magnetic resonance imaging scan depicting the compression fracture of T12 vertebra (black arrow), adapted from Kim *et al.* 2010 [69].

In addition to the significant impact VBFs have on patient well-being, these fractures constitute a major societal burden worldwide, both in terms of loss of quality of life and healthcare costs [4]. In the United States over 10 million individuals have osteoporosis, a figure that is expected to increase to 14 million by 2020 [65, 70]. It is estimated that $16.9 billion was spent to treat the more than 2 million Americans who experience an osteoporotic fracture, a figure forecasted to increase to $25 billion by 2025 [65]. In Europe, the costs associated with the treatment, pharmacological prevention and long-term care of osteoporosis related fractures exceeded €37 billion in 2010, and are forecasted to rise to €46 billion by 2025 [71]. The costs associated with the treatment of osteoporotic fractures in Canada are lower due to its smaller population, but still amounted to $2.3 billion in 2010 [72]. VBFs are the most common type of osteoportic

fracture, and there are more VBFs each year in Canada than heart attacks, strokes, or breast cancer cases [3].

Developing a true understanding of the global incidence of VBFs is complicated by the fact that up to three quarters of such fractures are not recognized clinically [73, 74]. From the data that is available, the three leading causes of VBFs are osteoporosis, metastatic bone disease, and trauma [62-64]. Two epidemiological studies conducted by the Mayo Clinic on the population of Rochester, Minnesota (published 20 years apart), found 83 % of VBFs are due to osteoporosis, 12-14 % are the result of trauma, and 3-4 % are caused by pathologies such as metastatic bone disease [75, 76].

With regards to osteoporosis, the incidence of VBFs is higher amongst women than men, and the risk increases with age (Figure 2a). The prevalence of VBFs with age is consistent across the globe, and appears to be the highest in countries with largely Caucasian populations, and lower in Latin American and Asian populations (Figure 2b). Estimates regarding the average number of VBFs are difficult to accurately identify from the literature. In the United States the annual incidence of VBFs as been reported as low

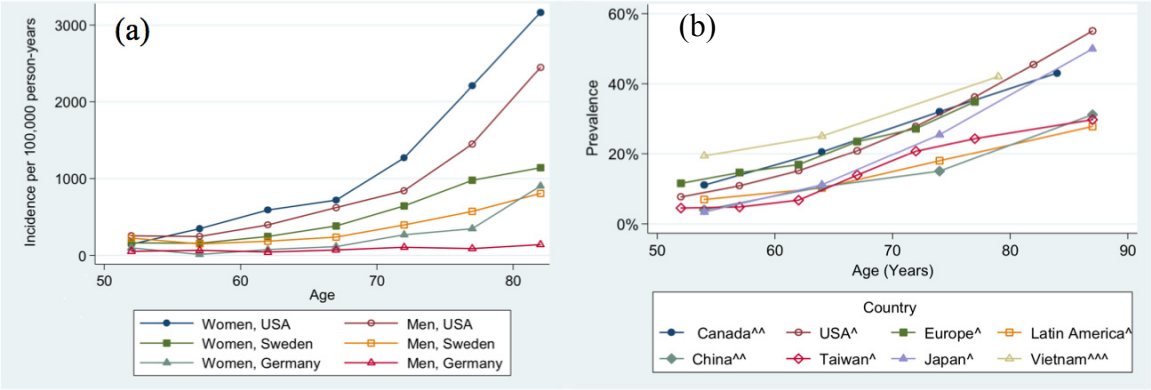

Figure 2: Epidemiological data of vertebral body fractures; (a) incidence rate amongst women and men in the USA, Sweden, and Germany; (b) Global comparison of prevalence amongst women, adapted from Schousboe [4].

210,000 [77], and as high as 700,000 per year [78]. Applying an analytical approach, Burge *et al.* combined population data of the United States with incidence rates of VBFs to calculate the average number of VBFs per year to be 550,000 (390,000 women; 160,000 men) [1]. More objective data exists for the European Union, where an analysis of the healthcare databases of 27 member states revealed an average of 520,000 VBFs occur each year [2]. In Canada, the number is much smaller, at an estimated 37,000 VBFs per year [3]. The majority of these fractures are asymptomatic or mildly symptomatic, allowing them to be treated with only minimal intervention [79]. However in *c.* 10 % of case, symptoms become severe enough that hospitalization is required [80].

There is far less literature dedicated to the epidemiology of VBFs secondary to metastatic bone disease than there is for the osteoporotic fractures. This is likely due to the fact that there are far fewer pathologic VBFs than there are osteoporotic VBFs [4]. However, what can be said is that skeletal metastases are the third most prevalent form of metastases, surpassed only by the liver and lung [81]. Osteolytic lesions most commonly metastasize from breast (21 %), lung (14 %), prostate (8 %), renal (5 %), gastrointestinal (5 %), or thyroid tumors (3 %), but may also arise from multiple myeloma or lymphoma [7, 82]. Each year 5 % of patients with cancer develop spinal metastasis, which are the most common type of tumor in the spine [7, 83]. The highest incidence rates of spinal metastases are in the thoracic vertebrae (67 %), followed by lumbar vertebrae (22 %), then cervical vertebrae (11 %) [7]. In the United States, this level of metastatic bone disease results in an estimated 75,000 to 100,000 cancer-induced VBFs per year, primarily in patients with stage III and stage IV prostate cancers (32 %), all stages of

multiple myeloma (22 %), stage IV lung cancer (20 %), stage IV breast cancer (6 %), or other cancers (20 %) [84].

With regards to the incidence of fractures down the vertebral column, the distribution is as follows: 20 % of fractures occur in the cervical vertebrae, 30 % in the thoracic vertebra and 50 % in the lumbar vertebrae [85]. The locations of these regions along the spinal column are depicted in Figure 3. The highest incidence of VBFs occurs at the transition between the kyphotic curvature of the thoracic spine and the lordosis curvature of the lumbar spine [5]. This region, which extends from T11 to L2, is termed the thoracolumbar junction and a reported 62% of VBFs occur in this location [86]. The higher prevalence of fractures in this region is attributable to the diminished stability and

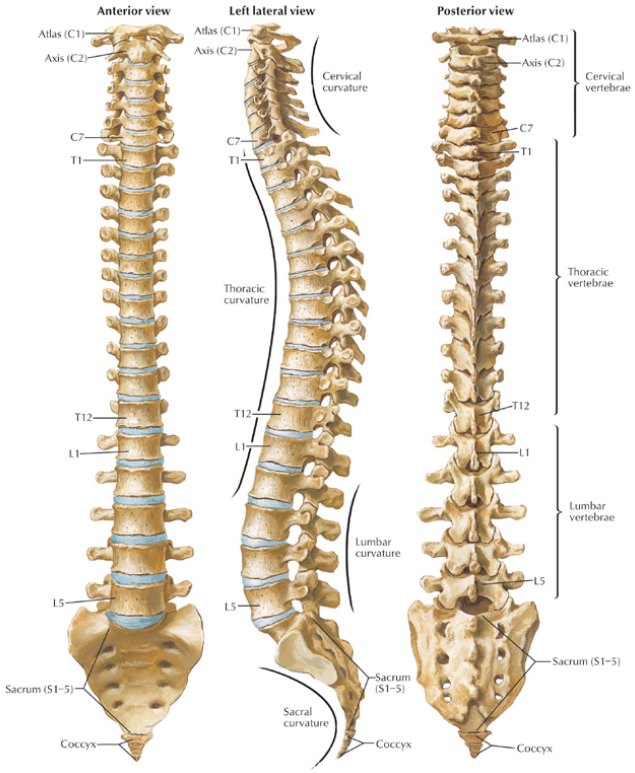

Figure 3: The spinal column, viewed from the anterior, lateral, and posterior. Adapted from Filler [87].

greater flexion/extension of lumbar vertebra *vs.* thoracic vertebrae, which combine to increase the biomechanical loading of the T11-L2 vertebrae [86].

Given the complexity of VBFs, there are multiple systems used to classify VBFs. However, the AO/ASIF (Arbeisgemenischaft für Osteosynthesefragen/Association for the Study of Internal Fixation) classification introduced by Margerl *et al*. [88] is becoming the gold standard for documentation and treatment of injuries of the vertebral column [86]. This system describes three general types of fractures pertaining to the type of biomechanical loading that caused the injury: compression (Type A), distraction (Type B), and rotational (Type C). Each fracture type is subdivided into groups (*i.e.* 1, 2, or 3),

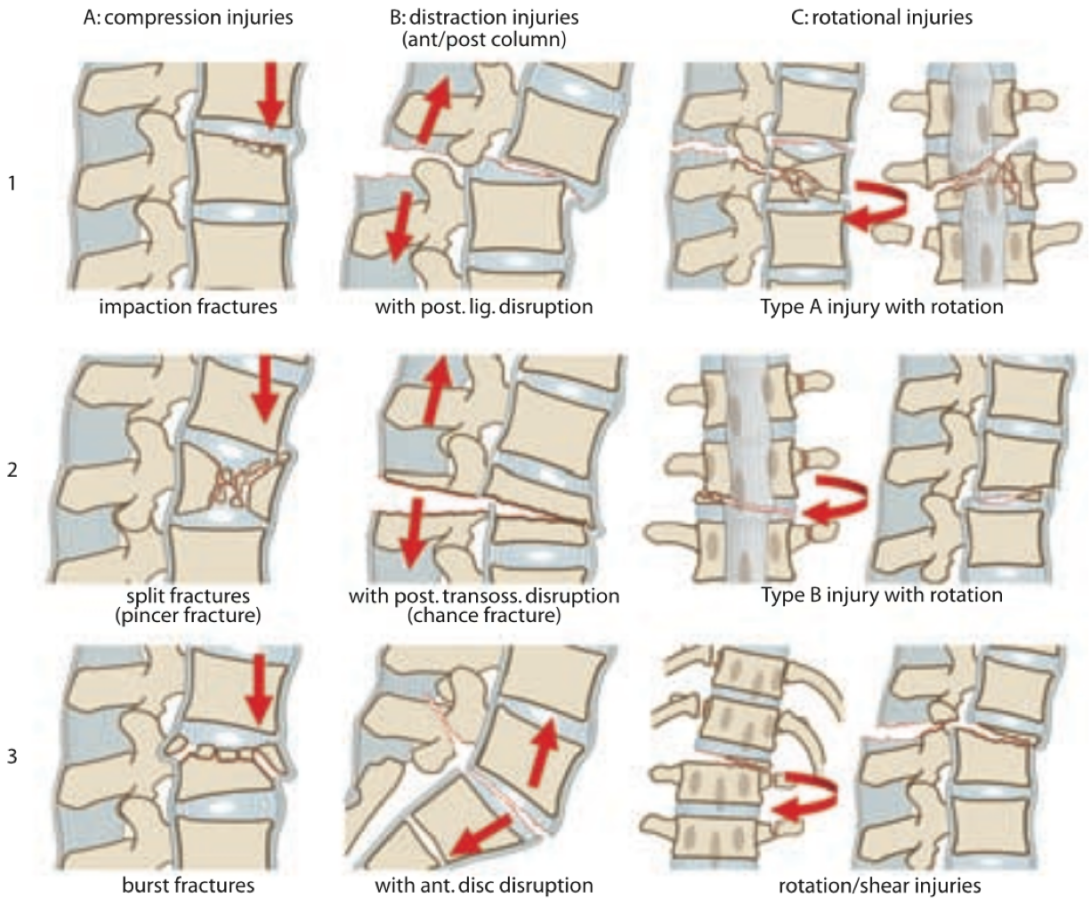

Figure 4: AO/ASIF classification system of VBFs, adapted from Margerl *et al.* [88].

which are descriptive of the magnitude of damage to the vertebral body. Finally, each descriptive group can be further classified according to the degree of instability of the fracture. For example, the fracture classification Type A3.1 describes incomplete burst fractures, which are more stable than Type A3.3, complete burst fractures [86]. The severity of the fracture increases from A to C, and from group 1 to 3. This classification system is illustrated in Figure 4. The most common VBFs are Type A compression fracture, accounting for *c.* 66% of clinically reported fractures, followed by Type C (*c.* 19%), and then Type B (*c.* 15%) [86]. Amongst compression fractures, impaction fractures (A1) and burst fracture (A3) are the most prevalent of Type A at 53% and 43% fractures [86]. Type A VBFs are typically treated by non-invasive means, but less stable fractures, or those associated with neurological deficit (*i.e.* Type A3.3, B, or C), often require surgical interventions [86, 89]. Chapter 3 discusses the relevant treatment options in more detail.

Chapter 3: Vertebral Body Augmentation

Treatment modalities for VBFs strive to achieve two goals: (i) pain relief and rehabilitation, and (ii) management of the underlying disease [6, 7]. The current standard of care is conservative therapy, which uses a combination of pain management and bed rest [6, 90]. In some instances, immobilization of the spine *via* back brace or external casting is necessary to facilitate healing of the fracture. Further, antiresorptive and anabolic agents are included in this approach to manage underlying osteoporosis [6, 90]. Lastly, when the patient's mobility allows, physical therapy is administered to mitigate the risk of future fractures [6, 90]. However, considerable risks are associated with various aspects of this conservative approach. These risks include exacerbation of bone fragility due to bed rest, severe gastrointestinal complications associated with the use of non-steroidal anti-inflammatory drugs, and cognitive impairment due to narcotic use [8, 9]. Surgical repair has been used to circumvent some of the inherent risks of conservative therapy by using internal fixation devices (*e.g.* plate, rods, screws) for the immediate stabilization of VBFs [86]. However, patients can suffer from chronic pain, loss of function, immobility, and excessive kyphosis resulting from internal fixation devices [10]. Additionally, these consequences are further complicated by the risk of instrumentation failure due to poor bone quality [10]. These factors limit the success of the surgical technique in patients with poor tolerance for operative trauma, such as the elderly [91]. As such, surgery is commonly reserved for patients with severe types of VBFs (*i.e.* Type A3.3, Type B, and Type C, injuries), suffering with intractable pain, and or display serious neurological deficits [86, 89].

To avoid the risks associated with conservative therapy or when pain cannot be adequately controlled, one of two vertebral augmentation procedures may be indicated, either percutaneous vertebroplasty (PVP) or kyphoplasty (KP). PVP is a minimally invasive procedure where radiopaque bone cement is injected into a fractured vertebra *via* a uni- or bi-transpedicular approach, under fluoroscopic guidance (Figure 5). PVP stabilizes the fracture to provide pain relief for the patient and to return mechanical integrity to the vertebral body; this procedure is performed as a treatment option for thoracic and lumbar VBFs [10]. Galibert and Deramond were the first to perform this procedure in 1984, injecting polymethyl methacrylate (PMMA) into a vertebral body to treat a vertebral haemangioma [34]. However, the procedure was popularized for the palliative treatment of osteoporotic VBFs in the 1990s [92]. Lewis described these procedures in detail in a 2007 review; they are summarized as follows [10]. The procedures are performed with the patient lying supine on the table under conscious sedation [93]. The clinician, using a mallet, taps 11 G or 13 G cannulae percutaneously through one or both pedicles of the fractured vertebra into the anterior third of the vertebral body. Bone cement is then injected through these cannulae under fluoroscopy

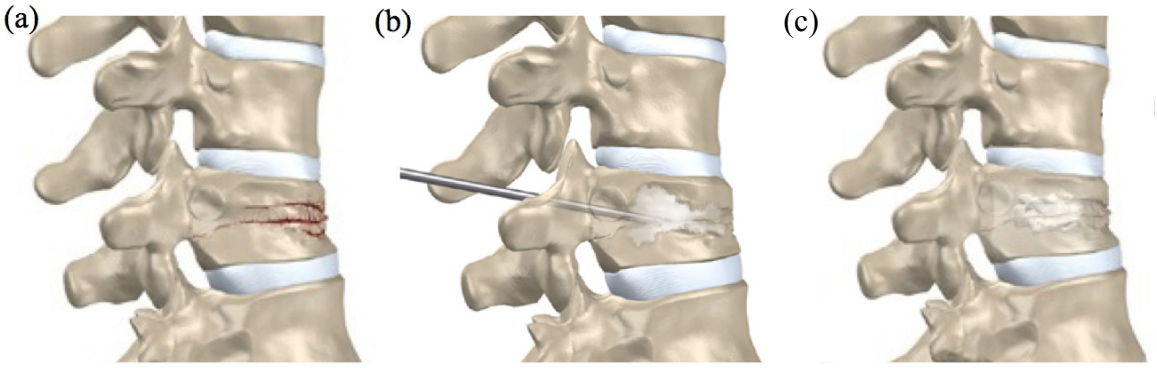

Figure 5: Graphical representation of the PVP procedure - (a) fractured vertebrae, (b) injection of bone cement, (c) stabilized vertebra. Adapted from proactiverehab.com [94].

guidance until the vertebral body has been filled sufficiently, typically requiring *c.* 4 mL of cement [26]. The cannulae are then removed and the patient remains stationary on the table for 15 to 20 minutes after the cement has been injected, allowing the material to set. After an observational period, the patient is free to go home [95], as PVP provides immediate pain relief [14, 15, 96], enabling a shorter hospital stay. On average, PVP patients leave the hospital within 3-6 days [97], with some able to leave the same day [29], compared to 10 days when VBFs are treated with conservative therapy [98].

KP is similar to PVP from a procedural standpoint, however, it includes the additional step of inflating a balloon tamp with the intent to restore vertebral height and correct the kyphotic deformity of the spine (Figure 6) [99]. More recently, alternative devices have been used in place of the conventional balloon to restore vertebral height, including titanium meshes, polymer coils, and mechanical jacks [100, 101]. KP is a more complicated procedure: firstly, it requires the use of general anesthesia; secondly, a drill to create a void to facilitate the placement of the balloon tamp; and thirdly the inflation of the balloon tamp further damages the trabeculae of cancellous bone within the vertebral

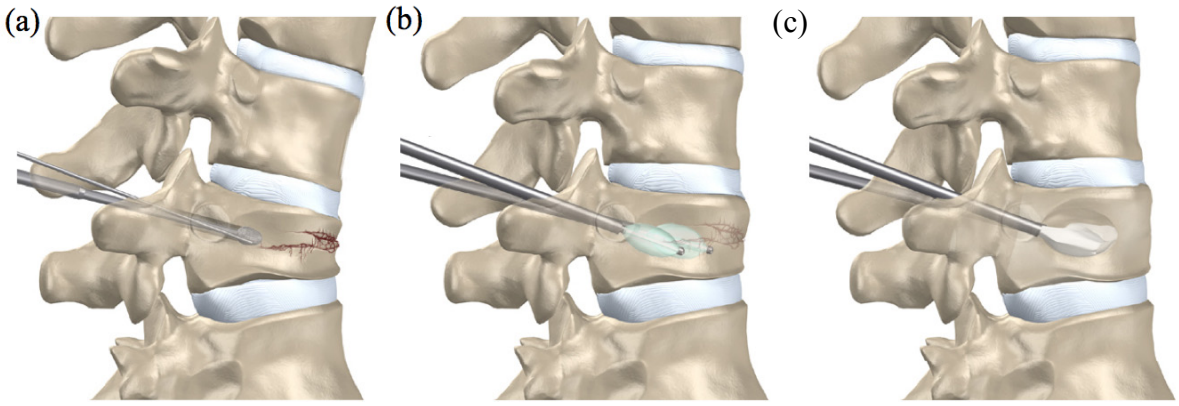

Figure 6: Graphical representation of the KP procedure - (a) drill into fractured vertebrae, (b) inflation of balloon tamp, (c) injection of bone cement. Adapted from proactiverehap.com [102].

body. The benefit of KP is the creation of a void by the balloon tamp that allows bone cement to be injected under lower pressure, potentially reducing cement extravasation [93, 103]. The primary goal of both PVP and KP is to reduce pain and improve functional status, while the secondary goal is to stabilize vertebrae weakened by fracture or tumors [104]

3.1 Palliative Mechanisms of Vertebral Body Augmentation

The mechanism of pain relief associated with vertebral body augmentation is likely associated with the mechanical stabilization of VBFs [93]. The pain associated with VBFs is caused by the either mechanical or chemical stimuli of nociceptors, sensory neurons responsible for transmitting pain signals [105, 106]. Mechanical stimulus involves the relative motion between top and bottom endplates of vertebrae, which induces micromotion in the trabeculae within the fractured vertebral body [107]. Chemical stimulus is attributed to bone marrow edema arising in part due to the inflammatory response associated with the fracture [108]. Internal fixation of the VBF is achieved by the interdigitation of the cement with the trabecular bone of the vertebrae. Once the cement has hardened, it forms an internal cast that stabilizes the fracture to prevent micromotion of the trabeculae, ceasing the mechanical stimulation of the nociceptors [109, 110], and providing patients with immediate and significant pain relief [22, 35, 111]. Mechanical stabilization does not address the pain associated with the chemical stimulus of nociceptors by the presence of bone marrow edema. However, edema is known to dissipate from the fracture site during the healing process, which may explain the continuous gradual reduction in pain over time, subsequent to the initial post-procedure decrease [22, 35, 108].

Further evidence to support mechanical stabilization as the most likely palliative mechanism comes from reports that calcium sulfate and calcium phosphate cements have been successfully used in PVP or KP applications. In contrast to PMMA, these cements do not have high setting temperatures and do not contain toxic monomers; thus, fracture stabilization is the only possible mechanism of pain relief [112]. Masala *et al.* performed PVP on 80 patients using sulfate hydroxyapatite cement, and observed significant drop in initial pain scores after 1 day and a continued decrease over the 12 month observation period [113]; it should be noted there was no control group in this study. Grafe *et al.* compared the efficacy of calcium phosphate cement to PMMA in KP in a prospective trial on 40 patients (n=20 patients per cement) with osteoporotic VBFs. They found the calcium phosphate to provide statistically similar levels of pain relief as PMMA immediately following the procedure and up to the final endpoint at 3 years [114].

Two additional, although less probable, palliative mechanisms have been postulated in the PVP and KP literature: thermal and chemical necrosis of the neural tissue specifically related to the use of PMMA [93]. The palliative mechanism of thermal necrosis was proposed due to the exothermic setting reaction of PMMA; free-radical polymerization has been recorded to produce peak temperatures in excess of 100 ˚C *in vitro*, which is believed to damage neural tissue [115]. However, *in vivo* investigations in both animal and human subjects revealed PMMA setting temperatures to be much lower, ranging from 40 to 76 ˚C for periods of less than 5 minutes, thus failing to exceed the thermal necrosis threshold of neural tissue (*i.e.* 45 ˚C for a period of greater than 30 minutes) [116, 117]. The basis of argument pertaining to chemical necrosis is related to the toxicity of the methyl methacrylate monomer of the liquid component of PMMA

[112]. However, despite the capability of PMMA ingredients to cause chemical necrosis of the surrounding tissue, the magnitude of their release is well below the levels required to kill neural tissue [107].

3.2 Clinical Efficacy of Vertebral Body Augmentation

In order to effectively treat VBFs, therapies must (i) relieve pain to facilitate rehabilitation and (ii) manage of the underlying disease [6, 7]. Although PVP and KP do not directly address the latter, these treatments have been clinically proven to be safe and effective, providing immediate and lasting pain relief for patients suffering from VBFs [11-15, 26-28]. Further, PVP and KP promote reduced analgesic use and improve functionality, thus mitigating the risks associated with conservative therapy [11, 12, 26]. Table 1 chronologically summarizes the seven randomized clinical trials (RCTs), that have evaluated PVP to date, and Table 2 summarizes the two RCTs that have been evaluated KP to date. These summaries include: the design, primary results, conclusions, levels of evidence, and limitations for each trial. Section 3.2.1 provides greater detail regarding each of the most pertinent PVP trials, and section 3.2.4 discusses the most relevant KP trials in greater detail. From the clinical evidence, PVP and KP are equally effective in the treatment of VBFs, and both are clinically proven to be superior to conservative therapy for the reduction of pain, disability, and improving quality of life [11-13, 26, 27].

3.2.1 Percutaneous Vertebroplasty

Seven RCTs have been published between 2007 and 2012 [14, 15, 17, 18, 26-28]. The enrollment periods for all of these trials were between July 2003 (Voormolen *et al.* 2007)

Table 1: Summary of PVP randomized controlled trials.

Study	Design	Level of Evidence	Limitations	Primary Results	Conclusions
Voormolen e*t al* 2007 [15]	Randomized, prospective, controlled trial, conducted at three centers between July 2003 and June 2005 in the Netherlands. 34 patients with osteoporotic VBFs between 6 weeks and 6 months old were treated with PVP (n=18) or conservative therapy (n=16). Pain, disability and quality of life were assessed at baseline, 1 day, 2 weeks, 3, 6, and 12 months	Level 2 - Lesser quality RCT	Short Follow up due to cross over; no blinding; no placebo control; small sample size	**PVP patients**: 34% decrease in pain score, significant improvements in disability and quality of life, and less analgesic use 1 day after treatment maintained until 2-week endpoint. **Control patients**: 7% decrease in pain after 1 day, and 16% reduction after 2 weeks.	Pain relief and improvement of mobility, function, and stature after PVP is immediate and significantly better in the short-term compared with conservative treatment. Study terminated after 2 weeks due to high crossover rates from the control group to the treatment group
Rousing *et al*. 2009 [120], 2010 [14]	Randomized, prospective, controlled, single-center trial conducted between January 2001 and January 2008 in Denmark; Acute <2wks (n=40) or suba-cute 2-8 weeks (n=10) osteoporotic VBF treated with PVP (n=26) or conservative therapy (n=24). Pain, disability, and quality of life were assessed at Baseline, 3 6, and 12 months after intervention	Level 2 - Lesser quality RCT	Small Sample size; No blinding; no sham control; Only 75% of patients were quantitatively assessed at baseline	**PVP patients**: 73% reduction in pain with 24 hours of procedure, which was sustained for 12 months. **Control patients**: 70% reduction in pain after 3 and 12 months, which was statistically similar to PVP patients.	PVP is comparable to conservative treatment for painful acute and semi acute osteoporotic VBFs at 3 and 12 months. PVP provides immediate pain relief of acute or semi acute osteoporotic VBFs, which is superior to conservative therapy until 3 months.

American Academy of Orthopaedic Surgeons and North American Spine Society Levels of Evidence [118, 119]

Level 1	High quality randomized controlled trial (RCT) with statistically significant difference or no statistically significant difference but narrow confidence intervals, or systematic Review of Level I RCTs (and study results were homogenous)
Level 2	Lesser quality RCT (e.g. < 80% follow-up, no blinding, or improper randomization); Prospective comparative study; Systematic review of Level II studies or Level I studies with inconsistent results
Level 3	Case control study; retrospective comparative study; systematic review of Level III studies
Level 4	Case Series
Level 5	Expert Opinion

Table 1 continued: Summary of PVP randomized controlled trials.

Study	Design	Level of Evidence	Limitations	Primary Results	Conclusions
Buchbinder *et al.* 2009 [17]	Randomized, prospective, placebo-controlled trial conducted between April 2004 and October 2008 at 5 centers in Australia. 78 patients with 1 or 2 osteoporotic VBFs that have been symptomatic for 12 months or less were treated with PVP (n=38) or placebo sham procedure (n=40). Pain, disability, and quality of life were assessed at baseline, 1 week, 1, 3, and 6 months, with Kroon et al. reporting outcomes after 12 and 24 months [121]	Level 1 - RCT; Level 2 - lesser quality RCT for 12 and 24 month follow up [121]	Small sample size; age of the fracture; lack of non-interventional control; strict inclusion criteria; Poor follow-up at 24 months, 76% PVP and 70% Control.	**PVP patients:** 20% reduction in pain after 1 week, which continually decreased to a 41% total reduction after 2 years. **Placebo patients**: 30% reduction in pain after 1 week, a decrease which was maintained over time, with a 27% reduction from baseline after 2 years.	Patients with treated with the sham procedure demonstrated improvements that were statistically similar to those patients treated by PVP after 1 week, 3, 6, 12 and 24 months.
Kallmes *et al.* 2009 [18]	Randomized, prospective, placebo controlled trial conducted between June 2004 and August 2008 at 11 centers in the United States, United Kingdom, and Australia. 131 patients with osteoporotic VBFs that had been symptomatic for one year or less were treated with PVP (n=68) or placebos sham (n=63). Crossover between treatment groups was allowed after 1 month. Pain and disability were assessed at 3 days, 2 weeks, and 1 month, with Comstock *et al.* reporting 6 and 12-month data [122].	Level 1 - RCT	Age of fracture; Validity of the sham procedure; high crossover rates from sham to PVP group; lack of non-interventional control group; strict enrolment criteria, and improper blinding	**PVP patients:** 27.9% reduction in disability, 45.3 % decrease in pain at 1 month. **Placebo patients:** 25.7% reduction in disability and 36.1% decrease in pain. Results were statistically similar at 1 month, but at 1 year PVP experienced greater decrease in pain (50 % vs. 35% $p = 0.042$)	Improvements in pain and disability associated with osteoporotic VBFs in patients treated with PVP were similar to the improvements in a sham control group. However, after 1 year there is evidence to suggest PVP provides modest reduction in pain compared to the shame control, although no difference in disability was observed.
Klazen *et al.* 2010 [26]	Randomized, prospective, controlled trial conducted between October 2005 and June 2008 at 6 centers in the Netherlands and Belgium. 202 patients with osteoporotic VBFs $\leq$ 6weeks old were treated with PVP (n=101) or conservative therapy (n=101). Pain, disability, and quality of life were assessed at baseline, 1 day, 1 week, 1, 3, 6, and 12 months.	Level 2 - Lesser quality RCT	No blinding; no placebo control.	**PVP patients**: 53% decrease in pain after 1 day, 73% decrease after 1 year. **Control patients**: 11% decrease after 1 day, 48% decrease after 1 year. PVP patients had significantly greater improvements in, pain, quality of life and disability scores, as well as lower drug use than control patients.	PVP is a safe and effective procedure for patients with persistent pain caused by osteoporotic VBFs. Further PVP provides immediate and lasting pain relief that is superior to conservative treatment

Table 1 continued: Summary of PVP randomized controlled trials.

Study	Design	Level of Evidence	Limitations	Primary Results	Conclusions
Farrokhi *et al.* 2011 [27]	Randomized, prospective, single-blinded, controlled trial conducted between September 2004 and January 2006 at a single center in Iran. 82 patients with osteoporotic VBFs refractory to analgesic therapy for > 4 weeks and < 1 year were treated with PVP (n = 40) or conservative therapy (n = 42). Crossover was allowed after 1 month. Patients were assessed for quality of life and pain at baseline, post procedure (pain only), 1 week, 2, 6, 12, 24, and 36 months.	Level 2 - Lesser quality RCT; although it should be noted blinding the physicians diminishes the chance of bias	Single center; small sample size; no discussion of statistical power to determine sample size; fracture age; patients were not blinded; crossover allowed	**PVP patients**: 58% decrease in pain after 1 day, 78% decrease after 3 years. **Control patients**: 11% decrease after 1 week, 49% after 3 years. PVP patients had significantly greater improvements in quality of life scores than control patients at all time points. PVP resulted in statistically greater pain relief up until 1 year, where further improvements were statistically similar to control patients. However, by 1 year 25% of control patients (n=10) crossed over to PVP group, which the intention-to-treat method could artificially lower the average pain reductions of the control group.	Compared to conservative therapy, PVP results in statistically significant greater pain relief and improvements in quality of life which lasted for 2 years.
Blasco *et al.* 2012 [28]	Randomized, prospective, controlled trial conducted between April 2006 and June 2010 at a single center in Spain. 125 patients with symptomatic osteoporotic VBFs ≤ 12 months old were treated with PVP (n=64) or conservative therapy (n=61). Patients were evaluated for pain and quality of life, assessed at baseline, 2 weeks, 2, 6, and 12 months.	Level 2 - Lesser quality RCT	Single center; fracture age; failed to enrol a sufficient number of patients to achieve 80% power of trial; high attrition rate; high rates of new fracture PVP patients, which may influence long-term pain scores of PVP	**PVP patients**: 42% decrease in pain after 2 months, which remained statistically similar for the remainder of the study. Further, PVP led to significant improvements in quality of life at all time points. **Control patients**: 25% decrease in pain after 2 months, which did not statistically change for the remainder of the study. Conservative therapy did not statistically improve patients' quality of life until 6 months.	Both PVP and conservative therapy are associated with significant improvement in pain and quality of life in patients with osteoporotic VBFs over a 1-year period, but PVP resulted achieve faster pain relief.

Table 2: Summary of KP randomized controlled trials.

Study	Design	Level of Evidence	Limitations	Primary Results	Conclusions
Wardlaw *et al.* 2009 [12]	Randomized, prospective, controlled trial conducted between February 2003 and December 2003 at 21 sites in 8 countries. 300 patients with osteoporotic VBFs ≤ 3 months old were treated with either KP (n=149) or conservative therapy (n=151). Patients were assessed for quality of life, disability and pain at baseline, 1, 3, 6, 12 months and 24-month data provided by Van Meirhaeghe *et al.* [123]	Level 2 - Lesser quality RCT	No blinding; Industry sponsor (Medtronic Spine LLC, USA); high presence of new fractures in both groups; high attrition rate	**KP patients**: 48% decrease in pain at 1 week and 60% reduction after 6 months, where it remained constant for remainder of study. **Control patients**: 21% decrease in pain at 1 week and 47% decrease after 2 years. KP patients experienced significantly greater improvements in quality of life, disability and pain as compared to patients treated with conservative therapy.	KP is effective and safe. Compared to conservative therapy, KP resulted in improvements in quality of life and disability measure and reduction of back pain in patients with acute painful VBFs, although the differences in improvement between KP and conservative therapy narrowed by 1 year.
Berenson *et al.* 2011 [11]	Randomized, controlled, prospective trial conducted between May 2005 and March 2008 at 22 sites in Australia, Canada, Europe, and the USA. 134 patients with cancer and 1-3 VBFs were treated with either KP (n=70) or non-surgical management (n=64). Patients were assessed for disability and pain at baseline, 1, 3, 6, and 12 months. Crossover was allowed after 1 month	Level 2 - Lesser quality RCT	No blinding; Cross-over allowed after 1 month; high attrition rates - only 6 control patients completed the 12 month study; industry sponsored study (Medtronic Spine LLC, USA)	**KP patients**: 52% decrease in pain at 7 and 30 days. **Control patients**: No pain reduction at 1 month. KP patients had significantly greater improvements in disability, quality of life and pain at 1 month, however due to crossover, difference between treatment groups became statistically similar by 3 months for pain and 12 months for disability and quality of life. Control patients who crossed-over significantly improved after KP.	KP is safe and effective for painful VBFs in patients with cancer, and rapidly reduces pain and improves function. As such, KP should be considered as an early treatment option for patients with cancer and symptomatic VBFs.

and January 2010 (Blasco *et al.* 2012). Due to the overlapping time frames of these trials, the research questions of each study have a common theme. The first RCT, published by Voormolen *et al.* in 2007 [15], prospectively assessed the short-term clinical outcome of sub-acute VBFs treated with PVP compared to conservative treatment (*i.e.* analgesic therapy and bed rest), where the analgesic regiments were tailored for each patients. Thirty-four patients with VBFs, refractive to medical therapy for at least 6 weeks, but not longer than 6 months and with MRI scans to confirm the presence of bone marrow edema, were enrolled in the 2-week study. Results showed that PVP patients (n=18) experienced significantly greater pain reductions and less analgesic use 1 day and 2 weeks after treatment versus conservative therapy patients (n=16). After 2 weeks, 14 of the 16 patients in the conservative therapy group requested crossover, which resulted in the early termination of the study. This short follow-up period and the small sample size limit Voormolen's findings, requiring additional study with a greater number of patients and longer follow periods.

To assess the long-term clinical outcomes of PVP, Rousing *et al.* conducted a prospective RCT that compared PVP to conservative therapy in patients with acute and subacute VBFs [14]. Fifty patients with VBFs less than 8 weeks old were randomized to either PVP (n=25) or conservative therapy (n=25) groups. PVP treatment resulted in a significant reduction in pain 1 day after the procedure. At the 3-month and 12-month time points, both groups exhibited statistically similar levels of pain. Rousing *et al.* concluded that PVP is an effective treatment for VBFs, but most fractures heal with 8 to 12 weeks; as such, PVP should be reserved only for patients that cannot tolerate conservative therapy, *e.g.* patients with chronic obstructive lung disease who cannot be treated as

analgesics due to poor lung function, or weak patients who risk serious debilitation with 2 to 3 months of the immobilization. However, the validity of this study is limited due to a small sample size and the fact that only 75 % of patients were assessed at baseline.

In 2010 Klazen *et al.* provided more definitive evidence regarding the efficacy of PVP from the largest PVP trial to date. This multicenter, prospective, RCT investigated the efficacy of PVP to treat osteoporotic VBFs versus conservative therapy [26]. Patients who experienced back pain for 6 weeks or less, confirmed by the presence of bone edema on MRI images, were randomized in to PVP (n=101) or conservative therapy (n=101) treatment groups. PVP treatment resulted in significantly greater pain relief than conservative therapy at the primary end points of 1 month and 1 year. A larger sample size and more complete follow-up compared to Rousing led Klazen *et al.* to conclude PVP was a safe and effective procedure that is superior to conservative therapy for patients suffering persistent pain from acute VBFs.

A key limitation of the studies relating to PVP efficacy versus conservative therapy up until 2011 was the lack of blinding. Farrokhi *et al.* published the findings of a single-center, prospective, RCT that used individuals blinded to the treatment modality to assess patient outcomes [27]. This study compared the efficacy of PVP versus conservative therapy to control pain and improve the quality of life of patients. Although patients were aware of their treatment, the single-blinding methodology of this study reduced the bias of those who assessed clinical outcomes. Inclusion criteria included pain associated with VBFs, confirmed by the presence of edema on MRI scans, that were refractory to analgesic medication with symptoms between 4 weeks and 1 year. Patients were randomized in to PVP (n=40) and conservative therapy (n=42) treatment groups. After 1

week, patients in the PVP group demonstrated statistically lower pain scores and a greater quality of life than the patients treated with conservative therapy over the remainder of the 3-year study.

Blasco *et al*. published the most recent RCT in 2012 [28]. This randomized, prospective, controlled, single-center study compared PVP versus conservative therapy. Patients with VBFs less than 12 months old, confirmed by the presence of edema on MRI scans, were randomized between PVP (n=64) and conservative therapy groups (n=61). Both groups demonstrated significantly less pain at the initial 2-week assessment, and pain levels continued to decrease over the 24-month study period, with PVP patients experiencing a greater overall reduction in pain. PVP patients also saw an immediate and significant improvement in quality of life, whereas conservative therapy patients did not see a significant improvement for 6 months. These findings led Blasco *et al*. to conclude PVP provides faster pain relief, with more significant improvement in the pain score at the 2-month follow-up than conservative therapy. Cumulatively, the aforementioned RCTs demonstrate PVP to be a safe and effective procedure, particularly in acute VBFs.

3.2.2 Percutaneous Vertebroplasty Controversy

Despite the considerable body of evidence that demonstrates PVP to be effective in the treatment of VBFs, the use of this procedure has declined *c.* 20 % since the release of two placebo-controlled RCTs were published in the New England Journal of Medicine (NEJM) in 2009 [16, 124]. Buchbinder *et al.* [17] and Kallmes *et al.* [18] both concluded a sham procedure to be as effective as PVP in the palliative treatment of osteoporotic VBFs. However, the validity of the findings presented by both Buchbinder and Kallmes

have been questioned in the literature due to the design, execution, results, and interpretation of the data [19-24].

The trial published by Buchbinder *et al.* was a, randomized, double-blinded placebo-controlled trial conducted at 5 centers across Australia [17]. Patients with one or two osteoporotic vertebral compression fractures less than 12 months old (with the presence of edema as detected by MRI) were randomized into PVP (n=38) and placebo-control (n=40) treatment groups. The placebo procedure entailed several elements to mimic the PVP procedure, including tapping a blunt-tip cannula positioned on the lamina of the vertebral arch, mixing but not injecting PMMA bone cement, and movement of the fluoroscopy equipment. Buchbinder *et al.* observed modest, and comparable, decreases in pain in both the PVP and placebo groups at time points from 1 week to 6 months, but the decreases of both groups were statistically similar. These results led Buchbinder *et al.* to conclude that PVP had no beneficial effect compared to the sham procedure for treating patients with painful osteoporotic VBFs [17]. Furthermore, in 2014 Kroon *et al.* published the 1 and 2-year follow-up results of this study, with 67 patients (33 PVP, 34 placebo) completing all follow up visits [121]. PVP patients demonstrated a continuous decrease in overall pain scores over time (20% reduction from baseline at 1 week, 42% reduction from baseline at 2 years), while the initial decrease report by placebo patients at 1 week remained constant over time pain (30% reduction from baseline at 1 week, 28% reduction from baseline at 2 years). Neither Buchbinder *et al*., or Kroon *et al.* discussed whether the reduced pain over time was statistically significance in either group [121, 125].

The second blinded, randomized, controlled trial conducted by Kallmes *et al.* had a similar design to that of Buchbinder *et al.* The multicenter trial was conducted at 11 centers across the United States, United Kingdom and Australia [18]. Patients were randomly assigned to either the PVP (n=68) or the sham control (n=63), and blinded to which procedure they received. Prior to treatment, all patients received an injection of 1% lidocaine in the tissues overlying the pedicles of the target vertebra(e), followed by an injection of 0.25% bupivacaine into the periosteum of the pedicles. The sham procedure took place after the bupivacaine injection, and consisted of verbal and physical cues to give the patient the perception they were undergoing PVP. These cues included pushing on the patient's back, talking about placement of the needle, and opening and mixing PMMA, but needles were not placed and cement was not injected. Both the PVP and sham control groups experienced statistically similar reduction in pain and disability immediately following the procedures, which continued until the 1-month primary endpoint of the studies. It was noted that 64% PVP patients demonstrated a trend toward a higher rate of clinically meaningful improvement in pain (*i.e.* 30% reduction from baseline) at the 3-month time point, compared to 48% of control patients, but this observation did not reach the point of significance by the end of the 3-month study ($p = 0.06$). Patients were allowed to cross over to the opposite group after 1 month, and significantly more control patients crossed over to the PVP group after 3 months (51% *vs.* 13% $p<0.001$) [18]. Given that both the PVP and control groups experienced similar results at 1 month, Kallmes *et al.* concluded that further studies are required to shed light on the long-term efficacy of PVP [18]. However, and critically, in 2013 by Comstock *et al.,* published the 1-year follow up analysis of the Kallmes *et al.* trial, where it was

revealed that significantly more PVP patients (70 %) experienced reduced scores [122]. Ultimately, it was noted that PVP patients experienced significantly greater reduction in pain than control patients (visual analog score: control 3.52 ± 2.89 *vs.* PVP 4.50 ±2.70, p = 0.042).

Despite the positive findings of Comstock *et al.,* the studies by Buchbinder *et al.* and Kallmes *et al.* sparked a significant debate across PVP communities regarding the validity of cement augmentation as a treatment method for osteoporotic VBFs [19, 21, 126-129]. These two studies had profound effects on the number of PVP procedures performed, with the number of both PVP and KP procedures dropping sharply from 2009 to 2010 [16, 130, 131]. The American Academy of Orthopaedic Surgeons, citing Buchbinder *et al.* and Kallmes *et al.*, published clinical practical guidelines in 2011 recommending against the use of PVP, instead recommending KP [132]. Analyzing Medicare procedural codes from 2006 to 2013, Cox *et al.* reported that PVP rates have been declining since 2009, but the annual rate of KP procedures has been increasing since 2010 (Figure 7) [16].

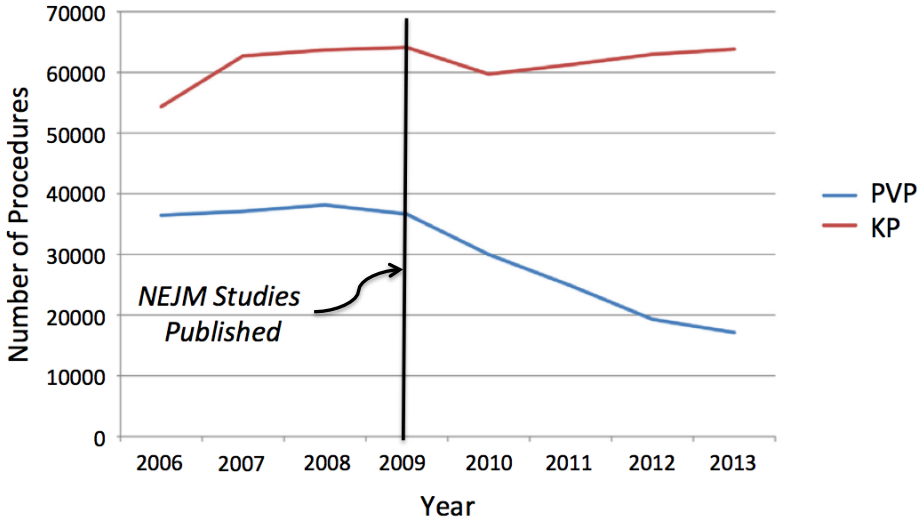

Figure 7: Trends in the annual number of PVP and KP procedures performed in the United States between 2006 and 2013, adapted from Cox *et al.* 2016 [16].

The findings presented by Buchbinder *et al.* [17] and Kallmes *et al.* [18] contradicted the findings of the previous two decades regarding the efficacy of PVP to treat osteoporotic VBFs [133]. As a result, members of the PVP community have scrutinized these studies, specifically with regards to the (i) design (*e.g.* acuity of the fractures, restrictive inclusion criteria, lack of non-interventional control groups, validity of placebo procedure used in Kallmes *et al.*), (ii) execution (*e.g.* deviation from required number of subjects, lack of detection of edema in Kallmes *et al.*), and (iii) results interpretation (*e.g.* high crossover rate from placebo to PVP in Kallmes *et al.*) [19-24]. Both trials deviated from their designed sample size, cutting enrollment short and thereby reducing statistical power [134, 135]. Although both argued that samples size where sufficient to detect their self defined minimum between-group differences, a reduction in sample size will broaden the distribution of results in both groups making it less effective in deciphering statistical significant between-groups differences. In a paper about sample size and statistical power of clinical trials, Lachin argues clinical trials with inadequate sample sizes are doomed to failure before they begin and serve only to confuse the issue of determining the most effective therapy for a given condition [136]. This effect has been the consequence of the 2009 NEJM papers on the treatment of VBFs, which has prompted greater analysis of all published data. Two meta-analyses of the data generated from all RCTs to date have concluded that PVP remains an effective procedure, but identify that the best outcome arise when the VBFs are less than 7 weeks old [25, 137]. Furthermore, upon a thorough review of all clinical evidence, the National Institute for Health and Care Excellence, as organization with the mandate to provide evidence-based

guidance to improve health in the United Kingdom, concluded PVP to be more effective than conservative therapies [138].

Ultimately, the goal of clinicians is to improve the lives of patients by reducing the pain and disability associated with VBFs. Edidin *et al.* identified 858,978 patients with osteoporotic VBFs between 2005 and 2008, of whom 63,693 underwent PVP. They found that that the mortality of patients suffering from a VBF was significantly reduced; after 4 years of follow-up, 57.3 % of patients who had undergone PVP were alive compared with 50.0 % of patients who had not undergone any intervention [139]. This combined with the evidence provided above suggests PVP to be an effective treatment for osteoporotic VBFs. The authors of the Kallmes *et al.* trial acknowledge the need for further investigation on this topic, stating that due to the significant improvements associated with PVP described by Comstock *et al.,* it is possible that PVP might be effective in a subgroup of patients [122]. Two such studies currently under way are the Vertos IV and Vertos V trials. Vertos IV investigates the efficacy of PVP to treat acute (< 6 weeks) VBFs in a blinded randomized controlled trial using the same sham procedure as Kallmes *et al.* [140]. Vertos V has a similar design but will investigate the efficacy of PVP to treat chronic (> 3 months) VBFs [141]. Both studies have been completed, Vertos IV in January 2014, Vertos V in June 2015, although no results have yet been released [142, 143].

3.2.3 Kyphoplasty

To date, the safety and efficacy of KP has been clinically demonstrated in two RCTs: (i) the Fracture Reduction Evaluation trial (FREE), which compared the efficacy of KP to treat primarily osteoporotic VBFs versus non-surgical care [12, 123, 144]; and (ii) the

Cancer Patient Fracture Evaluation study (CAFE), which compared the efficacy of KP versus non-surgical care to treat VCBFs in patients with cancer [11]. The FREE study was carried out at 21 sites in 8 countries, and evaluated the quality of life with regards to physical abilities in 149 KP patients and 151 control patients with VBFs less than 3 months old with presence of edema assessed by MRI. At the 1-month primary endpoint of the study, KP patients had significantly faster and greater improvements in quality of life, function, mobility and pain than those treated with non-surgical care [12]. KP patients did report greater pain relief at 1 and 2 years [144], which was determined to be a key driver in the improved quality of life of patients treated with KP [145]. The differences in quality of life and disability scores narrowed over time, becoming statistically similar at the 1 and 2-year time points as the condition of the control group improved [123]. Importantly, one of the aims of the KP procedure is to correct the kyphosis associated with VBFs. In the FREE trial KP patients experienced significant improvement in kyphotic angle compared to the control group (3.13˚ vs. 0.82˚, p=0.003) which in a follow up publication by Van Meirhaeghe *et al.,* was found to correlate with improved physical abilities [123].

The CAFE trial was conducted at 22 sites across Europe, USA, Canada, and Australia and it investigated the efficacy of KP to treat VBFs in patients who had cancer [11]. Patients were randomized into KP (n=65) and non-surgical (n=52) treatment groups, and had access to analgesics, bed rest, bracing, physiotherapy, rehabilitation programs, and walking aids. The primary end point of the study was the assessment of disability at 1-month, where it was observed that patients treated with KP had a superior functional outcome than patients who received non-surgical management. Additionally, at the 1-

month time point KP patients showed marked reduction in back pain, improvement in quality of life, and less medication use; trends that continued for the remainder of the 12-month study. These improvements led to 73% of KP patients being able to care for themselves. Improvements in the control group came about slower and were less substantial, with only 39% of patients gaining sufficient functional improvement to care for themselves at 1 year. The limited improvement in the control group led Berenson *et al.* to conclude that KP should be considered as an early treatment option for patients with cancer who have symptomatic VBFs [11]. Together, the data from the FREE and CAFE provide clinical evidence that KP is a safe and effective procedure for the treatment of VBFs.

3.2.4 Percutaneous Vertebroplasty versus Kyphoplasty

Clinical evidence has demonstrated that PVP and KP are equally effective in treating the symptoms of VBFs [13, 29, 30]. However, currently 75% of the vertebral augmentation procedures in the United States are KP [146, 147]. The 3:1 ratio of KP to PVP procedures is largely due to (i) the controversy regarding PVP brought about by the 2009 NEJM articles, and (ii) the perception that KP is more effective than PVP [16]. With regards to the former, Figure 8 depicts the transition by clinicians from PVP to KP, with the largest shift occurring in Interventional Radiology, the most prominent specialty for conducting PVP. With regards to the latter point, three recent prospective RCTs compared the clinical efficacy of PVP to that of KP in the treatment of VBFs, with follow-up periods of between 1 and 5 years, and all three *disproved* the perception that KP is more effective than PVP [13, 29, 30]. In all three trials, both PVP and KP were observed to significantly reduced the pain and disability of patients, improvements that were sustained over the

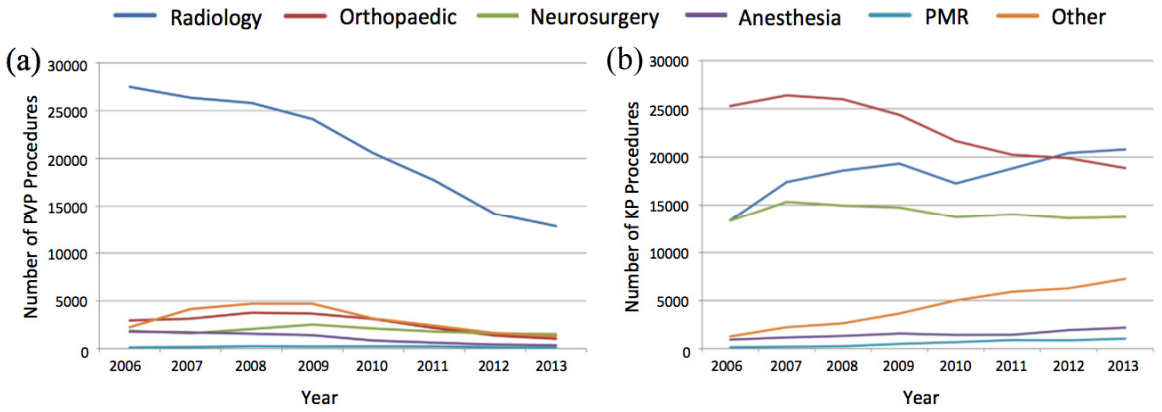

Figure 8: Number of (a) PVP and (b) KP performed in the United States between 2006 and 2013, categorized by speciality. Note PMR stands for Physical medicince and rehabilitation. Adapted from Cox *et al.* 2016 [16].

entirety of the follow-up periods. However, in each study, the improvements in pain and disability in both PVP and KP treatment groups were found to be statistically similar at all time points. These findings led the authors of all three studies to conclude that PVP and KP are equally effective treatments for patients suffering from VBFs [13, 29, 30]. Further, KP costs more than PVP; in the United States, KP is between $4000 and $5000 more than PVP [16]. In a cost analysis conducted by the National Institute for Health and Care Excellence as part of their assessment of vertebral body augmentation, it was identified that KP costs three times more to achieve the same clinical outcome as PVP [138]. Given the similar clinical efficacy and the higher cost of KP, unless a demonstrable clinical advantage is revealed in the future, there is no appreciable benefit of treating VBFs with KP as opposed to PVP.

3.2.5 Complications of Vertebral Body Augmentation

Both PVP and KP are safe procedures and complications are rare, occurring in 1 to 3% of patients [148]. The most common adverse event associated with vertebral body

augmentation is cement extravasation, although complications arising from cement extravasation are uncommon [149]. In clinical studies, the rate of cement extravasation has been reported as high as 85% for PVP procedures and 73% for KP procedures, with the most common sites being the intervertebral disc, paravertebral tissue, vasculature, and spinal canal [29]. Although these rates are higher than most published in the literature, they are consistent in the fact that extravasation is more prominent during PVP procedures than it is during KP [150]. In most cases cement extravasation is asymptomatic. However, in a small number of patient serious complications can arise. In exceptional instances, extravasation into the spinal canal can cause cord compression leading to limb ischemia or paralysis [151, 152]. More frequently cement leaks into the venous system, with pulmonary embolisms being to most common result, which are reported to occur in 2 to 26% of patients [152]. There have been at least 6 fatalities reported in the literature associated with either pulmonary or brain embolisms subsequent to PVP [153]. To mitigate against these risks, the radiopacity and viscosity of the cements are critical to ensure sufficient visualization and control of the cement during delivery. Additionally, post-procedural scans (*e.g.* radiographs, echocardiogrpahy, computed tomography, pulmonary angiography) should be conducted to detect any cement that may have leaked and poses a risk to the patient [152, 153].

Another complication commonly attributed to PVP and KP is the development of new fractures subsequent to cement injection; however, clinical evidence suggests vertebral body augmentation is not the cause of these fractures [25]. It has been argued in the literature that these new fractures are the result of altered biomechanical loading within the spinal column due to the increased stiffness of the augmented vertebra [154].

However, of the 9 clinical trials that compared either PVP or KP to conservative therapy, only Blasco *et al.* found a statistically significant greater number of new fractures in patients who underwent vertebral augmentation (29 new VBFs in 17 of 64 PVP patients *vs.* 8 new VBFs in 8 of 61 control patients, $p = 0.0462$). Unfortunately, this study was statistically underpowered to draw any legitimate conclusion regarding the cause of new VBFs subsequent to PVP [28]. Instead, it is more likely that subsequent VBFs are caused by either the natural progression of an existing pathology, or the biomechanical alterations associated with the preexisting VBFs [68, 155].

3.3 Injectable Bone Cements for Vertebral Body Augmentation

Any clinical bone cement used today for either PVP or KP falls into one of four categories: acrylic based cements, composite cements, calcium phosphate cements, or calcium sulfate cements [156]. To date, none of these existing cements have been able to demonstrate appropriate levels of biocompatibility whilst balancing practical injection characteristics with sufficient mechanical durability. Table 3 outlines the most desirable properties of an ideal bone cement for PVP and KP. From this list, the key properties are: excellent biocompatibility; easy injectability for a *minimum* of 5 to 10 minutes; with some clinical experts preferring 15 to 30 minutes [157, 158]; a setting dough viscosity that does not change much between mixing and subsequent delivery into the vertebral body; a resorption rate that is neither too fast nor too slow; and mechanical properties that are comparable to those of healthy intact trabecular bone [159]. Vertebral trabecular bone has compression strength in the order of 1-20 MPa, which have led to the suggestion PVP and KP bone cements should have compressive strengths of at least 30 MPa [160-163].

Table 3: Desirable properties of injectable bone cement for use in PVP and/or KP, adapted from Lewis [112].

	Desired Atrributes
a)	Very high radiopacity
b)	Ease of preparation and handling
c)	Working time of about 6-10 min
d)	Setting time of about 15 min
e)	Very easy injectability into the collapsed vertebral body
f)	Requisite mechanical properties that would allow for immediate reinforcement of the vertebral body and ensure early ambulation of the patient; for example, values of modulus of elasticity and strength should be comparable to those of a healthy vertebral body
g)	Appropriate cohesion; that is, dough sets in a fluid without disintegration (this is achieved by keeping a high viscosity for the dough)
h)	A curing dough whose initial viscosity is low (but not low enough to have the potential for extravasation) and a change in that viscosity that is practically invariant with setting time)
i)	Microporosity (mean pore diameter < 10 μm), to allow circulation of body fluid
j)	Macroporosity (mean pore diameter > 100 μm), to provide a scaffold for blood – cell colonization
k)	No toxicity
l)	Low curing temperature
m)	Low cost

3.3.1 Acrylic Bone Cements

PMMA is a two part self-polymerizing cement, with liquid and powder components [164]. The liquid component consists of a methyl methacylate monomer (*c.* 95 wt%) and benzoyl peroxide, or N,N, dimethyl-p-toluidine (*c.* 0.89 - 2.7 wt%), an accelerator that will break down the catalyst of the powder and initiate free radical polymerization. Hydroquinone is added as a stabilizer to prevent polymerization caused by the physical extremes of heat or light [44, 164, 165]. The powder component consists of pre-polymerized PMMA particles and/or copolymers of acrylic acid, ethyl acrylate, methyl acrylate, methyl methacrylate, and styrene. Additionally, benzoyl peroxide is included (*c.* 0.75-2.5 wt%) as a polymerization initiator, along with radiopacifying agents such as

barium sulfate, zirconium dioxide, tantalum, or tungsten powders [44, 164-166]. When cured, PMMA bonds to bone *via* mechanical interdigitation only [112, 156].

PMMA is the gold standard cement for PVP and KP, and has been since the inception of the procedures [34, 35]. However, in a review of acrylic bone cements, Lewis [164] listed six inherent disadvantages with the material, in particular: (1) high temperatures achieved during polymerization (recorded as high as 125°C [167]), (2) possibility of chemical necrosis of tissue caused by liquid component (*i.e.* methyl methacrylate monomer, NN-dimethyl-p-toluidine, benzoyl peroxide, or hydroquinone [168, 169]) (3) shrinkage of cement during polymerization, (4) large mismatch of mechanical properties between implant material and the bone being augmented, (5) weak cement-bone interface, and (6) cement particles that evoke an inflammatory response with deleterious effects on local tissue. These disadvantages have the potential to destabilize the PMMA implants, resulting in micromotion that may compromise the palliative relief provided by vertebral body augmentation [37]. In respect to the latter, a key contributor to the potential destabilization of the implant is the development of fibrous connective tissue around the PMMA bone cement, which may weaken the cement-bone interface (Figure 9) [38]. The development of the fibrous capsule is part of the inflammatory reaction of the body to isolate the implant [170]. This is generally initiated in response to substances leached from the PMMA cement mantel, including unreacted methyl methacrylate monomer (MMA), or radiopacifying agents such as barium sulfate [36, 38, 40, 171]. Fibrous encapsulation of PMMA implants has been reported in the literature [37, 38], including evidence from augmented human vertebrae

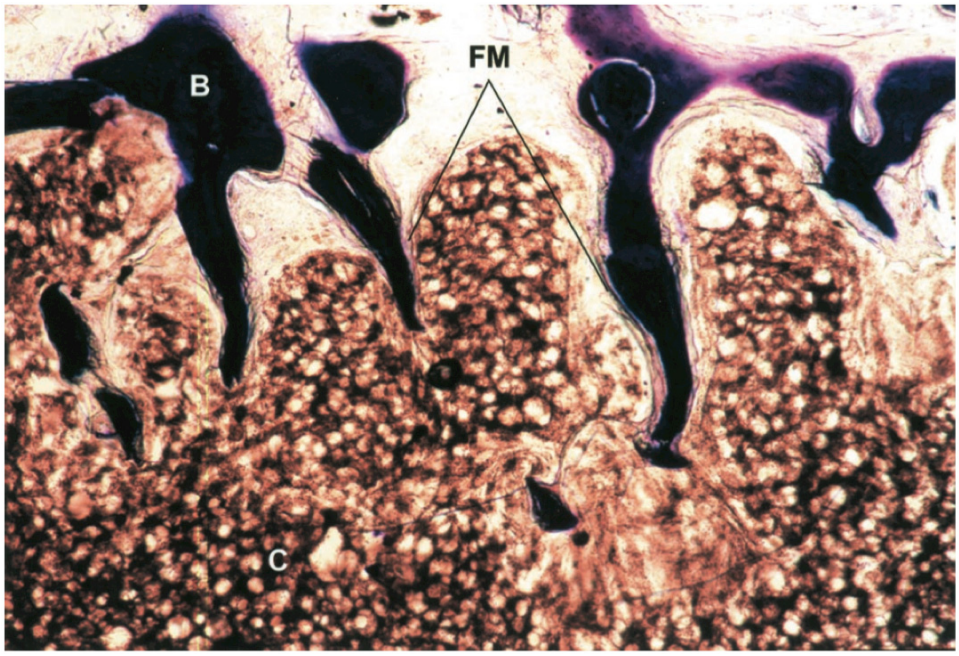

Figure 9: A fibrous membrane (FM) can be seen preventing the direct apposition of PMMA cement (C) to vertebral bone (B). This histological section is of a vertebral body resected from a 42-year old woman who had undergone KP (Giemsa stain at X 50 magnitfication, adapted from Togawa *et al.* 2003 [36]).

resected from deceased [36, 40], neurologically compromised [37], or severely kyphotic patients [36]. Additionally, the cement-bone interface may be further be compromised, increasing the risk of implant destabilization due to the potential osteonecrosis associated with either thermal injury or chemical insult from MMA [36, 37, 39, 40]. It has been hypothesized that the clinical efficacy of PVP is limited when cement interdigitation with surrounding cancellous bone is inhibited, which results in poor fracture stabilization and little pain relief [172].

3.3.2 Composite Resins

Composite resin bone cements have been created to improve upon the shortcomings of PMMA [173]. One commercially available composite resin is Cortoss (Stryker Orthobiologics, USA). It is a paste-paste system containing bisphenol-a-glycidyl

dimethacylate, bisphenol-a-ethoxy dimethacrylate, and triethylene glycol dimethacrylate resins combined with glass-ceramic particles to stimulate bone apposition at the interface. The cement also includes barium boroaluminosilicate glass for improved radiopacity and strength and silica for improved viscosity [173]. Advantages of Cortoss include reduced toxicity of liquid monomer achieved by a more complete reaction, improved handling properties, lower polymerization exotherm (63°C), bioactivity of the combeite glass-ceramic to induce the growth of hydroxyapatite on the cement surface, and a bone-cement interface that strengthens over time [112, 174]. In rabbit and sheep models, Erbe *et al.* observed mild to moderate inflammatory response by the host to Cortoss, with evidence of foreign-body reaction and fibrosis over an observation period of 4 to 52 weeks [38]. However, the evidence of direct bone apposition to Cortoss at 24 weeks in rabbits and 52 weeks in sheep (*e.g.* Figure 10) led Erbe *et al.* to state that Cortoss cement

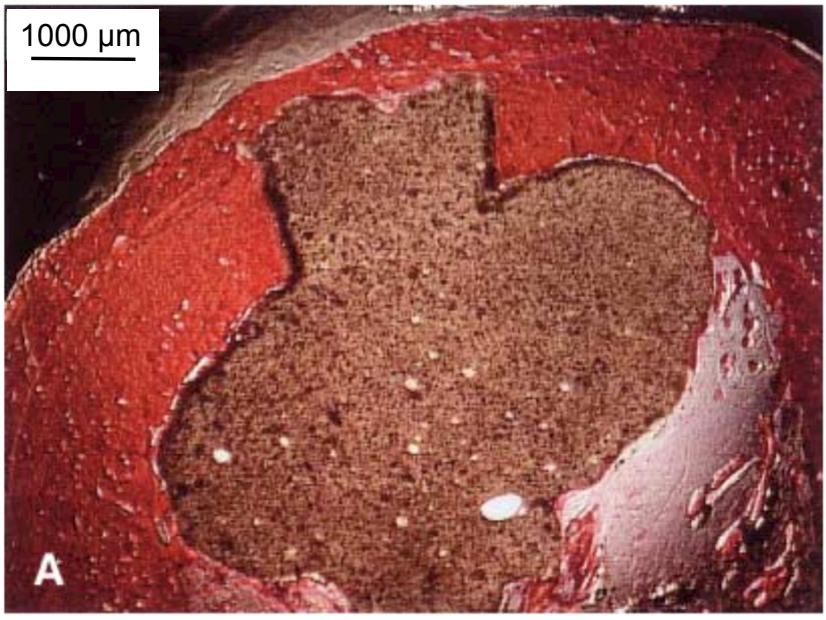

Figure 10: Histological image of Cortoss in rabbit specimen with evidence of direct cement - bone contact at 4 weeks (adapted from Erbe *et al.* 2001[38]).

is more biocompatible than PMMA [38]. Further, Erbe *et al*. found this direct bone contact made Cortoss 4.5 to 100 times more adhesive to bone than PMMA [38]. In humans, prospective, non-controlled clinical investigations have shown Cortoss to be a safe and effective implant material for use during PVP or KP [175-177]. Most recently in 2012, Bae *et al.* published findings of a prospective, randomized, controlled trial that concluded Cortoss is as effective as PMMA in providing pain relief to patients subsequent to PVP [178].

However, despite this clinical success, poor handling characteristics have prevented the wide spread adoption of Cortoss by the PVP and KP communities. Specifically, Cortoss is provided in a mix-on-demand system. Once expelled, it sets hard within 5 minutes in ambient air, and within 2-4 minutes at body temperature of 37 ˚C [38, 179]. This quick setting nature hinders the injectability of Cortoss, as proficient users recommend 5-10 minutes of injection time as a minimum to perform PVP procedures [31, 32]. In an attempt to circumvent this short-coming, the manufacturer (Stryker Orthobiologics) recommends that vertebral body augmentation with Cortoss to be completed using multiple ≤1 cc injections, each within a 1.5 minute window [179]. However, clinicians prefer to have more time to ensure precise control of cement during injection, with some clinical experts desiring the cement to be injectable for 15 to 30 minutes [157]. Furthermore, the hydrophilic nature of Cortoss has been associated with an elevated risk of cement extravasation [180], the setting temperature (63 ˚C) is sufficient to cause thermal necrosis of bone [32], and the cement's chemistry contains allergenic agents [181]; these factors, in addition to the sub-optimal handling characteristics, may explain in the limited adoption and success of Cortoss [182].

3.3.3 Ceramics

There are two types of ceramic bone substitutes, calcium phosphate cements (CPCs) and calcium sulfates cements (CSCs). First developed by Brown and Chow in 1983, CPCs can be molded into specific bone cavities and are currently used as bone graft substitutes to aid in the healing process of bone defects due to disease or trauma [183, 184]. CPCs consist of a liquid and a powder, which when mixed together undergo a dissolution and re-precipitation process [185]. This is a slow exothermic reaction, which keeps setting temperatures low and yields an entangled network of crystals that hardens over time as the network becomes denser due to crystals growth [185]. This produces a calcium deficient hydroxyapatite with similarities to the mineral phase of natural bone [163]. Depending on material composition and the nature of the hydration product, which is dictated by the pH of the cement paste, CPCs are classified as either apatites or brushites [44, 112]. Apatites comprise alpha-tricalcium phosphate powder that is combined with water, while brushites involve an acid-base reaction with a beta tricalcium phosphate powder [163]. At physiological pH, brushite cements are one to two orders of magnitude more soluble than apatite cements which, along with low mechanical strength and poor handling characteristics, limits their clinical utility [44].

Apatite CPCs show potential for PVP and KP applications because of their inherent resorption, allowing for bone integration and remodeling at the implant site, as well as displaying excellent biocompatibility [156]. However, three critical issues exist which impede the use of CPC in vertebral augmentation procedures. Firstly, CPCs have poor injectabilty due to the fact the cements undergo separation of their liquid and solid phases when injected [41]. Secondly, it has been shown that CPCs have poor cohesion,

disintegrating into small particles on contact with blood or biological fluids, which can induce an inflammatory response [42, 185]. Lastly, CPCs generally have poor mechanical properties (*e.g.* strength, toughness) that limit their clinical applications [44, 185]. In 2009, Schmelzer-Schmied *et al.* published a non-randomized prospective trial that found CPCs to be effective in KP (where lower injection pressures are required [186]), providing immediate pain relief for patients with trauma-induced VBFs and allowing for significantly better outcomes for up to 6 months compared bracing and analgesic therapies [187]. However, Schmelzer-Schmied *et al.* caution that the difficult injectability of CPC requires considerable training to ensure successfully applications. Additionally, they expressed caution regarding the use of CPCs in the treatment of unstable A3 VBFs (*i.e.* incomplete burst fractures [188]) due to the insufficient strength of the materials. Blattert *et al.* also published a randomized trial in 2009 that compared the efficacy of CPCs to PMMA in KP to treat A1 VBFs (wedge or impact fracture [188]) and A3 VBFs [189]. Blattert *et al.* found KP with CPC led to statistically improved pain relief of A1 VBFs at 1 year. Despite this success, all patients with A3 VBFs treated with CPC reported the same level of pain at 1 year, which Blattert *et al.* attributed to the inability of CPC to resist the flexural, tension, and shear forces applied in the vertebral body [189]. Further, in one patient, the CPC implant was observed to disintegrate prior to setting due to the profuse intraoperative hemorrhage form the vertebral cancellous bone. These results led Blattert *et al.* to recommend against the use of CPCs in KP procedures [189].

Calcium sulfate cements (CSCs) were first proposed as a biomaterial in the late 19th century, and have been successfully used as bone void filler for more than 100 years [112, 190]. Surgical grade CSCs are calcium sulfate hemihydrate mixed with water to

become calcium sulfate dihydrate [191]. Clinically, CSCs are used for bone defects, drug delivery, endodontic surgery, and sinus augmentation [191]. Calcium sulfate cements are of interest as injectable bone cement because they are biocompatible materials that provoke minimal inflammatory response in surrounding tissue, encourage angiogenesis and osteogenesis. As well they are resorpable *in vivo*, allowing the cement to be replaced by new bone over time [112]. However, in PVP/KP applications, the quick rate of resorption of CSCs raises concerns regarding their ability to provide sufficient stabilization to the fracture for the 6-8 weeks required for the fracture to heal [156, 192]. Alternatively, Cerament (Bonesupport**,** Sweden) is a bi-phasic material comprising calcium sulphate (60%) mixed with hydroxyapatite (40%) and a contrast agent (iohexel/iodine solution) to form an injectable paste indicated for use in PVP [193, 194]. This material has been evaluated as PVP cement in prospective, non-randomized trials and has been approved for use in Europe. The clinical literature has found it to be effective in providing pain relief to patients suffering from A1 vertebral compression fractures up to 1 year [192, 194, 195]. The hydroxyapatite phase is intended to slow the resorption rate of the calcium sulphate and add strength to the cement matrix [195]. This material is designed to balance its resorption rate to the rate of bone remodeling [193]. However, early remodeling (as soon as 1 month post implantation) is still a concern, which combined with their weak mechanical properties (compression strength *c.* 10-30 MPa) inhibits its use in unstable VBFs (*e.g.* A2 split fractures or A3 burst fractures) [192, 194, 196].

Chapter 4: Glass Ionomer Cements

Despite the beneficial attributes, and the clinical success, of the four types of cements described in Chapter 3, their deficiencies impel further advancement of new materials towards the ideal bone cement for vertebral body augmentation to optimize outcomes for patient suffering from VBFs. A class of dental cements know as glass ionomer cements (GICs), or glass polyalkenoate cements (GPCs), possesses qualities that are consistent with the majority of those described as ideal for vertebral body augmentation [32]. Specifically, GICs demonstrate: (i) excellent biocompatibility owing to their adhesive nature, low setting temperatures, and potential bioactivity *via in situ* ion release; (ii) mechanical properties suitable for withstanding loading scenarios within the spine; and (iii) inherent radiopacity, an obligatory requirement for these minimally invasive procedures conducted under fluoroscopy. Additionally, intrinsic benefits of GICs include their abilities to chemically adhere to calcium in the hydroxyapatite phase of bone, whilst exhibiting negligible shrinkage. However, in order to adapt GICs for suitable use in vertebral body augmentation, a fundamental limitation must be overcome; aluminum must be removed from their glass chemistry, due to safety concerns [46, 47], whilst appropriately balancing their handling and mechanical properties.

Wilson and Kent invented GICs in 1969 in response to clinical dissatisfaction with dental silicate cements [197]. GICs made their clinical debut in 1975 [45, 198], and today, GICs are a versatile material that is used throughout dentistry in luting, lining, and restorative applications [199-201]. GICs are multi-component systems consisting of an acid degradable glass powder mixed with an aqueous solution of polyalkenoic acid. When mixed together, an acid-base setting reaction takes place that produces a cement

consisting of residual glass particles embedded within a polysalt matrix, which can also be considered as a particulate-filled polymer composite [202].

4.1 Ionomer Glasses

4.1.1 Structural Theories of Glass Formation

In the most basic sense, a glass is an amorphous solid exhibiting glass transformation behavior [203]. Although there are multiple glassy materials that fit this description, the most common are inorganic oxide glasse. It is these oxide glasses that are used in GICs systems, particularly aluminosilicate glasses. Zarcharaiasen was the first to describe the atomic structure of oxide glasses, hypothesizing they form an extended three-dimensional interconnected network that lacks symmetry and periodicity [204]. This network comprise of cation species known as network formers, randomly linked together by oxygen anions. These oxygen atoms perform two distinct roles in the network: (i) as bridging oxygen (BO) linking two adjacent network formers together, and (ii) as non-bridging oxygen (NBO) that terminate the polyhedral network and do not link adjacent structural units [205]. Depolymerization of the network occurs when a modifying oxide is included in the melt compositions, which changes the oxygen content within the glass, and results in scission of the of a covalent A–O–A bond to produce an ionic bond $A–O^{-}$ M^{z+} $^{-}O–A$, where A is termed a network former and the M^{z+} cation is termed a network modifier. Additionally, these network disruptions impart basic character to the glass, with the NBO sites susceptible to acid attack [198].

There are several ways to classify network forming and network modifying species. Sun suggested that the process of forming glass involves the inability to rearrange bonds in the liquid state during crystallization. As such, a good network former

has a higher bond strength, calculated as the energy required to dissociate a single A–O bond [206]. According to Sun's calculations, a glass former has high single bond strengths, exceeding 80 kcal mol^{-1}. The most common network forming species is silicon (Si), which has a single bond strength of 106 kcal/mol and forms SiO_4 tetrahedral structural units [203]. Oxides species with a single bond strength less than 60 kcal/mol are deemed to be glass modifiers. Typical network modifiers include sodium (Na) and calcium (Ca), which have single bond strengths of 20 kcal/mol and 32 kcal mol^{-1} respectively [203]. Based on Sun's model, metal oxides that have single bond strengths between 60 and 80 kcal mol^{-1} are termed intermediates. Depending on the chemical environment of the glass composition, intermediates will change their coordination state to act as either a network former or modifier. Aluminum (Al), with a single bond strength of 53-67 kcal mol^{-1}, is an example of an intermediate used in the glass chemistry of dental GICs. Alternatively, Dietzel classified vitreous elements into the same three categories, but did so according to field strength (F_S) of the cation in relation to oxygen ion (Eq. 1), where Z_c is the valency of the cation and a is the distance in Å between the cation and oxygen anion [207].

$$F_S = Z_c/a^2 \qquad \textbf{(Equation 1)}$$

According to Dietzel, forming cations have a high field strength (*c.* 1.3 – 2 $Å^{-2}$); modifying cations have a lower field strength (*c.* 0.1 – 0.4 $Å^{-2}$); and intermediates have field strengths between *c.* 0.5 –1.0 $Å^{-2}$. In this model, Si is again a former with a field

strength of 1.57 $Å^{-2}$, Na is a modifier (0.19 $Å^{-2}$) and Al is again an intermediate (0.87 – 0.96 $Å^{-2}$, depending on its coordination state) [203].

The structural units that build the glass network, such as SiO_4 tetrahedra, are made up of central network forming cations bonded with multiple oxygen atoms. Q^n speciation refers to the number of BO (n) bonded to the central former 'Q', where n ranges from 0 to 4. An entirely linked network, consisting of only BO will have a Q^4 speciation. In a GIC system, a Q^4 glass will be impervious to acid attack, as there are no NBO. However, as modifying species are added to the glass composition, the network will depolymerize, lowering the value of n until it is fully disrupted with a Q^0 speciation, representing a network with only NBO [208]. As the modifier contents in ionomer glasses increases, there is a proportional increase in their reactivity as more NBO are formed [209, 210]. In fact, an influential structural parameter of glass properties is the ratio of BO to NBO oxygen atoms bonded to each network former. The network connectivity (N_C) is a numerical average representation of the ratio of BO to NBO determined using equation 2 [211].

$$N_c = \frac{No.\ BO - No.\ NBO}{Total\ No.\ of\ Bridging\ Species} \qquad \textbf{(Equation 2)}$$

Boyd *et al.* have used N_C to support their findings regarding the structural changes in the glass network and their impact on the setting characteristics of GICs. They observed that increasing the modifier content of SiO_2-CaO-ZnO glasses, resulted in a more disrupted glass network with lower N_C. These more reactive glasses produced stronger GICs with shorter working and setting times [212].

4.1.2 Glass Chemistry of Aluminosilicate GICs

The ion leachable glass powders used in conventional GICs for dental applications are based on aluminosilicate chemistries. There exist a multitude of compositions, broadly separated into two categories; those that contain fluorine, and those that do not. Their basic compositions are SiO_2–Al_2O_3–CaO, and SiO_2–Al_2O_3–CaF_2 [45]. Other compositional constituents have included are: Na_2O, NaF, Na_3AlF_6, P_2O_5, $AlPO_4$ [45, 213]. In contemporary GICs compositional changes to the glass typically involve changes to the modifier content, such as the replacement of CaO with alternative modifiers or intermediates, including SrO, LaO, BaO, and or ZnO to enhance radiopacity for increased diagnostics sensitivity [214, 215].

In the aluminosilicate glasses of conventional GICs, the primary network forming species is silica (SiO_2), which forms tetrahedral structures of SiO_4. Aluminum has a substantial influence on the properties of GICs, behavior that is due in part to the structural role Al takes in aluminosilicate glasses. As an intermediate, Al has the ability to take either a forming or modifying role; which role depends on the Al_2O_3/MO ratio, where MO represents a modifying oxide [216]. The ability of Al to adopt a four-fold coordination, *i.e.* Al(IV), is closely related to the total amount of alkali and alkaline earth oxide in the glass. For Al^{3+} to become Al(IV), two things are required. Firstly, Al_2O_3 only brings 1.5 oxygen per Al^{3+}, but requires 2 oxygen per Al^{3+} to be a network former. This extra oxygen is provided by modifiers such as Na_2O or CaO. Secondly, Al(IV) have a tetrahedral structure of $[AlO_4]^-$ which has a net negative charge due to the formal charge of 3+ on Al but the 4- charge provided by coordinated oxygen. This negative charge requires compensation to ensure electroneutrality within the glass network. This charge

compensation is provided by modifying cations (*e.g.* Na^{+}) that have already donated their oxygen to $[AlO_4]^{-}$ [208]. However, in conventional aluminosilicate GICs, CaO is the typical modifying species and one Ca^{2+} charge compensates two $[AlO_4]^{-}$ tetrahedra. In situations where Ca:Al ≥ 1:2, all Al^{3+} is Al(IV) [45]. According to Loewenstein's rules, Al^{3+} is forced to take up a four-fold coordination [217] and considering aluminum ions have similar ionic radii as Si^{4+}, this allows Al(IV) tetrahedron to replace SiO_4 tetrahedron within the glass network [218]. Loewenstein's rules restrict the formation of glass with two Al(IV) structure linked *via* a central BO; therefore Al(IV) structures have to be surrounded by other network forming structures such as SiO_4 or PO_4 [208]. Whenever two Al^{3+} are neighbors to the same oxygen, then one of them must adopt a higher coordination, such as five- or six-fold structures, *i.e.* $[AlO_5]^{-}$ or $[AlO_6]^{-}$. The Si:Al ratio plays an important role in dictating the structure of the Al^{3+} in the glass phase. For Si:Al above 1:1, all Al^{3+} will be Al(IV), but if the ratio falls below unity, then Al^{3+} is no longer forced to adopt a tetrahedral structure, taking an octahedral structure [198]. Similarly, if Ca:Al < 1:2, Al^{3+} is not forced to take Al(IV) structure. Octahedral aluminum structures, Al(VI), are presumed to have 3 BO and 3 NBO [203].

Aside from changes in the modifier or intermediate content of the glass, other compositional modifications to the glass include the addition of fluoride and/or phosphorous. The introduction of F^{-}, typically by CaF_2, Na_3AlF_6, or AlF_3, is done for a variety of reasons. In the applications of GICs, fluoride release is beneficial for its anticariogenic effect [219]. In the glass, fluoride is very influential on network structure. Probing the structure of SiO_2-Al_2O_3-P_2O_5-CaO-CaF_2 glasses with magic angle spinning nuclear magnetic resonance spectroscopy (MAS-NMR) revealed that as F content

increases, aluminum shifts to more of a modifying role instead of a forming role as evidenced by an increase of Al(V) and Al(VI) structures [220]. Additionally, incorporating F results in more Si-O-Si bonds, fewer Si-O-Al bonds, and more Al-O-P linkages [220]. There is also evidence that fluoride forms Ca–F bonds, reducing the potential for Ca^{2+} to form NBO; or Al–F–Ca bonds, which may be a part of aluminum structural units [221]. However, as part of structural units, fluorine will replace BO with non-bridging fluorines, disrupting the network and lowering the glass transition temperature [222]. Along with fluorine, phosphorus is used to modify the setting characteristics of the GIC [199]. Phosphorus is a network former, and can typically take a tetrahedral structure [PO_4], where one oxygen atom is double bonded and thus nonbridging to satisfy the formal +5 charge on the P^{5+} ion. In the presence of $[AlO_4]^-$ the net positive charge of PO_4 tetrahedra can be used to balance the negative charge of the Al(IV) structures [223].

4.2 Polyalkenoic Acid

The acid component of a GICs is a polyelectrolyte that dissociates into polyanion chains and counterions when mixed into an aqueous solution [45]. The development and properties of various polyalkenoic acids used in GICs have been described in detail elsewhere [45, 224, 225]. This thesis focuses specifically on manipulation of the glass component of GICs. However, a general discussion is included below for readers to appreciate the role of polyalkenoic acid in GIC systems.

In the first iterations of GICs, a 50 % aqueous solution of polyacrylic acid (PAA) was used. However, the high viscosity of these PAA solutions made mixing of the GIC difficult and led to poor handling characteristics and unstable cements, which converted

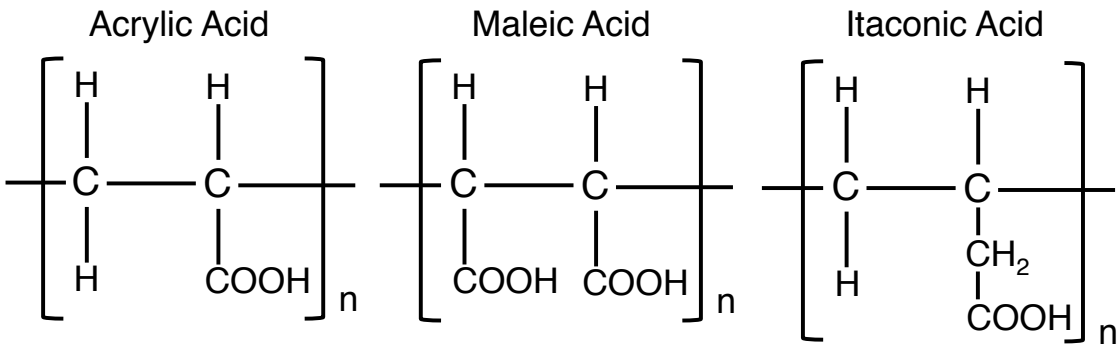

Figure 11: Polyalkenoic acid units used in typical GIC formulations, adapted from Smith 1998 [213] and Lohbauer 2010 [226].

into a gel form after only a few months because of the presence of inter-molecular hydrogen bonds [199, 224]. The issue of gelation was rectified by the use of copolymers of acrylic–itaconic acids instead of homopolymers of only acrylic acid [213]. Copolymers of acrylic-maleic acids and acrylic–3-butene-1,2,3-tricarboxylic acids are also commonly used (Figure 11). The number of functional carboxyl (COOH) groups varies amongst these acid types, resulting in different functionality and acid strength [227]. The strength of the GIC will increase as the number of functional COOH groups per chain increase; however, this may lead to the potential embrittlement of the matrix over time which can reduce the strength and toughness of the cements [228]. Today the most common polyacid components of GICs are either homopolymers of PAA, *c.* 45 wt% (either in liquid form or as a dry powder blended with water during GIC mixing), or co-polymers of acrylic-maleic acid, although dry PAA powders blended with glass and activated by water are also used [198, 229]. The mechanical performance of GICs and their handling properties can be influenced by the concentration, molecular weight, and polydispersity of the acid, as well as the ratio at which the acid and glass are mixed [230-235]. Generally, as the molecular weight and acid concentration increases, there is a

corresponding increase in mechanical properties and a decrease in setting time. However, past a certain molar mass and or acid concentration, there is a reverse in these trends associated with some combination of: i) impaired mixing of cement due to more viscous PAA solutions, ii) greater amount of time required for PAA particles to dissolve and cations to migrate from the glass, and iii) increased polydispersity inherent to higher molecular weight PAA [215, 236-238].

Finally, an attribute that is critical to the clinical success of GICs is their ability to chemically adhere to both bone and stainless steel [239]. This adhesive character arises from the carboxylate groups (COO^-) of the polyalkenoic acid which form either polar or ionic chemical bonds with reactive polar substrates [239]. With regards to bone, the adhesive chemical bonds are formed by COO^- displacing PO_4^{3-} and Ca^{2+} from the hydroxyapatite ($Ca_5(PO_4)_3(OH)$) phase at the surface of bone (Figure 12). These ionic

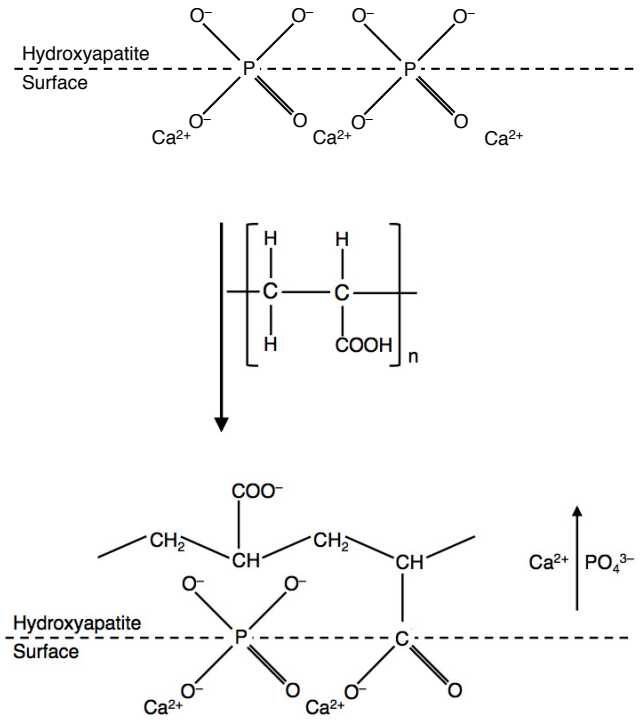

Figure 12: The adsorption of polyacrylate on hydroxyapatite, adapated from Wilson *et al.* 1983 [240].

species are released together, which results in a net positive charge of 1+ on the hydroxyapatite substrate. This 1+ charge is neutralized by the 1– charge of a COO^- group of the polyalkenoic acid to maintain electroneutrality [240].

4.3 GIC Failure Theory

Conventional alumniosilicate GICs demonstrate compressive strengths up to 300 MPa and flexural strengths in excess of 50 MPa [226]. Experimental results indicate that failure of GICs occurs due to crack propagation through the polysalt matrix of the cement (GIC structure is discussed in detail in sections 4.4 4.5) [241]. Further, the concentration and molar mass of the polyacrylic acid have been found to be the most important parameters determining the mechanical properties of GICs [228, 232, 237, 241, 242]. Hill *et al.* investigated the viscoelastic behaviors of GICs using dynamic mechanical thermal analysis [237]. This analysis revealed a sharp loss peak, behavior that is typical of thermoplastics. Thus, Hill *et al.* proposed the use of the reptation model, the theory that governs the failure of thermoplastic polymers, to explain the mechanisms control the mechanical behavior of GICs [237].

4.3.1 Reptation Model

The strength of glassy polymers is based upon the long-range entanglement of neighboring chains, which restricts their relative motion [243]. Additionally, chain mobility can be restricted further due to interactions between subtitutents (*e.g.* PAA carboxylate groups) of adjacent chains [241]. These entanglements can be viewed to form hypothetical tubes (Figure 13a), with the fracture surface energy, or the toughness of the material coming from the energy required to extricate the chains from these tubes. The

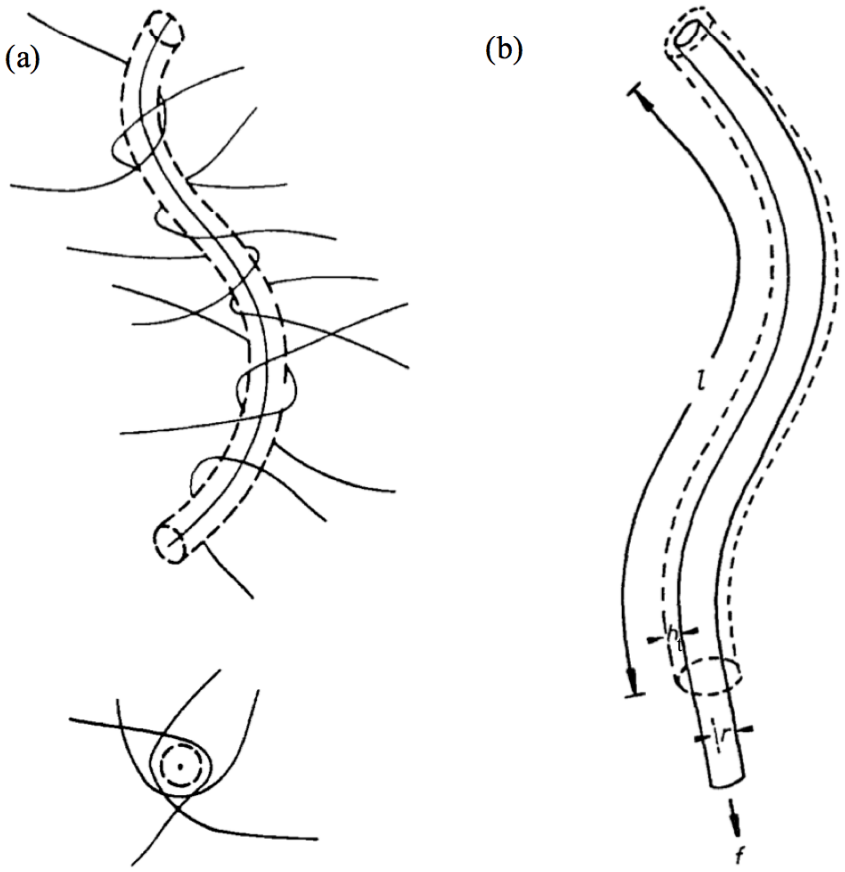

Figure 13: Schematics of reptation theory, (A) polymer chain trapped in a tube of entanglements and (B) mechanism of chain removal, adapted from Prentice 1985 [243].

reptation model provides a mathematical justification for the 'snake-like' motion of polymer chains as they are pulled out of these tubes. Analysis of this theory was originally conducted by Prentice [243], and applied to the GIC system by Hill *et al.* to explain the failure theory of GICs [237]. The following summary of the reptation model is based on work by Hill [237, 241].

Using a power-law viscous model, schematically depicted in Figure 13b, the shear stress (τ) experienced by the chain in will be proportional to the apparent strain rate (γ).

$$\tau = \mu(\gamma)^n \qquad \textbf{Equation 3}$$

where μ is the coefficient of viscosity resulting from the interactions of the substituents on neighboring chains and *n* is the power law index. However, the shear stress is also proportional to the applied force *(f)* over the effective surface area of the chain (*a*):

$$\tau = \frac{f}{a} \qquad \textbf{Equation 4}$$

where *a* is:

$$a = 2\pi r l \qquad \textbf{Equation 5}$$

and *r* is the radius of the polymer chain and *l* is the contour length of tube in which the chain is contained. The apparent strain rate can be defined as per equation 6, where v is the rate of removal of the chain and h_t is the spatial gap between the surface of the chain and the hypothetical tube.

$$\gamma = \frac{\mathrm{v}}{h_t} \qquad \textbf{Equation 6}$$

Combining equations 3-6 gives:

$$f = 2\pi r \mu \left(\frac{\mathrm{v}}{h_t}\right)^n l \qquad \textbf{Equation 7}$$

which states that at a constant v, the force acting on the chain in the tube direction is proportional to the length of the tube remaining occupied. The energy required to extract the chain then becomes:

$$\tau = \int_{l=0}^{l=L} f \, dl \qquad \textbf{Equation 8}$$

where L is the total length of the tube. Substituting equation 7 into equation 8 gives:

$$\tau = \int_{l=0}^{l=L} 2\pi r\mu \left(\frac{\mathrm{v}}{h_t}\right)^n l \, dl \qquad \textbf{Equation 9}$$

which, at a constant v becomes:

$$\tau = \pi r\mu \left(\frac{\mathrm{v}}{h_t}\right)^n L^2 \qquad \textbf{Equation 10}$$

Considering the total number of segments, m, that cross a unit area of the fracture plane, the work done per unit area will be:

$$\tau = \tau_0 m \qquad \textbf{Equation 11}$$

It is assumed that each chain will only cross the fracture plane once, which is likely an oversimplification of the actual material structure but streamlines this analysis. Combining equations 10 and 11 yields:

$$\tau = \pi r\mu m \left(\frac{\mathrm{v}}{h_t}\right)^n L^2 \qquad \textbf{Equation 12}$$

The chain length (L) of a polymer is proportional to its molar mass. Therefore, when the crack opening velocity, v, is constant, the work done in extracting a chain from a unit area of the crack plane is proportional to the square of the molar mass (M) of the polymer (equation 13).

$$\tau \propto M^2 \qquad \textbf{Equation 13}$$

This analysis reveals that two distinct failure modes exist for glassy polymers: (i) chain pullout, or (ii) chain scission. From equation 7, it is noted that the force *(f)* to extract a chain from its tube is proportional to its length (*l*). The transition between these two failure modes occurs at a critical chain length (l_c), when the extraction force exceeds the force required to break the carbon-carbon backbone of the polymer. Prentice experimentally observed the critical chain length in PMMA (Figure 14), where a shoulder

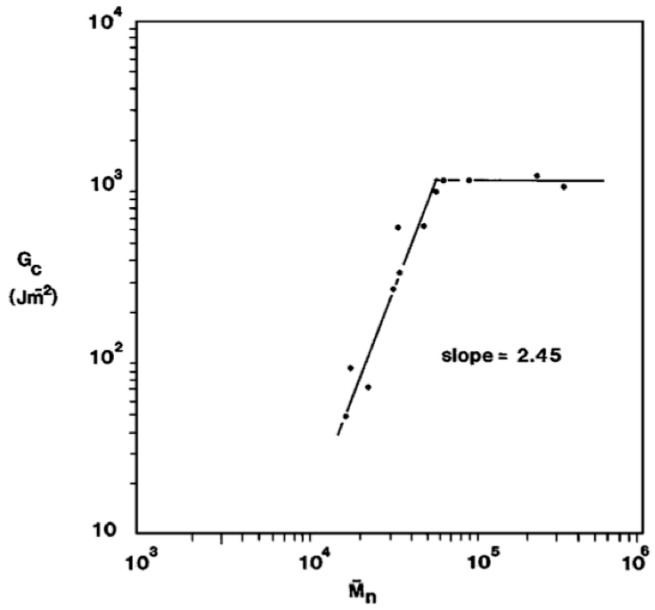

Figure 14: Toughness (G_C) *vs.* average molecular weight (M_n) of PMMA. The plot depicts the transition from chain pullout to chain scission failure at *c.* 10^5 g mol^{-1}, from Prentice 1985 [243].

is clearly visible at molar mass of *c.* 10^5 g mol^{-1}, above which no further improvement in toughness is achieved. Below l_c, chain pullout is the predominant failure mechanism.

Equation 13 can be adjusted slightly. Prentice found that below a certain molar mass, the chain length was too short to produce entanglements with one another. This is believed to occur in chains consisting of 100 to 300 mer units [237]. For PAA, its mer unit ($CH_2CHCOOH$) has a molar mass of 72 g mol^{-1}. Therefore, the minimum molar mass of PAA to produce entanglements (M_e) is between 7200 to 21600 g mol^{-1} [235, 237], although more recently M_e has been argued to be as low as 5000 g mol^{-1} [244]. Therefore equation 13 becomes:

$$\tau \propto (M - M_e)^2 \qquad \textbf{Equation 14}$$

There are two key limitation of the reptation model when applied to GIC systems. Firstly, the reptation model does not consider crosslinking bonds between substituents (*i.e.* metal-carboxylates within the GIC matrix) [232]. The compressive and flexural strengths of GICs have been observed to both increase [245, 246] and decrease [246, 247] over time. These changes are commonly attributed to an increased crosslink density of the GIC matrix due to the ongoing acid-base setting reaction [232]. The greater crosslink density increases the force required to pullout the polyacrlic chains, thus increasing the strength of the cement. However, Hill introduced the concept of 'over-crosslinking', where excessive crosslinking within the GIC matrix decreases the toughness of the cement and reduces the crack tip opening displacement, resulting in fewer polymer chains crossing the fracture plane and thereby decreasing the materials strength [228].

This concept was expanded by de Barra and Hill, who argue that increased crosslinking reduces the amount of molecular motion and plasticity at the crack tip, which results in fewer polyacrylic chains undergoing pullout [232]. Essentially, increasing the crosslink density within the GIC matrix effectively lowers the critical threshold of PAA molar mass that dictates whether the dominant failure mechanism of the cement is chain pullout or chain scission. This critical molar mass is *c.* 80,000 to 100,000 g mol^{-1} [237, 244].

Secondly, the reptation theory assumes all chains in the matrix have the same length, *i.e.* a monodisperse polymer. In reality, the PAA used in GICs has a polydisperisty that ranges over several orders of magnitude [235]. Both Hill *et al.* [237] and later Griffin and Hill [241] found that their experimental data did not fit the reptation model. Specifically they observed that toughness increased with PAA molar mass, but it did not keep pace with the toughness predicted by the reptation model. One explanation given was that the polydispersity of high molar mass PAA means a fraction of the polyacid chains exceed the l_c, and thus add to the viscosity of the cement paste but do not contribution towards the mechanical properties of the set material [237, 241]. Fennell and Hill also noted discrepancies between observed and predicted mechanical properties of GIC comprising low molar mass PAA (*c.* 9000 - 25000 g mol^{-1}), which they attributed to the polydispersity of these PAA compositions to contain a significant proportion of polymer chains below the M_e, the minimum molar mass to produce entanglements [235]. Despite these criticisms, the reptation model remains the most suitable model for analyzing the fracture behavior of GICs that is capable of making quantitative predictions [241].

In dental applications, the primary mechanical limitations of GICs are their low fracture strengths, brittle nature, and poor resistance to wear [226, 227, 248]. Wilson *et al.* found wear resistance to be proportional to fracture toughness [242]. Current commercially available restorative grade GICs have fracture toughness values in the range of 0.3-0.55 MPa $m^{1/2}$ [249-251], compared to that of dentin which is 2.4 MPa $m^{1/2}$ [232]. The most effective way to improve the toughness properties of GIC is to increase the molar mass of PAA [235]. However, this negatively impacts the handling characteristics of the cement. Therefore, it is necessary to tailor the PAA molar mass, concentration, and powder to liquid ratio to ensure the handling characteristics of the cement remain practical in the presence of maximized mechanical properties [233-235].

4.4 GIC Setting Reaction

The cement matrix of GIC is the product of acid-base neutralization between the liquid polyelectrolyte acid and the basic glass powder (Figure 15) [198]. Wilson describes the general process taking place in a number of overlapping stages [45]. The decomposition

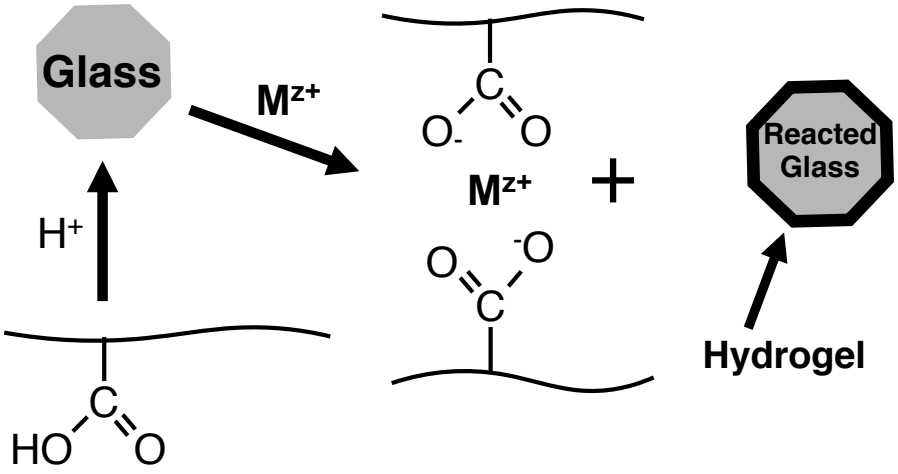

Figure 15: Schematic of GIC setting reaction, protons attack the glass particles to release metal cations (M^{z+}), which then react with available COO^- groups and crosslink the polyanion chains, while reacted glass particles develop a hydrogel layer. Adapted from Griffin and Hill, 1999 [252].

of the powder is initiated by the mixing of the aluminosilicate glass and PAA liquid. The acid degrades the glass by ion exchange with hydrogen protons from the polyacid, releasing metallic cations (*e.g.* Al^{3+}, Ca^{2+}, Zn^{2+}) and silicic acid ($Si(OH)_4$); subsequently, the silicic acid condenses to form a silica gel around residual glass particles. The increase in concentration of cations, and potential positively charged complexes increases the pH of the aqueous phase. This causes the polyacid to ionize to a greater extent, thereby increasing its electromotive force, aiding migration of the liberated cations into the aqueous solution. As the polyacid ionizes, the polymer chains experience electrostatic repulsion between negatively charged carboxylate groups, causing the chains to unravel and expand, which increases the viscosity of the cement. Cation concentration increases until they condense on the polyacid chains. Desolvation occurs and insoluble salts precipitate, first as a sol, which then converts to a gel. This gelation represents the initial set of the GIC. After gelation, the cement continues to harden as more crosslinking salts are formed within the cement matrix. The microstructure of the final cement consists of reacted glass particles embedded in a polysalt matrix, sheathed in a siliceous hydrogel layer (Figure 16) [45, 252].

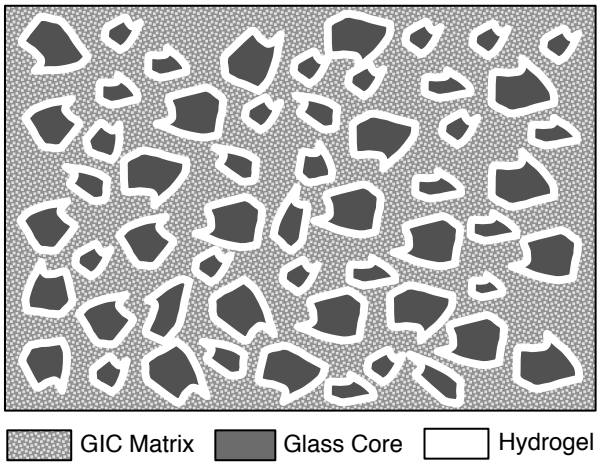

Figure 16: Schematic representation of set GIC microstructure, adapted from Wilson and Nicholson 1993 [45].

The structure of the glass plays an important role in the GIC setting reaction. A glass comprising only *vitreous* SiO_2 contains only BO, and thus is impervious to acid attack [198]. The introduction of modifying oxides such as CaO or SrO depolymerizes the glass network through the creation of NBO; it is these NBO which serve as sites of acid attack, releasing the corresponding M^{z+} cations (*e.g.* Ca^{2+}, Sr^{2+}). A second molecular structure susceptible to acid attack involves intermediate oxides (*e.g.* Al_2O_3) acting in a forming capacity. An example of this is Al in a four-fold coordination state, *i.e.* $[AlO_4]^-$. The negative charge of the $[AlO_4]^-$ structure is compensated by cations such as Ca^{2+}. However, the negative charge and basic nature of the $[AlO_4]^-$ tetrahedra make them susceptible to acid attack [198]. Structural analysis of the GIC setting reactions suggest ions are released from the bulk of the glass particles in addition to their surface, with Billington *et al.* [253] using data generated by Hatton and Brook [254] to determine that total glass degradation is *c*. 10% during GIC setting. The reactivity of the glass is a significant contributor to the GIC setting rate. Wilson used the principals of acidobasicity (*i.e.* the acid-base balance of an oxide material that governs whether it will accept or donate electrons) to assess the cement-forming capabilities of SiO_2-Al_2O_3-CaO glasses [255]. The acidobasicity of these glasses were based on their overall field strengths and ionization potentials, and compared to the setting times of their corresponding GIC. From the results, a strong correlation was noted between glasses with greater durability, *i.e.* lower acidobasicity, and slower setting cements [255].

4.5 Molecular Structures of GICs

The molecular structures of polyelectrolyte cements, including GICs, can be identified through infrared measurements of the asymmetrical stretching modes of carboxylate

groups, which experience a shift in frequency when coordinated with metal cations [45]. Nicholson described common bonding modes of zinc polycarboxylate cements that can be applied to GICs (Figure 17) [45, 256]. These structures are presented in order of increasing covalent-like character: (i) purely ionic, (ii) bridging bidentate, (iii) chelating bidentate, and (iii) asymmetric unidentate [256]. The cationic species that form the polyacrylate crosslinks play an important role in the strength and stability of the cement due to their charge and ionic size [45]. The metal-carboxylate salts comprising Ca^{2+} and Mg^{2+} cations are primarily ionic in nature, thus they are less hydrolytically stable and provide less strength to the matrix [45]. Metal-carboxylate bonds involving Na^{+} are also ionic in nature. However, since Na^{+} is monovalent, it only bonds to one COO^{-} group and does not crosslink PAA chains. For this reason, adding Na_2O to ionomer glasses results in slower setting GICs that have weaker mechanical properties [202]. Alternatively,

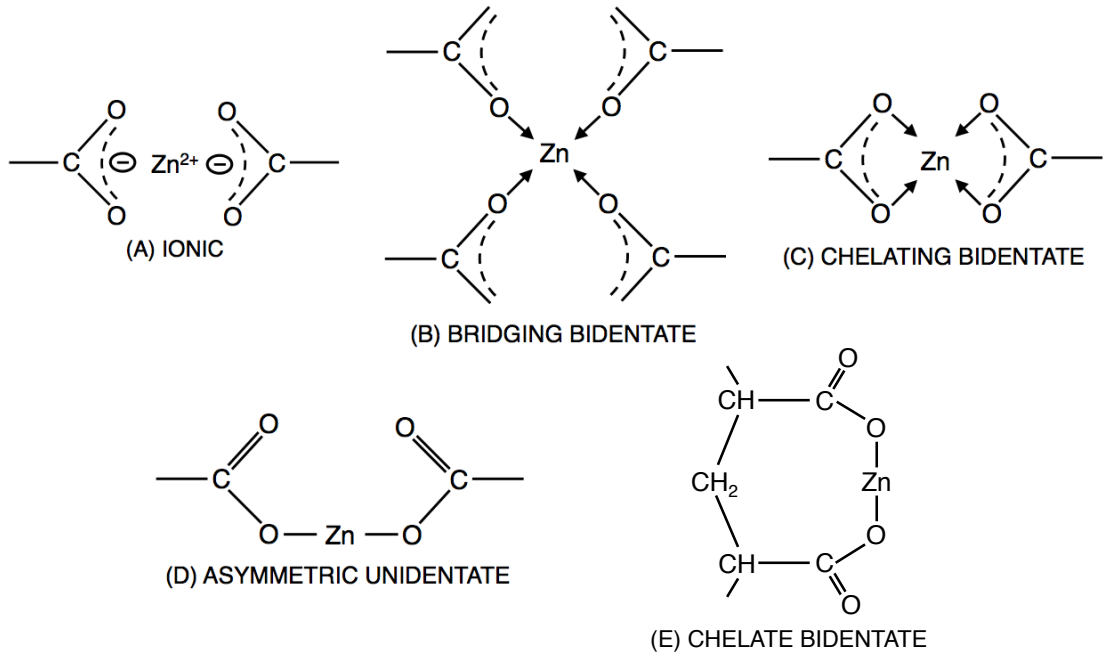

Figure 17: Metal polyacrylate structures - (a) purely ionic, (b) bridging bidentate, (c) chelating bidentate, (d) asymmetric unidentate, (e) chelate bidentate 8-member ring (Nicholson *et al.* 1988 [256]).

Al^{3+} and Zn^{2+} cations show evidence of forming bonds with more covalent-like character [45, 256]. The strength and stability of crosslinking species are influenced by their charge-to-size ratio and parallel the magnitude of the complexation constant, where $Al^{3+} > Cu^{2+} > Zn^{2+} > Ca^{2+} > Mg^{2+}$ [45, 52, 257]. Finally, it should be noted that Al^{3+}, has a formal charge of 3+, compared to the 2+ of the other divalent ions. Theoretically, this allows Al^{3+} ions to bond with 3 carboxylate groups and crosslink up to three polyanion chains, although this is sterically improbable [45]; rather, it has been suggested that Al^{3+} forms complexes with H_2O and or F^- (*e.g.* $[AlF(H_2O)_3]^{2+}$), and it is these complexes that crosslink the polyanion chains [45].

Another influential component on the properties of the GIC is water, and the structural role that it takes within the cement determines what impact it has. In the GIC structure, water can exist in several different states depending on its location within the molecular structure. In the vicinity of the glass network, water hydrates the silica gel layer surrounding reacted glass particles [45]. In the GIC matrix, water exists in one of two states, evaporable or non-evaporable [45]. Evaporable water, also referred to as loosely bound water, forms sheaths around the acrylic chains in the polysalt matrix. This labile water can be lost or gained to the surrounding environment, important for clinical applications is important as water absorption counteracts the shrinkage associated with the setting reaction as the cement hardens [45]; however, absorption of too much water can have a deleterious influence on mechanical properties of the GIC, as it acts as a plasticizer [45, 258]. Alternatively, non-evaporable water is tightly bound within the molecular structure of the cement. Tightly bound water is coordinated to cations that form the metal-carboxylate salts within the matrix. To determine the impact of hydration

on the mechanical properties of dental cements, Wilson *et al.* compared the ratio of non-evaporable to evaporable water and the strengths of dental silicates, zinc polycarboxylate, zinc phosphates, and GICs [258]. Over a 2-week period, the ratio of non-evaporable to evaporable water was observed to increase in all four cements as did the strength and moduli of the cements. However it was noted that with the increases to mechanical properties, the plasticity of the cements decreased. The GIC had the greatest improvement in mechanical properties, a 290 % increase in compressive strength and a 260 % increase in modulus [258]. However, it is likely that the on-going setting reaction also contributed to this increase the increased mechanical properties [232]. It is clear that the structural role of water has considerable impact on the mechanical integrity of the GIC.

4.6 Aluminosilicate GICs as Orthopaedics Bone Cements

Owing to the clinical success of GICs in dentistry, the expanded use of aluminosilicate GICs was explored in other fields, including orthopaedics, ontological, neuro-otological, and skull-based procedures [259, 260]. Jonck was the first to propose the use of GICs in orthopaedic applications, motivated by the clinical need to replace acrylic bone cements (*i.e.* PMMA) in order to improve the long-term success of total joint arthorplasties [259]. Specifically, Jonck cites the intrinsic potential of PMMA to cause thermal and or chemical necrosis of bone, and the effects of leaching residual monomer to the surrounding tissues as major disadvantages that contribute to the pathogenesis which leads to failure of total joint replacements [259]. Furthermore, revision surgeries are complicated by the reduced quality of remaining bone stock, which motivated Jonck to identify alternative bone cements with surface characteristics that enable direct bone

contact and enhanced osseointegration [259]. Aluminosilicate GICs were considered on the bases of: (i) their negligible setting exotherm, (ii) the fact their polymer content is pre-polymerized and contains no monomer component, (iii) their intrinsic ability to leach potentially therapeutic ions, and (iv) their ability of chemically adhere to bone.

Jonck and Grobbelaar began investigating GICs based on SiO_2–Al_2O_3–CaF_2–Na_3AlF_6–$AlPO_4$ glass chemistry mixed with a co-polymer consisting of acrylic and maleic acids (Ionocem, Ionos GmBH & Co., Seefeld, Germany) [259]. Initial biocompatibility studies, reported by Jonck in 1989, examined Ionos GIC implanted in a microporous diffusion chamber on the tibial plateau of baboons. The results demonstrated that within the diffusion chamber, Ionos was biocompatible, non-toxic and did not inhibit cell proliferation [261]. Furthermore, it was noted that the GICs were osteoconductive, exhibiting no inhibitory effect on bone tissue development, and appeared to promote osteoblastic activity. Normal differentiation of haemopoetic tissue on the surface of the cement was also observed [259, 262, 263].

The positive result in the baboon model led Jonck and Grobbelar to evaluate Ionos GIC as a cementing agent in hip arthroplasties in a limited human clinical study [263]. Between 1984 and 1987, 33 patients received primary (n=11) or revision (n=22) total hip arthroplasties cemented with Ionos GIC. The use of Ionos was justified on the basis that all patients required surgery, but were contraindicated for PMMA on the basis of poor bone stock or, thinning out of compact bone, the presence of granuloma and the possibility of acrylic hypersensitivity. However, the arthroplasties were only successful in 65 % of patients, as the remaining patient experienced significant implant migration, which led to failure in 35 % of arthroplasties within 2.5 to 5 years of implantation [263].

The low success rate was seen as a clinical failure of Ionos bone cement, as by comparison, PMMA cemented total hip replacements have a survivorship of *c.* 80 % after 25 years [264]. Jonck attributed the low success rate to inappropriate cement handling technique during the surgery or insufficient mechanical properties of the cement [259]. However, the design of Jonck's study, which used patients with pre-existing poor bone quality, likely introduced bias into the evaluation and may have obscured the meaningful assessment of aluminosilicate GICs in orthopaedic applications.

Concurrent to the aforementioned investigations, Ionos bone cement was also being clinically evaluated in otological, neuro-otological, and skull-based procedures. In 1990 Geyer and Helms reported the successful use of Ionos GIC in 163 out of 167 patients undergoing middle-ear procedures; cement resection was required in 4 patients due to persistent infections, which were present before the surgeries [265]. In 1992, Babighian reported preliminary data describing the successful use of Ionos GIC in 56 out of 59 patients who underwent middle ear reconstructions [266]. Also in 1992, Ramsden *et al.* used Ionos GIC in 80 cases without incident, and described the cement as an easy-to-use, versatile material that is valuable in the preventing leaks of cerebral spinal fluid subsequent to acoustic neuroma surgeries and other skull based procedures [260]. Two years later, Helms and Geyer successfully used Ionos GIC as a hard tissue substitute in translabyrinthine surgeries to remove acoustic neuroma in 5 patients. They found that Ionos diminished the risk of post-operative meningitis when the surgical defect is closed reliably in a watertight fashion [267]. Kempf *et al.* used Ionos GIC to fix the electrode array of cochlear implants in 244 patients without incidence over a 2 year follows up [268]. In 1997, Geyer and Helms reported 343 ossicular reconstruction surgeries, where

Ionos GIC achieved a 91 % success rate, and only 1 % rejection rate, (manifested as persistent infection) [269]. Additional examples of ossicular reconstruction are provided by Masseen and Zenner in 1998 [270] and Kjeldsen and Grontved in 2000 [271]. Both studies found Ionos GIC to be capable of reconstructing ossicular bones during tympanoplasty type II procedures. This success found Ionos to be less of a risk than alternative ossicular reconstruction techniques [271] and led to the recommendation that Ionos be used in all ossicular reconstructions [269].

4.7 Contraindication of the Use of Aluminosilicate GICs in Orthopaedics

Despite the aforementioned positive achievements of Ionos aluminosilicate GIC described above, this material has been contraindicated outside the field of dentistry due to its aluminum-containing glass chemistry, which has been implicated in impaired bone mineralization and at least three fatal cases of aluminum induced encephalopathy [46, 47]. Dollken made the first mention of the neurotoxic properties of aluminum in 1897 [272]. In 1942, Kopeloff *et al.* demonstrated recurrent epileptic seizures by direct application of aluminum paste to the cortex of monkeys [273]. In humans, the introduction of hemodialysis in 1964 caused an endemic of aluminum-induced encephalopathy [274]. In 1994, four cases of aluminum-induced encephalopathy were reported in the literature, with 2 in France and 2 in Belgium [275, 276]. Renard *et al.* reported the first two cases, involving a 55-year old male and a 72-year old female. Both underwent translabyrinthine otoneurosurgery and bone reconstruction involving Ionos GIC. Within two months of the procedures, both patients presented with subacute coma and epileptic seizures, and their conditions continued to deteriorate. An adverse event

associated with effect to the Ionos GIC was assumed, and measurements of the cerebral spinal fluid found aluminum levels to be 135 μg/L and 185 μg/L for the two patients, where the norm is < 3.5 μg/L [275]. Fortunately, resection of the cement, the use of an external lumbar drainage system, and treatment with desferrioxamine stabilized the conditions of both patients. These events led national authorities in France to ban the use of Ionos GIC in 1994. However, this ban did not deter its use in Belgium, and Hanston *et al.* reported on the death of two patients subsequent to implantation of Ionos GIC [276]. Similar to the French cases, both patients (29-year old man and 54-year old women) underwent translabyrinthine otoneurosurgery with bone reconstruction involving Ionos GIC. Subsequent to the procedures, the neurological condition of both patients deteriorated, and despite the best efforts of their clinical care team, both patients ultimately expired within 6 months due to brain failure. Again, the aluminum levels in the cerebral spinal fluid were elevated, measured as 112 μg/L and 63 μg/L in the two patients. Hanston *et al.* attributed the encephalopathy to aluminum release from the cement [276]. Reusche *et al.* reported the third fatality and fifth case of aluminum-induced encephalopathy involving Ionos GIC in 2001 [46]. Consistent with the other four cases, high levels of aluminum (82-188 μg/L) were measured in the cerebral spinal fluid attributed to excessive release of aluminum from the cement subsequent to translabyrinthine otoneurosurgery. Reusche *et al*. stressed the importance of regular dural closure to ensure the avoidance of any direct contact of cerebral spinal fluid and brain paranchyma with Ionos GIC. In many instances, when proper surgical technique is adhered to, the use of Ionos GIC has shown to be safe and effective. However, after

Reusche *et al.* showed their results to Ionos GmBH & Co., the distribution and application of their GIC became strictly forbidden [46].

In addition to neurotoxicity, aluminum has also been associated with impaired bone mineralization and ostoblastic activity [277-280]. Engelbrecht *et al.* performed 45 revision hip arthoplasty surgeries between 1991 and 1994, cementing the femoral component with PMMA and used Ionos GIC in a granular form mixed with homologus bone as a bone substitute to fill voids surround the acetabular cup [47]. Early re-loosening of the acetabular component was observed in 10 patients (22%) after an average of 30 (15–50) months, much higher than the 7 % of arthroplasties that re-loosen after 8 years when homologus cancellous bone was used alone [47]. The authors attributed this unacceptably high failure rate to high concentration of aluminum release from the GIC in the local surrounding tissues, which impaired mineralization of the osteoid and ultimately compromised the stability of the prostheses. Further, the aluminum serum levels were evaluated in 6 patients, 3 with stable prostheses and 3 with loosened prostheses; all had elevated levels but patients with loosened prostheses were much higher. This is a risk as the impaired bone mineralization associated with the release of high concentrations of aluminum can lead to osteoporosis, with increased risk of fracture and unfavorable conditions for implantation of prostheses [281]. For these reasons Engelbrecht *et al.* stated [47]:

"We do not recommend continuation of the use of this material in orthopaedic surgery."

This body of evidence as a whole has led to contraindication of aluminum-containing GICs for use beyond their native field of dentistry [48]. Today,

aluminosilicate GICs for otoneurosurgery are still available (Serenocem, Corinthian Surgical, Nottingham, United Kingdom), however there are explicit warnings that Serenocem not be used for acoustic neuromas or skull based surgeries [282]. GICs remain a versatile material, which when applied correctly can be effective. However, their aluminum content will always represent an inherent safety risk to patients, whether it be risk of neurological deficit in othoneurological applications, or the risk of compromised bone quality in orthopaedic applications. Therefore, to mitigate against these risk for future patients, the aluminum content of GICs must be eliminated.

4.8 Aluminum-free GICs

The intrinsic properties of GICs, including their low exotherm, ability to chemically adhere to bone, and their potential for bioactivity remain desirable characteristics in orthopaedic applications, including vertebral body augmentation. However, as previously mentioned, in order to ensure the safe use of GIC outside of dentistry and limited applications in middle-ear surgies, aluminum must be removed from the glass chemistry. This is not a trivial challenge. Aluminum undertakes a critical role in glass composition, exerting significant influence on the structure and properties of both the glass and the corresponding cement. In particular, aluminum has considerable impact on the ability of a GIC to blend high strength with appropriate handling characteristics.

Darling and Hill were the first to report the development of aluminum-free GICs [52]. They investigated zinc silicate glasses in attempt to improve the fracture toughness and the wear resistance of aluminosilicate GICs in dental applications. This investigation included two aluminum-free glass series based on R_2O-ZnO-SiO_2 (R = Na, K, Li) and CaO-ZnO-SiO_2 glass chemistries. Zinc was explored for two reasons: (i) zinc

polycarboxylate cements have fracture toughness values that are 2 to 3 times greater than GICs [52], and (ii) like aluminum, zinc is considered a network intermediate capable of acting as either a former or modifier depending on the glass composition [203]. The use of zinc in hard tissue biomaterials is appropriate because it can increase the DNA of osteoblasts [283], which lead to increased bone mass [284]. Furthermore, zinc is the second most prevalent trace element in the body [285] and is also bactericidal, a desirable properties for a bone cement [286]. Darling and Hill noted that the alkali zinc silicate series failed to yield hydrolytically stable cements. Two GICs were successfully produced with two calcium-zinc-silicate glasses ($0.57SiO_2$, 0.29ZnO, 0.14CaO and $0.42SiO_2$, 0.53ZnO, 0.05CaO mole fraction). However, these zinc silicate GICs were found to be mechanically inferior to their aluminosilicate counterparts [52]. Boyd and Towler investigated the impact PAA molecular weight and concentration had on the mechanical properties of these zinc silicate GICs [49]. Boyd noted that the compressive strengths of these materials did not meet the clinical requirements defined by either the ISO9917 or ISO5833 standards, which dictate the minimum strengths required of dental restorative ($\geq$ 100 MPa) or orthopaedic ($\geq$ 70 MPa) cements [287, 288]. However, in subsequent work by Boyd, it was noted that the strength of the zinc silicate GICs are appropriate for less mechanically demanding applications, such as PVP and or KP where the compressive strength of the cement must exceed 30 MPa [54, 184]. The experimental results of Boyd and Towler show the mechanical and handling properties of the zinc silicate GICs to be inversely related. For example, the GIC with the longest working time, 218 seconds, had a corresponding 1-day compression strength of *c.* 7 MPa. Alternatively, the cement with the strongest 1-day compression strength, 40 MPa, had the

shortest working time, only 24 seconds [49]. This innate relationship represents a critical impediment to the development of aluminum-free GICs for clinical use in orthopaedics.

Brauer *et al.* developed an alternative aluminum-free GIC based on magnesium (Mg) containing glasses (47.32SiO_2, 10.41CaO, 11.04CaF_2, 31.23MgO mol%) [50]. Like aluminum and zinc, magnesium is also considered an intermediate capable of crosslinking polyacylic chains in GIC systems [203, 257]. These Mg-containing GICs were developed in response to biocompatibility concerns associated with zinc-based GICs, which arose due to evidence that high concentrations of zinc may induce a cytotoxic response *in vitro* [50]. The Mg-containing GICs were found to be less cytotoxic, but where not hydrolytically stable [50]. In a subsequent paper, Brauer *et al.* reported that substituting up to 50 % of the calcium content with strontium in the Mg-containing glasses (*i.e.* 47.32SiO_2, 5.21CaO, 5.52CaF_2, 5.21SrO, 5.52SrF_2, 31.23MgO mol%) improved the hydrolytically stability of the cements [257]. Although these Mg-containing GICs were reported to be "rubbery" when first placed in deionized water for incubation, after four weeks they exhibited compressive strengths of 19 to 29 MPa. The enhanced stability associated with the incorporation of strontium was found to decrease working time from 120 seconds to 90 seconds; however, these handling and mechanical properties remain clinically impractical for non-dental applications. To further improve the hydrolytic stability of the Mg-containing GIC, a copolymer of vinylphosphonic (*i.e.* $[CH_2CH(PO(OH)_2)]_n$) and acrylic acids was investigated [289]. Vinylphosphonic acid has two functional phosphonic acid groups per mer unit, which when combined with the one carboxyl acid group of PAA, produced GICs with 1-day compressive strength of *c.* 23 MPa and Young's moduli of 4 to 7 GPa [289]. Quantitative data pertaining to the impact

of the copolymer on the handling characteristics of the cements was not reported in the study. Despite the improved stability of these Mg-containing GICs, the mechanical properties of the cements still remain insufficient for load bearing orthopaedic applications (*e.g.* PVP and or KP).

For completeness, Hurrell-Gillingham *et al.* investigated Fe_2O_3 based glass chemistries as a third potential alternative to aluminum [290]. It was hypothesized that since Al^{3+} is a trivalent metal, Fe^{3+} would be capable of performing a similar role in the GIC chemistry. The authors based their glass compositions on the aluminosilicate GIC of Serenocem (Corinthian Medical, United Kingdom), which they had previously determined (*i.e.* 31.6SiO_2, 22.0Al_2O_3, 9.2P_2O_5, 26.0CaO, 11.3CaF_2 mol% [291]), with the exception that Al_2O_3 was replaced with Fe_2O_3. Unfortunately, the authors found that the P_2O_5 content of the glass became highly corrosive towards their alumina ceramic crucibles during melting, resulting in 4 of the 5 glasses becoming contaminated with aluminum. The only glass composition that was substantially free of aluminum (*c.* 0.4 mol%) was found to be highly reactive and produced GICs that set too quickly to be evaluated in any meaningful way. This investigation was further compromised by the fact that Fe^{3+} partially reduced to Fe^{2+} when present in high concentrations, resulting the spontaneous crystallization of magnetite. The authors argued the crystallized glass reduced the rate of ion release from the cement, which was believed to reduce the potential of cytotoxic effects of the cement. No further studies have been published exploring Fe_2O_3 based GICs.

To date, zinc silicate GICs have been the most extensively investigated class of aluminum-free GICs. These cements have been proposed for a variety of clinical

applications, such as: dental restorative cements [52], arthroplasty [49], antibacterial coatings on medical devices [292, 293], bone void fillers [55, 58, 59], adhesives for sternal closures [294], cranioplasty applications [295], and injectable bone cements for PVP and/or KP [53, 54, 56, 296, 297]. With respect to the latter, zinc silicate GICs possess many of the desirable properties defined by Lewis [112] (Table 3, page 36), making them a suitable alternative to existing injectable bone cements. Unlike PMMA, zinc silicate GICs can chemically adhere to bone, do not contain toxic monomers and have a negligible exotherm, properties which enhance their biocompatibility profile compared to the gold standard cement [53]. Although zinc silicate GICs are non-resorbable, this allows these cements to possess mechanical properties that are capable of providing long-term stability to fractured vertebral bodies, a key limiting factor with regards to calcium sulfate cements [54]. In contrast to calcium phosphate cements, zinc silicate GIC pastes are cohesive and have the capability to set in a wet environment [55]. However, despite these positive attributes, zinc silicate GICs are not injectable due to their quick setting nature. Attempts to improve the handling characteristics of zinc silicate GICs have failed sufficiently to extend the setting reaction to levels that are practical for clinical application [53, 54, 56, 296, 297]. Furthermore, strategies to delay GIC setting are coupled with significant reductions in corresponding strengths [53, 54, 56, 296, 297]. This combination of properties is a critical flaw, which obstructs the clinical use of zinc silicate GICs in orthopaedic procedures including vertebral body augmentation.

Chapter 5: Statement of the Problem

There exists a fundamental limitation that inhibits the clinical deployment of silica-based, aluminum-free GICs for percutaneous applications – an inability to balance practical handling characteristics with adequate mechanical performance. Figure 18 depicts the dichotomous nature between theses two properties. When GICs exceed the recommended minimum compressive strength of 30 MPa for PVP/KP, their corresponding working times range within *c.* 1 – 3 min, well short of the recommended 5-10 min of injection time required for proficient users, and impractical compared to the *c.* 15 minutes requested by common end users [157, 158]. Potential modifications have been explored to extend the setting reaction, including: changing the molar mass, quantity, and or the concentration of PAA in the GIC system [49, 54]; using of trisodium citrate as an additive to extend the GIC setting reaction [56]; and most extensively, altering the modifier and/or intermediate content of SiO_2-based glass chemistries [49, 54, 58, 59, 294, 298, 299]. However, regardless of the modification, the same inverse relationship prevails: GICs can either be strong, but set quickly, or GICs can set slowly, but exhibit inadequate mechanical properties (Figure 18). For example, when the strongest zinc silicate GIC increased from *c.* 55 MPa to 70 MPa (Wren *et al*. 2010), the working time fell from *c.* 3 min to 1 min. By comparison, when the slowest setting cement exhibited a working time increase from *c.* 1 min to 4 min, the compression strength decreased from 80 MPa to 6 MPa. Therefore, in order for aluminum-free GICs to become viable medical devices for vertebral body augmentation, their setting reactions must be extended without succumbing to this inverse relationship.

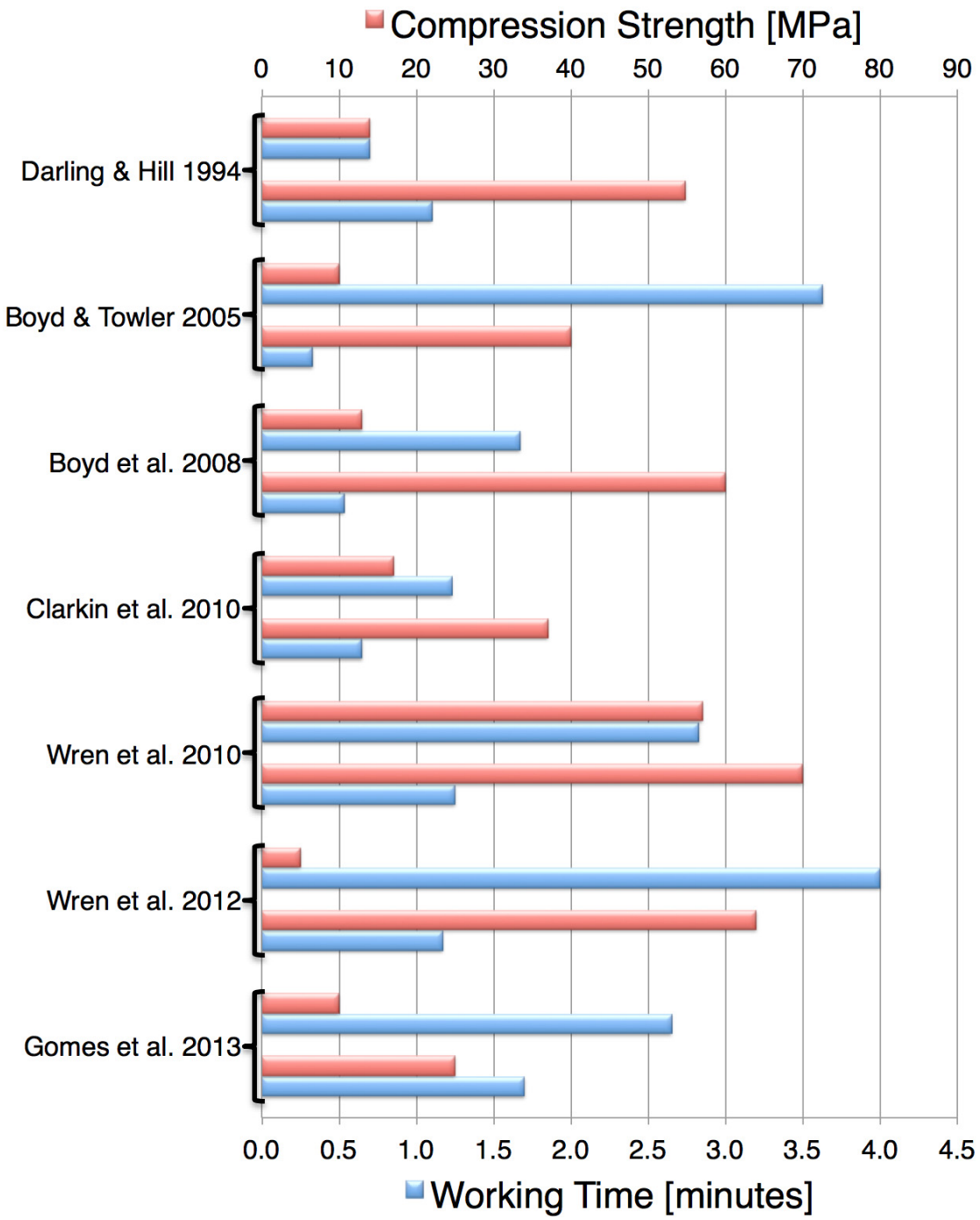

Figure 18: Graphical representation of the inverse relationship that exists between handling and mechanical properties of zinc silicate GICs. Each data set from the associated reference comprises of two pairs; (i) the cement composition with the longest working time and its corresponding 1-day compressive strength, and (ii) the cement composition with the maximum strength and its corresponding working time [49, 52, 53, 56-59]

Despite the fact that glass structure exerts significant influence on GIC properties, the conventional philosophy of adjusting modifier and/or intermediate content of the glass to balance reactivity has failed to rectify this inverse relationship [54, 57, 58, 294, 295, 299-301]. With this approach, in order to extend GIC handling characteristics, it is required that the modifier and/or intermediate content be reduced to lower degradability of the glass. This will diminish the release of divalent cations and slow the crosslinking of the polysalt matrix. However, lower release of divalent cations reduces the quantity of metal-carboxylate crosslinks within the GIC matrix, which has a deleterious impact on the strength of the cement. Therefore, in order to extend the setting of GICs whilst ensuring their mechanical integrity, it is necessary to identify an alternative method of reducing glass reactivity without limiting ion release. Accordingly, the philosophy of this thesis research explores replacing silicon as the primary network forming species in the glass as a novel means to control its degradation and consequently the handling and mechanical properties of the associated GIC.

Two elements with network forming capabilities identified for this research are germanium (Ge) and zirconium (Zr). Germanium has a formal charge of 4-plus (Ge^{4+}) and is considered a network former similar to Si^{4+} [203, 302]. In vitreous GeO_2, Ge^{4+} forms tetrahedral structures coordinated to 4 oxygen atoms (GeO_4), similar to vitreous SiO_2 [303]. However, in the presence of modifying oxides, GeO_4 has the ability to transform to higher coordinated structures, *i.e.* $[GeO_5]^-$ or $[GeO_6]^{2-}$ [303]. Similar to the $[AlO_4]^-$ tetrahedra in aluminosilicate glasses, the negative charge on the higher coordinated germanium structures must be charge compensated by cations in the glass (*e.g.* Ca^{2+} or Zn^{2+}) to ensure the electroneutrality of network [304, 305]. The potential

shift of divalent cations, like Ca^{2+} or Zn^{2+}, from modifying roles in zinc silicate glasses to charge compensating the $[GeO_5]^-$ or $[GeO_6]^{2-}$ structures in germanium-based glasses, may further polymerize the glass network and make it less degradable. However, from the aluminosilicate GIC literature, the bridging oxygens coordinated to these charge compensated forming unit are known to be basic and remain vulnerable to acid attack [198, 255]. Therefore, it is hypothesized that the replacement of SiO_2 by GeO_2 will delay, but not prevent, the release of divalent cations (*e.g.* Ca^{2+}, Zn^{2+}) from the glass, which will slow the formation of the polysalt matrix and thereby extend the handling characteristics of zinc silicate GICs without impairing their strengths.

In addition to replacing SiO_2 with GeO_2, the inclusion of zirconium dioxide (ZrO_2) in the glass chemistry is also being explored in this work. Zirconium is used as a nucleating agent in the glass-ceramic industry and has a low solubility in glass, typically on the order of 1-8 mol% [306-308]. The solubility of ZrO_2 in a glass is dependent on its compositional proportion to alkali oxide content (*e.g.* Na_2O), or to a lesser extent alkaline oxides (*e.g.* CaO) [309]. With regards to glass structure, Zr^{4+} is consider an intermediate, although it is commonly observed as a former, taking a $[ZrO_6]^{2-}$ octahedral structure and forming Si-O-Zr linkages in silicate glasses [310]. The negative charge of the $[ZrO_6]^{2-}$ structure must be charge compensated, a role commonly filled by Na^+ or Ca^{2+} ions, hence the dependence of ZrO_2 solubility on alkali and alkaline oxide content [306, 309]. ZrO_2 is attractive for the inclusion in ionomer glasses as it significantly reduces the degradability of glass, even in small amounts (*c.* 2-3 mol%) [306, 307, 310, 311]. This is due to the ability of Zr to polymerize a gel-like layer at the surface of the glass, preventing ions from attacking the silica network [308, 311, 312] Therefore, it is hypothesized that

including ZrO_2 will decrease the degradability of zinc silicate glasses and extend the handling characteristics of the corresponding GIC.

To test the hypotheses associated with the replacement of Si by Ge and Zr in the glass chemistries of zinc silicate GICs, three investigations have been designed (Figure **19**). The first investigation, presented in Chapter 6, conducts a preliminary screening to assess the potential and practicality of Ge and Zr to extend the GIC setting reaction, by evaluating their impact on the handling and mechanical properties of a well-characterized zinc silicate GIC from the literature. The second investigation presented in Chapter 7 conducts an in-depth examination of the GIC setting reaction in an attempt to elucidate the mechanisms associated with the changes in the handling characteristics of the cement. Lastly, Chapter 8 investigates the GIC molecular architecture over time to explain changes in mechanical properties. For clarity purposes, each of these experimental chapters are preceded by a brief rationale outlining: (i) the motivation of the chapter and its context in the overall body of work; (ii) the objective and/or hypothesis specific to this chapter; and (iii) an introduction to the experimental architecture used for the investigation.

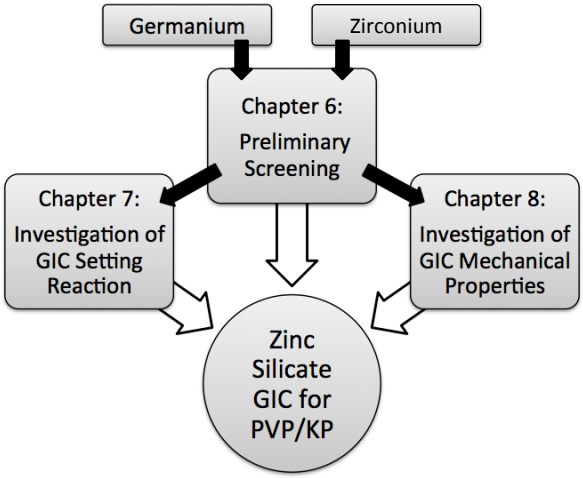

Figure 19**: Research overiew**

Chapter 6: Novel Adaptations to Zinc Silicate Glass Ionomer Cements – The Unexpected Influences of Germanium Based Glasses on Handling Characteristics and Mechanical Properties

6.1 Rationale

Aluminum-free glass ionomer cements (GIC) have been hindered for use as injectable bone cements by their inability to balance handling characteristics with mechanical integrity. The mechanical and handling properties of zinc silicate GICs have been well characterized in the literature, where they have demonstrated compression strengths up to 70 MPa but with working times of less than 3 minutes (Figure 18). Previous efforts to extend the setting reaction have remained clinically insufficient and are typically accompanied by significant reductions in strength. This chapter tests the hypotheses that i) the replacement of SiO_2 with GeO_2, and ii) the inclusion of ZrO_2 in zinc silicate glass chemistries will extend the GIC setting reaction and improve handling characteristics of the cement without effecting strength. In order to efficiently evaluate these two compositional changes, a design of mixtures (DoM) approach was employed. DoM is a statistical based approach to compositional design that allows for the simultaneous evaluation of multicomponent substitutions across wide compositional ranges whilst evaluating a minimum number of compositions [313-319]. Further, the DoM method yields mathematical models that relate compositional factors to material characteristics across the entirety of the design space. Thus, this chapter serves as a screening exercise to evaluate the effectiveness of GeO_2 and ZrO_2 to improve the handling characteristics of zinc silicate GICs, as well as assessing the impact of these inclusions on the mechanical properties of the resultant cements.

6.2 Introduction

Percutaneous vertebroplasty (PVP) and kyphoplasty (KP) are minimally invasive procedures for the palliative treatment of pathological fractures of vertebral bodies typically associated with osteoporosis or metastatic disease [320]. Both PVP and KP involve the injection of radiopaque bone cement through percutaneous cannulae into the fractured vertebrae to stabilize the fracture, which provides pain relief [22, 35] and returns mechanical integrity to vertebra [166]. KP differs from PVP in that it has an added step whereby a balloon tamp is inserted into the fracture and inflated, facilitating cement injection and correcting the kyphotic deformity by returning some of the height to the collapsed vertebra [166]. Glass ionomer cements (GICs) have been identified as potential alternatives to conventional PVP and KP bone cements, such as polymethyl methacrylate, because of their positive intrinsic attributes, including: excellent biocompatibility, bioactivity *via* the *in vivo* release of therapeutic ions, ability to chemically bond to both bone and surgical metal, inherent radiopacity, and a negligible exotherm during setting [198, 321]. GICs are multi-component systems consisting of a degradable glass powder mixed with an aqueous solution of polyalkenoic acid, usually polyacrylic acid (PAA). When mixed, the acid attacks the network modifiers of the glass, liberating metal cations that crosslink the polyanion chains of the acid, resulting in a cement consisting of a polysalt matrix reinforced with reacted glass particles [198].

Conventional dental GICs are comprised of an aluminosilicate glass [198], and are contraindicated for orthopaedic use [322]. Dental GICs previously used in cases of reconstructive otoneurosurgery or wider orthopedic applications, caused fatal aluminum-induced encephalopathy, impaired osteoblastic function, and hindered bone

mineralization due to the release of Al^{3+} ions [323-326]. Aluminum (Al) is an important part of the setting process of GICs, and its absence hinders cement formation [49]. Al facilitates three important characteristics in conventional GICs [45]. Firstly, in the presence of a sufficient amount of silica, Al^{3+} may isomorphically replace SiO_4 tetrahedra when charge compensated by cations like Na^+ or Ca^{2+}, creating a charge imbalance in the glass network that allows for degradability of the glass [327]. Secondly, Al^{3+} forms complexes with other ions (such as Ca^{2+} or F^-) that are believed to slow the setting reaction of the cement. Finally, although sterically improbable, Al^{3+} trivalent charge may bind three PAA chains, increasing entanglement of the polyanions and strength of the cement matrix [45]. However, for GICs to be reconsidered for orthopaedic applications, Al must be removed to ensure patient safety. Different components have been proposed in the literature as alternatives to Al, including iron [328], magnesium [50] and zinc [329]. Towler and Boyd developed a zinc-based GIC (ZnGIC) for orthopaedic applications comprising a zinc-calcium-strontium-silica glass ($0.48SiO_2$, 0.36ZnO, 0.12CaO, 0.04SrO2). Zn^{2+} has the potential to perform the same roles as Al^{3+} in glass, as both a network modifier, chelating the carboxylate groups on the acid chains and crosslinking the matrix, and as a network former with charge compensation of $[ZnO_4]^{2-}$ tetrahedral structures coming from cations such as Ca^{2+} [49]. These ZnGICs have been well documented in the literature, demonstrating acceptable biocompatibility and strength [49, 161, 211, 330], but are prevented from PVP/KP applications by poor handling properties due their quick setting nature, *c.* 30-60 sec [160, 331].

Bone cements indicated for PVP/KP are required, as a minimum, to be injectable for 5-10 min, combined with strengths of at least 30 MPa [33, 159]. Various methods

have been employed to extend working times of Al-free GICs, including, most obviously: decreasing both the molecular weight and concentration of the PAA [332], adding trisodium citrate (TSC) during mixing of the GIC mixture to reduce viscosity [321], and incorporating novel reagents in the glass network, such as titanium (Ti) [333]; none have led to sufficient extensions in working time. Of these alterations, the incorporation of Ti into the glass network showed the most promise, increasing the working time to *c.*180 sec whilst maintaining compression strength of 45 MPa. Adding 15%wt TSC in the ZnGIC mixture increased working time to *c.*120 sec from 32 sec whilst maintaining compression strength of 60 MPa. Smaller amount, up to 10% TSC, increased mechanical strength but had a reduced impact on working times. Lowering the PAA molecular weight and concentration produced a six-fold increase in working time (120 sec *vs.* 20 sec), but saw a significant reduction in the compressive strength of the cement, 20 MPa *vs.* 60 MPa [160, 321]. Despite the best efforts, all of these alterations saw insufficient extensions in working times when compared to the desired injection times of 5-10 min. More recently, Wren *et al.* [210] have investigated a gallium (Ga) containing, Al-free GIC for the purposes of filling bone cavities subsequent to tumor resections. Ga was incorporated on the basis that it is known to have a therapeutic effect for treating bone cancer. Surprisingly, the Ga GICs showed improved working times over zinc silicate GICs, reaching a maximum of *c.* 4 min; however, this was accompanied by a significant decrease in compression strength from *c.* 80 MPa to *c.* 6 MPa; further demonstrating the challenge to balance working time and strength. To date there has yet to be an Al-free GIC for orthopaedic applications with appropriate levels of both strength and appropriate clinical handling.

Traditionally, changes made to the glass network to improve on the setting characteristics of Al-free GICs have primarily focused on varying the network modifying components of the glass, leaving silicon (Si) as the primary network forming component [210, 211, 333]. However, the philosophy of this work is to explore alternative network forming components to improve the handling characteristics of the Al-free GICs. One such component is zirconium (Zr), which may be useful in extending the acid-base setting reaction of GICs, as there is evidence that Zr slows glass degradation in acidic environments [334]. Additionally, ZrO_2 is a common radiopacifer in current bone cements, where it has been shown to improve their mechanical strength whilst demonstrating good biocompatibility [335, 336]. The solubility of Zr in a glass network is controlled by the availability of alkali ions. Zr is often found in the octahedral coordination of $[ZrO_6]^{2-}$ within the glass networks, requiring charge compensation [337]. Reagents such as sodium (Na) have been shown to be effective at fulfilling this role at a suggested ratio of 1:1 for ZrO_2 : Na_2O [309]. Na has also been suggested to slow setting of GICs by inhibiting crosslinking of PAA chains [202]. Yet, given the insufficient extensions to Al-free GIC's working time *via* the various modalities described above, this thesis chose to employ a different approach. Instead of simply incorporating Zr and Na as alternative network modifying components, this work investigates changing the primary network-forming component within the glass as well. Germanium (Ge), is a known network-forming component, and is theoretically capable of isomorphically replacing Si in the glass network [203]. As well, Ge compounds have been shown to inhibit cancer development [338, 339], an attribute that could be exploited given both the ion release

capabilities of GICs and the indication of PVP/KP for vertebral body fractures resulting from metastatic disease.

This chapter aims to investigate the incorporation of Ge, Zr and Na into the ZnGIC glass composition (0.48SiO_2, 0.36ZnO, 0.12CaO, 0.04SrO_2) and the effects this will have on the handling (working and setting times) and mechanical properties (compression strength, biaxial flexural strength and modulus) of the resulting GIC. These findings will be used to evaluate the novel Al-free GICs as injectable bone cements for the indication of procedures such as PVP and KP.

6.3 Materials and Methods

6.3.1 Design of Glass Mixtures

Experimental glass melts determined the ranges that GeO_2 could be substituted for SiO_2, and that ZrO_2/Na_2O (equally matched on the basis of charge compensation) could be substituted for CaO in the ZnGIC predicate glass composition. These ranges were used to develop the constraints for a mixture design using Design Expert 8.0.4 (Stat-Ease Inc., USA), employed to establish the necessary design points to evaluate the effects of the substitutions on the properties of the GIC. To estimate the effect of each substitution, the vertices and constraint plane centroids and overall centroid of the defined domain were selected to construct 12 compositions, the ZnGIC predicate and 11 experimental GICs (Table 4), using a quadratic Scheffé Model. The amounts of ZnO and SrO were fixed at a total of 0.40 mol. fraction, and the remaining 0.60 mol. fraction of the glass comprising SiO_2, GeO_2, ZrO_2/Na_2O, and CaO was constrained as follows:

- Constraint 1: $0.00 \leq (SiO_2+GeO_2) \leq 0.48$

- Constraint 2: $0.00 \leq SiO_2 \leq 0.48$
- Constraint 3: $0.00 \leq GeO_2 \leq 0.48$
- Constraint 4: $0.00 \leq ZrO_2/Na_2O \leq 0.10$
- Constraint 5: $0.02 \leq CaO \leq 0.12$

Table 4: DG Glass compositions (mol. fraction). The zinc silicate predicate composition of Boyd *et al.* [161] is in the first row, followed by the 11 experimental compositions.

	ZnO	SrO	SiO_2	GeO_2	ZrO_2	Na_2O	CaO
ZnGIC	0.36	0.04	0.48	0	0	0	0.12
DG201	0.36	0.04	0	0.447	0.0335	0.0335	0.087
DG202	0.36	0.04	0	0.48	0	0	0.12
DG203	0.36	0.04	0.215	0.215	0.05	0.05	0.07
DG204	0.36	0.04	0.48	0	0.05	0.05	0.02
DG205	0.36	0.04	0	0.38	0.05	0.05	0.12
DG206	0.36	0.04	0.447	0	0.0335	0.0335	0.087
DG207	0.36	0.04	0.38	0	0.05	0.05	0.12
DG208	0.36	0.04	0	0.48	0.05	0.05	0.02
DG209	0.36	0.04	0.215	0.215	0.025	0.025	0.12
DG210	0.36	0.04	0.223	0.223	0.0335	0.0335	0.087
DG211	0.36	0.04	0.24	0.24	0.025	0.025	0.07

6.3.2 Glass Synthesis

Each glass in Table 4 was prepared by weighing out appropriate amounts of analytical grade reagents zinc oxide, strontium carbonate, silica, germanium oxide, zirconia, sodium carbonate, and calcium carbonate (Sigma-Aldrich Co., Canada). Powder compositions were mixed for 1 hour in a mechanical mixer and then dried in an oven (100 ˚C, 1 h). Compositions were then packed into platinum crucibles (Alfa Aesar, USA) and fired (1520 ˚C, 1 h) in a high temperature furnace (Carbolite RHF 1600, UK) and quenched into deionized water at room temperature. The resulting glass frit was then dried overnight in an oven (100 ˚C) and subsequently ground using a planetary ball mill (Laval

Labs Inc., Canada) and sieving to yield a particle size less than 45 μm. All ground glass powders were than annealed in the high temperature furnace at temperatures 30 ˚C less than their respective glass transition temperatures for 3 h and left to furnace cool. All glasses were subsequently stored in a desiccant environment prior to analysis.

6.3.3 Glass Transition Temperature

All glass powders were analyzed with a differential scanning calorimeter (Q200 DSC, TA Instruments, Canada) to determine the glass transition temperature (T_g). Fifty milligrams of glass powder were placed into stainless steel closed pans, while the reference pan was left empty. Samples were heated at a rate of 10 ˚C min^{-1} to a maximum temperature of 725 ˚C. Q Series software (TA Instruments, Canada) was used to determine T_g (point of inflection).

6.3.4 Cement Preparation

Cements were prepared by mixing glass powder with a 50 wt% aqueous solution of PAA, M_w = 12,700 g mol^{-1} (E6, Advanced Healthcare Ltd., UK) and deionized water on dental mixing pads using a dental spatula at a ratio of 2:1.5 glass powder to liquid acid.

6.3.5 Determination of Working and Setting Times

Both working and setting times were evaluated based on the procedures defined in ISO9917 [287]. The working time of the cements was measured in ambient air using a stopwatch, and was defined as the period of time from the start of mixing during which it was possible to manipulate the material without having an adverse effect on its properties [340]. Setting times were determined by filling an aluminum mold (10 mm x 8 mm x 5 mm) to excess with each experimental cement, which was placed on an aluminum plate

(75 mm x 100 mm x 8 mm) wrapped in aluminum foil. Sixty seconds after the end of mixing, the assembly was placed in an oven at 37 ˚C. Sixty seconds prior to the compositions working time, a Gilmore needle (mass 453g, flat tip Ø1.1mm) was placed on the surface of the material. This process was repeated intermittently until the cement could take the full weight of the indenter for 5 sec, whilst making a full circular indentation in the cement. The indentation process then continued every 30 sec until the indenter tip failed to make a complete circular impression in the cement's surface when viewed at 2X magnification [340]. Both evaluations were performed in triplicate.

6.3.6 Generation and Application of Mathematical Models

The design method described in section 6.3.1 was used to produce equations that link the properties of working time and setting time to the four compositional factors (SiO_2, GeO_2, ZrO_2/Na_2O and CaO).

The general forum of the Scheffé quadratic polynomial equation [341] which connects the working time response (Y_Q) to the compositional factors is:

$$Y_Q = \sum_{i=1}^{q} \beta_i X_i + \sum_{i=1}^{q-1} \sum_{j=i+1}^{q} \beta_{ij} X_i X_j + e \qquad \textbf{Equation 15}$$

where X_i represent the i^{th} compositional factor, $q = 4$, β_i coefficients represent the effect of the individual compositional factors X_i , β_{ij}, are the coefficients of regression which represent the effects of two-way interactions between the compositional factors, and e is the residual. The general form of the Scheffé cubic polynomial equation [341] fitted to the setting time response (Y_C) is:

$$Y_C = \sum_i^q \beta_i X_i + \sum \sum_{i<j}^q \beta_{ij} X_i X_j + \sum \sum_{i<j}^q \gamma_{ij} X_i X_j (X_i - X_j) + \sum \sum_{i<j<k} \sum^q \beta_{ijk} X_i X_j X_k + e \quad \textbf{Equation 16}$$

where γ_{ij} represents the coefficients of the cubic blending binaries and β_{ijk} are the coefficients of regression representing the three-way interactions between compositional factors. The coefficients were derived *via* a backwards regression method and are presented in pseudo values, which represent the effect of each component [342]. All mixture experiment models were developed relating the response variables to proportions of pseudo-components. Pseudo-component proportions (z_i) are calculated as:

$$z_i = \frac{x_i - L_i}{l - L_z} \quad \textbf{Equation 17}$$

where x_i stands for the original component proportion, L_i stands for the lower bound constraint (limit) for the i^{th} component, L_z stands for the sum of all lower bound constraints (limits) for all components in the design, *i.e.* $L_z = \Sigma L_i$, and l represents the total mixture. The pseudo-components are combinations of the original (actual) components, which rescale the constrained composition region so that the minimum allowable proportion of each pseudo-component is zero. This transformation may provide for more precisely estimating model coefficients compared to using the actual component system; as such, the coefficients derived based on the pseudo-component scaling are referred to in the context of the discussion to follow.

Low standard deviations were observed for the developed mixture regression models and verified *via* the F-Test. F_R is the F-ratio which is defined as the ratio between

the model summation of squares (MSS) and the residual summation of squares (RSS) [343]:

$$F_R = \frac{MSS/dfM}{RSS/dfE} \qquad \textbf{Equation 18}$$

where dfM and dfE denote the degree of freedom of the obtained model and the overall error respectively. It is a comparison between the model explained variance and the residual variance. It should be noted that high F_R values indicate the reliability of the models.

In order to visualize the relationship between each property and variation in glass component, the regression coefficients were used to generate 2D and 3D surface contour from the fitted polynomial equations (Figure 20 through Figure 23).

6.3.7 Determination of Compression Strength

The compressive strength was determined using a procedure based on ISO9917 [340]. Stainless steel split ring molds (Ø4 mm x 6 mm) were filled to excess with cement, covered with acetate, and then clamped between two stainless steel plates and incubated (37 ˚C, 1 h). Upon removal from the oven the assembly was broken down, cement flash was removed, and the ends of the samples were ground flat using wet 800 grit silicon carbide paper prior to removing from the molds. Samples were incubated at 37 ˚C in distilled water for 1, 7, 30, and 180 days under static conditions. After each time period, samples were removed from incubation environment and immediately loaded on an Instron 3344 mechanical testing system (Instron, USA) with a 2 kN load cell and compressed with a crosshead speed of 1 mm min^{-1}. Five samples for each cement formulation were tested in ambient laboratory air.

6.3.8 Determination of Biaxial Flexural Strength and Modulus

Biaxial flexural strength (BFS) of the cements was determined according to the methods presented by Williams *et al.* [344]. Teflon molds (Ø15 mm x 1 mm) were filled to excess with cement, covered with acetate, and then clamped between two stainless steel plates and incubated (37 ˚C, 1 h). Upon removal from the oven the assembly was broken down, cement flash was removed, and the samples' top and bottom surfaces were ground flat using wet 800 grit silicon carbide paper prior to removing from the molds. Samples were incubated at 37 ˚C in distilled water for 1, 7, 30, and 180 days under static conditions. After each time period samples were removed from the incubation environment and immediately loaded on an Instron 3344 mechanical testing system with a 2 kN load cell and compressed with a crosshead speed of 1mm min^{-1}. Five samples for each cement formulation were tested in ambient laboratory air. BFS was calculated according to:

$$BFS = \frac{P}{t^2}\left[0.63 \ln\left(\frac{r}{t}\right) + 1.156\right] \qquad \textbf{Equation 19}$$

where P is the applied point load (N), t is the specimen thickness (mm), and r is the radius of the support ring (mm).

The biaxial flexural modulus of each sample was calculated according to the method of Higgs *et al*. [345], using the BFS force-displacement data and assuming a Poisson's ratio of 0.3.

6.3.9 Statistical Analysis

One-way analysis of variance (ANOVA) was employed to compare the different cement compositions. Mean values of working times and setting times data were compared using

the Tukey post-hoc test. The mean values of compression strength, BFS, and modulus data were compared using the Bonferroni post-hoc test. Differences were deemed significant when $p \leq 0.05$. All calculations were done using Prism 5 (GraphPad Software Inc., USA).

6.4 Results

6.4.1 Glass Transition Temperature

Results in Table 5 demonstrated that Ge based glasses have a lower T_g than Si based glasses. T_g was only used to determine the annealing points required for the methodology of glass synthesis, and will not be discussed further in this chapter.

Table 5: Experimental results for T_g, working time (W_t) and setting time (S_t) of the 11 experimental glass compositions and the ZnGIC predicate glass and resulting GIC. Standard deviation presented in parentheses.

Composition	T_g [˚C]	W_t [min:sec]	S_t [min:sec]
ZnGIC	677	1:17 (0:03)	2:05 (0:02)
DG201	593	5:18 (0:02)	13:58 (0:31)
DG202	605	5:58 (0:20)	16:06 (1:30)
DG203	613	7:05 (0:07)	104:19 (0:25)
DG204	657	7:08 (0:13)	DID NOT SET
DG205	601	4:58 (0:13)	14:07 (1:41)
DG206	645	1:09 (0:31)	3:16 (0:06)
DG207	640	0:22 (0:05)	1:03 (0:12)
DG208	582	10:02 (0:09)	35:55 (2:11)
DG209	624	5:02 (0:13)	14:13 (2:11)
DG210	612	6:56 (0:26)	36:05 (2:38)
DG211	622	7:54 (0:21)	75:23 (4:43)

6.4.2 Handling Characteristics

Table 5 demonstrates the complex relationship between glass composition and handling characteristics of resultant GICs within the pre-defined design space. General observations showed that the inclusion of Ge consistently slowed the setting reaction. Ge based GICs possessed working times of *c.*5-10 min and setting times of *c.*14-36 min. The Si based GICs were more sporadic, with working times ranging from 22 sec to 7 min and setting times from 1 min to > 720 min *(DG204 failed to set, as it remained pliable after 12 hours)*. Compositions containing both Ge and Si possessed working times of 5-8 min, but showed a strong compositional dependency with regards to setting times, as some set in a reasonable amount of time (DG209 and DG210), while other set much more slowly (DG203 and DG211).

No clear trends were observed from Table 5, but the regression models presented in Table 6 are a useful tool to help correlate the influence glass composition has on the response properties (working and setting time) of the resultant GIC. The backwards regression method was selected to determine the significant model coefficient terms automatically. The working time was fitted with a quadratic model, and the setting time was fitted with a cubic model. DG204, which did not set, was omitted from the setting model. Table 7 ranks the influence, either positive or negative, of each coefficient within their respective models. This table indicated that the most influential factors on the working and setting time responses were the interactions between multiple components. The models are graphically represented in Figure 20 through Figure 23.

Table 6: Final regression models in terms of L-pseudo components, and R^2 values, and summarized ANOVA for each response.

			Summarized ANOVA				
Response	Regression Model		R^2	R^2adj.	R^2pred.	P Value	F_R
Working Time (sec)	+386.56	* SiO_2	0.9872	0.9648	0.9240	0.0013	44.06
	+589.09	* GeO_2					
	+627.88	* ZrO_2/Na_2O					
	+7462.16	* CaO					
	+1196.78	* SiO_2 * GeO_2					
	-10890.71	* SiO_2 * CaO					
	-9956.51	* GeO_2 * CaO					
	-13144.13	* ZrO_2/Na_2O * CaO					
Setting Time (sec)	+1568.67	* SiO_2	0.9168	0.8337	0.8056	0.0099	11.02
	+2569.36	* GeO_2					
	+146.00	* ZrO_2/Na_2O					
	-6774.50	* CaO					
	+2.797E+5	* SiO_2 * GeO_2 * ZrO_2/Na_2O					
	-1.262E+5	* SiO_2 * GeO_2* CaO					

Table 7: Summary of the significant (positive and negative), individual and interaction effects associated with compositional factors (order of significant effects: highest to lowest, ↑represents positive effects, and ↓ represents negative effects).

Working Time (sec)		Setting Time (sec)	
Ranking Effect	***Effect Coefficients***	***Ranking Effect***	***Effect Coefficients***
↓ ZrO_2/Na_2O * CaO	- 13144.13	↑ SiO_2 * GeO_2 * ZrO_2/Na_2O	2.797E+5
↓ SiO_2 * CaO	- 10890.71	↓ SiO_2 * GeO_2 * CaO	- 1.262E+5
↓ GeO_2 * CaO	- 9956.51	↓ CaO	-6774.50
↑ CaO	7462.16	↑ GeO_2	2569.36
↑ SiO_2 * GeO_2	1196.78	↑ SiO_2	1568.67
↑ ZrO_2/Na_2O	627.88	↑ ZrO_2/Na_2O	146.00
↑ GeO_2	598.09		
↑ SiO_2	386.56		

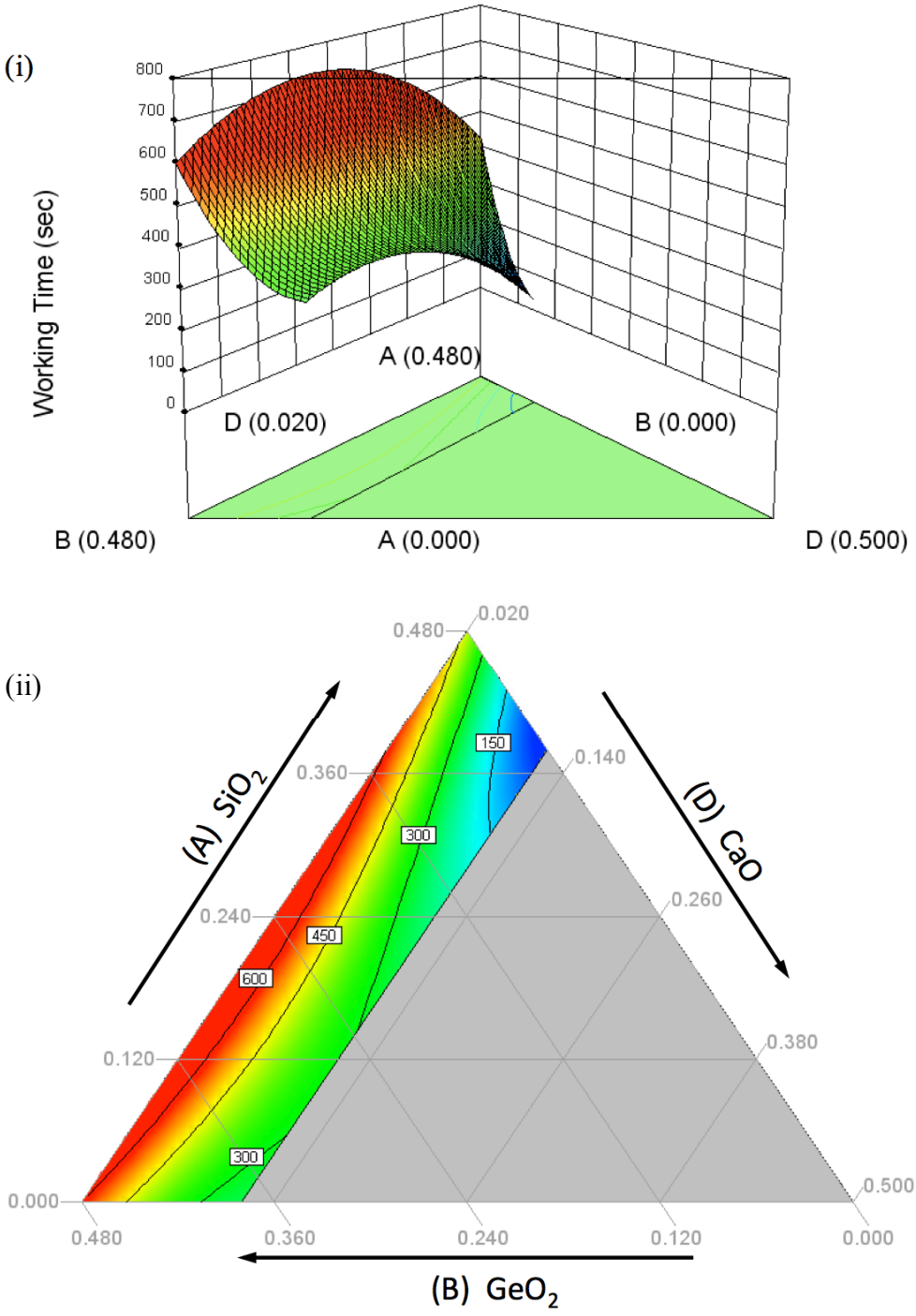

Figure 20: The 3D (i) and 2D (ii) contour plots show the effect of varying glass composition within the confines of the design space and the resultant working time based on the regression model. These plots are confined to within the design space where (A) SiO_2 0-0.48mol fraction, (B) GeO_2 0-0.48mol. fraction, (D) CaO 0.02-0.12mol. fraction, and ZrO_2/Na_2O fixed at 0.1mol. fraction.

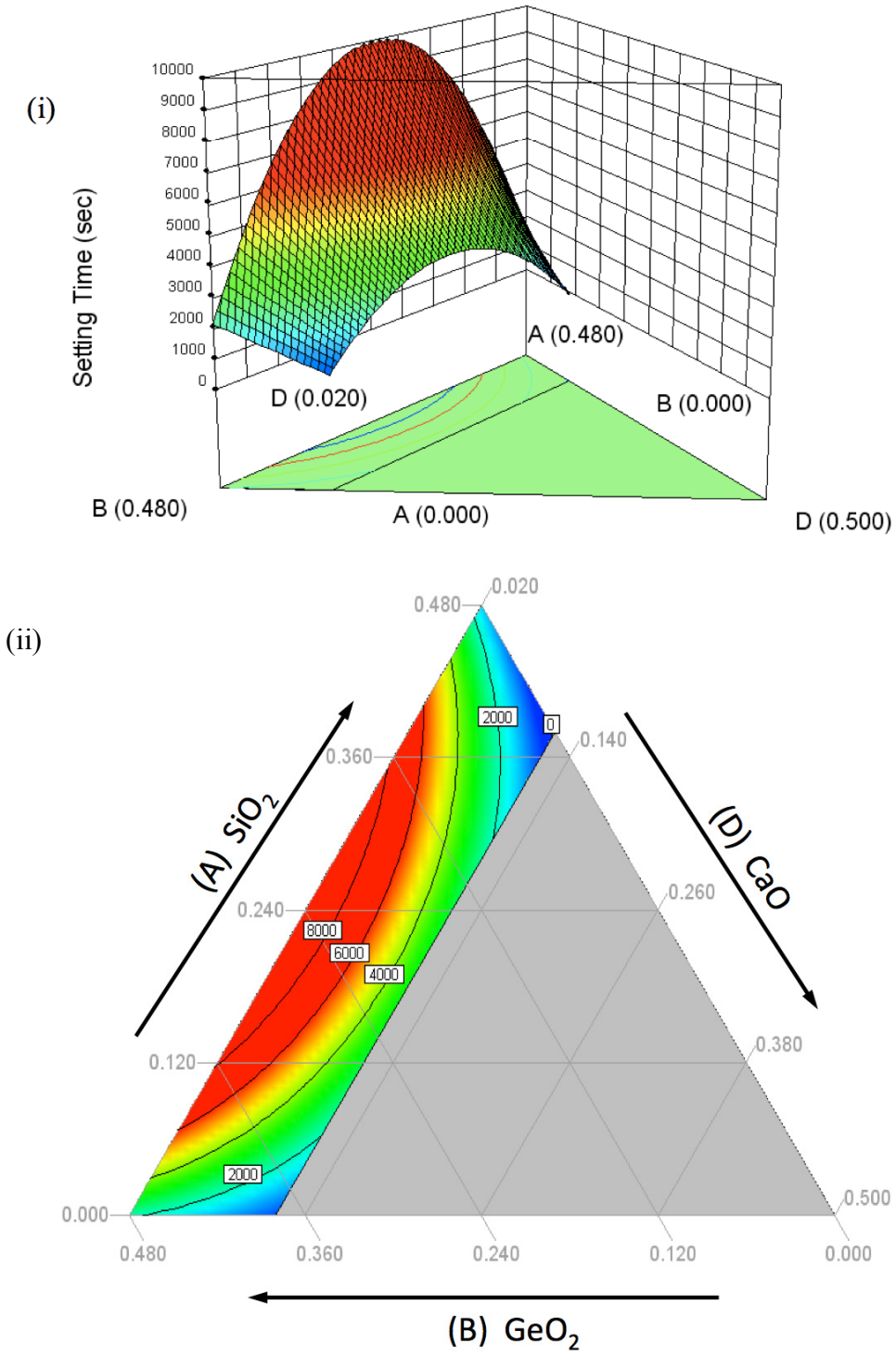

Figure 21: The 3D (i) and 2D (ii) contour plots show the effect of varying glass composition within the confines of the design space and the resultant setting time based on the regression model. These plots are confined to within the design space where (A) SiO_2 0-0.48mol fraction, (B) GeO_2 0-0.48mol. fraction, (D) CaO 0.02-0.12mol. fraction, and ZrO_2/Na_2O fixed at 0.1mol. fraction.

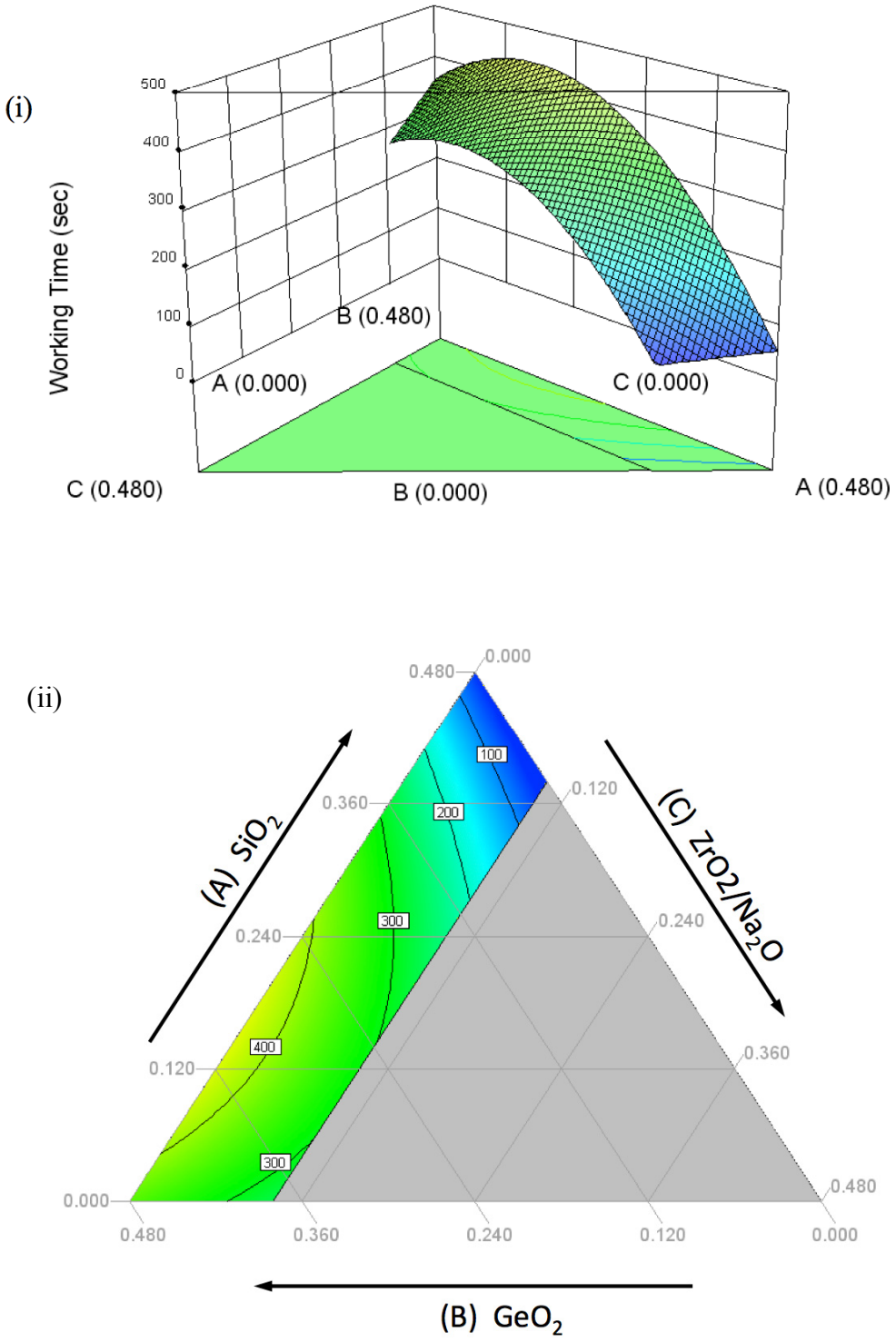

Figure 22: The 3D (i) and 2D (ii) contour plots show the effect of varying glass composition within the confines of the design space and the resultant working time based on the regression model. These plots are confined to within the design space where (A) SiO_2 0-0.48mol fraction, (B) GeO_2 0-0.48mol. fraction, (C) ZrO_2/Na_2O 0-0.10mol. fraction, and CaO fixed at 0.12mol. fraction.

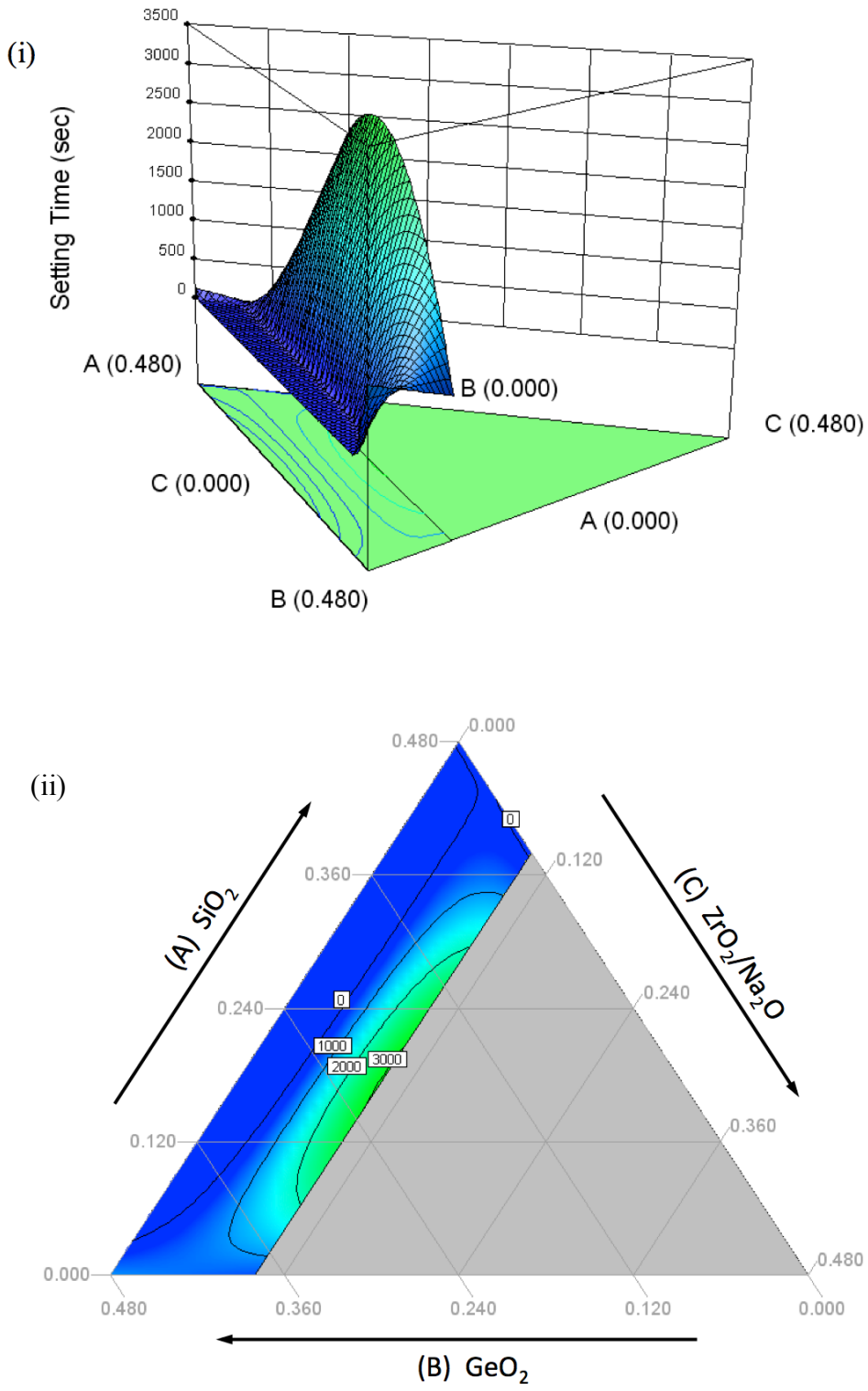

Figure 23: The 3D (i) and 2D (ii) contour plots show the effect of varying glass composition within the confines of the design space and the resultant setting time based on the regression model. These plots are confined to within the design space where (A) SiO_2 0-0.48mol fraction, (B) GeO_2 0-0.48mol. fraction, (C) ZrO_2/Na_2O 0-0.10mol. fraction, and CaO fixed at 0.12mol. fraction.

6.4.3 Mechanical Properties

Three compositions were chosen from the full mixture design space for the characterization of mechanical properties. Compositions with working times less than *c.*5 min (ZnGIC, DG206, DG207) or setting times greater than 60 min (DG203, DG204, DG211) were omitted on the basis their properties are clinically impractical for use in PVP and KP. DG208 was moved forward because it exhibited the longest working time. The remaining compositions, DG201, DG202, DG205, DG209, and DG210, were subjected to a 1-day compression test. From this test DG205 and DG202 were chosen for mechanical testing because DG205 was identified as the strongest composition amont that group, and DG202 exhibited a reasonable balance between strength and working time. The compression strengths are presented in Figure 24. All three compositions exhibited compression strengths in excess of 30 MPa for the first 30 days. DG202 and DG208 exhibited a significant decrease in strength at the 180 day time point. DG205 possessed the highest strength, peaking at 7 days (49.6 MPa), but was statistically similar across all four time points.

DG202 displayed a decreasing trend in BFS over time (Figure 25), culminating in a significant drop from 11 MPa at 1 day to 6.5 MPa at 180 days. Again, DG205 was the strongest material, this time peaking at 30 days (13.4 MPa) but similar to the compression data, DG205 weakened after 180 days (9.4 MPa). There was no statistically significant change of DG208 over the 180 days like the other two materials, as it remained between 7 and 9 MPa, ($p > 0.05$).

The moduli of these three experimental GICs are presented in Figure 26. Typically DG202 was the stiffest material and DG208 was the least stiff. All three

materials see a drop in modulus from 30 to 180 days, but only DG205 and DG208 to the point of significance ($p < 0.05$).

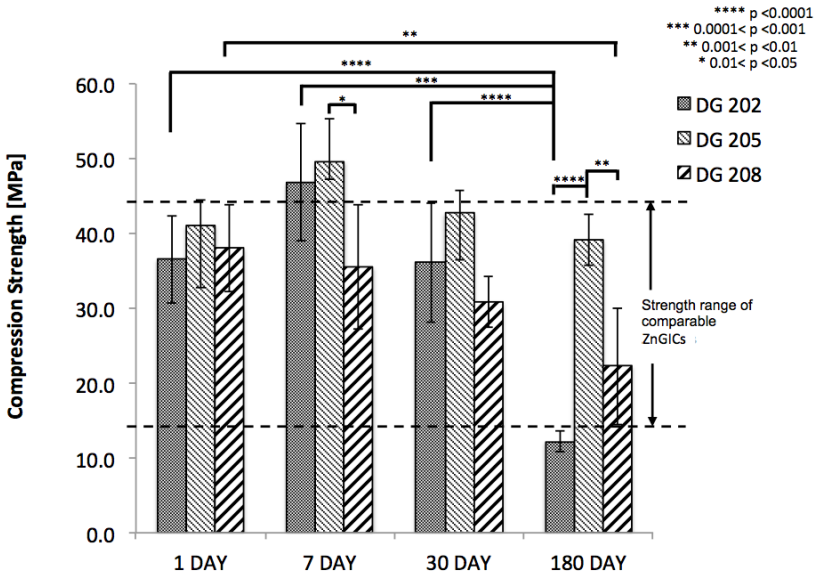

Figure 24: The compression strength of three experimental GIC compositions, DG202, DG205, and DG208 over 1, 7, 30 and 180 days. Comparable ZnGIC strengths from Clarkin *et al.* [332] and Boyd *et al.* [49].

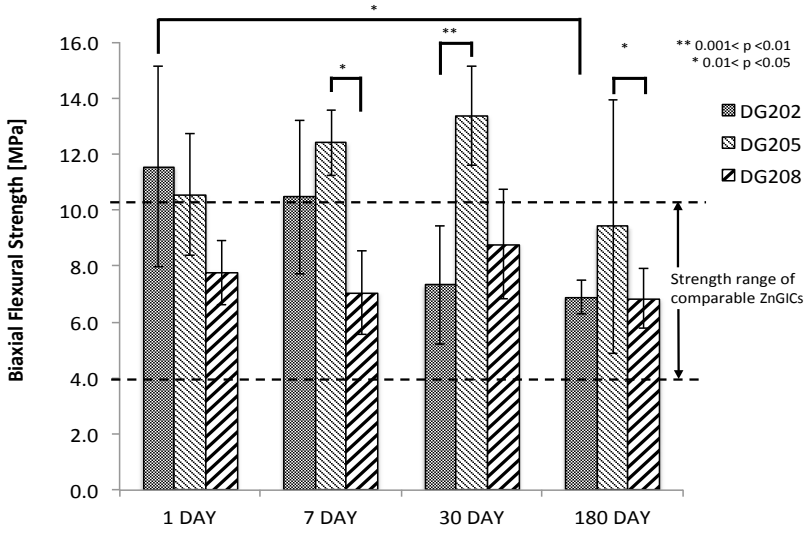

Figure 25: The biaxial flexural strength of three experimental GIC compositions, DG202, DG205, and DG208 over 1, 7, 30 and 180 days. Comparable ZnGIC strengths from Clarkin *et al.* [332] and Boyd *et al.* [49].

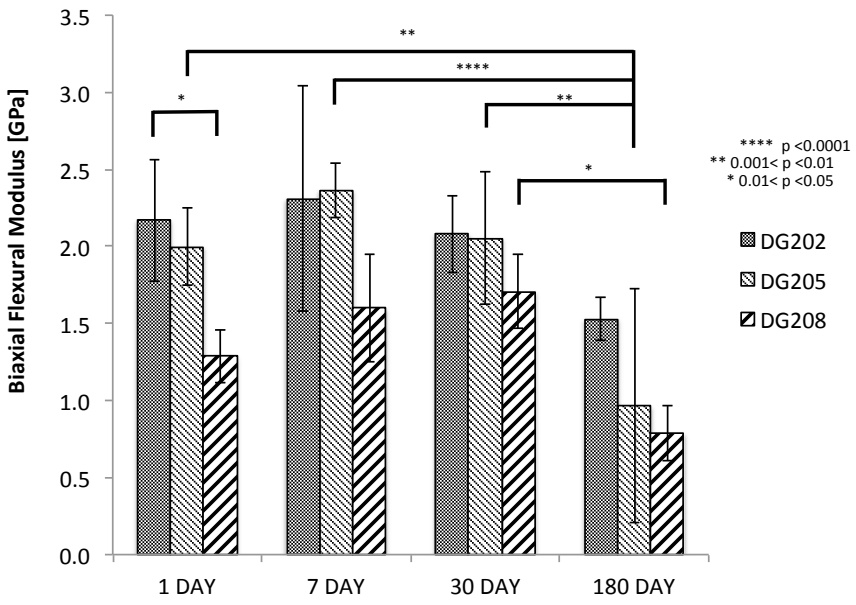

Figure 26: The moduli of DG202, DG205, and DG208 experimental GIC compositions over 1, 7, 30 and 180 days.

6.5 Discussion

6.5.1 Handling Characteristics

The most significant observations of this chapter are that clinically useful handling characteristics can be achieved in Ge-based GICs without compromising their strength. Such significant increases to the setting reaction were unexpected, since Ge was believed to simply isomorphically replace Si within the glass network. GIC setting reactions are dictated by the rate at which cations are released from glass during the acid attacks and chelated by the PAA polyanion chains [45]. In ZnGICs, the Zn^{2+}, Ca^{2+}, and Sr^{2+} cations take on roles as network modifiers, depolymerizing the glass network by producing non bridging oxygen [211, 299, 346]. The less polymerized a glass network is, the more susceptible it is to acid attack and faster the materials will set, evident by the significant

influence CaO has on the both the working and setting time models (Table 7, and graphically in Figure 20 and Figure 21). The effect of Ge on the handling characteristics is best demonstrated by comparing DG202 and the ZnGIC predicate. These two materials have the same compositions, except in DG202 GeO_2 entirely replaced SiO_2. Here, a 360% increase in working time and a 670% increase in setting time was observed. The regression models interpolate the results across the design space and the plots in Figure 20 through Figure 23 show working and setting time increasing as GeO_2 content increases, peaking when Si and Ge are present in the glass at approximately equal levels. Thus, these experiments allows me to definitively say Ge is a leading factor in extending the setting reaction of the DG Series GICs.

The fact that all Ge based GICs set in under 40 min suggest that Ge limits the reactivity during the initial set, but does not impede the entire cement forming reaction. Literature discusses two potential intrinsic qualities of Ge glasses that may provoke the reduced reactivity and longer setting reactions observed in this investigation. First, GeO_4 tetrahedra have lower bond angles than those of SiO_4 (132° *vs.* 154°), with the presence of smaller three membered rings in the vicinity of alkali cations resulting in smaller network cavities [347-349]. This characteristic may trap such cations, delaying their release until a sufficient number of protons have been donated from the polyanions to produce an electromagnetic force large enough to initiate the release and subsequently the participation of said cations in the setting reaction. Secondly, GeO_4 tetrahedra have been found to take on higher coordination, either $[GeO_5]^-$ or $[GeO_6]^{2-}$, requiring charge compensation by cations to promote electroneutrality. Should this be the case, it could reduce the number of network modifying cations responsible for producing the non

bridging oxygen sites susceptible to acid attack, resulting in a less reactive glass [347]. Evidence to support these theories is provided by the comparison of DG205 and DG207, which are compositionally similar, save for DG205 is a Ge based glass, and DG207 is a Si based glass. DG205 exhibits a working time of *c.* 5 min, compared to that of DG207 at just 22 sec. The quick setting nature of DG207 is indicative of a GIC mixed with an inverted glass, which are very reactive due to a highly disrupted glass networks caused by an increased number of network modifiers [346, 350]. The slower setting reaction of DG205 is characteristic of a less reactive network, with fewer and or more difficult-to-access modifiers.

The effects of Zr and Na on the GIC setting characteristics are less clear. In some instances in inclusion of ZrO_2/Na_2O in the glass compositions extended the setting reaction of the resultant GICs (DG208 > DG202; DG204 > ZnGIC). However, in other instances the inclusion of ZrO_2/Na_2O in the glass shortened the setting reaction (DG202 > DG205 & DG201; ZnGIC > DG207). This sporadic nature is represented by the contrasting model responses, where prominent effects of increasing ZrO_2/Na_2O content reduces the working time response (Figure 22) but increases the setting time response (Figure 23). The impact of ZrO_2/Na_2O on GIC handling characteristics is significant, as combined they represent no more than 10% of the glass, yet are part of the most influential interactions in both the working and setting time responses (Table 7). Table 8 highlights the working time portion of these observations and presents an interesting trend. There is consistency between glass compositions, whether Ge or Si based, and the ranking order of the corresponding working times – the same compositions are ranked in the same order. Two observations are drawn from this. First, Ge seems to produce GICs

with more consistent setting reaction. Our results show working times between 5 and 10 min, and setting time in between 14 and 36 min. In contrast, Si based glasses exhibit wildly varying handling characteristics, with working times ranging from 22 sec to 7 min and setting times from 1 min to those which do not set. Second, despite the apparent randomness of the influence of Zr and Na have on the GIC setting reaction, the trend of Table 8 demonstrates some consistency between the concentration of ZrO_2/Na_2O in the glass network and the role they play during the initial setting reaction. Ultimately, this suggests that the influence of Zr and Na on the setting reaction may not be dependent on the quantity of each component, but rather on their interactions with other components within the glass composition.

Table 8: Ge and Si based GICs ranked in order of ascending working times.

Rank	W_t [min:sec]	Ge based compositions	W_t [min:sec]	Si based compositions
1	4:58	DG205 ($0.38GeO_2$, 0.36ZnO, $0.05ZrO_2$, $0.05Na_2O$, 0.04SrO, 0.12CaO)	0:22	DG207 $0.38SiO_2$, 0.36ZnO, $0.05ZrO_2$, $0.05Na_2O$, 0.04SrO, 0.12CaO)
2	5:18	DG201 ($0.447GeO_2$, 0.36ZnO, $0.0335ZrO_2$, 0.033d5Na_2O, 0.04SrO, 0.087CaO)	1:09	DG206 ($0.447SiO_2$, 0.36ZnO, $0.0335ZrO_2$, $0.0335Na_2O$, 0.04SrO, 0.087CaO)
3	5:58	DG202 ($0.48GeO_2$, 0.36ZnO, 0.04SrO, 0.12CaO)	1:17	ZnGIC ($0.48SiO_2$, 0.36ZnO, 0.04SrO, 0.12CaO)
4	10:02	DG208 ($0.48GeO_2$, 0.36ZnO, $0.05ZrO_2$, $0.05Na_2O$, 0.04SrO, 0.02CaO)	7:08	DG204 ($0.48siO_2$, 0.36ZnO, $0.05ZrO_2$, $0.05Na_2O$, 0.04SrO, 0.02CaO)

Nonetheless, the handling characteristics and corresponding strength presented by the Ge based GICs are a significant improvement over previous Al-free GICs as, for the first time, the working and setting times are within the range of clinical practicality and

balanced with reasonable strength. Further investigations are required into the injectability of these materials, but with working times up to 10 min, the rheology is promising. Future work can also exploit the optimization process of the mixture design methodology to identify a novel glass composition within the compositional design space that may produce a GIC to meet the clinical requirements of injectability of 5-10 min, or greater.

6.5.2 Mechanical Properties

Three specific observations highlight the unexpected mechanical properties and the unique nature of Ge-based GICs. Firstly, given the experimental evidence from the literature that demonstrates increased working times are accompanied by decreased strength for Al-free GICs, it was expected the Ge based experimental GICs would do the same; yet they do not. Figure 24 and Figure 25 show the compression and biaxial flexural strengths of the three DG series GICs and, how they compare to the ranges of compression and biaxial flexural strengths published for zinc silicate GICs made with PAA of similar strength. Typically, less reactive glasses result in a lower crosslink density and thus weaker cement. However, despite the reduced reactivity of the Ge based glasses and the significant extension to the setting reaction associated with the corresponding GICs, we see that they exhibit strengths comparable to, or even greater, than those of the quick setting ZnGIC predicate compositions [49, 332]. With compression strengths in excess of 30 MPa for the first 30 days being greater than that of vertebral cancellous bone, *c.* 20 MPa [161], it shows these materials adhere to clinical philosophy which PVP and KP cements should have mechanical properties matched closely to those of healthy vertebrae [159].

The second unexpected observation is that the moduli of Ge based GICs are much higher than expected. The moduli of the experimental GICs range between 0.8 GPa (DG208, 180 d) to 2.4GPa (DG205, 7 d) where DG202 is generally the stiffest material, although not significantly so. Literature has shown ZnGICs to have biaxial flexural modulus less than 0.5 GPa [160, 161] – up to an order of magnitude lower than the values observed in this work. Comparing the moduli of the compositionally similar DG202 and ZnGIC suggests, like the setting reaction, Ge is the component responsible for the increased stiffness. Mechanical properties of GICs, such as strength and modulus, have been attributed to the crosslink density of cations that chelate the polyanion chains of the acid, and the extent to which these chains are entangled with one another [232]. It is unlikely an increased crosslink density of divalent cations is responsible for the increase in stiffness because such a mechanism would see a concurrent increase to strength, and as indicated above the strengths of DG202 are similar to those of the zinc silicates in the literature. Hill *et al.* described the entanglement of polyanion chains to restricting their lateral movement, while interactions with neighboring chains restrict their longitudinal movement [237]. Therefore, it is possible that interactions between multivalent Ge^{4+} ions, or complexes thereof, interact with more than two polyanions to increase chain entanglement thereby reducing reptation to produce stiffer cements.

The third unexpected observation is the marked decrease in mechanical properties for all three cements over time. Typically, GICs (*including ZnGICs*) have demonstrated an increase in mechanical properties as the cement matures [49, 232, 332, 351]. Wilson attributes this characteristic to the continuous and more complete acid-base reaction between the glass and the PAA [45]. Increases in mechanical properties of the Ge-based

GICs are displayed intermittently in Figure 24, Figure 25, and Figure 26, although never to the extent of significance. Ultimately, all tested materials see significant decreases in strength and or modulus from 1 to 180 days. This is not a novel characteristic, as some GICs have demonstrated a decline in strength with respect to time [351, 352]. This behavior has been attributed to either hydrolytic instability and a plasticizing action of water [234], or over crosslinking of the polyanion chains caused by the continuous setting reaction [352]. The latter cause is less likely, as over crosslinking would likely be accompanied by an increase in modulus, as shown by Wren *et al.* [351]; yet a reduction in modulus was observed for all three Ge-based GICs. Regardless of the cause, this characteristic could have negative clinical implications, and will require further investigation to identify the underlying mechanisms and whether alterations can be made to the cements to mitigate the decline of mechanical integrity whilst maintaining a appropriate clinical handling characteristics.

6.6 Limitations

Limitations exist in this study. The lack of a molecular investigation of either the glass or the resulting GIC only allows the authors to postulate what might be happening on a molecular level of the experimental materials. Additional key limitations with the experimental methodology are:

- Working times were meant to offer a simple approximation of GIC rheology. A full injection study is required to definitively understand whether these GICs are suitable as injectable bone cements.
- Fixing the compositional ratio of ZrO_2:Na_2O at 1:1 allowed the production of Zr containing glasses, but did not allow for independent analysis of how Zr or Na

might affect the handling or mechanical properties of the GIC as individual elements.

- Fixing the mole fraction of ZnO and SrO at 0.36 and 0.04 greatly reduced the complexity of the design of mixtures presented in Table 4. However, this eliminated the ability to investigate the influence ZnO and SrO may have had as individual components, or as part of interactions with other components on the handling characteristics and mechanical properties of the resultant GIC.
- With only three of the twelve compositions undergoing mechanical evaluation, the understanding of how GeO_2 and ZrO_2/Na_2O affect the mechanical properties is limited solely to the observations made from the experimental results presented in this work. Additionally, this prevents the development of regression models to map the effect of glass composition on GIC mechanical properties across the entire design space.

6.7 Conclusions

Previous Al-free GICs are not clinically practical as injectable bone cements because they fail to achieve an appropriate balance between handling and mechanical properties, despite numerous attempts to alter their performances. In agreement with the hypothesis of this thesis, it has been shown that carefully controlled additions of GeO_2, ZrO_2, and Na_2O to the glass component of a zinc silicate GIC significantly extends the setting reaction without sacrificing mechanical integrity. Thus, for the first time, Al-free GICs are clinically viable as injectable bone cement for PVP or KP with regards to handling characteristics and mechanical properties.

6.8 Supplementary Data

Only 3 of the 12 DG series GICs compositions were evaluated in Chapter 6. For completeness, 8 or the remaining 9 compositions (DG204 did not set and thus could not be evaluated) were evaluated for compressive strength (Figure 27), biaxial flexural strength (Figure 28) and biaxial flexural modulus (Figure 29). The key findings of these data were that the glass composition with both Si and Ge, and *c.* 1.5-3.5 mol% of ZrO_2 produced GICs with mechanical properties that increased over time (*i.e.* DG209 and DG210).

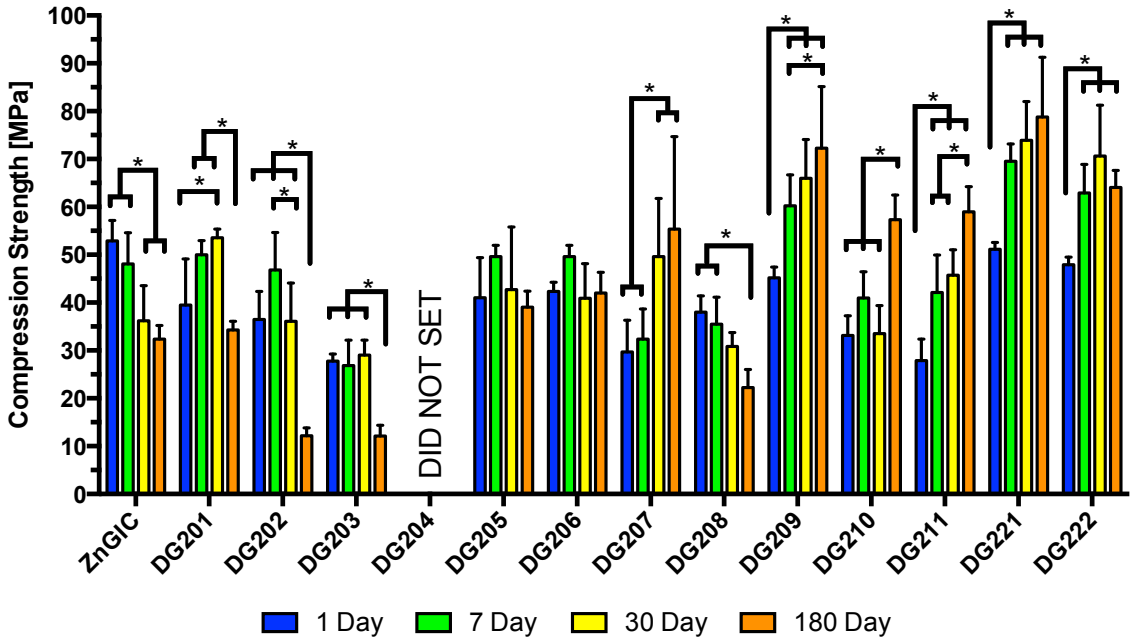

Figure 27: Compression strengths of DG series GICs. DG204 did not set, thus could not be evaluated. * denotes statistically significant differences ($p < 0.05$).

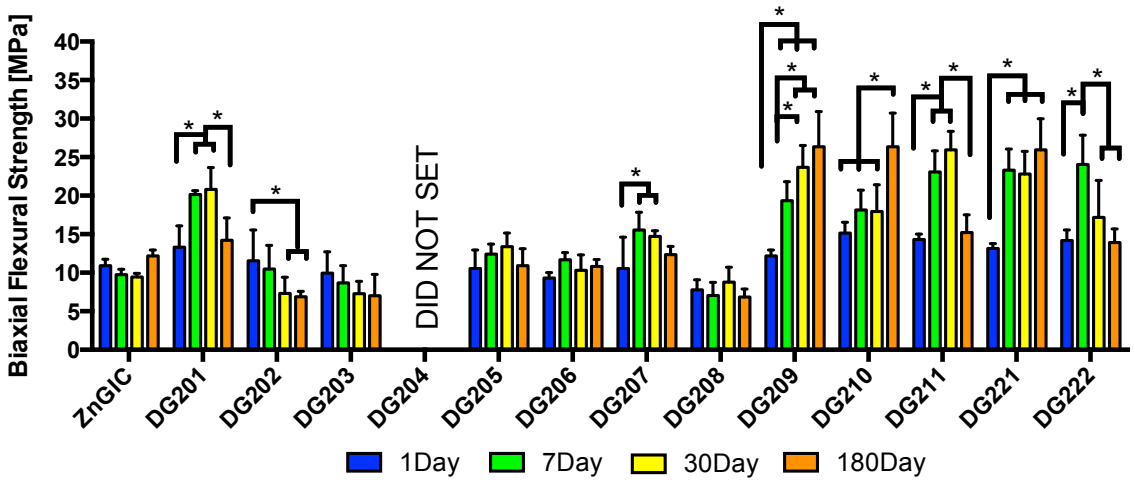

Figure 28: Biaxial flexural strengths of DG series GICs. DG204 did not set, thus could not be evaluated. * denotes statistically significant differences ($p < 0.05$).

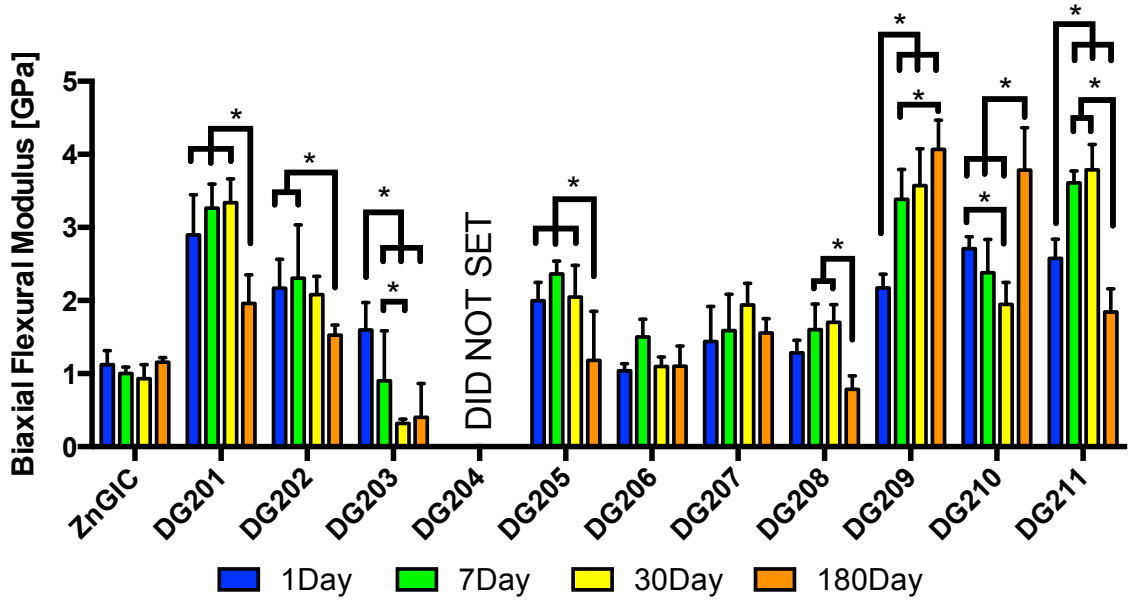

Figure 29: Biaxial flexural modulus of DG series GICs. DG204 did not set, thus could not be evaluated. * denotes statistically significant differences ($p < 0.05$).

DG302, a new formulation of glass, was interpolated from within the DG design space and used to validate the DoM handling models present within Chapter 6 and the mechanical models listed in Appendix 1. This composition was observed to have the best combination of handling and mechanical properties (Table 9) for use as injectable bone cement for PVP or KP of any cement composition produced in this work, where ideal cements are required to be injectable for a minium of 5-10 minutes, combined with lasting compressive strength in excess of 30 MPa. Further details regarding DG302 and the validation process are provide in Appendix 1.

Table 9: DG302 glass composition (mol. fraction) and cement properties when mixed at 1:0.75 ratio with 50 wt% aq. solution of PAA Mw = 12,500 g mol^{-1}. Data presented as mean with standard deviation in parentheses.

Composition							
	ZnO	GeO_2	SiO_2	CaO	SrO	ZrO_2	Na_2O
DG302	0.36	0.269	0.206	0.09	0.04	0.0175	0.0175
Handling Characteristics [min:sec]							
Working Time	6:41 (0:04)						
Setting Time	50:47 (0:50)						
Injectability: Measured as the force applied to plunger of 1cc syringe with a 4-inch 12G cannula. 5 minutes after the initiation of cement mixing, the plunger of syringe was loaded at 60mm/min for 10s repeated every minute for 10 minutes using an Instron 3344 mechanical test unit with 2kN load cell (n=3). Blue line is avg. max thumb force (36 N) [353] Test completed by L. Kiri	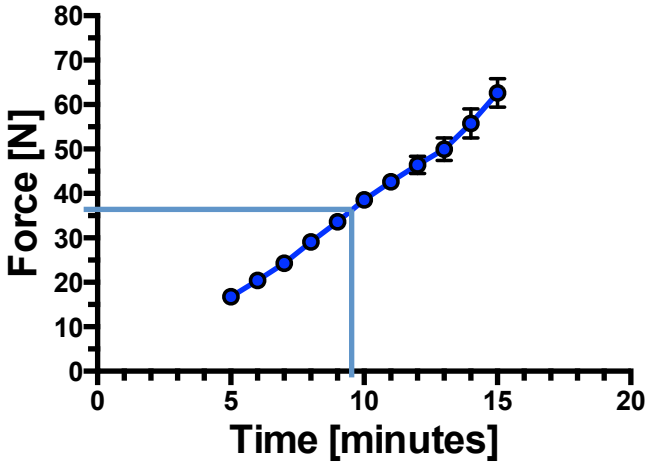						
Mechanical Properties [MPa]							
Time Point	**1 day**		**7 days**		**30 days**		**180 days**
Compression Strength	51.1 (1.5)		69.5 (3.7)		73.9 (8.1)		78.8 (12.5)
Biaxial Flexural Strength	13.1 (0.6)		23.3 (2.5)		22.8 (3.3)		25.9 (4.3)
Biaxial Flexural Modulus	2120 (300)		3320 (388)		2820 (1010)		4275 (263)

Chapter 7: Evidence of a Complex Species Controlling the Setting Reaction of Glass Ionomer Cements

7.1 Rationale

The evidence presented in Chapter 6 identified that Ge, not Zr, is the critical component that enables the balancing of handling and mechanical properties in zinc silicate GICs. Ge delays the GIC setting, whilst maintaining mechanical properties. Although the mechanical data indicate Zr to be useful in maximizing strength when it was included in minimal amounts, Zr alone was not capable of balancing this strength with practical handling characteristics. Ge exhibits stronger evidence to support the approach that manipulating glass reactivity by varying the network former can control GIC properties.

Consequently, the objective of this chapter is to elucidate the mechanism(s) responsible for the profound impact Ge has on the setting reaction of zinc silicate GICs. Given the innate complexities of the DoM methodology and the unique behavior of Ge-containing GICs to decouple handling characteristics from mechanical properties, it was determined that a more simplified approach was necessary to identify the potential mechanisms involved. Therefore, a "one-variable-at-a-time" approach is employed to investigate the incremental replacement of SiO_2 with GeO_2 as the primary network-forming component in a quaternary (1-x SiO_2, x GeO_2, 0.36 ZnO, 0.16 CaO) glass series. This glass series was used to explore various aspects of the GIC setting reaction, including glass degradation, formation of the GIC matrix, and cement rheology.

7.2 Introduction

Glass ionomer cements (GICs) demonstrate an innate relationship between handling characteristics and mechanical behavior. Both of these properties are highly dependent on

the reactivity of the glass, and altering one often has a reciprocal effect on the other [49, 52, 218, 354]. GICs are the product of mixing a basic glass powder with an aqueous solution of polyalkenoic acid. Initial setting of the cement results from the formation of a polysalt matrix produced as multivalent cations (*e.g.* Al^{3+}, Ca^{2+}, Zn^{2+} leached from the acid degradable glass) crosslink the polyanion chains of the deprotonated acid [45]. After the initial set (*i.e.* gelation), GICs continue to harden over time due to continued crosslinking [232] and as hydrated silicate or phosphate networks are formed [198, 355]. This setting reaction serves as the origin for the innate relationship between the handling and mechanical properties of GICs. Setting times can be adjusted by controlling the rate and the extent to which the glass degrades, but mechanical integrity is dependent on the number and strength of the metal-carboxylate crosslinks within the matrix [45]. This imbalance is present in both conventional GICs (*i.e.* those comprising aluminosilicate glasses) used in dentistry [218, 223, 356], and aluminum-free GICs (*e.g.* zinc silicates) proposed for various orthopaedic applications [49, 54, 56, 58, 257, 290]. For conventional cements, this issue has been practically circumvented through application of fluoride-containing glasses, or the use of (+)-tartaric acid as an additive in GIC systems [198]. However for the aluminum-free compositions, this correlation has yet to be adequately addressed and represents a fundamental obstacle towards their clinical applicability.

Chapter 6 reported the unexpected findings that a full replacement of SiO_2 with GeO_2 in zinc silicate glasses significantly extends the setting time of GICs while maintaining their strength [60]. These slow setting and high strength characteristics have potential implications to the use of GICs in both dental and orthopaedic applications, but

are completely counterintuitive given the innate relationship between handling and mechanical performance described above. Current knowledge regarding the impact of germanium (Ge) on the GIC setting reaction is limited, as only discrete data derived from the assessment of handling characteristics (*i.e.* working and setting times) of cement systems comprising overly complex glasses have been obtained [60, 357, 358]. The present chapter addresses this knowledge gap by examining various stages of the cement setting reaction over time in simplified Ge-modified zinc silicate GIC systems, specifically: (i) the assessment of glass reactivity by profiling glass degradation rates under simulated setting conditions; (ii) profiling in situ structural changes as the GIC matrix is formed using attenuated total reflectance Fourier transform infrared spectroscopy; (iii) directly measuring the progression of GIC setting using rheology to obtain viscosity profiles; and (iv) monitoring the post-gelation hardening of the GIC matrix by measuring the biaxial flexural strengths. The objective of this chapter is to elucidate the mechanism(s) associated with the delayed setting of GICs containing Ge.

7.3 Materials and Methods

7.3.1 Glass Synthesis

Five experimental glasses (BD1-5) were synthesized with molar compositions of: (0.48 – x) SiO_2, xGeO_2, 0.36 ZnO, 0.16 CaO; where x = 0, 0.12, 0.24, 0.36, 0.48 mol. fraction. Analytical grade reagents silica, germanium dioxide, zinc oxide and calcium carbonate (Sigma Aldrich, Canada) were weighed out and blended together for 1 h in a mechanical mixer. Post-mixing, powder compositions were packed into platinum crucibles (Alfa-Aesar, USA) and fired (1500 ˚C, 1 h) in a high temperature furnace (Carbolite RHF 1600, UK) then subsequently quenched in water at roomd temperature. The resultant glass frit

was dried overnight (120 ˚C) then ground in a planetary ball mill (Fritsch Pulverisette 7, Germany) and sieved to retrieve a particle size less than 45 μm. All glass powders were subsequently annealed in platinum crucibles in a high temperature furnace at T_g – 30 ˚C for 3 hours and left to furnace cool (T_g provided in Table 10). All prepared glass powders were stored in a desiccator for subsequent analysis.

7.3.2 Differential Scanning Calorimetry

The glass transition temperature (T_g) for each glass composition was determined using a differential scanning calorimeter (Netzsch STA 409PC, USA). Approximately 30 mg of glass powder was placed into a platinum closed pan with the reference pan left empty. Samples were heated at 10 ˚C min^{-1} to 1000 ˚C. Proteus Thermal Analysis software (Netzsch Instruments, USA) was used for data analysis with T_g taken as the point of inflection.

7.3.3 X-ray Diffraction

Prior to heat treatment, glass powders were analyzed with an x-ray diffractometer (Bruker, D8 Advanced, Canada) equipped with a LynxEye silicon strip detector and Cu Kα radiation generated at 40 kV and 40 mA. Specimens were pressed in round polymethyl methacrylate holders and exposed to x-ray beam incident at 5˚ with the detector collecting scatters between $5^\circ < 2\theta < 100^\circ$ over 950 seconds.

7.3.4 Glass Ion Release Profiles Under Simulated Setting Conditions

To simulate the setting process of a GIC, each experimental glass was mixed with acetic acid for 0.5, 1, 2, 5, 10, 15, 30, and 60 minutes and concentration of released ions were subsequently measured, similar to the method described by Wasson [359]. Extracts (n=3

per glass per time point) were prepared by mixing 0.15 g of annealed glass powder with 10 mL of 2.8 M aqueous acetic acid (Sigma-Aldrich, Canada), with a starting pH of 2.2 (*i.e.* typical pH level at the start of GIC mixing [360]) in 15 mL polystyrene tubes. Samples were mixed using a rotational mixer (Rotamix, ATR Inc., USA) at 1 Hz for the time periods of 0.5, 1, 2, 5, 10, 15, 30, and 60 minutes at 22 ˚C, then immediately centrifuged for 1 minute after which 5 mL of extract was drawn off the top of each sample for ICP-OES analysis.

7.3.5 ICP-OES

Ion release extracts were analyzed using inductively coupled plasma optical emission spectroscopy (ICP-OES). Extracts were diluted at a 1:100 ratio in 2% aqueous nitric acid (Sigma-Aldrich, Canada) for ICP-OES analysis. An Optima DV8000 ICP-OES system (Perkin-Elmer, Canada) was calibrated with certified solutions (Perkin-Elmer, Canada) and used to measure the concentration of Si, Ge, Zn^{2+}, and Ca^{2+} ions released into the acetic acid solution. From the measured concentrations of each ion, the percent release of each component was calculated according to equation 20, where the numerator is the concentration of Y as measured in the extract solution and the denominator is the theoretical mole fraction of Y (Table 10), where Y represent either Ge, Si, Zn^{2+}, or Ca^{2+}. The release profiles of each ion were modeled as one-phase associations with the y-intercept set to zero using statistical software (Prism 6, Graph Pad, USA).

$$\%\, release\ of\ Y = \frac{mol^{Y}_{extract}}{mol^{Y}_{glass}} \times 100 \qquad \textbf{Equation 20}$$

7.3.6 Cement Preparation

Cements derived from BD glasses were prepared by mixing annealed glass powders with 50 wt% aqueous solution of polyacrylic acid (PAA) with a molecular weight of 12,500 g mol^{-1} (Advanced Healthcare, UK) and deionized water at a ratio of 1:0.75. Mixing was complete within 30 seconds. The naming convention for these cements was cBDZ, where Z identifies the parent glass (*e.g.* cBD1 is the cement derived from BD1 glass).

7.3.7 ATR-FTIR of Setting GIC

Attenuated total reflectance Fourier transform infrared spectroscopy (ATR-FTIR) was used to examine the structure of cements as they set. Ninety seconds from the commencement of mixing cement components, their contiguous pastes were placed directly on a temperature controlled diamond ATR element (Golden Gate, Specac, USA) maintained at 22 ˚C. Cement structures were probed using an infrared spectrometer (Tensor 27, Bruker, USA); the final spectra at each time point were recorded as the average of 17 runs collected over one minute. Each run consisted of 32 scans in the mid-IR region (400-4000 cm^{-1}) at a resolution of 4 cm^{-1}. Spectra were collected at 2, 5, 10, 15, 30, and 60 minutes after the commencement of cement mixing. The resulting spectra (*i.e.* Figure 34) represent the average of n=3 replicates for each cement composition. To identify and isolate potential interactions between Ge and PAA, both aqueous PAA alone and aqueous PAA mixed with crystalline powder GeO_2 (Sigma Aldrich, Canada), in accordance with the methodology of section 7.3.6 were examined with ATR-FTIR under the conditions described above.

To assess the progress of GIC setting, the ratio between *c.* 1700 cm^{-1} and *c.* 1550 cm^{-1} band heights were calculated from each spectrum identified in Figure 34, where the

band heights were taken as the absorbance magnitudes of the spectra with a horizontal baseline. For clarity, each *spectrum* is averaged from three *replicates*, where each replicate comprises 17 *runs*, and each run consists of 32 *scans*. The 1700 cm^{-1} band corresponds to C=O in the un-reacted carboxyl (COOH). The bands in the range of 1537-1562 cm^{-1} correspond to metal-carboxylate structures ($COO^{-}M^{z+}$) identified in Table 3. The difference in the $COO^{-}M^{z+}$/COOH band height ratio, as a function setting time (at 2, 5, 10, 15, 30, and 60 minutes), was defined as per equation 21 (graphically represented in Figure 30).

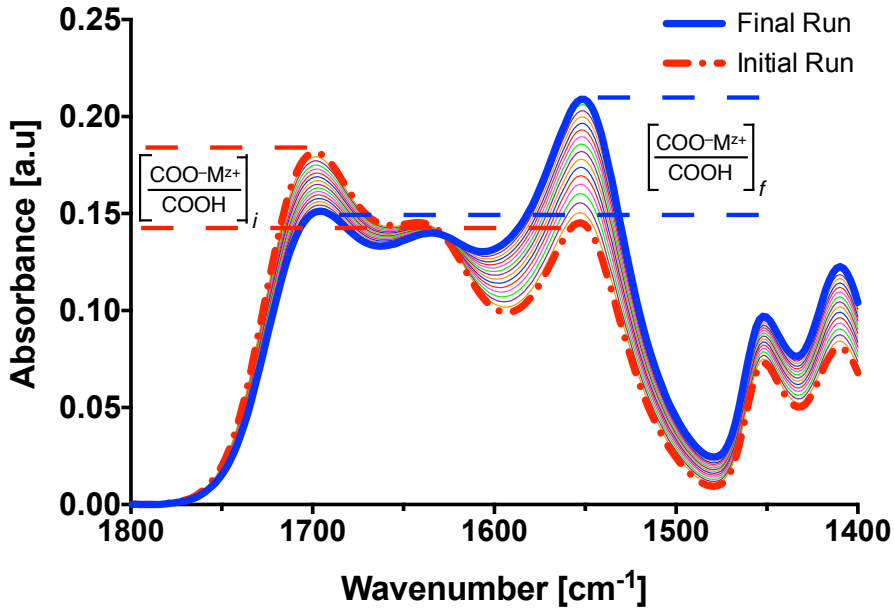

Figure 30: An example of the shift in absorbance height of COOH (*c.* 1700 cm^{-1}) and $COO^{-}M^{z+}$ (*c.* 1550 cm^{-1}) bands across the 17 runs collected over a 1-minute acquisition during ATR-FTIR probing of GIC structure undergoing setting, in this plot cBD1 at 2 minutes. The difference in the $COO^{-}M^{z+}$/COOH band height ratio is evident when comparing the initial run (dashed red line) with the final run (thick blue line).

$$Rate\ of\ COO^{-}M^{z+}\ formation = \frac{\left[\frac{COO^{-}M^{z+}}{COOH}\right]_{final} - \left[\frac{COO^{-}M^{z+}}{COOH}\right]_{initial}}{1\ minute} \qquad \textbf{Equation 21}$$

Where,

$$\left[\frac{COO^{-}M^{z+}}{COOH}\right]_{initial} = ratio\ of\ run\ 1$$

$$\left[\frac{COO^{-}M^{z+}}{COOH}\right]_{final} = ratio\ of\ run\ 17$$

7.3.8 Rheology

Rheological profiles (n=3) of each GIC were measured using an oscillating constant stress rotational rheometer (Bohlin CS Rheometer, Malvern, UK) equipped with Ø20 mm parallel plates. After mixing, the cement pastes were spatulated onto the fixed lower plate of the rheometer. The top plate was lowered to a gap height of 1 mm and excess cement was trimmed away within 3 minutes from the start of mixing. Immediately following cement trimming the rheology program was initiated, applying a 3000 Pa shear stress to the cement at a frequency of 1 Hz and a constant temperature of 22 ˚C. Measurements were recorded every 10 seconds until the complex viscosity reached steady state or a maximum elapsed time of 60 minutes, whichever came first.

7.3.9 Biaxial Flexural Strength

The biaxial flexural strengths (BFS) of the cBD series GICs were determined according to the methods presented by Williams *et. al*. [344]. Teflon molds (Ø15 x 1 mm) were filled to excess with cement, covered with acetate, and then clamped between two stainless steel plates and incubated (37 ˚C, 1 h). Upon removal from the oven, the assembly was broken down, cement flash removed, and samples (n=5) placed in 10 mL of deionized water and incubated for a further 23 h at 37 ˚C. After incubation, samples

were immediately placed on a 3-point support ring and loaded at 1 mm min^{-1} using an Instron 3344 mechanical testing system with a 2 kN load cell. BFS was calculated according to equation 19 where P is the applied load (N), with sample thickness t (mm) and r is the support ring radius (mm).

$$BFS = \frac{P}{t^2}\left[0.63 \ln\left(\frac{r}{t}\right) + 1.156\right] \qquad \textbf{Equation 19}$$

7.3.10 Double Torsion Fracture Toughness

The double-torsion (DT) test method (Figure 31) has been used extensively in the GIC literature to evaluate fracture toughness (K_{IC}) [232, 235, 237, 242, 252]. Polyvinylsiloxane (Kerr Corporation, USA) molds were cast from an aluminum plate (Figure 32a) with the same dimensions (25 x 65 x 3.5 mm) as reported by Hill [237], inclusive of the groove with 0.5 mm depth cut down the center aluminum cast, to produce a defect along the length of the sample (Figure 32b). Molds were filled to excess with cement, covered with an acetate sheet and incubated at 37 ˚C under the uniformly disturbed weight of a glass slab (10 x 20 x 1.5 cm) for 1 h. Samples were removed from

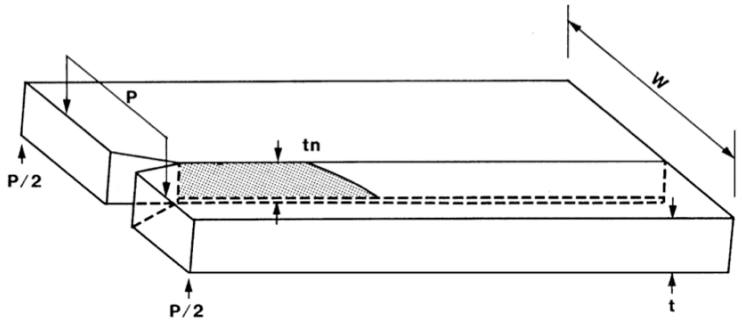

Figure 31: Schematic of double torsion fracture toughness test specimen, from Fennel and Hill 2001 [235].

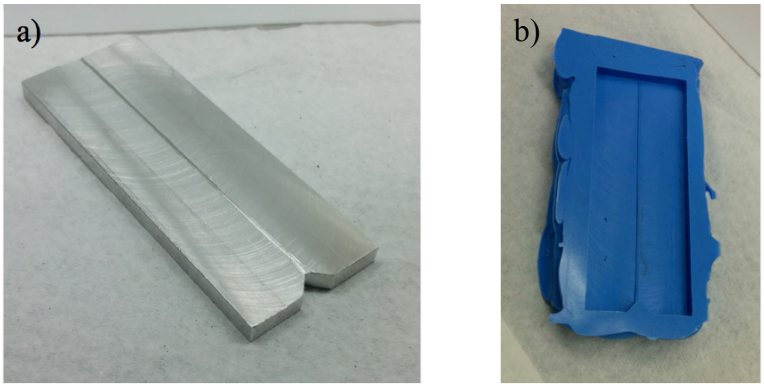

Figure 32: Double torsion fracture toughness (a) sample cast and (b) mold.

the mold, placed in petri dishes with 25 mL of deionized water, sealed with Parafilm (Bemis Company, USA), and incubated for 24 h at 37 ˚C. After the incubations period, samples removed from the petri dishes and a sharp slot was gently cut into the notch with a scalpel. Samples were positioned on a DT fracture toughness test fixture (based on that of Shyam and Lara-Curzio [361]) with four 6 mm steel ball bearing supports and loaded by two 3 mm steel ball bearing at 0.1 mm min^{-1} using an Instron 3344 mechanical testing system. Samples were kept hydrated by placing a piece of filter paper saturated with deionized water on the top surface, which was kept clear of the applied point loads. Load-displacement data was recorded and the K_{IC} was calculated using equation 22 [237], where P_c is the maximum load, W_m is the moment arm of test fixture, ν is the passion ratio (*i.e.* assumed to be 0.3), W is the sample width, t is the sample thickness, and t_n is the sample thickness in the groove. Each composition was tested in triplicate except cBD1, which was too reactive and set prior to proper filling of the mold and prevented the assessment of K_{IC}.

$$K_I = P_c W_m \left(\frac{3(1+\nu)}{W t^3 t_n}\right)^{\frac{1}{2}} \qquad \textbf{Equation 22}$$

7.3.11 Statistical Analysis

Statistical analysis of experimental results was conducted using Prism 6 (Graph Pad, USA). The BFS results were analyzed using one-way analysis of variance (ANOVA), while ICP and ATR-FTIR results were analyzed using two-way ANOVA. Tukey post-hoc tests were used to identify any statistically significant differences amongst measured results ($p<0.05$).

7.4 Results

7.4.1 Glass Synthesis

BD glasses were confirmed as amorphous using X-ray diffraction, lacking any identifiable crystalline species. Glass transition temperatures (T_g) (as per Table 10) was observed to linearly decrease, proportional to decreasing Si:Ge ratio ($T_g = -155X + 672$, $R^2 = 0.992$).

Table 10: Composition of 5 experimental BD series glasses (mol. fraction) with corresponding glass transition temperatures (T_g).

	Si : Ge Ratio	SiO_2	GeO_2	ZnO	CaO	T_g [˚C]
BD1	1:0	0.48	0	0.36	0.16	673
BD2	3:1	0.36	0.12	0.36	0.16	653
BD3	1:1	0.24	0.24	0.36	0.16	631
BD4	1:3	0.12	0.36	0.36	0.16	620
BD5	0:1	0	0.48	0.36	0.16	597

7.4.2 Glass Ion Release Profiles Under Simulated Setting Conditions

It was observed that decreased Si:Ge ratio (*i.e.* increased GeO_2 content) significantly increased the rate of release of all ions from the glass (Figure 33a-e). This observation is

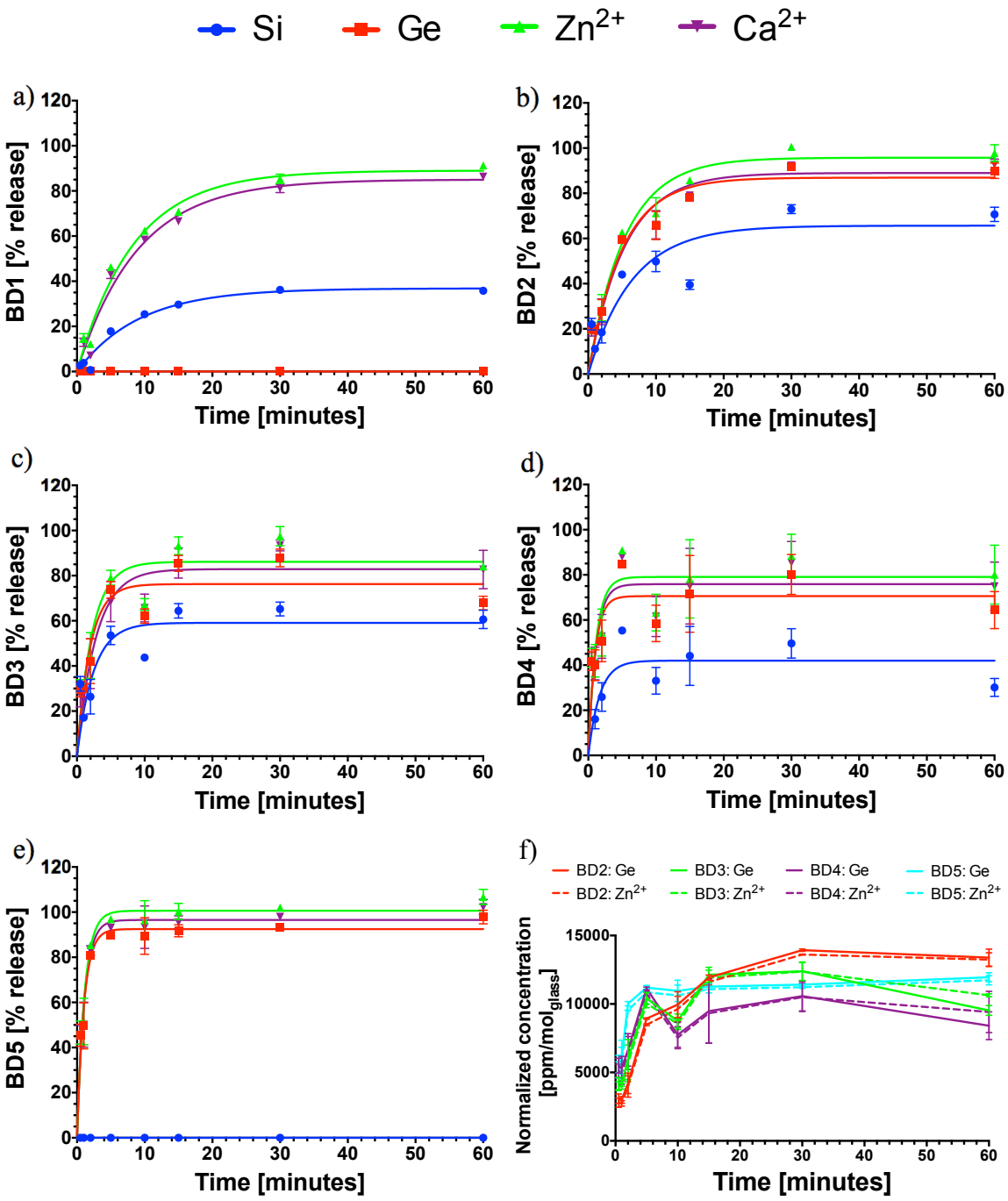

Figure 33: Glass ion release profiles (mean ± S.D.) from (a) BD1, (b) BD2, (c) BD3, (d) BD4, and (e) BD5 glass compositions (Si:Ge ratios as follows: BD1 1:0; BD2 3:1; BD3 1:1; BD4 1:3; BD5 0:1). Lastly, (f) illustrates normalized Ge and Zn^{2+} release concentration scaled to account for the discrepancies in mole fractions of GeO_2 and ZnO in BD2-5 (mean ± S.D.). BD1 is not included in (f) because it does not contain Ge. In BD2-5 at all times points, the normalized Ge and Zn^{2+} concentrations were statistically equivalent.

Table 11: Summary of the one phase association curve fits with associated R^2 values for glass ion release data. Curve fits are presented as best fit values with 95% CI in parentheses.

		Half-time [minutes]	Plateau [% release]	R^2
Si	BD1	6.32 (5.3 – 7.9)	36.8 (34.3 – 39.4)	0.9665
	BD2	4.74 (3.1 – 8.1)	65.7 (56.5 – 74.8)	0.7630
	BD3	1.69 (1.2 – 3.1)	59.1 (52.5 – 65.7)	0.6516
	BD4	1.16 (0.7 – 3.8)	42.0 (35.7 – 48.3)	0.4537
	BD5	–	–	–
Ge	BD1	–	–	–
	BD2	3.45 (2.8 – 4.4)	86.9 (81.5 – 92.4)	0.9404
	BD3	1.36 (1.0 – 2.0)	76.3 (70.2 – 82.4)	0.7968
	BD4	0.68 (0.5 – 1.3)	70.6 (63.6 – 77.5)	0.4815
	BD5	0.70 (0.6 – 0.9)	92.5 (88.8 – 96.2)	0.8874
Zn^{2+}	BD1	5.77 (5.1 – 6.6)	89.0 (85.1 – 93.0)	0.9835
	BD2	3.75 (3.1 – 4.7)	95.6 (90.1 – 101.4)	0.9509
	BD3	1.55 (1.2 – 2.3)	86.1 (79.7 – 92.6)	0.8351
	BD4	0.79 (0.6 – 1.4)	79.1 (71.6 – 86.6)	0.5631
	BD5	0.76 (0.6 – 0.9)	100.6 (96.6 – 104.6)	0.9019
Ca^{2+}	BD1	6.17 (5.3 – 7.4)	85.0 (80.3 – 89.8)	0.9765
	BD2	3.71 (3.1 – 4.7)	89.0 (83.6 – 94.4)	0.9486
	BD3	1.94 (1.5 – 2.9)	82.9 (76.2 – 89.6)	0.8459
	BD4	0.77 (0.5 – 1.3)	75.9 (68.7 – 83.0)	0.5607
	BD5	0.74 (0.6 – 0.9)	96.5 (92.7 – 100.4)	0.8961

evinced by the shift to burst-like release of all ions as the Si:Ge ratio transitioned from 1:0 (BD1) to 0:1 (BD5). From Table 11, it can be seen that as the Si:Ge ratio decreases, the half-times (the time to reach half of the plateau percent release) falls proportionally (BD1 > BD2 > BD3 = BD4 = BD5; $p<0.05$).

An interesting observation was made during the analysis of ion release concentrations for BD4 (*i.e.* where Ge and Zn are present in equimolar concentrations). It was noted that Zn^{2+} and Ge ions were released at equivalent concentrations at each time point under the simulated setting conditions utilized in this experiment (Figure 33f). Based on this observation, a comparison of the release data of the other compositions that

contained both Ge and Zn was performed (Figure 33f). From this comparison, it was observed that when Zn^{2+} and Ge release concentrations were scaled to account for variance in molar abundance, by normalizing to ZnO and GeO_2 mole fractions of the glass composition, their release concentrations were directly comparable. This type of relationship was only observed in Ge and Zn^{2+} release data.

7.4.3 ATR-FTIR of Setting GIC

The spectra presented in Figure 34 with associated reference structures and band assignments (Table 12) highlight the structural changes within the cement matrices during setting. In the initial stages, the dominant bands are associated with the structures of the polyacrylic acid: (i) *c.* 1700 cm^{-1}, which represents C=O in available carboxyl (COOH) functional groups; (ii) 1452cm^{-1} assigned to C–H_2 scissor, and (iii) a broad hump near *c.* 1250 cm^{-1} representing the C–O stretch [362, 363]. As the setting reaction proceeds, three bands develop that are common to all experimental GICs: (i) *c.* 1550 cm^{-1} corresponding to the asymmetric vibration of carboxylate groups that have reacted with Zn^{2+} or Ca^{2+} cations ($COO^{-}M^{z+}$) [256, 364]; (ii) *c.* 1405 cm^{-1}, characteristic of symmetric stretching of reacted $COO^{-}M^{z+}$ groups [365, 366]; and (iii) a third unassigned band which

Table 12: Significant reference structures and band assignments associated with cBD GICs.

Reference Structures*	Wavenumber [cm^{-1}]	Reference
Asymmetric Chelating Bidentate (Ca^{2+} - $2COO^{-}$)	1541-1547	[364]
Asymmetric Ionic (Zn^{2+} - $2COO^{-}$)	1562	[256]
Asymmetric Chelating Bidentate (Zn^{2+} - $2COO^{-}$)	1554-1548	[256]
Asymmetric Unidentate (Zn^{2+} - $2COO^{-}$)	1537	[256]
Amorphous SiO_2	1000-1200	[294, 362, 367]
Quartz-like GeO_2	886, 958	[368]

**Schematics of all structures are provided in* Figure 17*, pg. 64, and in the associated references.*

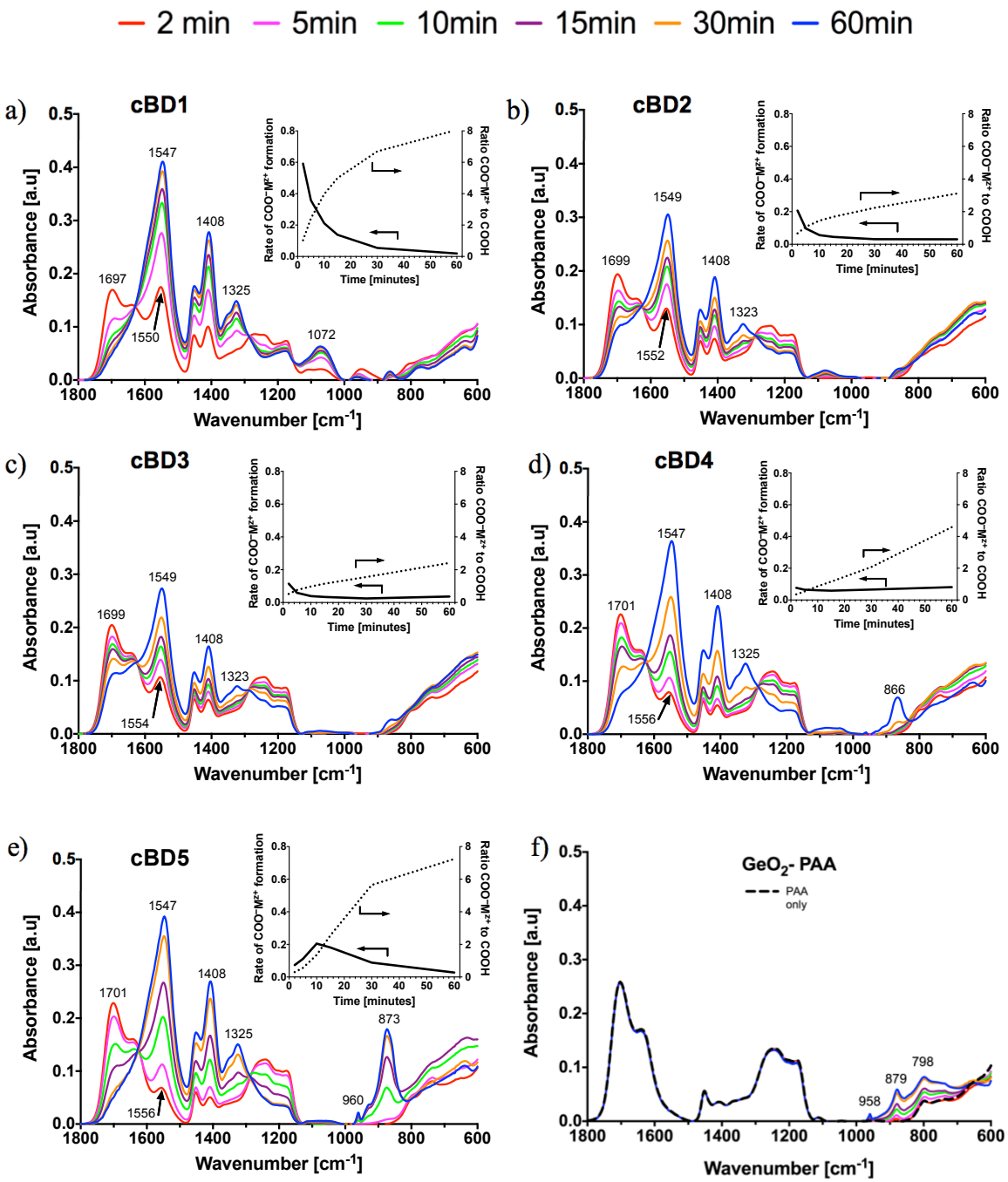

Figure 34: The plots in (a)-(e) depict FTIR spectra as a function of time for cBD series GICs. The plot in (f) depicts spectra of PAA only (dashed line) and the GeO_2 – PAA mixture. The subplots in the upper right of each spectra depict (i) the rate of change of these ratios over time (solid line) and (ii) the ratio of *c.* 1550 cm^{-1} to *c.* 1700 cm^{-1} band heights (dotted line).

develops at *c.* 1325 cm^{-1}. For completeness the band at *c.* 1070 cm^{-1} corresponds with the Si-O-Si bridges in the glass phase in cBD1 (*i.e.* Si:Ge 1:0) [294, 362, 367]. In cBD4 (*i.e.* Si:Ge 1:3) and cBD5 (*i.e*. Si:Ge 0:1), bands at 866 cm^{-1}, 873 cm^{-1}, and 960 cm^{-1} were observed. These bands correspond well with those present in Figure 34f (*i.e.* PAA and PAA-GeO_2) and are likely associated amorphous GeO_2 given their similar resonances to crystalline structures such as rutile and quartz-like GeO_2 [368]. Temporal changes in band intensities represent the progression of the acid-base reaction as the GICs sets. As Zn^{2+} and Ca^{2+} ions form salt bridges that crosslink the polyanion chains, the *c.* 1700 cm^{-1} band height decreases concurrent with an increase in the band heights of asymmetric and symmetric metal carboxylate bonds (*c*. 1550 cm^{-1} and *c.* 1405 cm^{-1}, respectively).

It is clear from the 2 minute spectra from Figure 34 that Ge impacts GIC formation at the earliest stages of setting: as Ge replaces Si, the *c.* 1550 cm^{-1} band drops in height and shifts to higher wavenumber, indicating (*i*) fewer crosslinks precipitating in the cement matrix and (*ii*) those which have precipitated are more ionic in nature. Further progression of the setting reactions was tracked by changes to the $COO^{-}M^{z+}$/COOH ratio; *i.e.* the ratio between *c.* 1550 cm^{-1} to 1700 cm^{-1} band heights (Figure 34a-e subplots). At 60 minutes, the $COO^{-}M^{z+}$/COOH ratios ranked as follows: cBD1 = cBD5 > cBD4 > cBD2 = cBD3, with cBD1 and cBD5 (Si:Ge 1:0 and 0:1) forming the most crosslinks, while cBD2 and 3 (Si:Ge 3:1 and 1:1) form the least. As Si:Ge ratio decreases two features of the setting reaction were evident. In the first instance, the ratio of $COO^{-}M^{z+}$/COOH appears to progress towards a decreased concentration of crosslinked carboxylate groups between cBD1 and cBD3; conversely this behavior reverses as the cement composition transitions from cBD3, to cBD4, to cBD5. In the second instance,

the rapid formation of crosslinks observed for cBD1 (*i.e.* Si-only glass) is replaced with slower, steady-state crosslink formation for cBD2-4 over the 60 minute period of observation. An interesting exception is noted where Si has been fully replaced with Ge (*i.e.* cBD5). Here, an *increase* in crosslinking rate during the first 10 minutes is observed, followed by a rate reduction to steady state formation of crosslinks thereafter. It is further noted that the maximum crosslinking rate of cBD5 (*i.e.* Ge-only glass) is at least three times less than that of cBD1 (*i.e.* Si-only glass).

7.4.4 Rheology

Figure 35 depicts the rheological profiles of the experimental GICs as they transitioned from viscous pastes to elastic solids (*i.e.* the gelation process) with relatively constant viscosities (except cBD3, which had not achieved a steady state viscosity by the maximum allotted time of 60 minutes). As the Si:Ge ratio decreased from 1:0 (cBD1) to

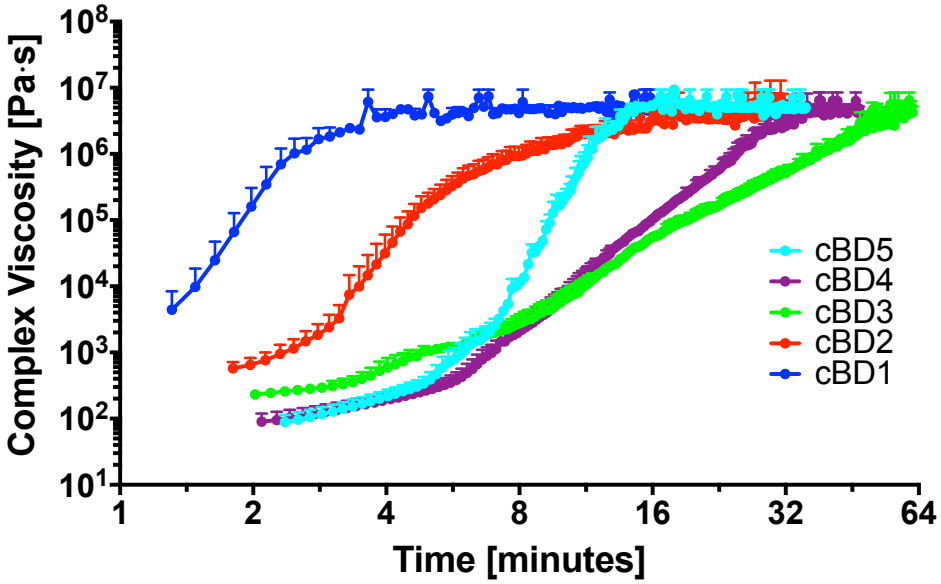

Figure 35: Change in complex viscosities (mean + SD) over time of the cBD series GICs during the setting process (Si:Ge ratios as follows: cBD1 1:0; cBD2 3:1; cBD3 1:1; cBD4 1:3, cBD5 0:1).

1:1 (cBD3), the rate at which gelation occurred was slower. However, a further reduction in the Si:Ge reversed this trend and sharpened the setting profiles, with cBD4 (Si:Ge 1:3) exhibiting a quicker increase in viscosity than cBD3, while cBD5 (Si:Ge 0:1) exhibited a faster gelation rate than cBD4. It was also noted that decreases in the Si:Ge ratio provided for a reduction in the initial viscosities of the cements, where cBD1 > cBD2 > cBD3 > cBD4, cBD5. Concurrently, cBD3, 4, and 5 experienced delayed initial gelation, with inflection points in their viscosity profiles at *c.* 5 minutes. By comparison, cBD1 and 2 exhibited rapid and almost immediate increases in viscosity. The ability of Ge to delay the onset of gelation appears to be maximized when SiO_2 and GeO_2 are included in the glass at equivalent mole fractions.

7.4.5 Biaxial Flexural Strength

The addition of germanium did not significantly change the strength of the cements, as the BFS of cBD2-5 were statistically similar to that of cBD1 (Si:Ge 1:0) (Figure 36). Comparing the compositions that contained Ge found cBD3, 4 and 5 (*i.e.* Si:Ge 1:1, 3:1, and 0:1, respectively) had statistically similar BFS values (13.2 – 13.9 MPa), which were all significantly greater than cBD2 (*i.e.* Si:Ge 3:1) at 10.5 MPa.

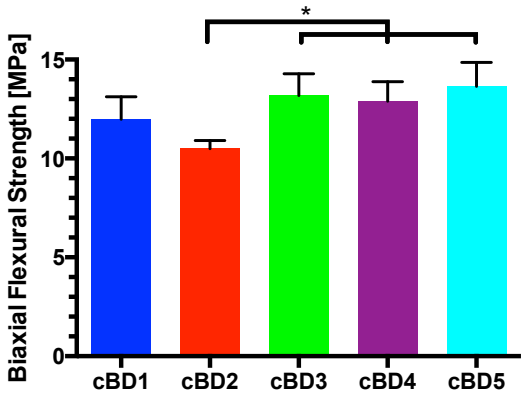

Figure 36: 24hr biaxial flexural strength of the cBD series GICs (mean + SD), * denotes statistically significant differences p < 0.05 (Si:Ge ratios as follows: cBD1 1:0; cBD2 3:1; cBD3 1:1; cBD4 1:3, cBD5 0:1).

7.4.6 Double Torsion Fracture Toughness

The 24 h fracture toughness (K_{IC}) of cBD GICs are depicted in Figure 37, which demonstrates that cBD3 (*i.e.* Si:Ge 1:1), had the highest resistance to crack propagation with a K_{IC} of 0.27 MPa $m^{1/2}$. The lowest K_{IC}, 0.17 MPa $m^{1/2}$, was demonstrated by cBD2 (Si:Ge 3:1), which was the quickest gelling cement of the four GICs tested. cBD4 and cBD5 (Si:Ge 1:3 and 0:1) were statistically similar at *c.* 0.22 MPa $m^{1/2}$. The cBD1 GIC set too quickly, which prevented the proper filling of the double torsion mold, therefore K_{IC} could not be measured for this composition.

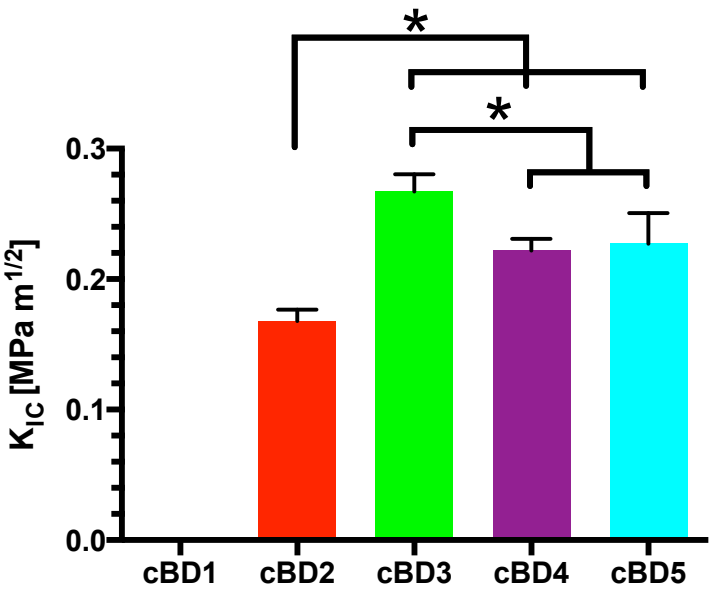

Figure 37: 24 h double torsion K_{IC} after of the cBD GICs (mean + SD). The fast setting behavior of cBD1 prevented sample preparation, thus K_{IC} could not determined. * denotes statistically significant differences $p < 0.05$ (Si:Ge ratios as follows: cBD1 1:0; cBD2 3:1; cBD3 1:1; cBD4 1:3, cBD5 0:1).

7.5 Discussion

The data provides clear evidence that germanium containing GICs have markedly different setting mechanisms compared to their silicon containing counterparts. The

design of this investigation revealed that this unique difference was due to the appreciable manifestation of a stage in the setting reaction that delays *but does not hinder* the crosslinking of the GIC matrix. The Si-based GIC (cBD1 Si:Ge 1:0) had the fastest gelation (*i.e.* initial set [45]). This behavior was attributable to the rapid formation of metal carboxylate crosslinks with more covalent-like character (Figure 34). Interestingly however, its contiguous glass (BD1) was observed to degrade the slowest of all five compositions (Figure 33a-e and Table 11). These results suggest that Zn^{2+} and Ca^{2+} cations (*i.e.* cations responsible for crosslinking the polyanion chains) derived from silicate glasses swiftly bond to available carboxylate groups, thus efficiently gelling the GIC matrix. This efficient crosslinking is contrasted by the behavior of the Ge containing compositions. For example, in the BD5 glass (Si:Ge 0:1), Zn^{2+} and Ca^{2+} ions were released 8 times faster than BD1, yet in its contiguous cement (cBD5) had (*i*) a lower initial viscosity relative to cBD1, and (*ii*) experienced a substantial delay in gelation (Figure 35). Concurrently, the structural data shows a low $COO^{-}M^{z+}$/COOH ratio for Ge containing GICs, indicating a higher proportion of unreacted carboxyl groups within the cement matrix. For completeness, it is also noted that the high wavenumber band positions of $COO^{-}M^{z+}$ structures in cBD5 indicate that the bonds present are more ionic in character at 2 min (Figure 34e). In contrast to conventional GICs, the delayed onset of gelation in Ge containing cements occurs despite the fast degradation of their related glasses. It appears reasonable to conclude, therefore, that cations released from Ge containing glasses (*i.e.* Ge, Zn^{2+}, Ca^{2+}) are liberated in a manner that suppresses their ability to precipitate and set the GIC matrix.

As the setting reaction proceeds, there is a sharp gelation in the cBD5 viscosity profile from 5 to 15 minutes. This coincides with an increasing rate of $COO^{-}M^{z+}$ formation resulting in rapid growth of the $COO^{-}M^{z+}$/COOH ratio and a trend towards more covalent-like crosslinks (*i.e.* lower wavenumber of $COO^{-}M^{z+}$ band) [256]. Although there exists obvious distinctions in the gelation profiles of the cBD1 (Si:Ge 1:0*)* and cBD5 (Si:Ge 0:1), once set their steady-state viscosities are similar and subsequent hardening leads to convergence of their structural characteristics (*i.e.* $COO^{-}M^{z+}$/COOH ratio, Figure 34a and e). Further manifestation of the structural similarities between cBD1 and cBD5 cements are their statistically similar biaxial flexural strengths (Figure 36), as initial GIC strength is heavily dependent upon the degree matrix crosslinking [232]. In fact, regardless of the setting behavior of Ge containing GICs, cBD2-5 all exhibit comparable levels of biaxial flexural strength to the Si based cement (cBD1). Thus, these results indicate that the Si:Ge ratio may be tailored to substantially alter GIC setting behavior with minimal impact to initial strength. Interestingly, the slowest setting cement (cBD 3 Si:Ge 1:1) also had the highest fracture toughness (additional details on the implications of this finding are provided in the general discussion of the work, Chapter 9, page 178). Therefore, slow setting of Ge containing GICs is not the result of delayed glass degradation, but rather the product of an alternative mechanism that delays, but does not obstruct, the crosslinking of the GIC matrix.

Wasson and Nicholson proposed the existence of $[Al_{13}O_4OH_{24}(H_2O)_{12}]^{7+}$ complex species as an explanation for the discrepancy between early release of Al^{3+} from the glass phase of alumniosilicate GICs and the late appearance of aluminum carboxylates in the GIC matrix [198, 359]. Accordingly, the existence of an ionic chemical complex may be

the alternative mechanism responsible for the slow setting behavior of Ge based GICs. The existence of an Al-complex in conventional GICs has yet to be proven with unequivocal experimental evidence. Most recently Munhoz *et al.* used ^{27}Al MAS-NMR and ^{27}Al 3QMAS-NMR to monitor the setting reaction of Fuji IX, an aluminosilicate GIC indicated for atrautmatic restorative techniques, from 5 minutes to 3 months [369]. In their ^{27}Al 3QMAS NMR examination of the GIC at 5 minutes, they observed a second site of tetrahedrally coordinated Al, *i.e.* Al(IV), in addition to the Al(IV) signal from the bulk glass. This second site was proposed to be part of the $[Al_{13}O_4OH_{24}(H_2O)_{12}]^{7+}$ structure, which is described as having one tetrahedral and twelve octahedral Al structures (Al(VI)) [369]. However the signal from the 12 Al(VI) sites was found to overlap with the Al carboxylates in the GIC, rendering the evidence for the presence of this Al complex inconclusive. In this study, evidence to suggest the existence of a chemical complex comes from: (i) the inverse relationship between the rates of ion release from the BD glasses and the speed of $COO^{-}M^{z+}$/COOH ratio growth in the cBD GICs, and (ii) the peculiar trait of BD series glasses to release Ge and Zn^{2+} proportionally. From the latter, it is hypothesized that the chemical complex species responsible for the slow setting of Ge containing GICs may be the product of interactions between Ge and Zn. Unfortunately, it is not possible from the current experimental results to determine the structural configuration or the genesis of any such complex. Neither Ge nor Zn are NMR active, as their respective NMR-active isotopes (*i.e.* ^{73}Ge and ^{67}Zn) have low gyromagnetic ratios, large quadrapole moments, and low natural abundances which yield spectra with low sensitivity and broad resonances [370, 371]. Nevertheless, the combination of the ion release, ATR-FTIR structural analysis, and

rheology data, yields strong experimental evidence to support the presence of a complex species which delays the onset of gelation without compromising the mechanical properties of the set cements. The fact that all metal carboxylate bands in the ATR-FTIR spectra (Figure 34) are consistent with those reported in the zinc-silicate GIC literature [57, 294] suggests that any potential complexes do not act as crosslinking species in the GIC matrix. Instead the complexes are likely transient species only, dissolving prior to crosslink formation to liberate their constituent cations, which subsequently precipitate as polysalts to form the GIC matrix (Figure 38). The significance of this interim step is it decouples glass reactivity from setting rate, which could have broad implications to the current and future clinical applications of GICs.

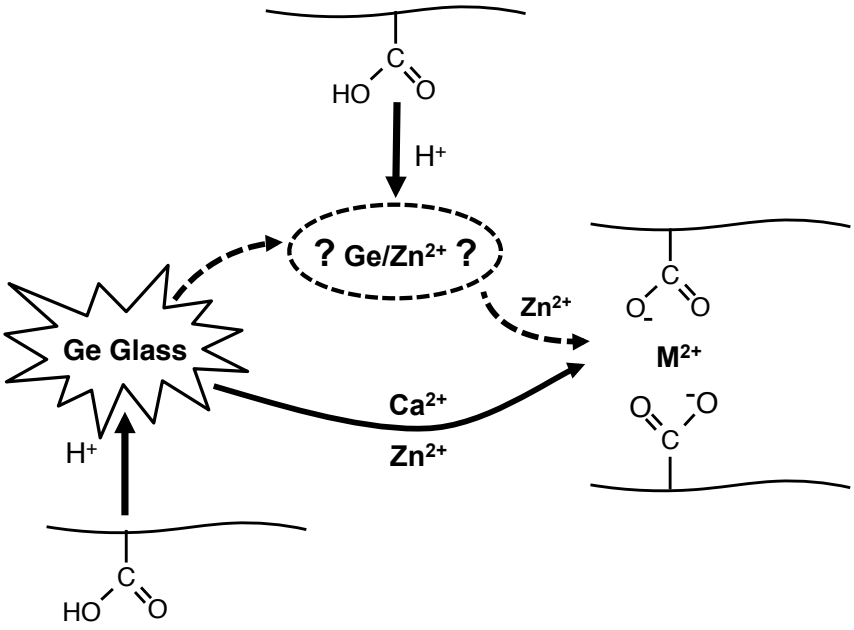

Figure 38: Schematic of Ge-based GIC setting reaction involving the potential ionic chemical complex. The complex species is hypothesized to involve interactions between Ge and Zn^{2+} ions.

Throughout the GIC literature there exists considerable evidence that demonstrates the opposing influence glass reactivity has on the GIC handling characteristics and mechanical performance [52, 58, 218, 354]. Glasses with low reactivity produce low viscosity cements that set slowly, but suffer from impaired mechanical performance due to an insufficient density of metal-carboxylate crosslinks in the GIC matrix. The use of more reactive glasses can improve the mechanical properties by increasing the crosslink density in the matrix. These more reactive glasses increase the rate of formation of the GIC matrix, which increases the viscosity of the cement paste and shortens the setting time. However, glasses can be too reactive and increase the viscosity to a point that prevents adequate mixing of the cement, which ultimately impairs the mechanical performance of the GIC. The ability of Ge containing glasses to decouple of glass reactivity from GIC setting rate disrupts these general tendencies, allowing more reactive glasses to produce strong GICs whilst maintaining a low viscosity during initial gelation. This combination of properties would be ideal for conventional aluminosilicate GICs currently used in the atraumatic restorative technique (ART). ART is performed in either a clinical or outreach setting as a minimally invasive intervention to prevent and/or stop the progression of dental caries [372]. This technique can be as basic as pressing high viscosity GICs into place using a finger for either preventative sealing of caries-prone pits and fissure, or the restoration and sealing of cavitated dentin carious lesions [373, 374]. High-viscosity GICs are preferred over their low- or medium-viscosity counterparts due to their better retention rates, mechanical performance, and wear properties [375]. However, low-viscosity GICs have demonstrated clinical success that has been attributed to their ability to penetrate deep into pits and fissures on the teeth

[376]. Thus, a GIC with high strength and low initial viscosity may improve efficacy of many dental procedures, including ART, by providing the mechanical performance required of a restorative material along with the ability to penetrate and seal pits and fissures of the tooth.

The ability to blend high strength with low viscosity would also benefit the development of aluminum-free GICs for future use in broader skeletal applications. One such indication is vertebral body augmentation, a palliative treatment for vertebral compression fractures. This is a minimally invasive procedure where bone cement is injected though percutaneous cannulae into the fracture for stabilization [10]. Si-based aluminum-free GICs developed for this procedure are impractical due to their rapid setting characteristics (*c.* 1-5 minutes [53, 56, 57, 257, 377]) that is well below the desired injection times for vertebral body augmentation that range from a minimum of 5 to 10 minutes [31]. The Ge containing GICs presented in this study, as well as those previously published by the authors (*i.e.* Chapter 6 and elsewhere) [60, 358], demonstrate significantly extended setting reactions that improve the viability of using Al-free GICs as injectable bone cements for broader skeletal applications, including vertebral body augmentation.

This investigation expands the utility of the Ge containing GICs by demonstrating that their setting profiles may be tailored through controlled manipulation of the Si:Ge ratio (Figure 35), whilst exerting minimal impact to their strengths (Figure 36). The evidence presented in Table 11 and Figure 33, along with the spectra in Figure 34 provide experimental evidence that Si-based glasses efficiently crosslink the GIC matrix, *i.e.* slow glass degradation with fast polysalt formation, while Ge-based glasses demonstrate

delayed crosslinking, *i.e.* fast glass degradation with slow polysalt formation. The authors speculate that the Si:Ge ratio controls whether efficient or delayed crosslinking is the dominant mechanism, which ultimately dictates GIC setting rate. In compositions where 1:0 > Si:Ge > 0:1 these two mechanisms may interfere with one another to decelerate GIC setting rate that reaches a minimum at Si:Ge 1:1. This evidence embodies the concept of complex formation as an alternative mechanism to be employed when designing glass compositions to produce GIC systems with specific handling performances.

7.6 Limitations and Future Work

The evidence presented in this chapter suggests a chemical complex species as the mechanism responsible for the delayed setting of Ge containing GICs. The authors acknowledge the limitations of this present chapter and the need for further experimentation to test the complex hypothesis. A key limitation of this chapter is the absence of structural data of the BD series *glasses*. Structural analyses of the glasses using techniques like Raman or FTIR spectroscopy may to provide insight as to whether or not the complex species originates in the glass network. The actual molar compositions of the BD series glasses were not experimentally determined and assumed to be the theoretical molar composition presented in Table 10. This assumption is likely the reason that the release percentage of some ions exceeds 100% in Figure 33a-e and Table 11. Additionally, further information regarding the complex species may be revealed through supplementary analysis of the ion release extracts from the glass degradation experiment. Unfortunately, the ionization process inherent to the ICP-OES technique limits the evidence of any potential complex species to only their possible constituents. Another

area that requires further experimentation is the mechanical analysis of the cBD series GICs. A more extensive mechanical investigation of these experimental cements regarding impact of Ge on the properties and structures of maturing GICs is pursued in Chapter 8.

7.7 Conclusion

This chapter shows that reducing the Si:Ge ratio in GICs based on SiO_2-GeO_2-ZnO-CaO glass chemistries delays, but does not hinder, crosslinking of the GIC matrix. The mechanism responsible for this delayed crosslinking is likely to be associated with a chemical complex species that imposes an additional stage to the GIC setting reaction. This complex species decouples the glass reactivity from cement setting characteristics without impairing mechanical performance. These findings indicate that the effects of complex species should be considered when designing GIC systems to achieve specific handling characteristics.

Chapter 8: Exploring the Unexpected Influence of the Si:Ge Ratio on the Molecular Architectures and Mechanical Properties of Al-Free GICs

8.1 Rationale

Functionally, it is understood that Ge balances the handling and mechanical properties of zinc silicate GICs. This is likely as a result of a complex species which delays but does not hinder the formation of the GIC matrix. However, there is insufficient evidence to develop robust composition-structure-property relationships regarding the mechanism(s) that control the mechanical properties of Ge-containing GICs over time. The mechanical data in Chapter 6 was complicated by DoM methodology, which obscured direct assessment of composition-property relationships. Although Chapter 7 provided information regarding the impact of Ge on GIC structure, this assessment was only conducted over the first 60 minutes post mixing. Therefore, to develop a more complete understanding of the mechanical performance of the Ge-containing GICs, the subsequent investigation explores the impact the Si:Ge ratio has on the mechanical properties and structure of the cBD GIC series over a period of up to 180 days. The mechanical assessment was confined to compressive strength and modulus testing. Although, there are concerns regarding the use of compression testing, such as interoperator error or complex failure mechanisms [378], the use of this test method in Chapter 8 was chosen on the basis of: (i) it is a common test methodology in ISO standards relating to the characterization of hard tissue cements [287, 288]; (ii) as a standardized test, it is applied throughout the literature, thus facilitating the comparison the strengths of the cBD GICs against others reported in the literature; and (iii) despite the aforementioned limitations,

Flemming *et al.* found compression testing to be reliable method [379], and Dowling *et al.* demonstrate the test has sufficient sensitivity to mechanically quantify changes in the GIC composition [215].

8.2 Introduction

Aluminum-free glass ionomer cements (GICs) have been proposed in the literature as an alternative to acrylic and ceramic-based cements for skeletal applications [49, 52, 257, 290, 380]. One such application is vertebral body augmentation, a minimally invasive procedure where bone cement is injected into fractured vertebral bodies as a palliative treatment for osteoporotic compression fractures [10, 32]. The most commonly investigated Al-free GICs in this regard comprise zinc-silicate ionomeric glasses; however, the quick setting nature (*c.* 1-3 min) of these cements render them impractical for vertebral body augmentation, as they are not injectable [49, 53, 56, 377]. A common philosophy that has been investigated in the literature to improve the handling characteristics of zinc-silicate GICs is to vary the network modifier and/or intermediate content of the glass in an effort to control its degradability [49, 54, 57, 58]. However, this approach has yet to produce a GIC that combines the requisite handling characteristics (minimum working times of 5-10 min) with sufficient levels of strength (compression strengths > 30 MPa) [31-33]. The origins of this imbalance are associated with an appreciable inverse relationship that is characteristic of silicon-based GICs, whereby extending the GIC setting reaction negatively impacts cement strength, or conversely improving GIC strength results in faster setting cements [49, 52, 54, 58, 295]. To overcome this limitation, Chapter 6 used a design of mixtures approach to investigate an alternative philosophy towards modulating the reactivity of zinc-silicate glasses, one in

which silicon (Si) is replaced as the primary network former in the glass with germanium (Ge) [60]. From Chapter 6, it was shown that the inclusion of Ge in zinc silicate glasses unexpectedly decoupled handling characteristics from strength. For example, the complete replacement of Si with Ge in the glass phase of these materials produced GICs with working times of up to 10 minutes and contiguous compression strengths of >35MPa at 24 h; thus, for the first time, Al-free GICs have become clinically viable as injectable bone cements for vertebral body augmentation [60].

To explore the mechanistic basis governing the chemistry that decouples the setting reaction from strength for Ge-based GICs, Chapter 7 used a simplified quaternary design space, where the Si:Ge ratio of the glass was the only variable [61]. From rheological measurements of the resultant cBD GICs in Chapter 7, it was observed that modulating the Si:Ge ratio exerted a significant influence on the setting reaction. In particular, it was concluded that (i) Ge substitutions decrease initial cement viscosity, and (ii) a parabolic trend in the gelation rate as a function of Si:Ge is minimized at 1:1. Rheological profiles were analyzed along with data pertaining to the influence of the Si:Ge ratio on: (i) the degradability of the glass, (ii) the structure of GIC matrices during the first 60 minutes of the setting reaction, and (iii) 24 h biaxial flexural strengths of the cements. From these data, the slow setting behavior of Ge-containing GICs was attributed to the emergence of an intermediate step in the setting reaction that delays, but does not hinder the crosslinking of the polysalt matrix. This intermediate step is hypothesized to be associated with the presence of a chemical complex species that disrupts divalent cations (*e.g.* Zn^{2+}) from crosslinking the polyacrylic acid during the initial stages of the GIC setting reaction. Ultimately, this mechanism allows the viscosity of the cement paste

to be modulated without compromising mechanical performance, providing a new approach to controlling cement properties and opening up expanded areas of utility for GICs, including vertebral body augmentation.

The philosophy to replace Si with Ge as the primary network former in zinc-silicate glass, although advantageous for in controlling GIC handling characteristics, was observed to be responsible for an unintended consequence. Complete substitutions of Si by Ge results in GICs that exhibit significant deteriorative losses in strength over time (*e.g.* DG202: 36 MPa compression strength at 1 day, which decreased to 12 MPa after 180 days) [60]. Given that vertebral body augmentation is performed on osteoporotic patients, for whom the ability to regenerate bone is already compromised, vertebral body augmentation cements are required to have lasting mechanical properties [31]. Thus, the mechanical instability be Ge-based GICs impairs the practicality of these materials for clinical applications. Accordingly, the objectives of this paper are to build on the existing, and nacent knowledge of Ge-containing GICs in order to (i) determine the influence of the Si:Ge ratio on compression strength over time, with a view to (ii) identifying the optimum ratio of Si:Ge that can provide for a clinically useful Ge-based GICs, and (iii) to establish, if possible, a mechanistic basis for the loss of strength of Ge-based GICs, such that any losses can be mitigated against.

8.3 Materials and Methods

8.3.1 Glass Synthesis

Five experimental glasses (BD1-5) were synthesized with molar compositions of: (0.48 – x) SiO_2, xGeO_2, 0.36 ZnO, 0.16 CaO; where x = 0.12, 0.24, 0.36, 0.48 mol. fraction. To synthesize the glasses, appropriate amounts of analytical grade reagents silica,

germanium dioxide, zinc oxide and calcium carbonate (Sigma Aldrich, Canada) were weighed out accordingly for each of the five compositions. Powder mixtures of each composition were then blended together for 1 h in a mechanical mixer. Post-mixing, powder compositions were packed into platinum crucibles (Alfa-Aesar, USA) and fired (1500 ˚C, 1 h) in a high temperature furnace (Carbolite RHF 1600, UK), then subsequently quenched in water at room temperature. The resultant glass frit was dried overnight (120 ˚C) then ground in a planetary ball mill (Fritsch Pulverisette 7, Germany) and sieved to retrieve a particle size less than 45 μm. All glass powders were subsequently annealed in platinum crucibles in a high temperature furnace at T_g – 30 ˚C for 3 h and left to furnace cool (T_g provided in Table 1). All prepared glass powders were stored in a desiccator for subsequent analysis.

8.3.2 Differential Scanning Calorimetry

The glass transition temperature (T_g) for each glass composition was determined using a differential scanning calorimeter (Netzsch STA 409PC, USA). Approximately 30 mg of glass powder was placed into a platinum closed pan with the reference pan left empty. Samples were heated at a rate of 10 ˚C min^{-1} up to 1000 ˚C. Proteus Thermal Analysis software (Netzsch Instruments, USA) was used for data analysis with T_g taken as the point of inflection.

8.3.3 X-ray Diffraction

Prior to heat treatment, glass powders were analyzed with an x-ray diffractometer (Bruker, D8 Advanced, Canada) equipped with a LynxEye silicon strip detector and Cu Kα radiation generated at 40 kV and 40 mA. Non-annealed glass powders were pressed into round polymethyl methacrylate holders and exposed to an x-ray beam incident at 5˚

with the detector collecting scatters between 5˚ < 2θ < 100˚ with a step size of 0.1012˚ over 950 seconds.

8.3.4 Cement Preparation

GICs were prepared by mixing annealed powdered glasses with a 50 wt% aqueous solution PAA (M_w = 12,500 g mol^{-1}; Advanced Healthcare Ltd., UK) at a powder to liquid ratio of 1:0.75. Mixing was complete within 45 seconds. To clearly distinguish between glass and cement materials this chapter adheres to the nomenclature introduced in Chapter 7: cBDZ *cement* consists of BDZ *glass, e.g.* cBD1 cement comprises BD1 glass.

8.3.5 Evaluation of Handling Characteristics

The handling characteristics of each cement were evaluated in accordance with the procedures outlined in ISO9917 [287]. Briefly, the working times were evaluated in ambient air by mixing 0.25 g of glass powder with 0.188 g of 50 wt% PAA aqueous solution and continuously spatulating the cement paste. A stopwatch was used to measure the length of time from the start of mixing until it was no longer possible to manipulate the cement paste without adversely affecting its properties [287]. For setting time evaluation, aluminum molds (10 x 8 x 5mm) were filled with cement placed on an aluminum block (75 x 100 x 8 mm) covered in aluminum foil. Sixty seconds after the end of mixing, the assembly was placed in an oven at 37 ˚C. Sixty seconds prior to the working time of the cement under investigation, a Gilmore needle (mass 454 g, flat tip Ø1.1 mm) was placed on the surface of the material. This process was repeated intermittently until the cement could take the full weight of the indenter for 5 sec, whilst making a full circular indentation in the cement. This indentation process then continued

every 30 sec. Setting time was recorded as the time from the end of mixing the cement until the indenter failed to make a complete circular impression in the surface of the cement surface when viewed at 2X magnification [287]. Both working time and setting time evaluations were performed in triplicate.

8.3.6 Compression Testing

Compression testing was conducted in accordance with the procedures outlined in ISO9917 [287]. Briefly, one side of stainless steel split ring molds (Ø4 x 6 mm) was covered with an acetate sheet. Subsequently, cement paste was spatulated (cBD1) or injected (cBD2-5) down the side of the cylindrical mold allowing air to escape from the opposite side in an attempt to minimize entrapment of air bubbles. Once molds were filled to excess, a second acetate sheet was used to cover the samples and the acetate-mold sandwich was clamped between two stainless steel plates and incubated (37 ˚C, 1 h). Upon removal from the oven, the clamps, steel plates, and acetate sheets were removed and the cement flash surrounding the specimens was carefully removed using a dental spatula. Subsequently, the top and bottom surface of each specimen in the mold was ground flat by hand using 400-grit silicon carbide paper to ensure both surfaces were parallel. Samples were then removed from the mold and placed in 15 mL falcon tubes filled with 10 mL of deionized water and incubated at 37 ˚C for 1, 7, 30, 90, and 180 days. After the appropriate amount of time, samples were removed from the incubation environment, and their dimensions (diameter, height) measured using digital calipers (Fowler Tools, Canada). Samples were then loaded on an Instron 3344 mechanical testing system (Instron, USA), equipped with a 2 kN load cell and compressed at 1 mm min^{-1} until fracture. Applied force-displacement data was recorded and used to calculate

maximum compression strength (CS) and modulus (E_C) (mean ± SD) of 5 samples for each cement formulation at each time point [381].

8.3.7 GIC Structural Analysis

Teflon molds (Ø7 x 1 mm), with the underside covered with an acetate sheet, were filled to excess with cement using a dental spatula, covered with a second acetate sheet, and then clamped between two stainless steel plates and incubated (37 ˚C, 1 h). Upon removal from the oven, cement flash was carefully removed around the specimens with a dental spatula. Samples were then removed from the molds, weighed, and subsequently placed in falcon tubes containing 5 mL of deionized water and incubated at 37 ˚C for 1, 7, 30, 90, and 180 days. After the respective incubation periods, samples were examined using attenuated total reflectance Fourier transform infrared spectroscopy and the extracts were examined using inductively coupled optical emissions spectroscopy. Subsequent to ATR-FTIR examination, 1 day and 180 day samples of cBD1 (Si:Ge 1:0) and cBD5 (Si:Ge 0:1) were flash frozen using liquid nitrogen to halt the setting reaction then placed in cold storage (-80 ˚C) until they were examined *via* scanning electron microscopy.

ATR-FTIR

Attenuated total reflectance Fourier transform infrared spectroscopy (ATR-FTIR) was used to probe the structure of cements over time. After the appropriate time period, samples were removed from the incubation environment, dried with absorbent paper, and placed on the diamond ATR element (Golden Gate, Specac, USA). Extracts were kept for later analysis. Cement surface structures were probed using an infrared spectrometer (Tensor 27, Bruker, USA). The resultant spectra obtained for each cement (Figure 42) at each time point (*i.e.* 1, 7, 30, 90, 180 d) were averaged of n=3 samples, where each

sample was examined at 2 separate locations on the same surface, each examination comprised 17 runs collected over one minute, and each run consisted of 32 scans in the mid-IR region (400-4000cm^{-1}) at resolution of 4 cm^{-1} [256, 382]. These spectra were normalized to the height of the *c.* 1452 cm^{-1} band. In an effort to mitigate the influence of the adjacent *c.* 1545 cm^{-1} and *c.* 1405 cm^{-1} bands on the height of the *c.* 1452 cm^{-1} band, the height of the *c.* 1452 cm^{-1} band was defined as the difference in intensities between the local maxima at *c.* 1452 cm^{-1} and the local minima at *c.* 1470 cm^{-1}. The *c.* 1452 cm^{-1} band was chosen as it corresponds to the CH_2 scissor vibration of the PAA [362, 382]. Since the ratio of PAA content to glass content was standardized across all cement samples, it was assumed that the proportional population of this molecular structure, as measured by ATR-FTIR, would not change over time and would be consistent across all cement compositions. This normalization was a necessary operation to conduct meaningful comparisons of key structural components within each cBD cement compositions. The comparisons made over time and across the various Si:Ge ratios were the (i) *c.* 1545 cm^{-1} band height, (ii) *c.* 1545 cm^{-1} full width at half maximum (FWHM), and (iii) the ratio between the areas under the *c.* 1545 cm^{-1} and *c.* 1452 cm^{-1} bands. The *c.* 1545 cm^{-1} band is important because it corresponds to the asymmetric vibration of the constituent metal-carboxylate salts, which reveals information regarding the GIC matrix [256, 364, 383].

ICP-OES of GIC Extracts

Inductively coupled optical emissions spectroscopy (ICP-OES) of GIC extracts was used to determine ion release from the cements over time. Extracts were diluted at a 1:5 ratio in 2% aqueous nitric acid (Sigma-Aldrich, Canada) for ICP-OES analysis. An Optima

DV8000 ICP-OES system (Perkin-Elmer, Canada) was calibrated with certified solutions (Perkin-Elmer, Canada) and used to measure the release concentrations of Si, Ge, Zn, and Ca into the deionized water. The concentrations of released ions from each cement sample were normalized on the basis of the mass of glass present in each sample according to the theoretical molar compositions of each glass (Table 13). This normalization established a total percentage of glass released from the cement as well as the release percentage of each glass constituent (*i.e.* Si, Ge, Zn and Ca) (mean ± S.D., n=3). To elucidate information pertaining to potential mechanisms that impact the mechanical properties of the cBD GICs, CS and E_C values were plotted against ion release data, and the resultant scatter plots underwent non-linear regression analysis (Prism 6, Graphpad Software Inc. USA).

Scanning Electron Microscopy

One-day and 180-day GIC samples of cBD1 (Si:Ge 1:0) and cBD5 (Si:Ge 0:1) were removed from cold storage and mounted to on SEM stubs using double-sided carbon tabs, and then coated with gold-palladium. The surface architecture of samples were inspected using an S-4700 SEM (Hitachi, USA) operating at 5 kV, 15μA.

8.3.8 Statistical Analysis

Statistical analysis was conducted using Prism 6 (GraphPad Software Inc., USA). Working times and setting times results were compared using a one-way ANOVA, while CS, E_C, ion release, and ATR-FTIR data were compared using two-way ANOVA. Statistical differences were determined using a Tukey post-hoc test where $p = 0.05$.

8.4 Results

All glasses were confirmed to be amorphous, exhibiting no identifiable crystalline species when examined by XRD. Table 13 contains T_g data for the 5 glass compositions and are provided for repeatability and reproducibility purposes. It was observed that T_g decreases linearly with the Si:Ge ratio as previously reported in Chapter 7.

Table 13: BD glass compositions (mole fraction) and the corresponding T_g values.

		Glass Composition				T_g [˚C]
	Si:Ge Ratio	SiO_2	GeO_2	ZnO	CaO	
BD1	1:0	0.48	0	0.36	0.16	673
BD2	3:1	0.36	0.12	0.36	0.16	653
BD3	1:1	0.24	0.24	0.36	0.16	631
BD4	1:3	0.12	0.36	0.36	0.16	620
BD5	0:1	0	0.48	0.36	0.16	597

8.4.1 Handling Characteristics

The addition of Ge to the glass compositions significantly extended the working times and setting times of the corresponding cements (Figure 39) to a maximum of *c.* 13 min and *c.* 37 min, respectively when the Si:Ge ratio was 1:1 (*i.e.* cBD3).

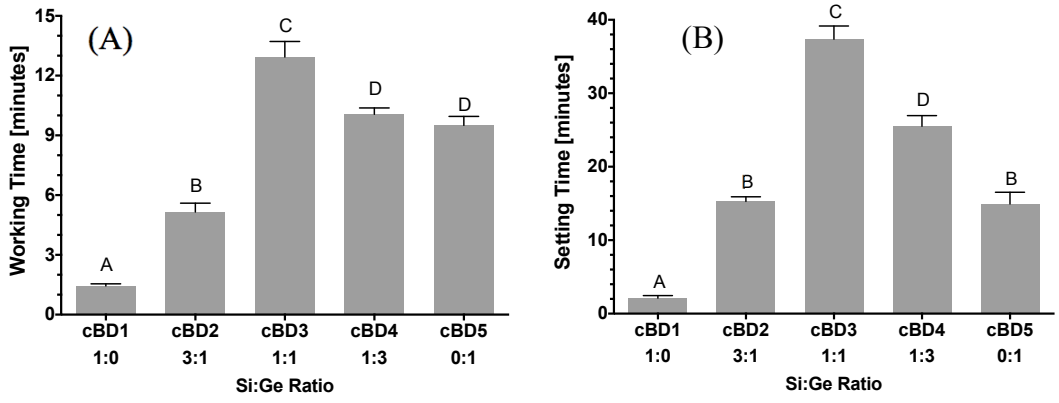

Figure 39: cBD Series GIC handling characteristics, (A) working time and (B) setting time (mean + SD). Compositions of the same letter group demonstrated statistically similar results (p >0.05).

8.4.2 Mechanical Properties

Notwithstanding occasional deviations in mechanical performance, the compression strengths and moduli of the cBD GICs were generally maintained up to 180 days for cements where Si:Ge ratio ≥ 1:1 (Figure 40 and Figure 41). However, when the Si:Ge ratio falls below 1:1 the cBD GICs (*i.e.* cBD4 and cBD5) suffered deteriorative losses in strength and modulus over time and become substantially weaker relative to cements with Si:Ge ≥ 1:1. The strongest cement was cBD3 (Si:Ge 1:1), which demonstrated CS in excess of 50 MPa at 1 and 180 days. The only composition to demonstrate a significant increase in strength with time was cBD2 between 1 and 7 days. Furthermore, the E_C of cBD series GICs were observed to increase linearly with CS ($E_c = 10CS + 350$, $R^2 = 0.82$).

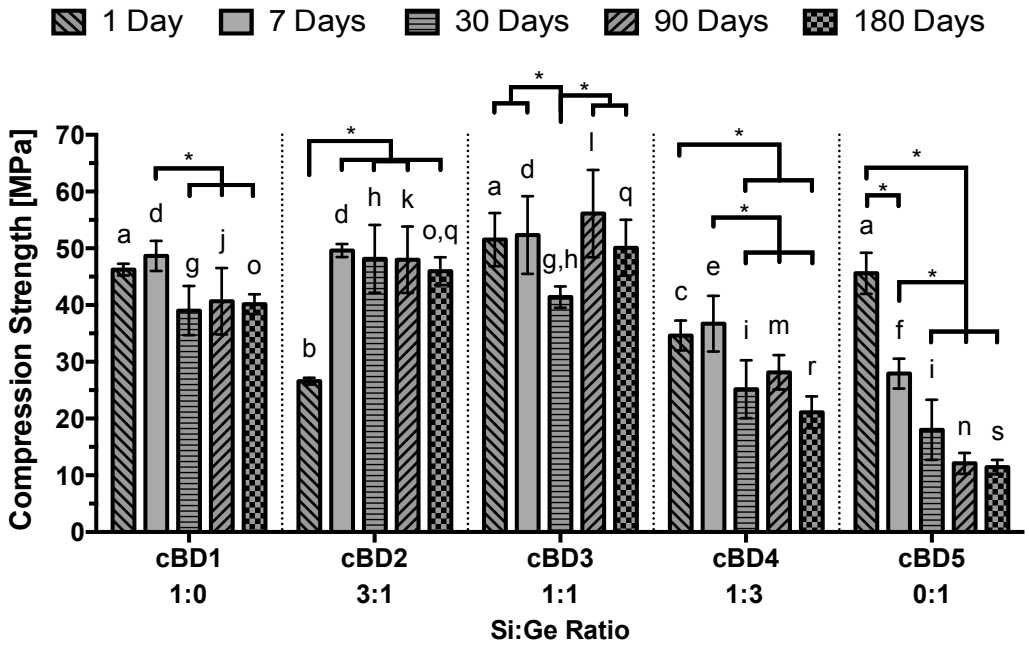

Figure 40: Compression strengths of cBD GICs over 1, 7, 30, 90, and 180 days. Data presented as mean ± SD, * denotes statistically significant differences within one compositional group ($p < 0.05$), and letters compare cement compositions across a specific time point, where values with the same letter are statistically equivalent ($p > 0.05$); letters a-c are used to indicate statistical significance at 1 day, letters d-f are used for 7 days, letters g-i for 30 days, letters j-m for 90 days, and letters o-s for 180 days.

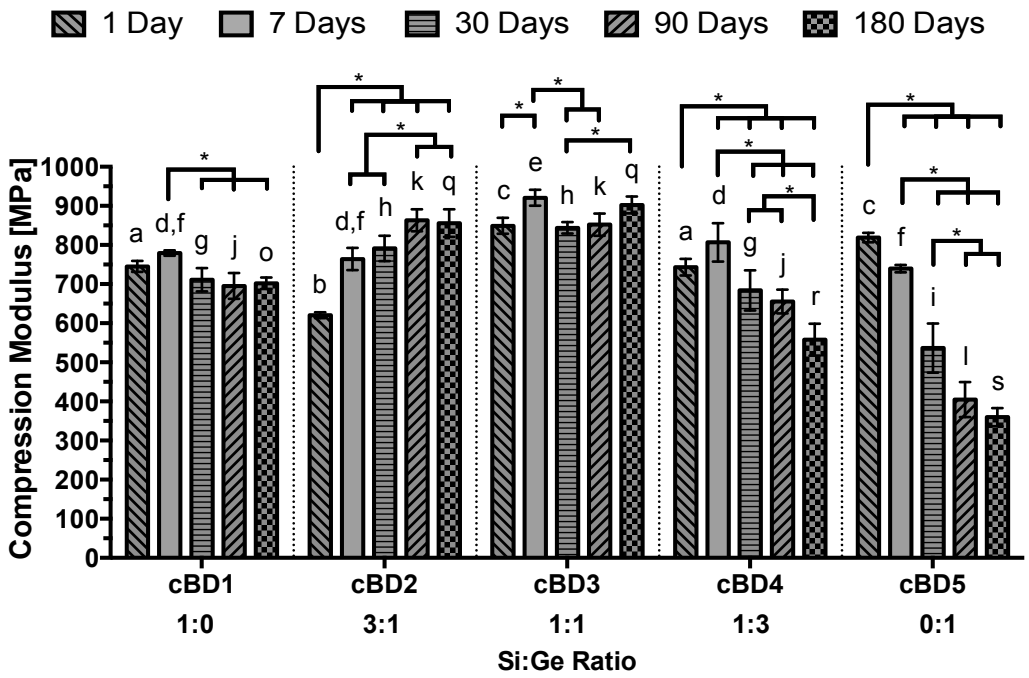

Figure 41: Compression moduli of cBD GICs over 1, 7, 30, 90, and 180 days. Data presented as mean ± SD, * denotes statistically significant differences within one compositional group ($p < 0.05$), and letters compare cement compositions across a specific time point, where values with the same letter are statistically equivalent ($p > 0.05$); letters a-c are used to indicate statistical significance at 1 day, letters d-f are used for 7 days, letters g-i for 30 days, letters j-m for 90 days, and letters o-s for 180 days.

8.4.3 ATR-FTIR

Figure 42 displays the ATR-FTIR spectra of the cBD GICs after the 1, 7, 30, 90, and 180-day incubation periods. Table 14 outlines the characteristic wavenumbers of the structures present in the cements. Interpretations of the spectra were limited to the region between 1800 cm^{-1} and 1100 cm^{-1}. Outside this range, large sample-to-sample variations in the signal obscured the identification of the associated molecular structures. Fortunately, resonant frequencies within this region are associated with defining structural features of GICs, namely the asymmetric (*c.* 1545 cm^{-1}) and symmetric (*c.* 1405 cm^{-1}) stretch of metal-carboxylate salts that crosslink the polyanion chains of the

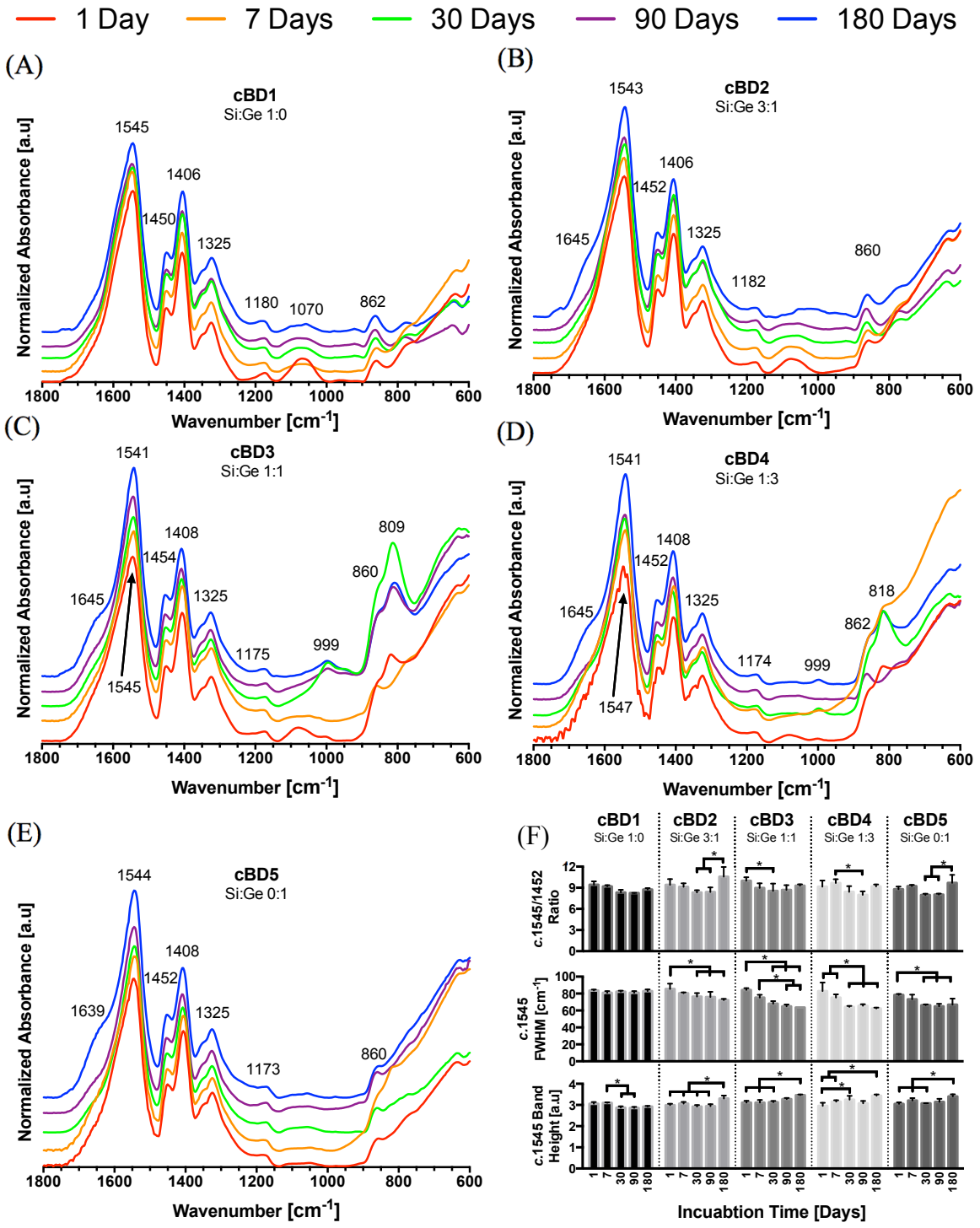

Figure 42: ATR-FTIR spectra of cBD GICs over time. Spectra represent the 1, 7, 30, 90 and 180 day time points of: (A) cBD1, (B) cBD2, (C) cBD3, (D) cBD4, (E) cBD5, and (F) (i) ratio of the areas underneath the 1545 cm^{-1} and 1452 cm^{-1} bands, (ii) *c.*1545 cm^{-1} band height, and (iii) *c.* 1545 cm^{-1} FWHM at each time point, plotted as mean ± SD, where * denotes statistically significant differences ($p < 0.05$).

Table 14: Peak assignment of characteristic FTIR wavenumbers associated with the cBD GICs.

Wavenumber [cm^{-1}]	Structure	Reference
1635	H-O-H bend	[362, 382, 384]
1540-1560	Asymmetric stretch metal-carboxylate bonds (e.g. Zn^{2+}- $2COO^{-}$, Ca^{2+}- $2COO^{-}$): 1537 cm^{-1} asymmetric unidentate Zn^{2+}- $2COO^{-}$ 1548-1554 cm^{-1} chelating bidentate Zn^{2+}- $2COO^{-}$ 1562 cm^{-1} asymmetric ionic Zn^{2+} - $2COO^{-}$ 1541 - 1547 chelating bidentate Ca^{2+}- $2COO^{-}$	[256, 364, 383]
1452	CH_2 scissor in PAA	[362, 382]
1405	Symmetric stretch metal-carboxylate bonds (e.g. Zn^{2+}- $2COO^{-}$, Ca^{2+}- $2COO^{-}$)	[256, 365]
1174	OH bending in carboxyl groups	[385]
860-1100	Si-O asymmetric stretch in SiO_4	[382, 386, 387]
680-900	Ge-O asymmetric stretch GeO_4 or GeO_6	[305, 388-392]

PAA to form the cement matrix (*i.e.* $2COO^{-}M^{2+}$, where M = Zn^{2+} or Ca^{2+}) [256, 364, 383]. The area under this band was taken as a representation of the total population of polysalt crosslinks in the GIC matrix. It was noted that the overall level of crosslinking in the GIC matrix remained relatively constant as a function of Si:Ge ratio or time. This is evinced by two observations: (i) the *c.* 1545/1452 cm^{-1} band area ratios across all five cements were statistically similar at each time point, and (ii) all compositions demonstrated statistically comparable ratios at the 1 and 180-day time points (Figure 42F). Ge-containing cements (cBD2-5, Si:Ge 3:1 – 0:1) appear to show two interesting features; (i) a convergence of the bond modes of metal-carboxylate salts over time, as illustrated by the simultaneous reduction in FWHMs and increase in height of the *c.* 1545 cm^{-1} bands (Figure 42F), and (ii) a shoulder at *c.* 1645 cm^{-1} developed over time. The latter first appeared in cBD2 (Si:Ge 3:1) at 180 days (Figure 42B), and as the Si:Ge ratio decreased, this shoulder appeared at earlier time points. The 1635 cm^{-1} wavenumber is

indicative of bending vibrations associated with H-O-H bonds in water molecules [362, 382].

8.4.4 GIC Ion Release

Figure 43 shows that increasing the concentration of Ge in the glass network resulted in an increased sum of degradation byproducts arising from their corresponding cements, as measured by ICP, following the order: cBD1 < cBD2 = cBD3 < cBD4 < cBD5. It was observed that for GICs comprising glasses where Si:Ge < 1:1 (*i.e.* cBD4 and 5), the total ion release significantly increased over time. Furthermore, Ge release from cements cBD2-5 (*i.e* cements containing Ge) was substantially greater than all other constituents elements, following the order: Ge > Si > Ca > Zn. Finally, it was noted that Zn release was on the order of 0.05%, equivalent to *c.* 1-3 ppm, and thus deemed to be negligible.

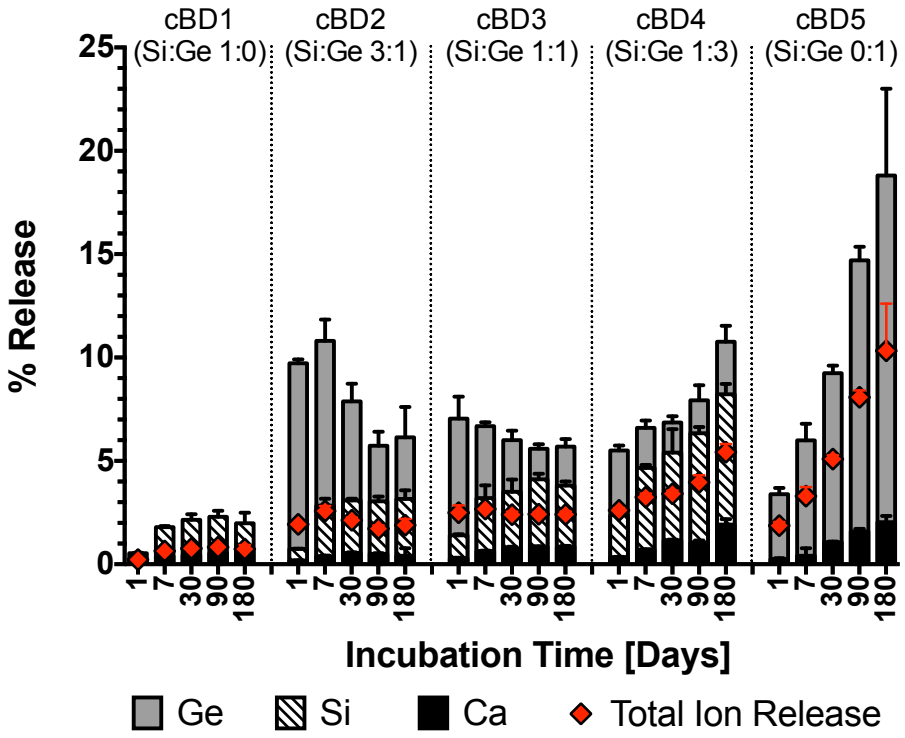

Figure 43: Ion release data from cBD series GICs presented as the percentage release of each compositional element and the total sum of all ions (mean + SD). Zn release is infinitesimal to the scale of the y-axis and thus omitted from figure.

Interestingly, it was observed that compositions exhibiting a significant decrease in mechanical properties over 180 days (*i.e.* cBD4 and cBD5 in Figure 40 and Figure 41) also generated significantly greater degradation byproducts over time (Figure 43). Quantitative assessment of this observation found that reductions in both CS and E_C were exponentially related to total ion release from the cBD4 and cBD5 cements (R^2 = 0.90 and 0.94, respectively) (Figure 44A). Further analysis revealed Ge release also displayed exponential correlations with and reduced CS (R^2 = 0.90) and Ec (R^2 = 0.93) of cBD4 and 5 (Figure 44B). Collectively this data indicates that loss of degradation byproducts, in particular Ge, is strongly correlated with the overall reduction of mechanical performance for Ge GICs.

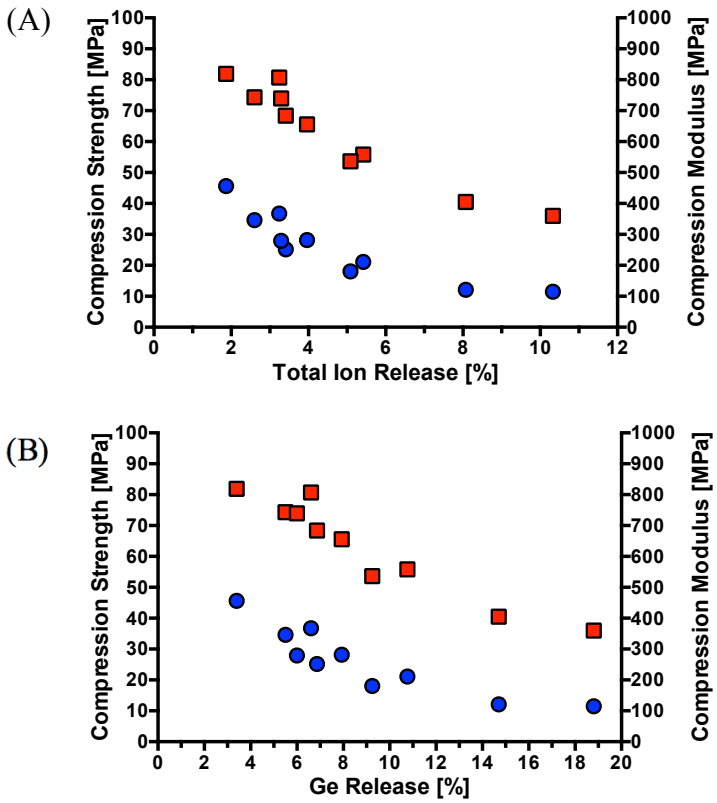

Figure 44: Regression analysis between ion release and mechanical properties. (A) Percentage of total ions released and (B) percentage of Ge released is compared against compression strength (blue) and modulus (red) for cBD4 (Si:Ge 1:3) and cBD5 (Si:Ge 0:1).

8.4.5 Scanning Electron Microscopy

Figure 45 exhibits the contrast in microstructures of cBD1 (Si:Ge 1:0) compared to cBD5 (Si:Ge 0:1). There were no visible pores presents in cBD1 at 1 day (Figure 45A), and only a minimal number of <5 μm pores at 180 days (Figure 45B). There was a higher density of pores in cBD5 at 1 day compared to cBD1, and pore diameters ranged from 3 to 80 μm (Figure 45C). This high density of pores was again observed in the 180-day cBD5 sample (Figure 45D). Cracks in the microstructure of the cements were caused by dehydration during sample preparation for SEM.

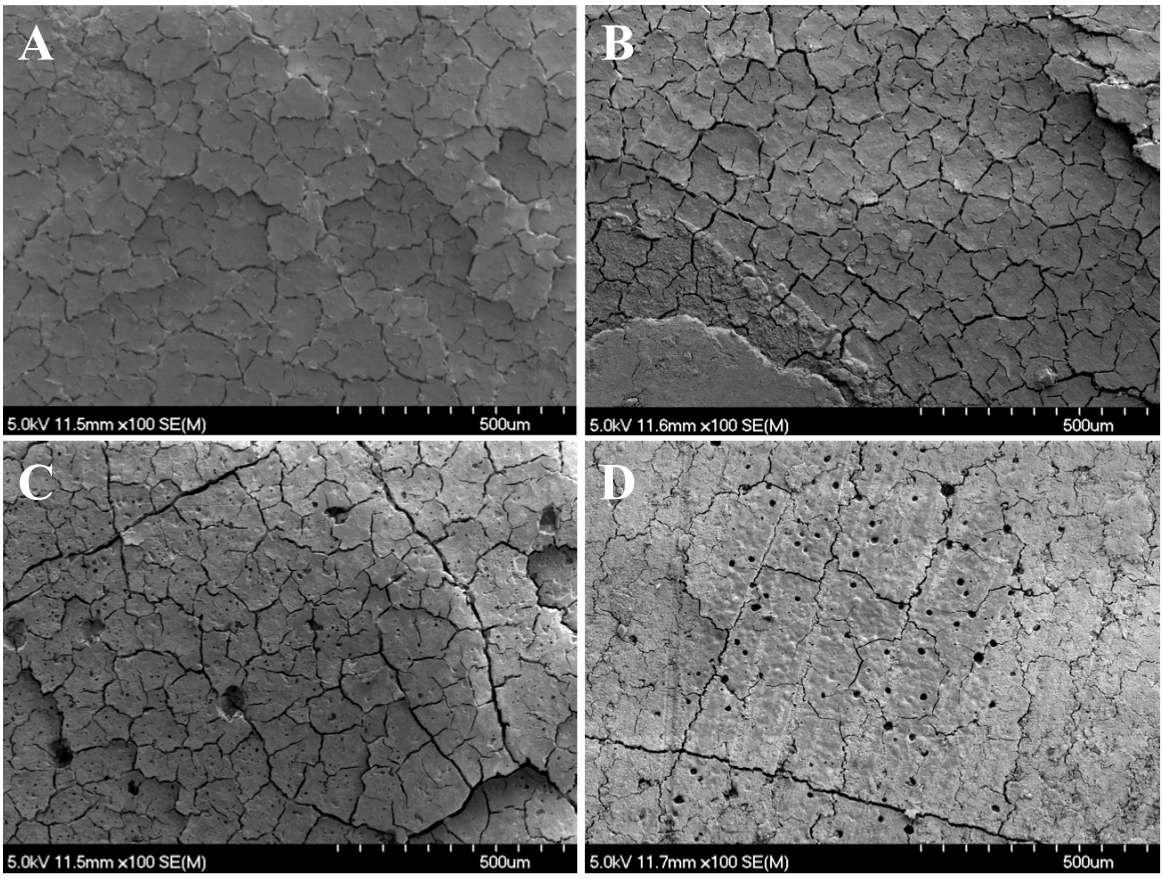

Figure 45: SEM micrographs (x100) of cBD1 (Si:Ge 1:0) after (A) 1-day and (B) 180-day incubation periods, and cBD5 (Si:Ge 0:1) after (C) 1-day and (D) 180 day incubation periods.

8.5 Discussion

The viability of Ge-containing GICs for clinical use in PVP was jeopardized because of deteriorative losses in strength over time. The data generated in this chapter clearly identifies that Ge-containing GICs can remain mechanically stable if the Si:Ge ratio in the glass is maintained at 1:1 or greater. The peculiarity of the performance of Ge-containing GICs presented in this chapter is emphasized by the observation that the slowest setting cement was also the strongest. This behavior occurred when half of the Si content in the glass was replaced by Ge, *i.e.* cBD3 (Si:Ge 1:1) *vs.* cBD1 (Si:Ge 1:0). This replacement resulted in an 8-fold increase in working time and a 16-fold increase in setting time of cBD3 over cBD1 (Figure 39), yet the CS of the two cements were statistically similar at 1 day, and after 180 days cBD3 was 25% stronger than cBD1 (Figure 40). The handling characteristics of cBD3 (*i.e.* 13 min working time, 37 min setting time) are consistent with those of Ge-containing GICs that are injectable [60, 393]. This fact, combined with the CS of cBD3 in excess of 50MPa at 1 and 180 days, demonstrates the practicality of Ge-containing GICs for clinical applications such as vertebral body augmentation where cements are required to have compressive strengths of at 30 MPa [33]. However, when the Si:Ge ratio decreases to less than 1:1, the long-term mechanical integrity of the cement is lost. This is evinced in Figure 40 and Figure 41 by the temporal reductions in both CS and E_C of cBD4 (Si:Ge 1:3) and cBD5 (Si:Ge 0:1). Thus it is imperative to conceptualize potential mechanism(s) responsible for the deterioration of strength to ensure the design of future Ge-containing GICs can practically balance extended handling characteristics with long-term mechanical stability.

The design space in this chapter was conceived where the only variable was the Si:Ge ratio such that investigations into the potential mechanistic bases associated with the loss of mechanical properties in Ge-containing GICs could be clarified. In the first instance, this chapter sought to correlate mechanical properties with potential changes in the molecular architecture of the polysalt matrix over a period of 180 days. With regards to the GIC molecular structure, no correlations were identified between the mechanical behavior of the cBD cements and the overall population of the ionic crosslinking bonds within their polysalt matrices. Varying the Si:Ge ratio in the glass composition resulted in only minor shifts of the asymmetric (*c.*1545 cm^{-1}) and symmetric (*c.*1405 cm^{-1}) resonance bands of the metal-carboxylate crosslinks in the corresponding GIC matrices. The positions of these bands are consistent with those reported for other zinc-silicate GICs [57, 294], suggesting that Ge does not act as a crosslinking element in the polysalt matrices. Instead, the primary metal-carboxylate bonds are likely to involve Zn and Ca, *i.e.* Ca^{2+}– 2(COO^{-}) or Zn^{2+}– 2(COO^{-}). The overall crosslink populations of cBD1-5 were observed to remain statistically similar between the 1 and 180-day times points (Figure 42F). This observation indicates that the polysalt matrices of these cements are hydrolytically stable, an argument that is supported by the low levels of Ca and Zn detected in the cement extract media over time. Therefore, the temporal decline of mechanical properties in Ge-containing GICs comprising glasses with Si:Ge ratios < 1:1 is not due to the dissolution of the polysalt matrix. Despite the consistent population of crosslinking bonds in Ge-containing GICs (*i.e.* cBD2-5), a convergence of the *c.*1545 cm^{-1} bands to lower wavenumbers was observed over time in the spectra of these cements (Figure 42B-E). This convergence is interpreted as a narrowing of the distribution of the

metal-carboxylate bonding modes within the GIC matrices to structures with more covalent-like character [256]. With an increased presence of stronger ionic crosslinks, there exist the potential to embrittle the GIC matrix due to over-crosslinking. Over-crosslinking restricts the relative motion amongst neighboring polyanion chains and reduces their flow at the crack tip, which increases the modulus of the cement but negatively impacts the strength [228, 232]. This argument of matrix embrittlement may explain the mechanical behavior of cBD2 (Si:Ge 3:1), where the E_C continually increased from 1 to 180 days and the CS increased from 1 to 7 days. However, the fact that both the CS and the E_C of cBD4 and cBD5 decrease significantly over time dispels matrix embrittlement as a leading contributor to impaired long-term strength of Ge-containing GICs with Si:Ge ratios $< 1:1$.

Since the deteriorative loss in mechanical properties over time cannot be attributed to structural changes in the polysalt matrix, alternative mechanisms must be considered. This chapter illustrates three potential mechanisms that likely contribute to this behavior. The first mechanism takes into consideration the strong correlation between an elevated release of degradation byproducts and lower cement strength and modulus (Figure 44). GICs can be regarded as particulate-filled polymer composites [202], comprising glass particles surrounded and supported by siliceous hydrogel depleted of crosslinking cations (*i.e.* Ca^{2+} and Zn^{2+}) [394]. Losing these residual glass particles would compromise the strength of the cement, as these particles act as reinforcing fillers to resist compressive forces and augment the mechanical integrity of the GIC provided by the polysalt matrix [395]. If the residual glass particles were degrading, release of *all* constituent ions would be expected. However, Figure 43 shows

the release of Ge is disproportionally high compared to other elements of the glass, making degradation of the residual glass particles unlikely. Instead, as Ge replaces Si in the glass, it is hypothesized that the hydrogel surrounding the glass particles becomes increasingly concentrated with Ge and progressively less hydrolytically stable. When Ge content surpasses that of Si in the glass composition, the diminished stability of the gel layer results in its degradation, releasing Ge and Si (if present). Loss of this gel layer would undermine the support of the residual glass particles, hindering their ability to reinforce the polysalt matrix, and may facilitate the creation of void and or cracks in the microstructure that would act as stress raisers, thus weakening the cement. The second mechanism that may contribute to the compromised mechanical integrity of Ge-based GICs is the possibility of greater porosity in their microstructure, as observed in the cBD5 SEM micrographs (Figure 45C and Figure 45D). It is possible that the appreciable degradation of the Ge-containing cements with a Si:Ge < 1:1 is a contributing factor in the development this porosity. However, given the previous argument that the degradation of residual glass particles is unliking, a more likely explanation of this porosisty comes from Nomoto *et al.* [396]. In their investigation of the effects of hand *vs.* encapsulated mixing of conventional GICs, they found that lower viscosity GICs capture more air bubbles in the cement during mixing, resulting in a cement with a more porous and thus weaker microstructure [396]. Therefore, the increased porosity seen in cBD5, which Chapter 7 has shown to be a less viscous cement than cBD1, may be due to the introduction of air bubbles during mixing. The third mechanism that may contribute to the mechanical decline of Ge-containing GICs is the plasticizing effect of water. The development of the *c.*1640 cm^{-1} shoulder in the FTIR spectra of cBD2-5 indicates an

increased presence of water in these cements over time (Figure 42). In GICs water exists in at least one of two states [45]:, a non-evaporable state where water molecules are tightly bound to (i) the crosslinking metal cations in the polysalt matrix and (ii) the gel layer surrounding the residual glass particles; and, an evaporable state where water molecules form loosely bound sheaths around the polyanion chains. The former increases the strength and modulus of GICs, while the latter reduces these properties [45, 232, 245, 397] – mechanical behavior that is consistent with that demonstrated by cBD GICs when Si:Ge < 1:1. Finally, it is possible that the propensity of GICs with Si:Ge < 1:1 to have greater porosity may facilitate water absorption, intensifing both the degradation of the gel layer and the plasticization of the cement matrix.

The practical benefit of including Ge in the glass composition of zinc silicate GICs is the manifestation of the extended handling characteristics. Figure 39 shows this benefit is realized with a Si:Ge ratio as high as 3:1, but to ensure strength is maintained and that this benefit remains practical, the Si:Ge ratio should not be less than 1:1 (Figure 40). The compositions which embody these ratios (*i.e.* cBD2 and cBD3, Si:Ge 3:1 and 1:1, respectively) were observed to release less than 3% of total ions (Figure 43). When total ion release exceeded 3%, the decline of mechanical properties of the Ge-containing GICs was exacerbated. Therefore, to sustain the strength of the Ge-containing GICs, the Ge content must be minimized and/or stabilized. Previous investigations by the authors support this hypothesis, as it was observed that reducing the Ge content in zirconia-stabilized glasses led to sustained strength of the corresponding GICs whilst maintaining extended handling characteristics [60, 357, 398].

The unexpected outcome of this chapter was the fact that the slowest setting cBD cement was also the strongest, behavior that is uncommon in conventional Si based GICs where extended setting times typically correlate with weaker cements [58, 222, 223, 252, 296, 300, 354, 395, 399]. The route of this unexpected behavior may lie in the ability of Ge to decouple glass reactivity from the setting rate of the cement [61]. This behavior of Ge-containing glasses may be useful beyond the proposed application of vertebral body augmentation, as such glasses may represent a new approach to improve the mechanical properties of conventional GICs, which have been criticized due to their brittle nature [226, 400]. Hill *et al.* demonstrated that the strength and toughness of GICs increased as the molecular weight (M_W) of the PAA increased due to i) the more appreciable entanglement of the polyelectrolyte chains, and ii) greater degree of crosslinking of said chains [237]. However, Wilson *et al.* described that in addition to the improved mechanical performance, increasing either the M_W or concentration of the PAA also raised the viscosity of the cement paste, rendering them more difficult to mix and resulted in shorter working times [242]. Furthermore, the thermoplastic nature of GICs yields a theoretical upper limit for the beneficial increases of M_W, between 80,000 and 100,000 dalton, above which the polymer matrix fails by chain scission rather than chain pull-out, which prevents further improvement of strength but will increase the viscosity of the cement paste [215, 237]. Thus, the contribution to mechanical performance provided by PAA cannot be maximized because trade-offs between the M_W, concentration, and powder to liquid ratio are required to ensure the handling characteristics of the resultant GIC remain practical [233-235]. The inclusion of Ge to the glass component of conventional GICs may facilitate mixing when high M_W or concentrations of PAA are

used by mitigating the contribution that the glass component has on the viscosity of the cement paste, due to the fact that Ge-containing glasses delay cement gelation [61]. In such a capacity, Ge-containing conventional GICs may allow for the mechanical benefits of increased M_W and or concentration of PAA to be optimized whilst maintaining practical handling characteristics.

Building on the work of this study, further investigation of the mechanical properties with a more sensitive test, such as fracture toughness (K_{IC}) to evaluate intrinsic material properties, may provide greater insight into the relationship between the strength and structure of Ge-containing GICs. Such an investigation would aid in clarifing several key aspects of the hypotheses generated in the present study. Firstly, the current chapter failed to substantiate correlations between the mechanical behavior of the cBD cements and the overall population of ionic crosslinking bonds within their polysalt matrices. The fact that K_{IC} measures a material's ability to resist crack propagation may provide additional insight into the relationship between molecular architecture and strength of the cBD cements. In particular K_{IC} may provide an enhanced understanding regarding the extent of polymer entanglement which, in addition to the ionic crosslinks, is a key contributor the mechanical performance of GICs [228, 249]. Secondly, correlating K_{IC} with changes in the ratio of evaporable to non-evaporable water in the cement over time as a function of Si:Ge ratio would provide more conclusive evidence regarding the plasticizing effect of water on the polysalt matrix as a mechanism that contributes to the mechanical decline of Ge-containing GICs. Finally, assessing K_{IC} of Ge-containing cements as a function of PAA M_W and/or concentration will determine whether or not their extended setting behavior is a practical platform to improve the toughness of GICs.

Ultimately, characterizing the K_{IC} of Ge-containing GICs will augment the understanding of their molecular architecture and yield an enhanced appreciation of potential benefits these novel cements may possess and how they can be applied to the clinical use of GICs.

8.6 Conclusion

This chapter explored the influence of the Si:Ge ratio in a quaternary glass system on the mechanical behavior of GICs over time. It was revealed the Si:Ge ratio should be within a 3:1 to 1:1 range to ensure extended GIC setting characteristics are appropriately balanced with sustained strength. Interestingly, both the Si:Ge ratio and time were observed to exert considerable influence on the compressive strengths of the cBD GICs but not on the populations of metal-carboxylate bonds within the polysalt matrices. Therefore, it appears that changes in mechanical properties of GICs arising from the replacement of Si by Ge in the glass chemistry are not the result of altering the number of divalent cations that crosslink the GIC matrix. Instead, the altered mechanical properties are likely associated with changes in the degree to which the polymer chains are entangled. The declining mechanical properties of Ge-containing GICs were found to be the result of the deleterious effects of an increased release of degradation byproducts from the cement when Si:Ge < 1:1 and the potential of water to plasticize the matrix. Ultimately, this chapter identified a Si:Ge ratio of 1:1 as providing the best combination of handling and mechanical properties to render Ge-containing GICs practical for clinical use as injectable bone cement in applications such as vertebral body augmentation.

Chapter 9: Conclusions and Future Work

The inverse relationship that couples the handling and mechanical properties of GICs has obstructed the clinical use of aluminum-free variants of these cements in orthopaedic indications. One such application is vertebral body augmentation, where bone cement must be injected through percutaneous cannulae into fractured vertebral bodies to stabilize the fracture and relieve the pain of the patient [12, 26]. The excellent biocompatibility and adhesive qualities of these cements motivated the research of GICs based on zinc silicate glass chemistries for use in vertebral body augmentation [53]. However, despite possessing adequate strength, the quick-setting nature of zinc silicate GICs makes these cements impossible to inject in a clinical setting. For the past decade, researchers have attempted to improve the handling characteristics of zinc silicate GICs but have failed to make these cements clinically practical [49, 54, 58, 59, 294, 298, 299]. The key limitation inhibiting the development of zinc silicate GICs for vertebral body augmentation is: an inability to extend the GIC setting reaction in order to improve the handling properties of the cement without negatively impacting its strength.

The glass chemistry plays a critical role in the GIC setting reaction and significantly impacts the properties of the cement [45], but a new approach is necessary to improve the clinical viability of aluminum-free GICs. To date, attempts to manipulate glass chemistry to improve GIC handling has focused on altering the modifier (*e.g.* Ca, Sr, Na) and/or intermediate (*e.g.* Zn, Ti, Mg) content of SiO_2 based glass compositions [50, 54, 57, 58, 295, 300], a practice that is inherently flawed. To slow GIC setting and improve handling in this manner, it is necessary to reduce the modifier and/or intermediate content of the glass to diminish its reactivity. However, it is the modifier and

intermediate elements of the glass that provide the multivalent cations which bond to carboxylate groups and crosslink the polyacrylic chains to form the GIC matrix [45]. Further, the quantity and strength of these bonds dictate the mechanical properties of the cement [45]. Thus, a new approach to controlling glass reactivity that does not impact the quantity of crosslinking cations is necessary to mitigate against this inverse relationship. Therefore, this body of work explored the philosophy that replacing SiO_2 as the primary network forming species in the glass will control its degradation and consequently the handling and mechanical properties of the resultant GIC.

Germanium and zirconium were chosen to investigate this approach, as both have glass network forming capabilities as well as interesting structural characteristics hypothesized to improve GIC handling characteristics. The inclusion of Ge was hypothesized to extend the GIC setting reaction by delaying, but not preventing, the release of divalent cations (*e.g.* Zn^{2+} and Ca^{2+}) due the potential presence of basic $[GeO_5]^{-}$ and $[GeO_6]^{2-}$ structures that require charge compensation from M^{z+} cations [303]. With regards to Zr, it was hypothesized that its ability to increase the durability of glasses in acidic environment would slow the GIC setting reaction and improve handling characteristics [308, 311, 312, 401]. Three broad investigations were completed to examine the impact of replacing Si and test the aforementioned hypotheses. The first investigation conducted a preliminary screening to assess the influence of Ge and Zr on the handling characteristics and mechanical properties of zinc silicate GICs. The second investigation focused on deducing the role of Ge in the GIC setting reaction using 4 experimental lines of enquiry. The final investigation examined the impact of Ge on the molecular architectures and strength of zinc silicate GICs over time. Cumulatively, these

investigations provide evidence that substantiates the ability to manipulate the handling and mechanical properties of zinc silicate GICs by controlling the Ge and or Zr content of the glass.

The first original contribution of this work is entitled "*Novel Adaptations to Zinc-Silicate Glass Ionomer Cements - The Unexpected Influences of Germanium Based Glasses on Handling Characteristics and Mechanical Properties*" and was published in the Journal of the Mechanical Behavior of Biomedical Materials, Vol. 23, 2013 [60]. This chapter used a design of mixtures (DoM) approach to produce 11 experimental glass compositions based on the control SiO_2-ZnO-CaO-SrO glass chemistry. GeO_2 was incorporated into the glass chemistry up to a full replacement of SiO_2. ZrO_2 was included up to a maximum of 5 mol%, evenly matched with Na_2O for solubility purposes. The impact of the GeO_2 and ZrO_2/Na_2O substitutions on the zinc silicate GIC properties as assessed by evaluating working and setting times, and compressive strengths, biaxial flexural strengths, and biaxial flexural moduli up to 180 days.

The most significant contribution of Chapter 6 was the finding that the comoplete replacement of SiO_2 by GeO_2 significantly improved GIC handling characteristics without adversely impacting initial strength. Specifically, it was observed that Ge-based GICs (*i.e.* DG202, 205, 208) had working times of 5 to 10 minutes, setting times of 14 to 36 minutes, and maintained compression strength in excess of 30 MPa for the first 30 days. These handling characteristics represented a 10-fold increase to working times, and up to an 18-fold increase in setting times over the zinc silicate GIC control.

Despite improvements to the handling characteristics of zinc-silicate GICs, the clinical practicality of these Ge-containing cements was jeopardized by marked decreases

in strength over time. The initial mechanical findings reported for 3 of the 12 GICs in this Chapter (*i.e.* DG202, 205 and 208) revealed that cements comprising glasses where Ge is the sole network former lost as much as 67% of their compressive strength over the 180-day observation period (*i.e.* DG202: 36 MPa at 1d, 12MPa at 180d). However, subsequent mechanical analysis of the remaining 9 compositions (supplementary data, Section 6.8 pg. 102) demonstrated that glasses with both SiO_2 and GeO_2 present in approximately equal molar concentration, along with the precise control of *c.* 2.5 mol% ZrO_2, produced cements with extended handling characteristics and high mechanical properties that were sustained over time. The mechanism behind this sustained strength was not clear from the evidence gathered during these initial investigations. However, subsequent studies (Chapter 8) revealed that a Si:Ge ratio of 1:1 was an important factor in minimizing the Ge release from the GIC, which correlated with improved mechanical performance (Figure 44, pg. 157). Also, it is likely that the ability of Zr to reduce glass degradability is a contributing factor in the sustained strength of the GICs investigated in the DoM design space of Chapter 6.

Three compositions that embody the balanced strength and handling properties of Ge-containing GICs are DG209, 210 and 302. All three had both Si and Ge, with Zr content between 1.5 and 3.5 mol%. These three cements possessed working times of 5 to 7 minutes, setting times of 14 to 52 minutes, and compression strengths of 33-51 MPa at 1 day, which increased to 57-79 MPa over the 180-day observation period. These long setting times and high strengths demonstrate the clinical viability of Ge-containing GICs for vertebral body augmentation, as they are consistent with the 5-10 minutes of working time and the minimum 30 MPa compressive strengths required of injectable bone cement

for use in vertebral body augmentation procedures [31, 33]. Furthermore, this evidence demonstrates that the inclusion of Ge decouples the handling and mechanical properties of zinc silicate GICs. The mechanisms responsible for this were explored in Chapter 7 and Chapter 8.

In addition to Ge, the impact of Zr on the handling and mechanical properties of zinc silicate GICs was also explored in Chapter 6. The inclusion of Zr significantly altered the reactivity of both Si-based and Ge-based glasses, although its effects on GIC properties were more extensive when incorporated into Si-based compositions. Only minor adjustments in the molar concentration of Zr are necessary to substantially change the cement-forming capabilities of the glass. In the Ge-based composition DG208, the replacement of 10 mol% CaO with 5 mol% each of ZrO_2 and Na_2O reduced glass reactivity, extending the GIC setting time to 36 minutes from 16 minutes when Zr/Na was not included (*i.e.* DG202), with no impact to the initial mechanical properties. Alternatively, in Si-based glass, this same level of Zr/Na addition to the composition inhibited its cement-forming capabilities. Figure 46 depicts the results from subsequent

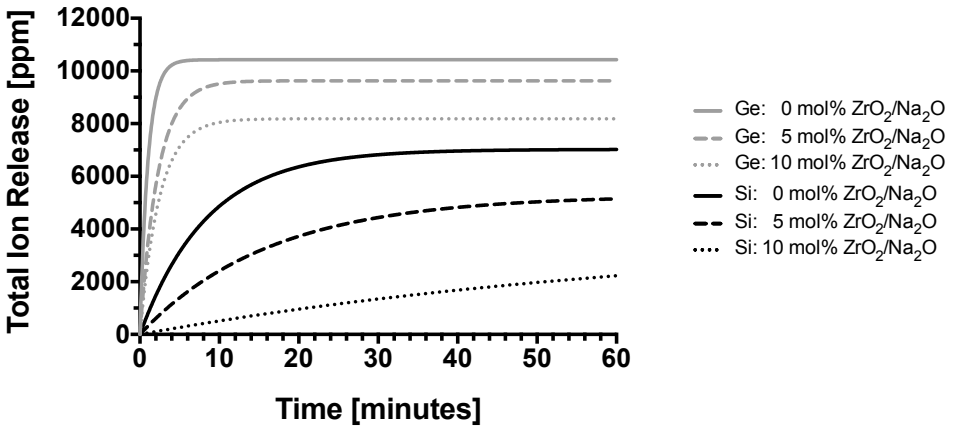

Figure 46: Ion release data demonstrating the reduced degradability of glasses when ZrO_2/Na_2O replaces CaO in GeO_2-ZnO-CaO and SiO_2-ZnO-CaO glass chemistries. Further details, including the materials and methods of this test are supplied in Appendix 2.

investigations; Zr significantly diminishes the reactivity of both Si and Ge based glasses, with up to 2.4-times slower ion release from Ge glasses and up to a 8.4-times slower ion release from Si glasses (Figure 46; Materials, Methods and Results in Appendix 2).

The mechanistic basis for the reduced reactivity of Zr-containing glasses may be deduced from the nuclear glass literature [308, 311, 312, 401]. Firstly, Zr commonly takes a network former role as a $[ZrO_6]^{2-}$ structure, which reduces NBO and polymerizes the glass network, as modifiers (*e.g.* Na^+ or Ca^{2+}) preferentially charge compensate the negative charge on the octahedral structure of Zr [312]. However, reduced cation release due the necessity to charge compensate the $[ZrO_6]^{2-}$ structures is unlikely the sole mechanism responsible for the reduced reactivity of Zr-containing glasses. This is evinced by two observations: (i) the extent to which Zr impacts the cement-forming capabilities of a glass, and (ii) the discrepancy between Si-based glasses, which did not form hardened cements, and Ge-based glasses, which successfully produced cements when the maximum amount of ZrO_2/Na_2O was included. The latter point also dispels the notion that the impaired cement-forming capabilities of glasses that contain ZrO_2/Na_2O is solely due to release of monovalent Na^+, which will inhibit the crosslinking of the GIC matrix as it only binds to one COO^- group [202]. Instead, the ability of Zr to diminish the rate of the GIC setting reaction is most likely due to its tendency to polymerize a thick gel-like barrier on the surface of the glass in aqueous environments, which has been found to prevent OH^- ions from attacking the silica network and limiting dissolution of neighboring atoms [308, 311, 312]. This mechanism has been found to significantly increase the durability of the glass in acidic environments, even when Zr makes up as little as 2 mol% of the glass composition [312, 401].

From the results of Chapter 6, it was determined that Ge was the critical factor in balancing the handling and mechanical properties of zinc silicate GICs. However, from the evidence of Chapter 6 the mechanistic basis for this balance was not clear. In contrast, glasses that contained Zr continued to obey conventional GIC behavior, *i.e.* where less reactive glasses yield slower setting and weaker GICs. Thus, Zr failed to exemplify the philosophy of this work, where the improvement of cement handling characteristics requires the GIC setting reaction to be delayed without limiting the release of divalent cations. Therefore, the investigations of Chapters 7 and 8 focused on the impact of replacing Si with Ge, not Zr, as the primary network former in the glass.

The objective of Chapters 7 and 8, respectively, were to elucidate the mechanisms responsible for the ability of Ge to decouple the handling and mechanical properties of zinc silicate GICs. Although DoM allowed for the efficient evaluation of the influences of Ge and Zr/Na on the handling characteristics of zinc silicate GICs, it failed to produce surface response models that accurately represented the mechanical properties of the DG GICs. Further, the complexity in the compositional design space obscured the assessment of the composition-property relationship between Ge and Zr/Na on the mechanical properties of zinc silicate GICs. Therefore, to simplify the investigations of Chapters 7 and 8 the BD glass series (0.48-x SiO_2, x GeO_2, 0.36 ZnO, 0.16 Ca, x = 0, 0.12, 0.24, 0.36, 0.48 mol. fraction) was designed where the divalent content was fixed (*i.e.* 0.36 ZnO and 0.16 CaO) and the only variable was the incremental replacement of Si by Ge. This glass series was used to investigate the impact of Ge on the GIC setting reaction (Chapter 7) and the long-term mechanical properties (Chapter 8).

The second original contribution of this work is entitled "*Evidence of a Complex Species Controlling the Setting Reaction Glass Ionomer Cements*", published in Dental Materials, Vol. 32, 2016 [61]. The objective of this chapter was to identify the mechanism(s) associated with Ge that are responsible for delaying the setting reaction of zinc silicate GICs. It was hypothesized that the replacement of Si by Ge would delay glass degradation, resulting in slower ion release and thus extend the GIC setting reaction. To test this hypothesis, Chapter 7 used the BD glass series and investigated the impact of the Si:Ge on four critical aspects of the GIC setting reaction (Figure 47).

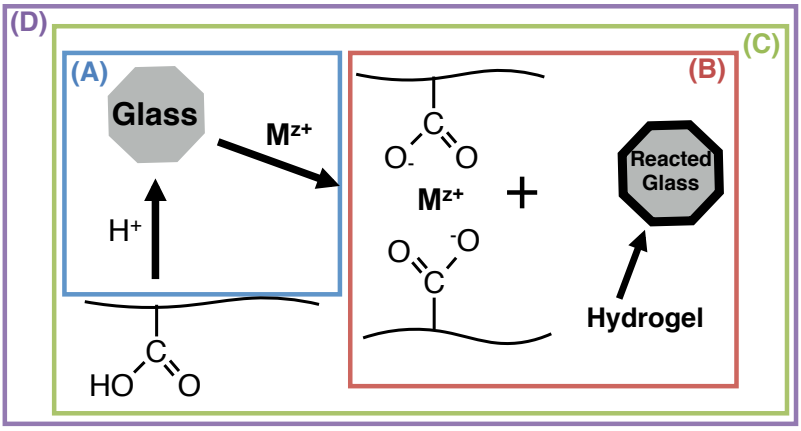

Figure 47: The experimental architectures of Chapter 7 explored four aspects of the GIC setting reaction: (A) glass reactivity; (B) formation of the GIC matrix; (C) GIC gelation, and (D) post-gelation hardening.

A. Glass reactivity was assessed by profiling glass degradation under simulated setting conditions.

B. Crosslinking of the GIC matrix was assessed by monitoring the formation of metal-carboxylate bonds *in situ* using ATR-FTIR spectroscopy.

C. Gelation of the cement was observed directly from the changes in the rheometer-derived viscosity profiles.

D. Post-gelation hardening of the GIC matrix was assessed by 24 h biaxial flexural strengths.

The critical finding of Chapter 7 was that Ge extends the GIC setting reaction through the introduction of an interim step that delays, but does not hinder, the formation of the GIC matrix. This conclusion was supported by the fact the reducing the Si:Ge ratio yields faster degrading glasses, yet contrary to expectation, the corresponding ATR-FTIR spectra indicated slower crosslinking of the GIC matrix. Further, the rheology testing demonstrated that the initial viscosity of cement pastes decreased as the Si:Ge ratio decreased and the onset of gelation was delayed. Finally, it was observed that as the Si:Ge ratio decreased, the rate of GIC setting was substantially reduced, reaching a minimum at Si:Ge 1:1, and sharpening as the ratio decreased futher. However, despite the considerable variation in the GIC setting behaviors, the biaxial flexural strengths remained consistent. The fact that Ge increases glass degradation but delays the formation of polysalt matrix is an inversion of the conventional theory of GIC setting [45]. This counter-intuitive combination of behaviors is attributed to the presence of a transient chemical complex species that delays, but does not prevent, divalent cations (*e.g.* Zn^{2+} or Ca^{2+}) from crosslinking GIC matrix.

The proposed complex is hypothesized to involve Zn and Ge, owing to their proportional release during the glass degradation study of Chapter 7 (Figure 33f). One possibility regarding the origin of this Ge/Zn complex may be the existence of $[GeO_5]^-$ or $[GeO_6]^{2-}$ structures in the glass that require charge compensation by Zn^{2+}. Support for the hypothetical Ge/Zn complex comes from their natural affinity for each other, as raw Ge is

primarily obtained as a by-product of refining zinc-based ores [402]. Furthermore, Zn and Ge are known to form oxide structures, mostly commonly $ZnGeO_3$ and Zn_2GeO_4, where Ge has an octrahedral and tetrahedral coordination, with the latter capable of forming in aqueous environments at room temperature [403-405]. Cumulatively, the evidence gathered throughout this chapter supports the formation of a chemical complex species as the likely mechanism that decouples the GIC handling characteristics from mechanical properties.

Interestingly, it was observed that the extended setting reaction of Ge-containing GICs was not linearly proportional to the Si:Ge ratio. As the Si:Ge ratio is reduced, a greater quantity of Ge and Zn are released from the glass in the form of the complex species, which slows the GIC setting reaction. However, as the Si:Ge ratio decreased past 1:1, the ATR-FTIR spectra, rheology, and handling characteristics of the cBD GICs indicated a shift in the influence of the complex mechanism from (i) *slowing* the setting reaction to (ii) *delaying* the onset of the setting reaction, a sharper rate of setting, following the trend: cBD1 < cBD2 < cBD3 > cBD4 > cBD5. This behavior parallels that of (+)-tartaric acid in alumniosilicate GICs, which inhibits the initial setting reaction by preventing premature crosslinking, thereby allowing the cement to retain fluidity for a longer time, while sharpening the final set [45, 383]. This shift is believed to arise from the reduced stability of the complex in the GIC solution associated with higher pH values, which arise from the faster acid-base neutralization that occurs in the presence of a more degradable glass. This is a significant finding as it reveals that manipulating the Si:Ge ratio directly controls the mechanism that governs the setting reaction, thus

allowing for tailored manipulations to the handling characteristics of the Ge-containing GICs.

The second critical finding of Chapter 7 was that the cement with the slowest setting reaction, *i.e.* cBD3 Si:Ge 1:1, also had the highest fracture toughness (K_{IC}) (Figure 37 pg. 132). The superior mechanical performance of this slow setting GIC is likely due to greater entanglement of the polycarboxylate chains within the GIC matrix. Although cement strength is influenced by both entanglement and extent of crosslinking within the polysalt matrix, the structural investigation of Chapter 8 found the population of metal-carboxylate bonds to be consistent regardless of the Si:Ge ratio (Figure 42f, pg. 154). Therefore, it is reasonable to consider that the delayed crosslink formation within the GIC matrix when Si:Ge 1:1 allows for greater entanglement of the chains prior to gelation of the cement. Evidence to support this theory comes from the observation that the K_{IC} values increased linearly with cBD GIC working times ($K_{IC} = 0.0126*W_t + 0.1022$, $R^2 = 0.98$). These K_{IC} results are promising, as they show that the setting reaction can be delayed with minimal impact on the initial mechanical properties of the cement; however, Chapter 6 raised concerns regarding the ability of Ge-containing GICs to maintain strength over time. Thus, it is necessary to develop an understanding of how manipulating the setting reaction of Ge-containing GICs effects their mechanical integrity over time.

The last original contribution of this body of work is entitled "*Exploring the Unexpected Influence of the Si:Ge Ratio on the Molecular Architectures and Mechanical Properties of Al-free GICs*", and is currently under consideration by the Journal of Biomaterials Applications for publications (status: under review May 13, 2016). The

objective of Chapter 8 was to expand the composition-structure-property relationships that describe the impact of replacing Si by Ge in zinc silicate GICs, with a focus on the mechanical properties. Specifically, this Chapter attempted to identify (i) the optimal Si:Ge ratio to maximize strength up to 180 days, and (ii) the potential mechanism(s) responsible for the time-induced mechanical instability of Ge-based GICs as discussed in Chapter 6. The influence of Si:Ge on the mechanical properties of the cBD GICs, was evaluated on the basis of compressive strength and modulus over a 180-day period. This mechanical data was compared against temporal changes in molecular architectures of the cements, assessed by: (i) structural investigations of the GIC matrix, (ii) quantification of the degradation by-products released from the cement, and (iii) electron micrographs of the surface microstructures of cBD1 and cBD5. For completeness, the working and setting times of the cBD GICs were also evaluated to allow for direct comparison within Chapter 8 regarding the influence of Si:Ge ratio on the GIC handling and mechanical properties.

The key finding of the Chapter 8 was that the Si:Ge ratio of 1:1 maximizes the compressive strength (> 50 MPa) at 1 and 180 days, in addition to having exhibited the longest working and setting time, *c.* 13 minutes and *c.* 37 minutes, respectively. This finding supports previous observations regarding the influence of Si:Ge ratio on balancing the handling and mechanical properties of zinc-silicate GICs. Chapter 8 confirms the finding of Chapters 6 and 7, in that the slowest setting cements yield the greatest mechanical properties. Additionally, Chapter 8 demonstrates that Zr is not an essential compositional element to ensure lasting mechanical integrity when 3:1 > Si:Ge ≥ 1:1. Lastly, Chapter 8 identified that the long-term instability of the Ge-based GICs

reported in Chapter 6 occurred when the glass had a Si:Ge < 1:1. The mechanistic basis for this decline is likely due to a combination of: (i) the increased porosity associated with low viscosities cement; (ii) the plasticizing effect of water on the matrix; and (iii) void creation within microstructure cement due to high level of Ge release. However, a Si:Ge of 1:1 mitigates against the deleterious effects of these mechanisms and, as mentioned above, ensures extended handling characteristics are balanced with sustained mechanical properties.

The mechanical and structural investigations conducted in Chapter 8 provided additional information regarding the impact of the complex-mediated setting reaction of the Ge-containing GICs. The compressive strength data indicates a minimum quantity of Ge (Si:Ge < 3:1) is required for the proposed complex mechanism to extended handling characteristics without reducing initial strength. Interestingly, the biaxial flexural and compressive strength data show cBD2 to be significantly weaker than other Ge-containing GICs at 1 day (except cBD4 CS). Given the consistent level of crosslinking in the matrices of all compositions at 1 day as measured by ATR-FTIR, the reduced mechanical performance of cBD2 is likely associated with a less entangled matrix, the other major contributing factor to GIC strength [45]. Further evidence to support this assertion comes from the fact that cBD2 had the lowest K_{IC} and working time values, two test that are sensitive to the degree of entanglement within the matrix [237]. From these data, it is reasonable to conclude that the mechanical impact of the complex formation is mediated by the magnitude of the delay it imposes on the GIC setting reaction.

The experimental evidence from this body of work demonstrates that replacing SiO_2 with GeO_2 in SiO_2-ZnO-CaO glass chemistry decouples the handling and

mechanical properties of GICs. Throughout the three investigative chapters of this work, several key composition-structure-property relationships were identified. DG302 is the embodiment of the sum total of these relationships. This glass has a molar composition of 0.36 ZnO, 0.269 GeO_2, 0.206 SiO_2, 0.09 CaO, 0.04 SrO, 0.0175 ZrO_2 and 0.0175 Na_2O, which was generated from the DoM methodology. The Si:Ge ratio of DG302 is 1:1.3, slightly above the 1:1 ratio identified throughout this work as necessary to maximize the handling characteristics. When DG302 was mixed with polyacrylic acid (50 wt% aq. sol., M_w=12,500 g mol^{-1}) the resultant cement had a working time of *c.* 7 minutes and a setting time of *c.* 51 minutes. The slow transition between the working and setting times is likely associated with the stability imparted to the glass by the 0.0175 ZrO_2 mol. fraction. Further, this steady rise in viscosity improves the injectability of the cement, which for DG302 yields injection times of *c.* 10 minutes (supplementary data, Table 9, pg. 113) when expelled from a 1cc syinge through a 10 cm long 12 G cannulae, (*i.e.* those conventionally used for vertebral body augmentation [10]). The Si:Ge ratio of 1:1.3 and the 0.0175 ZrO_2 mol. fraction are two compositional features that ensure high and sustained strengths up to 6 months. The 1 and 180-day compression strengths of DG302 were 51 MPa and 79 MPa, which made this GIC the strongest composition produced during this work. The last distinctive feature of the DG302 composition is the extended handling properties coupled with high strength that *increase* over time. The balance between the handling characteristics and mechanical properties of DG302 exemplifies the clinical viability of Ge-containing GICs in vertebral body augmentation, where cements are required to be injectable for at least 5-10 minutes and have compressive strengths in

excess of 30 MPa [31-33]. However, several critical areas remain to be investigated with respect to Ge-containing GICs, one of which is biocompatibility.

Owing to their adhesive nature, negligible setting exotherm, and potential bioactivity, GICs have been described as having excellent biocompatibility in dental applications [48, 406, 407]. However, as exemplified by the discussion in Section 4.7 , the *in situ* release of toxic ions (*e.g.* Al^{3+}) from the cements can be detrimental to patient safety [46, 47]. Key areas of concern regarding ion release from GICs are (i) susceptibility to washout of unset cement paste when delivered *in vivo*, and (ii) the elution of ions from hardened cements over time that may cause unfavorable host responses [46-48]. The primary concern regarding Ge-containing GICs is the release of Ge *in vivo.* As discussed in Chapter 8, the release of Ge from Ge-containing GICs is minimized when Si:Ge is 1:1, the same ratio that is necessary to achieve clinically practical handling and mechanical properties. Thus, the risk associated with Ge release will be curtailed in the event of clinical use of Ge-containing GICs in skeletal applications. The current understanding regarding the physiological effects of Ge on the skeletal system is limited. It appears that Ge performs the same role as Si in bone metabolism, and may exert beneficial effects on bone mineral density and bone mineral content [408, 409]. However, caution has been raised in the literature regarding potential toxicity associated with the over exposure of Ge *via* oral consumption of GeO_2, which has been reported to affect renal function [410, 411].

Concurrent with this body of work, investigations regarding the biocompatibility of Ge-containing GICs have been conducts by colleagues. Dickinson investigated the *in vitro* cytotoxicity of the DG series GICs from Chapter 6, using MTT assays with NIH

3T3 mouse fibroblasts cells exposed to 1, 7, 30 day cement extracts. Dickinson observed cell viability in excess of 90% at all time points for all Ge-containing GICs [412]. Further evidence to support the safety of Ge-containing GICs comes from a recent publication by Pierlot *et al.* [413]. The Ames assay was used to assess the genotoxicity of GICs comprising 0.48-x SiO_2, x GeO_2, 0.36 ZnO, 0.11 CaO, 0.025 ZrO_2, 0.025 Na_2O glass chemistries, where x = 0, 0.12, 0.24, 0.36, 0.48 mol. fraction, based on 72 h elution extracts of set cements. Results demonstrated that all compositions released less than 150 ppm Ge and were found to be non-mutagenic [413]. Together, these *in vitro* results demonstrate an initial promising biocompatibility profile for the Ge-containing GIC. However, *in vitro* results are intrinsically limited and there can be large disconnect between *in vitro* and *in vivo* findings primarily due to the lack of host response [170]. To the best of the author's knowledge, there have been no studies published that have investigated aluminum-free GICs in *in vivo* using hard tissue models to assess host response. Perhaps this is due to the dichotomous nature between the handling and mechanical properties of aluminum-free GICs, which hinders the practicality of delivering the material *in vivo*. However, the positive results *in vitro* combined with the balanced properties of Ge-containing GICs has allowed for their use *in vivo*. In a recently submitted paper, Pierlot *et al.* describes the outcome a pilot animal trial that evaluated DG302 in a sub-chronic, femur defect model in New Zealand White rabbits (n=4, 2 animals, 2 defect sites per animal) over an 8 week period [414]. The study found DG302 elicited a tissue response characterized by a mild incomplete fibrous layer, which was not considered to be encapsulating, as multifocal cement-bone apposition was observed. This result suggest that Ge-containing GICs have potential osteoconductive and/or

osseointergrative qualities (Figure 48) [414]. The lack of complete fibrous encapsulation is important as it shows that the Ge-containing GICs do not provoke a significant inflammatory response. Further, the direct cement-bone apposition is critical for the stability of the implant *in vivo* [38]. Thus, this pilot study demonstrates the promise of Ge-containing GICs to be safe and effective bone cement for the augmentation of hard tissues.

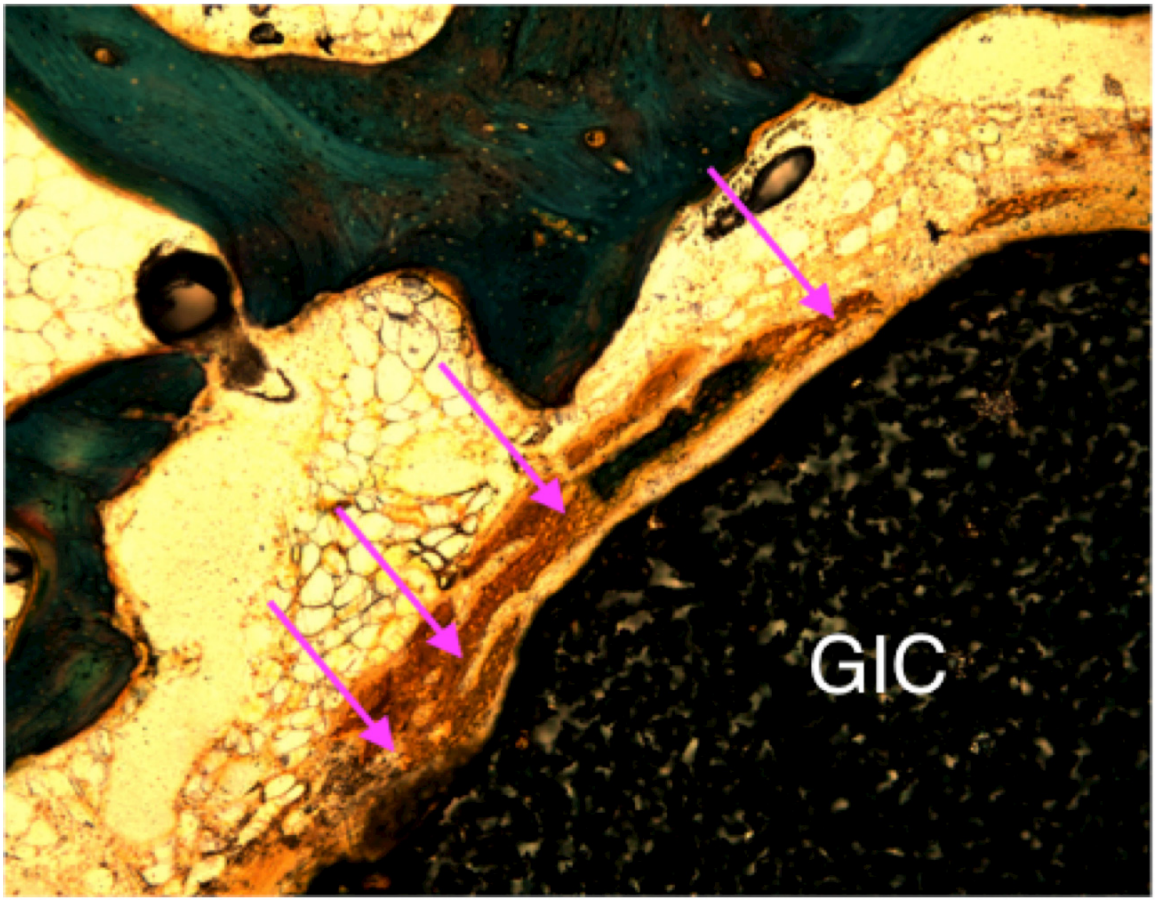

Figure 48: Histological image with Goldner's Trichrome stain of the DG302 (GIC) demonstrating multifocal bone-biomaterial appositions (arrows), adapted from Pierlot *et al.* 2016 [414].

In conclusion, this body of work revealed that changing the network former in the glass chemistry is an effective means of modulating GIC properties. The evidence herein

demonstrates replacing Si with Ge redresses the dichotomous nature between the handling and mechanical properties of aluminum-free GICs, which has been a critical limitation to clinical use of these materials in orthopaedic applications. The inclusion of Ge in zinc silicate glass composition yields counter-intuitive setting chemistry, where Ge delays the formation of the molecular structures, likely due to the development of intermediate step associated with the formation of a chemical complex species. Unexpectedly however, the slower a Ge-containing GIC sets, the stronger it becomes, behaviors that are uncharacteristic of conventional GICs. Ultimately, the precise control of the ratio between Si and Ge in the glass chemistry produces injectable zinc silicate GICs with handling and mechanical properties are practical for clinical use.

The properties of the Ge-containing GICs of this work, specifically DG302, are consistent with those described for an ideal bone cement. Their non-toxic composition, and potential for osteoconduction and/or osseintegration alleviates the concerns associated with PMMA bone cements. The steady rise in viscosity that DG302 exhibits lends itself to forgiving injection qualities for enhanced control, which addresses a key limitation expressed by clinicians regarding the use of Cortoss. Further, upon injection these cements remain cohesive, a barrier for the use of calcium phosphate cements in vertebral body augmentation. Lastly, the increasing strength of DG302 signifies its potential to provide lasting stability, a concern regarding calcium sulfate cements. For these reasons, Ge-containing GICs are clinically viable for use in vertebral body augmentation for the stabilization of fractures in the spinal column.

9.1 Future Work

This body of work has generated many intriguing and diverse questions. In general terms, future investigations should consider: the germanium glass structure and its role in the proposed creation of complex species during the setting reaction; the nature of the Si:Ge ratio of 1:1 in maximizing the handling and mechanical of GICs; and lastly, can the slow setting nature of Ge-containing GICs facilitate the use of higher molar mass PAA. Further work within these areas would be of value to the scientific communities in the fields of glass, glass ionomer cement, and hard tissue biomaterials.

The first suggested area for future work is the structural investigations of Ge-based glasses and GICs to investigate the hypothesized complex species. The complex-based mechanism considers the concept that Zn^{2+} charge compensates higher coordinated Ge structures, such as $[GeO_6]^{2-}$. Attempts within this work to elucidate the structural configuration of Ge in the glass network were unsuccessful. Specifically, Raman spectroscopy was used, but failed to correlate any substantive change in the glass network as Ge replaced Si (Figure 54, pg. 203). A more thorough investigation of the BD series glasses (0.48-x SiO_2, x GeO_2, 0.36 ZnO, 016 CaO) would help form a structural basis for the potential existence of a complex species. Unfortunately, NMR is not a suitable characterization technique for Ge-based glass, as ^{73}Ge has a low gyromagnetic ratio, large quadrapole moment and low natural abundance [370]. Further, Raman spectroscopy, a common technique used to investigate Ge-based glass [348, 415], was found to lack sufficient precision. Therefore, the use of alternative techniques should be considered to assess the structure of Ge-based Glass. One such technique is extended x-ray absorption fine structure (*i.e.* EXAFS), which is sensitive to changes in bond length. This technique

has been used to observe the lengthening of Ge–O bonds from 1.73 Å, characteristic of GeO_4, to 1.80 Å, characteristic of GeO_6 structures in the glass network [416, 417]. The provision of such data could help identify: (i) the coordination state of Ge in the glass (*i.e.* GeO_4 or $[GeO_6]^{2-}$), (ii) if the coordination state of Ge changes as a function of composition, and (iii) potential interactions between Ge and Zn in the glass, due to the sensitivity of EXAFS to near neighbors in the glass network [418, 419]. Such data may provide useful structural evidence in determining the origins of the proposed complex species.

The second area of proposed future work considers the hypothetical Ge/Zn complex species. A reasonable point to initiate subsequent investigations of this complex is the exploration of the existence of potential crystal structures in GIC pastes during the setting. Two such potential structures include $ZnGeO_3$ and Zn_2GeO_4, which comprise octahedral and tetrahedral coordinated Ge respectively. These structures have unique and discernable XRD patterns [371, 403-405, 420]. Additionally, the latter, is known to form in aqueous environments at room temperatures [371, 403, 404, 420]. One proposed methodology for the detection these oxides in GIC pastes during the setting reaction is to profile the XRD patterns at distinct and various time points. cBD5 (Chapter 7) demonstrates the most radical shift in setting behaviors, and thus represents a suitable glass composition to explore the existence of the complex. Briefly the methodology is envisioned as such: blend Ge-based glass (BD5: 0.48 GeO_2, 0.36 ZnO, 0.16 CaO mol. fraction) with a 50 wt% aqueous solution of PAA M_w=12,500 g mol^{-1} for 30 seconds. Allow the setting reaction to proceed for 1, 2, 5, 7, 10, 15, 20, 25, and 30 minutes, (n=3 samples per time point). After each allotted time point immerse the GIC paste in liquid

nitrogen to freeze and stop the setting reaction. Subsequently, powderize and store frozen specimens in cold storage (*c.* -20 ˚C) prior to XRD analysis using a < 0 ˚C substrate. The resultant XRD profiles should be examined for evidence of the transient presence of crystalline species, such as $ZnGeO_3$ and or Zn_2GeO_4.

The third area of potential investigation would refine the examination of the Si:Ge ratio. This work provided evidence of a parabolic trend in GIC properties centered about the Si:Ge ratio of 1:1. To highlight this observation Figure 49 illustrates the handling and mechanical data of the cBD series GICs normalized to the maximum value in each of the respective data sets (*i.e.* working times, setting times, K_{IC}, biaxial flexural strengths, and 1 and 180-day compressive strengths). The incremental steps of the BD series glasses (0.12 mol. fraction) investigated in Chapters 7 and 8 were too coarse to decipher if Si:Ge 1:1 is the actual maxima, or if there is a plateau in properties about the

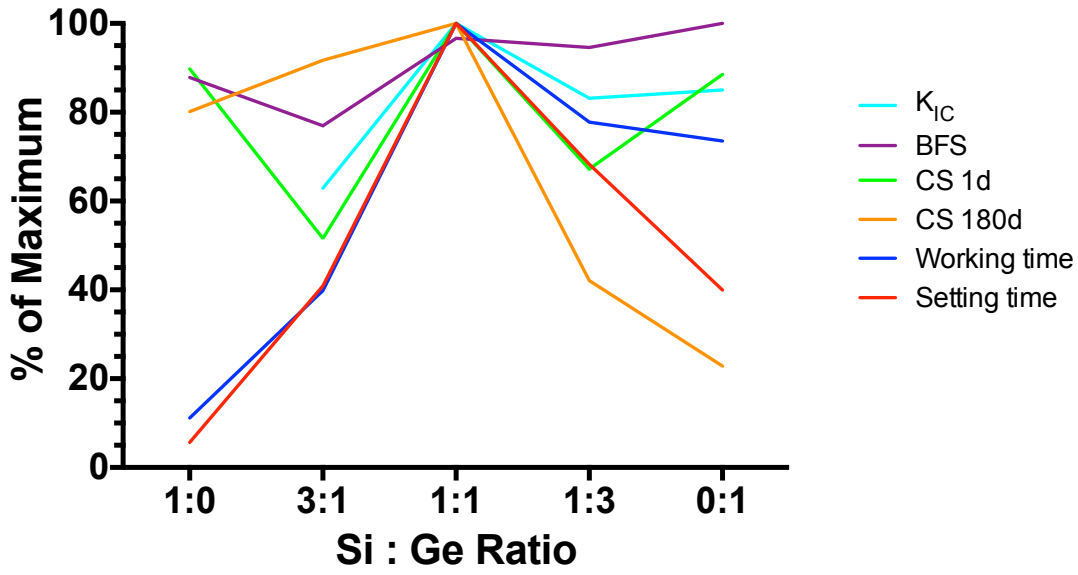

Figure 49: Normalized handling and mechanical properties of the cBD GICs demonstrating the maximizing effect of Si:Ge 1:1

1:1 ratio. Thus a new glass series is proposed with a more precise adjustment to the Si:Ge ratio: 0.28-x SiO_2, 0.20+x GeO_2, 0.36 ZnO, 0.16 CaO; x = 0, 0.02, 0.04, 0.06, 0.08 mol. fraction). The effect of this finer adjustment in Si:Ge ratio should be evaluated in terms of both GIC setting reaction and long-term mechanical properties. For the setting reaction, the methodologies utilized in Chapter 7 would be relevant; *i.e.* glass ion release under simulated setting, ATR-FTIR to follow the formation of GIC matrix structure during gelation, and rheology to develop gelation profiles all up to 60 minutes. Further, it may be the case that the complex acts in a similar fashion to (+)-tartaric acid, *i.e* its existence is mediated by the pH of the GIC solution [45]. These experiments should be supplemented by monitoring the pH as the GIC sets using a flat-ended pH probe [360]. Comparing pH changes with infrared spectra and rheological data may further elucidate the unique characteristics of Ge-containing GICs. With regards to mechanical properties, double torsion fracture toughness [235] evaluated up to 180 days may yield the most relevant information regarding structural changes in the GIC matrix over time. For completeness compression strength should be included to facilitate comparison between new and existing data.

Finally, as this work used only one PAA composition (50 wt% aq. sol. of M_W 12,500 g mol^{-1}), it would be beneficial to assess the impact of varying the PAA molar mass and concentration on the handling and mechanical properties of the GIC. Increasing the molar mass and concentration of PAA enhances the mechanical properties of the cement, but also raises the viscosity of the cement paste, making mixing more difficult [233-235]. It is hypothesized that the slow setting nature of Ge-containing GICs with Si:Ge *c.* 1:1 can facilitate the use of high molar mass PAA and thus augment the

mechanical properties of the cement. The objectives of this experiment would be: (i) to explore the relationship that Ge-containing GICs have with the critical PAA molar mass (*i.e.* 80,000-100,00 g mol^{-1}) where GIC failure transitions from chain pullout to chain scission [237, 244]; and (ii) to maximize mechanical properties and determine the suitability of Ge-containing GICs for other clinical applications. The materials for this investigation should include (i) the Ge-containing GIC with the best combination of strength and handling; and (ii) multiple PAA compositions with molar masses that range between 25,000 - 210,000 g mol^{-1} in aqueous solutions with concentrations of 35 to 55 wt% [233-235]. Rheology and ATR-FTIR structural analysis would be appropriate measures to determine the impact of PAA molar mass on the setting reaction of the Ge-containing GIC. As for the mechanical analysis, K_{IC} would be most appropriate to determine the impact greater chain length has on the mechanical properties of the cement. The benefit of such work would be to assess the potential of the Ge-containing GIC platform for use in more load intense clinical applications, such as total joint replacement.

Appendix I: Additional Information Regarding the DG Series Glasses and GICs

X-ray Diffraction of DG series Glasses

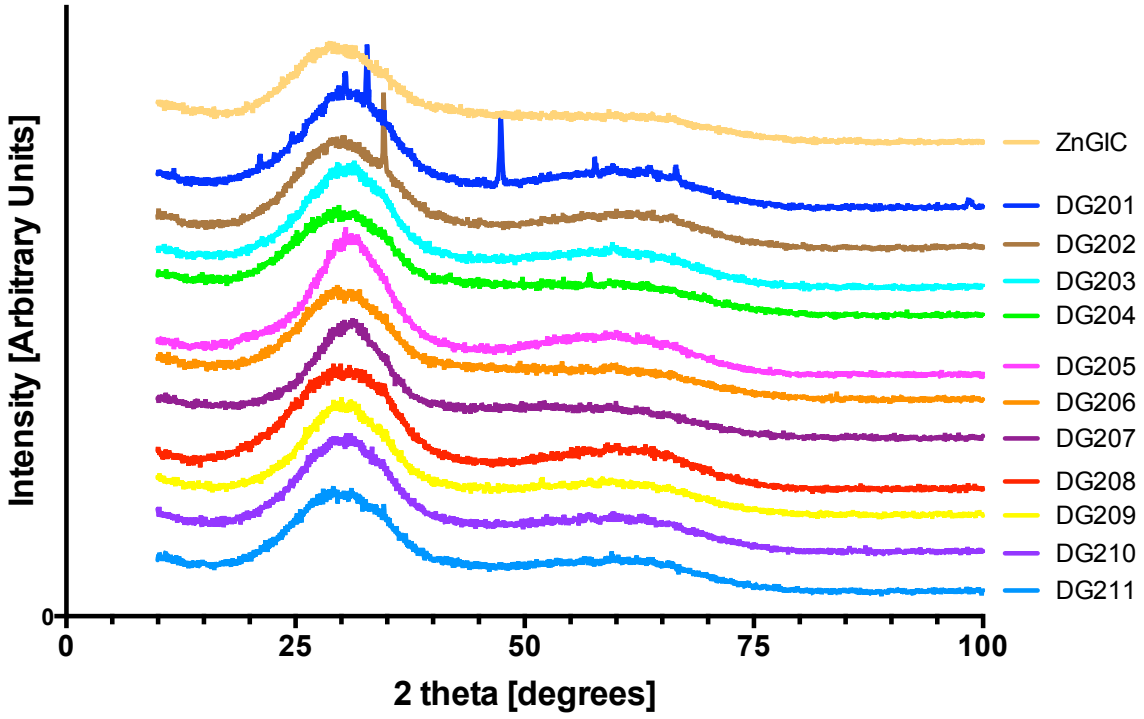

Figure 50: Representative XRD profiles of the DG series glasses used in Chapter 6.

^{29}Si MAS-NMR of DG series Glasses

Experiment and analysis conducted by Dr. Ulrike Werner-Zwansiger, Nuclear Magnetic Resonance Research Resource, Department of Chemistry Dalhousie University.

Methods

The structure of annealed SiO_2-containing DG series glass powders were probed with a ^{29}Si MAS NMR (Bruker Advance NMR spectrometer with a 9.4T magnet and a 79.51 MHz ^{29}Si Larmor frequency) using 7 mm rotor diamters. The samples were spu at 5.00 kHz. Between 132-320 scans were accumulated with single pulse excitation using a pulse length of 5.24 μs at 42 kHz rf field strength. The recycle delays were chosen to be five times the spin lattice relaxation times, which range between 17 and 30 seconds as determined by inversion recovery sequences. The chemical shift scale was referenced externally against Kaolin as secondary chemical shift standard at -91.65 ppm (center between doublet) as referenced against TMS. Lineshape fits were performed with the program dmfit (Version dm2010vs).

Results

Figure 51 presents an overview of all NMR spectra defined by their label and composition (mol%). All spectra, except DG203 and 204 were fit with two Gaussian functions centered around -76 ppm and -82 ppm at approximately a 1:1 ratio. DG203 and 204 were fit one Gaussian function centered at -76.8 ppm and -81.9 ppm respectively. These peaks are in the vicity of Q^2 and Q^3 depending on the composition of the glass. Maximum peak positions correlate roughly with the overall oxygen content and higher oxygen content relates to lower chemical shift values. DG200 deviates from this trend, as

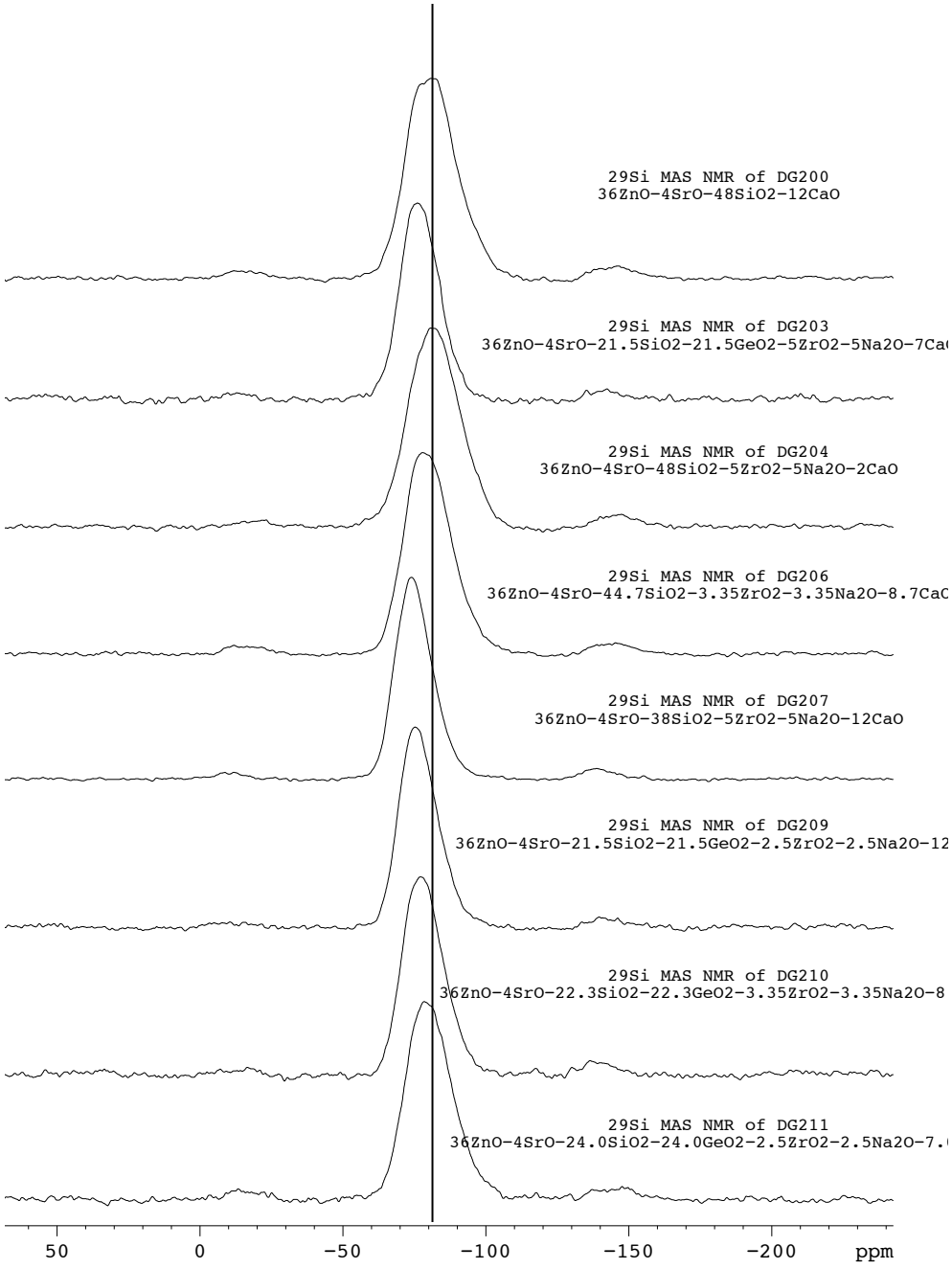

Figure 51: ^{29}Si NMR spectra of SiO_2-containing DG series glasses. Glass composition is listed to the right of each spectra

its oxygen content lies in the middle of all values, but it has a low chemical shift and thus higher network connectivity. Oxygen content is lowered by replacing SiO_2 with CaO or Na_2O, which corresponds to a shift to higher Q-species with lower frequencies. It was

observed that the line width and peak maximum are proportional to the sum of SiO_2 and GeO_2 concentrations, suggesting both act as network forming components. It seems that Ge-containing samples exhibit slightly higher liner width than those spectra from samples that only contain Si as network former. This behavior is attributed to the development of Si-O-Ge bonds in addition to Si-O-Si bonds, which have different chemical shifts. This indicates Ge acts similarly to Si in its network forming capability, as view from ^{29}Si NMR.

Assessment of Radiopacity

The minimally invasive procedures of PVP and KP are conducted under fluoroscopic guidance, thus the cements are required be radiopaque.

Methods

GICs were synthesized from the DG series glass in the same manner as described in Section 6.3.4 The radiopacity of the GICs were calculated according ISO9917 [340]. Cement discs (Ø14mm x 1.7mm) were prepared and irradiated groups alongside an aluminum step wedge (12 steps, 1.3mm to 12.6mm thick) at a distance of 400mm under 70kV and 7mA, using a Phot-X II x-ray source (Belmont Equipment, USA). Specimens were exposed on Kodak Insight IO-41 dental film (Carestream Dental, CAN). The optical density of each material and aluminum step was found using a QAS Densitometer (Picker International, USA). The 'equivalent aluminum thickness' was found by dividing the sample's thickness by the thickness of the aluminum step with an equivalent optical density. In instances where the density fell between two steps, the thicker step was taken, as per ISO 9917 procedure.

Results

All DG GICs are inherently radiopaque, as shown in Figure 52. When irradiated next to the aluminum step wedge, the 12 GICs demonstrated radiopacities equivalent to 1.8–3.1mm of aluminum (Table 15). The most radiopaque compositions were DG201 and DG210, both equivalent to 3.1mm of aluminum, while the least radiopaque composition was ZnGIC, at 1.8mm of aluminum. Generally, the addition of GeO_2 or ZrO_2/Na_2O increased the radiopacity of the materials. However, all compositions are statistically

similar, thus no strong conclusion can be made about the effects of glass composition on radiopacity.

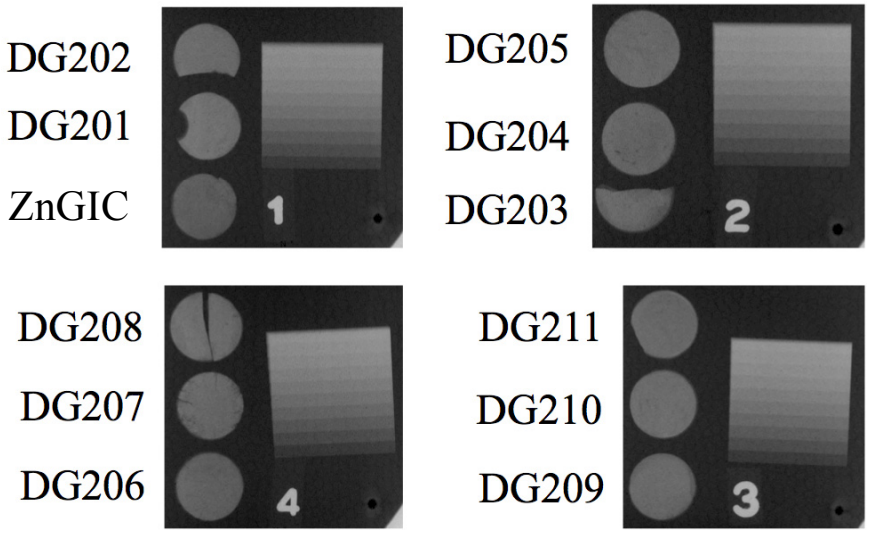

Figure 52 : Radiographs of the 12 GIC compositions, *c.* 1mm thick, irradiated next to an aluminum steph wedge, consisting of 12 equi-thickness steps between 1.3mm and 12.6mm thick.

Table 15: Radiopacity of DG series GICs, mean(SD).

Composition	Equivalent thickness of Al [mm]
ZnGIC	1.8 (0.4)
DG201	3.1 (0.0)
DG202	3.0 (0.0)
DG203	2.7 (0.4)
DG204	2.5 (0.0)
DG205	2.8 (0.4)
DG206	2.1 (0.4)
DG207	2.3 (0.4)
DG208	2.9 (0.4)
DG209	2.6 (0.4)
DG210	3.1 (0.0)
DG211	2.9 (0.4)

Mathematical Response Models of Mechanical Properties of DG Series GICs from Chapter 6

The design of mixtures (DoM) methods described in Sections 6.3.1 and 6.3.6 were used in an attempt to produce mathematical response models for the (i) compression strength (CS), (ii) biaxial flexural strength (BFS), and (iii) biaxial flexural modulus (BFM) responses, using the 1-day and 180-day data from Figure 27, Figure 28, and Figure 29. In each model, the quadratic Scheffé model (Equation 1) was found to provide the best-fit, based on the R^2 values. The regression models are summarized in terms of their L-pseudo components in Table 16 throughTable 18. For a model to represent the data to a statistically significant level requires the P-value to be less than 0.05. A significant model must yield R^2, $R^2_{Adjusted}$, and $R^2_{predicted}$ within 0.2 of each other for the model to be considered an accurate representation of the response across the entire design space [421]. Despite these shortcomings, significant models were successfully developed for CS at 1 day, and BFM at 1 day, indicated by P-value of less than 0.05. However, these four models yielded poor R^2_{pred} values, indicating the models were poor representations of how the properties changed across the design space. The models from the DoM analysis of the handling characteristics showed that this approach is valid for GICs (Section 0); however, it appears the complexity of the mechanical properties, which is only made worse by their temporal variations, may be too much for the DoM approach to successfully model. Future use of DoM modeling of GIC mechanical properties may be more successful if a greater number of design points (glass compositions) are used to improve the models' robustness, or, if the design space varies fewer than 4 components.

Table 16: Final regression models in terms of L-pseudo components, and R^2 values, and summarized ANOVA for compression strength (CS) of DG series GICs response.

			Summarized ANOVA				
Response	Regression Model		R^2	R^2adj.	R^2pred.	P Value	F
	+7.16	* SiO_2	0.9617	0.9043	0.3196	0.0083	16.75
1-day	–14.31	* GeO_2					
CS	–1016.06	* ZrO_2/Na_2O					
[MPa]	+273.75	* CaO					
	–51.02	* SiO_2 * GeO_2					
	+1365.94	* SiO_2 * ZrO_2/Na_2O					
	+1570.74	* GeO_2 * ZrO_2/Na_2O					
	+86.65	* SiO_2	0.9919	0.9193	N/A	0.2071	13.66
180-day	+133.58	* GeO_2					
CS	–3272.32	* ZrO_2/Na_2O					
[MPa]	+2675.16	* CaO					
	+92.25	* SiO_2 * GeO_2					
	+3396.76	* SiO_2 * ZrO_2/Na_2O					
	–3508.28	* SiO_2 * CaO					
	+3332.49	* GeO_2 * ZrO_2/Na_2O					
	–3924.55	* GeO_2 * CaO					
	+4068.29	* ZrO_2/Na_2O * CaO					

Table 17: Final regression models in terms of L-pseudo components, and R^2 values, and summarized ANOVA for biaxial flexural strength (BFS) of DG series GICs response.

			Summarized ANOVA				
Response	Regression Model		R^2	R^2adj.	R^2pred.	P Value	F
	+26.73	* SiO_2	0.6397	0.3996	0.1203	0.1365	2.66
1-day	+28.43	* GeO_2					
BFS	–90.68	* ZrO_2/Na_2O					
[MPa]	–66.60	* CaO					
	+673.77	* ZrO_2/Na_2O * CaO					
	–51.87	* SiO_2	0.6202	0.2404	–1.1469	0.3018	1.63
180-day	–56.32	* GeO_2					
BFS	–1458.27	* ZrO_2/Na_2O					
[MPa]	+322.81	* CaO					
	+2128.19	* SiO_2 * ZrO_2/Na_2O					
	+2147.11	* GeO_2 * ZrO_2/Na_2O					

Table 18: Final regression models in terms of L-pseudo components, and R^2 values, and summarized ANOVA for biaxial flexural modulus (BFM) of DG series GICs response.

			Summarized ANOVA				
Response	Regression Model		R^2	R^2adj.	R^2pred.	P Value	F
1-day BFM [GPa]	–0.67	* SiO_2	0.9695	0.88982	-1.4320	0.0277	13.61
	+4.87	* GeO_2					
	–16.06	* ZrO_2/Na_2O					
	–101.46	* CaO					
	+3.39	* SiO_2 * GeO_2					
	+135.10	* SiO_2 * CaO					
	+109.12	* GeO_2 * CaO					
	+229.81	* ZrO_2/Na_2O * CaO					
180-day BFM [GPa]	–9.89	* SiO_2	0.6580	0.3159	–0.4795	0.2450	1.92
	–9.18	* GeO_2					
	–248.81	* ZrO_2/Na_2O					
	+54.51	* CaO					
	+363.97	* SiO_2 * ZrO_2/Na_2O					
	+359.44	* GeO_2 * ZrO_2/Na_2O					

Validation of Mathematical Response Models

Two addition glass compositions (DG302 and DG303, Table 19) were designed and synthesized to test the predictive qualities of the mathematical response models produced by the DoM methodology. Due to the inability to adequately model the mechanical properties of the DG GICs, DG302 and DG303 were designed based on optimizing the GIC handling properties to maximize working time, and achieve a setting time between 10 and 20 minutes [31]. Table 20 compares the model predicted values against the experimentally determined 'actual' values. There was reasonable agreement in working time, although the model over-predicted the response for both compositions. The setting times model drastically under-predicted setting time of DG302, as the actual value was

30 minutes longer than the predicted value. DG303 was much closer. This discrepancy suggests it may be worthwhile to revisit the setting time model to see if it can be updated to more accurately represent this new design point. Despite the lack of predictive qualities amongst the mechanical DoM models (Table 16 through Table 18); there are some reasonably close comparisons between the predicted and actual values of CS, BFS and E_B in Table 20, more so for DG303 than 302. This is an important observation as it shows that models predict some regions of the design space better than others. By identifying these regions, users can have more confidence in the model, which may improve outcomes of the optimization process.

Table 19: Optimized DG GIC glass compositions.

	ZnO	SrO	SiO_2	GeO_2	CaO	ZrO_2	Na_2O
DG302	0.36	0.04	0.206	0.269	0.09	0.0175	0.0175
DG303	0.36	0.04	0.165	0.262	0.12	0.0265	0.0265

Table 20: Handling and mechanical properties of DG302 and DG303. The 'predicted' values are those predicted by the DoM models. The 'actual' values are the average experimentally determined results.

	DG302		DG303	
Property	Predicted	Actual	Predicted	Actual
Working time [min:sec]	7:11	6:41	6:01	5:02
Setting Time [min:sec]	20:00	50:46	15:55	20:43
CS [MPa]				
1 Day	29.0	51.1	43.7	47.9
180 Day	59.0	78.8	71.3	64.0
BFS [MPa]				
1 Day	14.2	13.2	11.4	14.6
180 Day	12.1	23.1	26.2	13.9
BFM [GPa]				
1 Day	2.62	2.11	1.97	2.93
180 Day	1.65	4.28	4.00	2.46

Appendix II: Additional Information Regarding the BD Series Glasses and GICs

X-ray Diffraction of BD Series Glasses

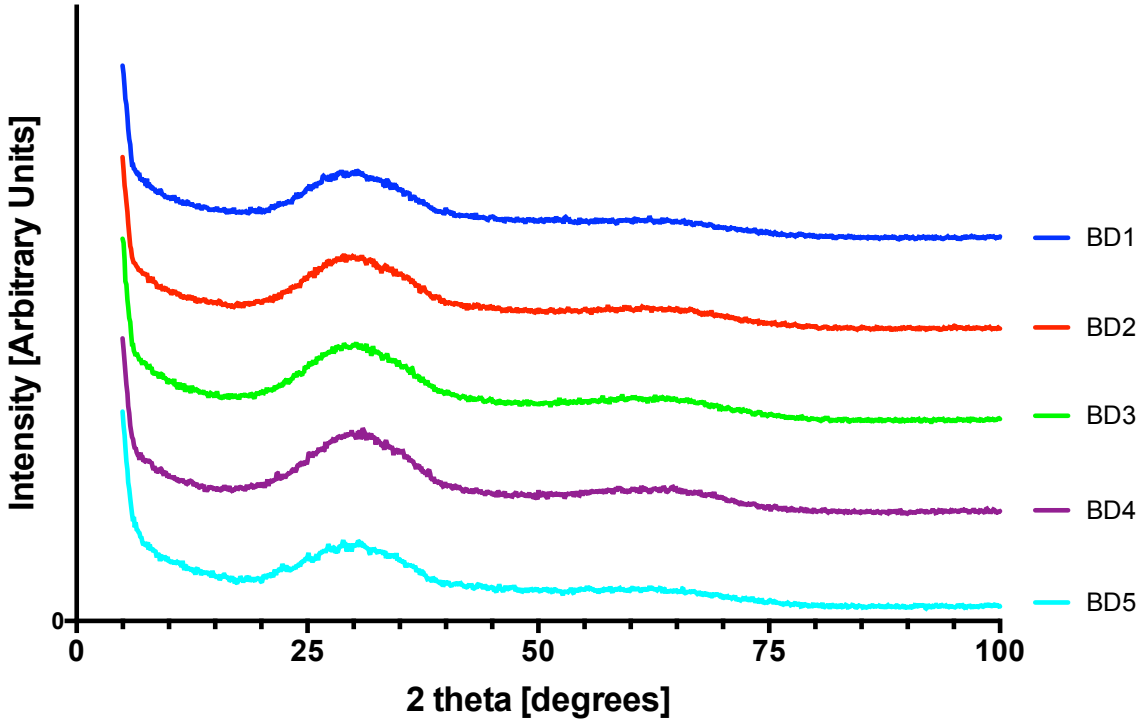

Figure 53: Representative XRD profiles of BD series glasses.

Raman Spectroscopy of BD Series Glasses

Experiment conducted by Michael Johnson, Department of Chemistry, Dalhousie University. Analysis conducted by Brett Dickey.

Methods

Spectra were collected using a Nicolet NXR 9650 FT-Raman spectrometer (Thermo Fisher Scientific Inc., CAN). Powder glasses were illuminated with YVO_4 1064 nm laser with Raman shifts being detected using an InGaAs detector with a resolution of 2 cm^{-1}.

Results

Raman analysis did not reveal any structural information regarding the Si phase in any of the glasses. This is best evidenced by the BD1 spectra in Figure 54 which presents a featureless ramps that decreases in intensity from low to high wavenumbers. With regards to the Ge in the glass, increased Ge content led to the development of three peaks in the Raman: (i) a low frequency peak which shifts from 98 cm^{-1} in BD1 to 90 cm^{-1} in

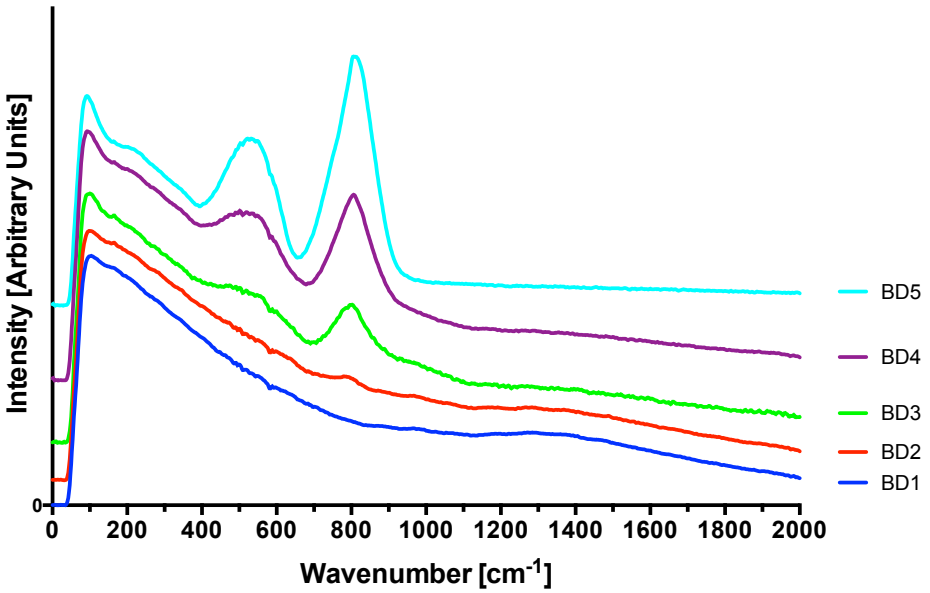

Figure 54: Raman spectra of BD series glasses.

BD5 and grows in intensity, developing a a shoulder around 200 cm^{-1}; (ii) a broad peak around 520 cm^{-1} that becomes more defined with increasing Ge content; (iii) and a high frequency peak that first appears in BD2, weakly centered about *c.*780 cm^{-1}, growing in intensity and shifting to *c.*800 cm^{-1} with increasing Ge content.

The low frequency peak is termed a Boson peak. The origins of Boson peak are unclear, but it is believed to be related to the overall network connectivity of the glass [422, 423]. The full impact of the shift to a lower wave number with increaseing Ge content is not fully understood at present and will require further analysis. The mid frequency peak, clearly visbile as a broad peak centered at 520 cm^{-1} in BD5, is characteristic of 3-member GeO_4 rings [348]. Wave numbers between 760 cm^{-1} and 790 cm^{-1} are characertic of GeO_4 tetrahedra with 2 BO and 2 NBO (N^2), while 860 cm^{-1} is accepted to represent GeO_4 with 3 BO and 1 NBO (N^3), so the high frequency peaks with lower wavenumbers represent less connected GeO_4 structures [415, 422, 424]. At higher Si:Ge ratios, the high frequency peak is centered about 780 cm^{-1} (BD2). As Si:Ge ratio decreases, this peak shifts to 800 cm^{-1} (BD5). This suggest as the Si:Ge ratio decreases, there is a slight increase in the average connectivity of GeO_4 tetrahedral structures, *i.e.* fewer NBO. However, the overall intensity of the 800 cm^{-1} peak increases, which indicated an increase in the overall distruption of the glass network. Noticeable absent from the Ge spectra is evidence of high coordinated Ge structures, *i.e.* GeO_5 or GeO_6, which are assigned wavenumber of between 710 cm^{-1} and 740 cm^{-1} [415]. It is possible such structure contribute to the overall envelope of the high frequency peak. However, the lack of a distinct peak within this range reduce the likelihood of higher cooridnated Ge structures existing in the BD series glasses.

Influence of Zirconium on Degradation of BD Series Glasses

Methods

Four additional glass compositions were designed to explore the mechanism associated with zirconium (Zr) that are responsible for delay the setting of GICs comprising Si-based or Ge-based glass chemistries (

Table 21). These four compositons were synthesized in the same manner as the other BD glasses, (Section 7.3.1), and their reactivities were investigated under similuated GIC setting conditions, as described in Section 7.3.4 .

Table 21: BD glasses with zirconium and their Tg.

	SiO_2	GeO_2	ZnO	CaO	ZrO_2	Na_2O	T_g [˚C]
BD1	0.48	-	0.36	0.16	0	0	673
BD6	0.48	-	0.36	0.11	0.025	0.025	654
BD7	0.48	-	0.36	0.06	0.05	0.05	652
BD5	-	0.48	0.36	0.16	0	0	597
BD8	-	0.48	0.36	0.11	0.025	0.025	588
BD9	-	0.46	0.34	0.10	0.05	0.05	586

Results

Figure 55 depicts the degradation profiles of the glasses outlined in Table 21. It was observed that as Zr and Na replace Ca, the reactivity of the Si-based glasses is substantially reduces, evinced by the flattening of the ion release profiles from Figure 55a, to Figure 55c, to Figure 55e. This same behavior was also observed in the Ge-based glasses (Figure 55b, d, and f), but to a much lesser degree. Therefore, it is reasonable to conclude that the inclusion Zr in the glass chemistry of Si and or Ge-based GICs reduces their reactivity, thus slowing the setting reaction by releasing fewer cations, which results in weaker cements due to a lower degree of crosslinkink in the GIC matrix.

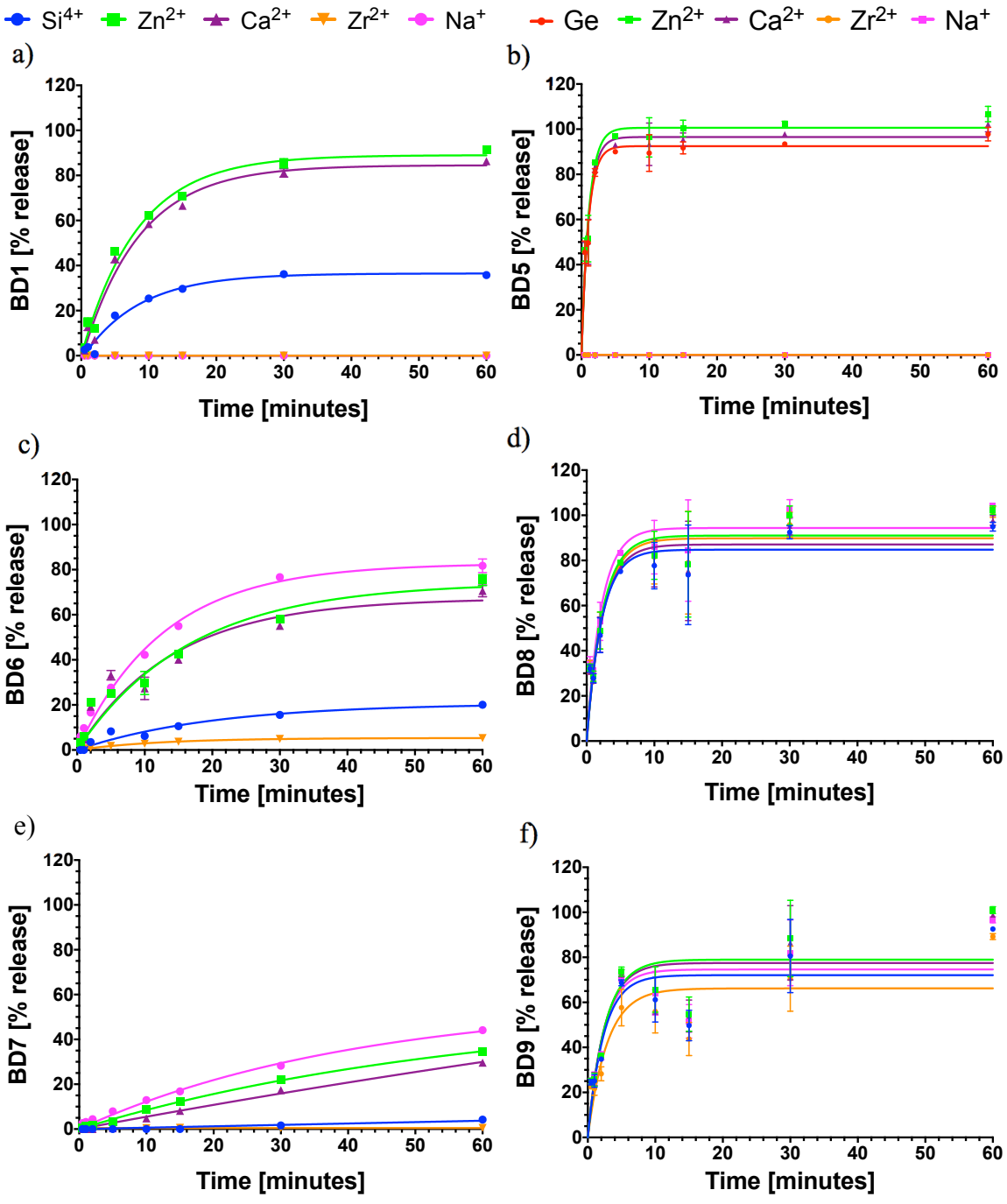

Figure 55: Impact of zirconium on the degradation of Si and Ge-based glasses. Figures a,c,e are Si-based glasses, and figures b, d, and f are Ge-based glasses.

Appendix III: Copyright Permission Letters

Copyright Permission – Chapter 6

ELSEVIER LICENSE
TERMS AND CONDITIONS

Jul 20, 2016

This Agreement between Brett Dickey ("You") and Elsevier ("Elsevier") consists of your license details and the terms and conditions provided by Elsevier and Copyright Clearance Center.

License Number	3913131170943
License date	Jul 20, 2016
Licensed Content Publisher	Elsevier
Licensed Content Publication	Journal of the Mechanical Behavior of Biomedical Materials
Licensed Content Title	Novel adaptations to zinc–silicate glass polyalkenoate cements: The unexpected influences of germanium based glasses on handling characteristics and mechanical properties
Licensed Content Author	B.T. Dickey,S. Kehoe,D. Boyd
Licensed Content Date	July 2013
Licensed Content Volume Number	23
Licensed Content Issue Number	n/a
Licensed Content Pages	14
Start Page	8
End Page	21
Type of Use	reuse in a thesis/dissertation
Portion	full article
Format	both print and electronic
Are you the author of this Elsevier article?	Yes
Will you be translating?	No
Order reference number	
Title of your thesis/dissertation	The Use of Germanium to Control the Properties of Glass Ionomer Cements
Expected completion date	Aug 2016
Estimated size (number of pages)	250
Elsevier VAT number	GB 494 6272 12
Requestor Location	Brett Dickey Dalhousie University 5981 University Avenue Halifax, NS B3H 4R2 Canada Attn: Brett Dickey
Total	0.00 CAD

Copyright Permission – Chapter 7

Title: Evidence of a complex species controlling the setting reaction of glass ionomer cements

Author: Brett Dickey,Richard Price,Daniel Boyd

Publication: Dental Materials

Publisher: Elsevier

Date: Apr 1, 2016

Logged in as:
Brett Dickey
Account #:
3001037705

LOGOUT

Order Completed

Thank you for your order.

This Agreement between Brett Dickey ("You") and Elsevier ("Elsevier") consists of your order details and the terms and conditions provided by Elsevier and Copyright Clearance Center.

License number	Reference confirmation email for license number
License date	Jul 20, 2016
Licensed Content Publisher	Elsevier
Licensed Content Publication	Dental Materials
Licensed Content Title	Evidence of a complex species controlling the setting reaction of glass ionomer cements
Licensed Content Author	Brett Dickey,Richard Price,Daniel Boyd
Licensed Content Date	April 2016
Licensed Content Volume	32
Licensed Content Issue	4
Licensed Content Pages	10
Type of Use	reuse in a thesis/dissertation
Portion	full article
Format	both print and electronic
Are you the author of this Elsevier article?	Yes
Will you be translating?	No
Order reference number	
Title of your thesis/dissertation	The Use of Germanium to Control the Properties of Glass Ionomer Cements
Expected completion date	Aug 2016
Estimated size (number of pages)	250
Elsevier VAT number	GB 494 6272 12
Requestor Location	Brett Dickey Dalhousie University 5981 University Avenue Halifax, NS B3H 4R2 Canada Attn: Brett Dickey
Billing Type	Invoice
Billing address	Brett Dickey Dalhousie University 5981 University Avenue Halifax, NS B3H 4R2 Canada Attn: Brett Dickey
Total	0.00 CAD

References

1. Burge, R., et al., *Incidence and economic burden of osteoporosis-related fractures in the United States, 2005-2025.* J Bone Miner Res, 2007. **22**(3): p. 465-75.

2. Svedbom, A., et al., *Osteoporosis in the European Union: a compendium of country-specific reports.* Arch Osteoporos, 2013. **8**: p. 137.

3. Canada, O. *What is Osteoporosis*. [cited 2016 June 18]; Available from: http://www.osteoporosis.ca/osteoporosis-and-you/what-is-osteoporosis/.

4. Schousboe, J.T., *Epidemiology of Vertebral Fractures.* J Clin Densitom, 2016. **19**(1): p. 8-22.

5. Kendler, D.L., et al., *Vertebral Fractures: Clinical Importance and Management.* Am J Med, 2016. **129**(2): p. 221 e1-221 e10.

6. Longo, U.G., et al., *Conservative management of patients with an osteoporotic vertebral fracture: a review of the literature.* J Bone Joint Surg Br, 2012. **94**(2): p. 152-7.

7. Georgy, B.A., *Metastatic spinal lesions: state-of-the-art treatment options and future trends.* AJNR Am J Neuroradiol, 2008. **29**(9): p. 1605-11.

8. LeBlanc, A., et al., *Spinal bone mineral after 5 weeks of bed rest.* Calcif Tissue Int, 1987. **41**(5): p. 259-61.

9. Dittmer, D.K. and R. Teasell, *Complications of immobilization and bed rest. Part 1: Musculoskeletal and cardiovascular complications.* Can Fam Physician, 1993. **39**: p. 1428-32, 1435-7.

10. Lewis, G., *Percutaneous vertebroplasty and kyphoplasty for the stand-alone augmentation of osteoporosis-induced vertebral compression fractures: present status and future directions.* J Biomed Mater Res B Appl Biomater, 2007. **81**(2): p. 371-86.

11. Berenson, J., et al., *Balloon kyphoplasty versus non-surgical fracture management for treatment of painful vertebral body compression fractures in patients with cancer: a multicentre, randomised controlled trial.* Lancet Oncol, 2011. **12**(3): p. 225-35.

12. Wardlaw, D., et al., *Efficacy and safety of balloon kyphoplasty compared with non-surgical care for vertebral compression fracture (FREE): a randomised controlled trial.* Lancet, 2009. **373**(9668): p. 1016-24.

13. Evans, A.J., et al., *Randomized controlled trial of vertebroplasty versus kyphoplasty in the treatment of vertebral compression fractures.* J Neurointerv Surg, 2015.

14. Rousing, R., et al., *Twelve-months follow-up in forty-nine patients with acute/semiacute osteoporotic vertebral fractures treated conservatively or with percutaneous vertebroplasty: a clinical randomized study.* Spine (Phila Pa 1976), 2010. **35**(5): p. 478-82.

15. Voormolen, M.H., et al., *Percutaneous vertebroplasty compared with optimal pain medication treatment: short-term clinical outcome of patients with subacute or chronic painful osteoporotic vertebral compression fractures. The VERTOS study.* AJNR Am J Neuroradiol, 2007. **28**(3): p. 555-60.

16. Cox, M., et al., *Vertebral Augmentation After Recent Randomized Controlled Trials: A New Rise in Kyphoplasty Volumes.* J Am Coll Radiol, 2016. **13**(1): p. 28-32.

17. Buchbinder, R., et al., *A randomized trial of vertebroplasty for painful osteoporotic vertebral fractures.* N Engl J Med, 2009. **361**(6): p. 557-68.

18. Kallmes, D.F., et al., *A randomized trial of vertebroplasty for osteoporotic spinal fractures.* N Engl J Med, 2009. **361**(6): p. 569-79.

19. Bono, C.M., et al., *North American Spine Society Newly released vertebroplasty randomized controlled trials: a tale of two trials.* Spine Journal, 2010. **10**(3): p. 238-240.

20. Clark, W., S. Lyon, and J. Burnes, *Trials of Vertebroplasty for Vertebral Fractures.* New England Journal of Medicine, 2009. **361**(21): p. 2097-2098.

21. Clark, W.A., et al., *Vertebroplasty for painful acute osteoporotic vertebral fractures: recent Medical Journal of Australia editorial is not relevant to the patient group that we treat with vertebroplasty.* Medical Journal of Australia, 2010. **192**(6): p. 334-337.

22. Klazen, C.A.H., et al., *Vertebroplasty versus conservative treatment in acute osteoporotic vertebral compression fractures (Vertos II): an open-label randomised trial.* Lancet, 2010. **376**(9746): p. 1085-1092.

23. Anderson, P.A., A.B. Froyshteter, and W.L. Tontz, Jr., *Meta-analysis of vertebral augmentation compared with conservative treatment for osteoporotic spinal fractures.* Journal of bone and mineral research : the official journal of the American Society for Bone and Mineral Research, 2013. **28**(2): p. 372-82.

24. Grafe, I.A., et al., *Calcium-phosphate and polymethylmethacrylate cement in long-term outcome after kyphoplasty of painful osteoporotic vertebral fractures.* Spine, 2008. **33**(11): p. 1284-90.

25. Anderson, P.A., A.B. Froyshteter, and W.L. Tontz, Jr., *Meta-analysis of vertebral augmentation compared with conservative treatment for osteoporotic spinal fractures.* J Bone Miner Res, 2013. **28**(2): p. 372-82.

26. Klazen, C.A., et al., *Vertebroplasty versus conservative treatment in acute osteoporotic vertebral compression fractures (Vertos II): an open-label randomised trial.* Lancet, 2010. **376**(9746): p. 1085-92.

27. Farrokhi, M.R., E. Alibai, and Z. Maghami, *Randomized controlled trial of percutaneous vertebroplasty versus optimal medical management for the relief of pain and disability in acute osteoporotic vertebral compression fractures.* J Neurosurg Spine, 2011. **14**(5): p. 561-9.

28. Blasco, J., et al., *Effect of vertebroplasty on pain relief, quality of life, and the incidence of new vertebral fractures: a 12-month randomized follow-up, controlled trial.* J Bone Miner Res, 2012. **27**(5): p. 1159-66.

29. Dohm, M., et al., *A randomized trial comparing balloon kyphoplasty and vertebroplasty for vertebral compression fractures due to osteoporosis.* AJNR Am J Neuroradiol, 2014. **35**(12): p. 2227-36.

30. Liu, J.T., et al., *Long-term follow-up study of osteoporotic vertebral compression fracture treated using balloon kyphoplasty and vertebroplasty.* J Neurosurg Spine, 2015. **23**(1): p. 94-8.

31. Heini, P.F. and U. Berlemann, *Bone substitutes in vertebroplasty.* Eur Spine J, 2001. **10 Suppl 2**: p. S205-13.

32. Lewis, G., *Injectable bone cements for use in vertebroplasty and kyphoplasty: state-of-the-art review.* J Biomed Mater Res B Appl Biomater, 2006. **76**(2): p. 456-68.

33. Jansen, J., et al., *Injectable calcium phosphate cement for bone repair and implant fixation.* Orthop Clin North Am, 2005. **36**(1): p. 89-95, vii.

34. Galibert, P., et al., *Preliminary note on the treatment of vertebral angioma by percutaneous acrylic vertebroplasty.* Neurochirurgie, 1987. **33**(2): p. 166-168.

35. Farrokhi, M.R., E. Alibai, and Z. Maghami, *Randomized controlled trial of percutaneous vertebroplasty versus optimal medical management for the relief of pain and disability in acute osteoporotic vertebral compression fractures.* Journal of Neurosurgery-Spine, 2011. **14**(5): p. 561-569.

36. Togawa, D., et al., *Histologic evaluation of human vertebral bodies after vertebral augmentation with polymethyl methacrylate.* Spine (Phila Pa 1976), 2003. **28**(14): p. 1521-7.

37. Urrutia, J., et al., *Early histologic changes following polymethylmethacrylate injection (vertebroplasty) in rabbit lumbar vertebrae.* Spine (Phila Pa 1976), 2008. **33**(8): p. 877-82.

38. Erbe, E.M., T.D. Clineff, and G. Gualtieri, *Comparison of a new bisphenol-a-glycidyl dimethacrylate-based cortical bone void filler with polymethyl methacrylate.* Eur Spine J, 2001. **10 Suppl 2**: p. S147-52.

39. Lewis, G., *Properties of acrylic bone cement: state of the art review.* J Biomed Mater Res, 1997. **38**(2): p. 155-82.

40. Srikumaran, U., et al., *Histopathologic analysis of human vertebral bodies after vertebral augmentation with polymethylmethacrylate with use of an inflatable bone tamp. A case report.* J Bone Joint Surg Am, 2005. **87**(8): p. 1838-43.

41. Habib, M., et al., *Mechanisms underlying the limited injectability of hydraulic calcium phosphate paste.* Acta Biomater, 2008. **4**(5): p. 1465-71.

42. Khairoun, I., et al., *Addition of cohesion promotors to calcium phosphate cements.* Biomaterials, 1999. **20**(4): p. 393-8.

43. Lieberman, I.H., D. Togawa, and M.M. Kayanja, *Vertebroplasty and kyphoplasty: filler materials.* Spine J, 2005. **5**(6 Suppl): p. 305S-316S.

44. He, Z., et al., *Bone cements for percutaneous vertebroplasty and balloon kyphoplasty: Current status and future developments.* Journal of Orthopaedic Translation, 2015. **3**(1): p. 1-11.

45. Wilson, A.D. and J.W. Nicholson, *Acid-base cements : their biomedical and industrial applications*. Chemistry of solid state materials. 1993, Cambridge England ; New York, NY, USA: Cambridge University Press. xx, 398 p.

46. Reusche, E., et al., *Subacute fatal aluminum encephalopathy after reconstructive otoneurosurgery: a case report.* Hum Pathol, 2001. **32**(10): p. 1136-40.

47. Engelbrecht, E., G. von Foerster, and G. Delling, *Ionogran in revision arthroplasty.* J Bone Joint Surg Br, 2000. **82**(2): p. 192-9.

48. Brook, I.M. and P.V. Hatton, *Glass-ionomers: bioactive implant materials.* Biomaterials, 1998. **19**(6): p. 565-71.

49. Boyd, D. and M.R. Towler, *The processing, mechanical properties and bioactivity of zinc based glass ionomer cements.* Journal of Materials Science-Materials in Medicine, 2005. **16**(9): p. 843-850.

50. Brauer, D.S., et al., *Benefits and drawbacks of zinc in glass ionomer bone cements.* Biomed Mater, 2011. **6**(4): p. 045007.

51. Hatton, P.V., K. Hurrell-Gillingham, and I.M. Brook, *Biocompatibility of glass-ionomer bone cements.* J Dent, 2006. **34**(8): p. 598-601.

52. Darling, M. and R. Hill, *Novel polyalkenoate (glass-ionomer) dental cements based on zinc silicate glasses.* Biomaterials, 1994. **15**(4): p. 299-306.

53. Boyd, D., et al., *Comparison of an experimental bone cement with surgical Simplex P, Spineplex and Cortoss.* J Mater Sci Mater Med, 2008. **19**(4): p. 1745-52.

54. Clarkin, O., D. Boyd, and M.R. Towler, *Strontium-based glass polyalkenoate cements for luting applications in the skeleton.* J Biomater Appl, 2010. **24**(6): p. 483-502.

55. Clarkin, O.M., et al., *Comparison of an experimental bone cement with a commercial control, Hydroset.* J Mater Sci Mater Med, 2009. **20**(7): p. 1563-70.

56. Boyd, D., et al., *Zinc-based glass polyalkenoate cements with improved setting times and mechanical properties.* Acta Biomater, 2008. **4**(2): p. 425-31.

57. Wren, A.W., et al., *A spectroscopic investigation into the setting and mechanical properties of titanium containing glass polyalkenoate cements.* J Mater Sci Mater Med, 2010. **21**(8): p. 2355-64.

58. Wren, A.W., et al., *Gallium containing glass polyalkenoate anti-cancerous bone cements: glass characterization and physical properties.* J Mater Sci Mater Med, 2012. **23**(8): p. 1823-33.

59. Gomes, F.O., R.A. Pires, and R.L. Reis, *Aluminum-free glass-ionomer bone cements with enhanced bioactivity and biodegradability.* Mater Sci Eng C Mater Biol Appl, 2013. **33**(3): p. 1361-70.

60. Dickey, B.T., S. Kehoe, and D. Boyd, *Novel adaptations to zinc-silicate glass polyalkenoate cements: the unexpected influences of germanium based glasses on handling characteristics and mechanical properties.* J Mech Behav Biomed Mater, 2013. **23**: p. 8-21.

61. Dickey, B., R. Price, and D. Boyd, *Evidence of a complex species controlling the setting reaction of glass ionomer cements.* Dental Materials, 2016. **32**(4): p. 596-605.

62. Leucht, P., et al., *Epidemiology of traumatic spine fractures.* Injury, 2009. **40**(2): p. 166-72.

63. Georgy, B.A., *Percutaneous image-guided augmentation for spinal metastatic tumors.* Tech Vasc Interv Radiol, 2009. **12**(1): p. 71-7.

64. Cummings, S.R. and L.J. Melton, *Epidemiology and outcomes of osteoporotic fractures.* Lancet, 2002. **359**(9319): p. 1761-7.

65. Armas, L.A. and R.R. Recker, *Pathophysiology of osteoporosis: new mechanistic insights.* Endocrinol Metab Clin North Am, 2012. **41**(3): p. 475-86.

66. Coleman, R.E., *Metastatic bone disease: clinical features, pathophysiology and treatment strategies.* Cancer Treatment Reviews, 2001. **27**(3): p. 165-176.

67. Fink, H.A., et al., *Disability after clinical fracture in postmenopausal women with low bone density: the fracture intervention trial (FIT).* Osteoporos Int, 2003. **14**(1): p. 69-76.

68. Broy, S.B., *The Vertebral Fracture Cascade: Etiology and Clinical Implications.* J Clin Densitom, 2016. **19**(1): p. 29-34.

69. Kim, J.H., et al., *The comparison of bone scan and MRI in osteoporotic compression fractures.* Asian Spine J, 2010. **4**(2): p. 89-95.

70. Kasturi, G.C., D.X. Cifu, and R.A. Adler, *A review of osteoporosis: part I. Impact, pathophysiology, diagnosis and unique role of the physiatrist.* PM R, 2009. **1**(3): p. 254-60.

71. Hernlund, E., et al., *Osteoporosis in the European Union: medical management, epidemiology and economic burden. A report prepared in collaboration with the International Osteoporosis Foundation (IOF) and the European Federation of Pharmaceutical Industry Associations (EFPIA).* Arch Osteoporos, 2013. **8**: p. 136.

72. Canada, O. *Osteoporosis Facts and Statistics*. [cited 2016 June 20]; Available from: http://www.osteoporosis.ca/osteoporosis-and-you/osteoporosis-facts-and-statistics/.

73. Cooper, C., T. O'Neill, and A. Silman, *The epidemiology of vertebral fractures. European Vertebral Osteoporosis Study Group.* Bone, 1993. **14 Suppl 1**: p. S89-97.

74. Fink, H.A., et al., *What proportion of incident radiographic vertebral deformities is clinically diagnosed and vice versa?* J Bone Miner Res, 2005. **20**(7): p. 1216-22.

75. Cooper, C., et al., *Incidence of clinically diagnosed vertebral fractures: a population-based study in Rochester, Minnesota, 1985-1989.* J Bone Miner Res, 1992. **7**(2): p. 221-7.

76. Amin, S., et al., *Trends in fracture incidence: a population-based study over 20 years.* J Bone Miner Res, 2014. **29**(3): p. 581-9.

77. Johnell, O. and J.A. Kanis, *An estimate of the worldwide prevalence and disability associated with osteoporotic fractures.* Osteoporos Int, 2006. **17**(12): p. 1726-33.

78. Kim, D.H. and A.R. Vaccaro, *Osteoporotic compression fractures of the spine; current options and considerations for treatment.* Spine J, 2006. **6**(5): p. 479-87.

79. Delmas, P.D., et al., *Underdiagnosis of vertebral fractures is a worldwide problem: the IMPACT study.* J Bone Miner Res, 2005. **20**(4): p. 557-63.

80. Cummings, S.R. and L.J. Melton, *Epidemiology and outcomes of osteoporotic fractures.* The Lancet, 2002. **359**(9319): p. 1761-1767.

81. Eleraky, M., I. Papanastassiou, and F.D. Vrionis, *Management of metastatic spine disease.* Curr Opin Support Palliat Care, 2010. **4**(3): p. 182-8.

82. Tancioni, F., et al., *Percutaneous Vertebral Augmentation in Metastatic Disease: State of the Art.* The Journal of Supportive Oncology, 2011. **9**(1): p. 4-10.

83. Krishnaney, A.A., M.P. Steinmetz, and E.C. Benzel, *Biomechanics of metastatic spine cancer.* Neurosurg Clin N Am, 2004. **15**(4): p. 375-80.

84. Strasser, J., et al., *Advancing the care of cancer patients with vertebral compression fractures: A radiation oncology expert panel discussion.* Oncol Hematol Rev, 2012. **8**: p. 12-17.

85. Hu, R., C.A. Mustard, and C. Burns, *Epidemiology of incident spinal fracture in a complete population.* Spine (Phila Pa 1976), 1996. **21**(4): p. 492-9.

86. Heinzelmann, M. and G.A. Wanner, *Thoracolumbar spinal injuries*, in *Spinal Disorders*. 2008, Springer. p. 883-924.

87. Filler, A. *Chapter 5 - Spine and Nerve Anatomy, The complete Spine*. 2011 [cited 2011 May 25]; Available from: http://www.backpain-guide.com/Chapter_Fig_folders/Ch05_Anatomy_Folder/Ch5_Images/05-4_Overall_Spine.jpg

88. Magerl, F., et al., *A comprehensive classification of thoracic and lumbar injuries.* Eur Spine J, 1994. **3**(4): p. 184-201.

89. Rhyne, A., 3rd, et al., *Kyphoplasty: report of eighty-two thoracolumbar osteoporotic vertebral fractures.* J Orthop Trauma, 2004. **18**(5): p. 294-9.

90. Miller, P.D., *Clinical Management of Vertebral Compression Fractures.* J Clin Densitom, 2016. **19**(1): p. 97-101.

91. Franck, H., et al., *Interdisciplinary approach to balloon kyphoplasty in the treatment of osteoporotic vertebral compression fractures.* Eur Spine J, 2003. **12 Suppl 2**: p. S163-7.

92. Lamy, O., B. Uebelhart, and B. Aubry-Rozier, *Risks and benefits of percutaneous vertebroplasty or kyphoplasty in the management of osteoporotic vertebral fractures.* Osteoporosis international : a journal established as result of cooperation between the European Foundation for Osteoporosis and the National Osteoporosis Foundation of the USA, 2014. **25**(3): p. 807-19.

93. Mathis, J.M., H. Deramond, and S.M. Belkoff, *Percutaneous vertebroplasty and kyphoplasty*. 2nd ed. 2006, New York, NY: Springer. xii, 309 p.

94. *Vertebroplasty*. [cited 2016 May 2]; Available from: http://www.proactiverehab.com/Injuries-Conditions/Mid-Back/Mid-Back-Surgery/Vertebroplasty/a~319/article.html.

95. Nussbaum, D.A., P. Gailloud, and K. Murphy, *A review of complications associated with vertebroplasty and kyphoplasty as reported to the Food and Drug Administration medical device related web site.* Journal of vascular and interventional radiology : JVIR, 2004. **15**(11): p. 1185-92.

96. Klazen, C.A., et al., *VERTOS II: percutaneous vertebroplasty versus conservative therapy in patients with painful osteoporotic vertebral compression fractures; rationale, objectives and design of a multicenter randomized controlled trial.* Trials, 2007. **8**: p. 33.

97. Ong, K.L., et al., *Two-year cost comparison of vertebroplasty and kyphoplasty for the treatment of vertebral compression fractures: are initial surgical costs misleading?* Osteoporos Int, 2013. **24**(4): p. 1437-45.

98. Papaioannou, A., et al., *Lengthy hospitalization associated with vertebral fractures despite control for comorbid conditions.* Osteoporos Int, 2001. **12**(10): p. 870-4.

99. Kim, D.H. and A.R. Vaccaro, *Osteoporotic compression fractures of the spine; current options and considerations for treatment.* The spine journal : official journal of the North American Spine Society, 2006. **6**(5): p. 479-87.

100. Tutton, S.M., et al., *KAST Study: The Kiva System As a Vertebral Augmentation Treatment-A Safety and Effectiveness Trial: A Randomized, Noninferiority Trial Comparing the Kiva System With Balloon Kyphoplasty in Treatment of Osteoporotic Vertebral Compression Fractures.* Spine (Phila Pa 1976), 2015. **40**(12): p. 865-75.

101. Vanni, D., et al., *Third-generation percutaneous vertebral augmentation systems.* Journal of Spine Surgery, 2016. **2**(1): p. 13-20.

102. *Kyphoplasty*. [cited 2016 May 2]; Available from: http://www.proactiverehab.com/Injuries-Conditions/Mid-Back/Mid-Back-Surgery/Kyphoplasty/a~318/article.html.

103. Saeed, K., E. Bayley, and B. Boszczyk, *Vertebroplasty and Kyphoplasty*, in *Manual of Spine Surgery*, U. Vieweg and F. Grochulla, Editors. 2012, Springer Berlin Heidelberg. p. 313-318.

104. Chandra, R.V., et al., *Vertebral augmentation: report of the Standards and Guidelines Committee of the Society of NeuroInterventional Surgery.* J Neurointerv Surg, 2014. **6**(1): p. 7-15.

105. Silverthorn, D.U. and B.R. Johnson, *Human physiology : an integrated approach*. 5th ed. 2010, San Francisco: Pearson/Benjamin Cummings. xxxiv, 867, 83 p.

106. Dubin, A.E. and A. Patapoutian, *Nociceptors: the sensors of the pain pathway.* J Clin Invest, 2010. **120**(11): p. 3760-72.

107. Mathis, J.M., H. Deramond, and S.M. Belkoff, *Percutaneous Vertebroplasty and Kyphoplasty*. 2nd ed. 2010, New York: Springer.

108. Black, J., *Biological performance of materials : fundamentals of biocompatibility*. 4th ed. 2006, Boca Raton: CRC Taylor & Francis. 497 p.

109. Belkoff, S.M., et al., *Biomechanical evaluation of a new bone cement for use in vertebroplasty.* Spine, 2000. **25**(9): p. 1061-1064.

110. Tohmeh, A.G., et al., *Biomechanical efficacy of unipedicular versus bipedicular vertebroplasty for the management of osteoporotic compression fractures.* Spine, 1999. **24**(17): p. 1772-1776.

111. Rousing, R., et al., *Percutaneous vertebroplasty compared to conservative treatment in patients with painful acute or subacute osteoporotic vertebral fractures: three-months follow-up in a clinical randomized study.* Spine, 2009. **34**(13): p. 1349-54.

112. Lewis, G., *Injectable bone cements for use in vertebroplasty and kyphoplasty: state-of-the-art review.* Journal of biomedical materials research. Part B, Applied biomaterials, 2006. **76**(2): p. 456-68.

113. Masala, S., et al., *Osteoporotic vertebral compression fractures augmentation by injectable partly resorbable ceramic bone substitute (Cerament|SPINE SUPPORT): a prospective nonrandomized study.* Neuroradiology, 2012. **54**(6): p. 589-96.

114. Grafe, I.A., et al., *Calcium-phosphate and polymethylmethacrylate cement in long-term outcome after kyphoplasty of painful osteoporotic vertebral fractures.* Spine (Phila Pa 1976), 2008. **33**(11): p. 1284-90.

115. Belkoff, S.M. and S. Molloy, *Temperature measurement during polymerization of polymethylmethacrylate cement used for vertebroplasty.* Spine, 2003. **28**(14): p. 1555-9.

116. Aebli, N., et al., *In vivo temperature profile of intervertebral discs and vertebral endplates during vertebroplasty: an experimental study in sheep.* Spine, 2006. **31**(15): p. 1674-8; discussion 1679.

117. Anselmetti, G.C., et al., *Temperature measurement during polymerization of bone cement in percutaneous vertebroplasty: an in vivo study in humans.* Cardiovasc Intervent Radiol, 2009. **32**(3): p. 491-8.

118. AAOS. *American Academy of Orthopaedic Surgeons: Levels of Evidence For Primary Research Question*. 2004 [cited 2016 July 2]; Available from: http://www.aaos.org/Research/Committee/Evidence/loetable1.pdf.

119. NASS. *North American Spine Society - Levels of Evidence For Primary Research Question*. 2005 [cited 2016 July 4]; Available from: http://www.spine.org/Portals/0/Documents/ResearchClinicalCare/LevelsOfEvidence.pdf.

120. Rousing, R., et al., *Percutaneous vertebroplasty compared to conservative treatment in patients with painful acute or subacute osteoporotic vertebral fractures: three-months follow-up in a clinical randomized study.* Spine (Phila Pa 1976), 2009. **34**(13): p. 1349-54.

121. Kroon, F., et al., *Two-Year Results of a Randomized Placebo-Controlled Trial of Vertebroplasty for Acute Osteoporotic Vertebral Fractures.* Journal of Bone and Mineral Research, 2014. **29**(6): p. 1346-1355.

122. Comstock, B.A., et al., *Investigational vertebroplasty safety and efficacy trial (INVEST): patient-reported outcomes through 1 year.* Radiology, 2013. **269**(1): p. 224-31.

123. Van Meirhaeghe, J., et al., *A randomized trial of balloon kyphoplasty and nonsurgical management for treating acute vertebral compression fractures: vertebral body kyphosis correction and surgical parameters.* Spine (Phila Pa 1976), 2013. **38**(12): p. 971-83.

124. Rosenbaum, B.P., et al., *Trends in Inpatient Vertebroplasty and Kyphoplasty Volume in the United States, 2005-2011: Assessing the Impact of Randomized Controlled Trials.* J Spinal Disord Tech, 2014.

125. Buchbinder, R., et al., *A Randomized Trial of Vertebroplasty for Painful Osteoporotic Vertebral Fractures.* New England Journal of Medicine, 2009. **361**(6): p. 557-568.

126. Buchbinder, R. and D.F. Kallmes, *Vertebroplasty: when randomized placebo-controlled trial results clash with common belief.* Spine Journal, 2010. **10**(3): p. 241-243.

127. Carragee, E.J., *The vertebroplasty affair: the mysterious case of the disappearing effect size.* Spine Journal, 2010. **10**(3): p. 191-192.

128. Gangi, A. and W.A. Clark, *Have Recent Vertebroplasty Trials Changed the Indications for Vertebroplasty?* Cardiovascular and interventional radiology, 2010. **33**(4): p. 677-680.

129. Buchbinder, R., R.H. Osborne, and D. Kallmes, *Invited editorial presents an accurate summary of the results of two randomised placebo-controlled trials of vertebroplasty.* Medical Journal of Australia, 2010. **192**(6): p. 338-341.

130. Goz, V., et al., *Vertebroplasty and kyphoplasty: national outcomes and trends in utilization from 2005 through 2010.* The Spine Journal, (0).

131. Smieliauskas, F., S. Lam, and D. Howard, *Impact of negative clinical trial results for vertebroplasty on vertebral augmentation procedure rates.* Journal of the American College of Surgeons, 2014.

132. Surgeons, A.A.o.O., *The treatment of symptomatic osteoporotic spinal compression fractures*, in *Guideline and Evidence Report*. 2010. p. 69-85.

133. McGirt, M.J., et al., *Vertebroplasty and kyphoplasty for the treatment of vertebral compression fractures: an evidenced-based review of the literature.* Spine Journal, 2009. **9**(6): p. 501-508.

134. Gray, L.A., et al., *INvestigational Vertebroplasty Efficacy and Safety Trial (INVEST): a randomized controlled trial of percutaneous vertebroplasty.* Bmc Musculoskeletal Disorders, 2007. **8**: p. 126.

135. Buchbinder, R., et al., *Efficacy and safety of vertebroplasty for treatment of painful osteoporotic vertebral fractures: a randomised controlled trial [ACTRN012605000079640].* Bmc Musculoskeletal Disorders, 2008. **9**.

136. Lachin, J.M., *Introduction to Sample-Size Determination and Power Analysis for Clinical-Trials.* Controlled Clinical Trials, 1981. **2**(2): p. 93-113.

137. Papanastassiou, I.D., et al., *Adverse prognostic factors and optimal intervention time for kyphoplasty/vertebroplasty in osteoporotic fractures.* Biomed Res Int, 2014. **2014**: p. 925683.

138. NICE. *National Institue for Health and Care Excellence: Percutaneous vertebroplasty and percutaneous balloon kyphoplasty for treating osteoporotic vertebral compression fractures*. 2013 [cited 2016 July 4]; Available from: https://http://www.nice.org.uk/guidance/ta279.

139. Edidin, A.A., et al., *Mortality risk for operated and nonoperated vertebral fracture patients in the medicare population.* Journal of bone and mineral research : the official journal of the American Society for Bone and Mineral Research, 2011. **26**(7): p. 1617-26.

140. Firanescu, C., et al., *A randomised sham controlled trial of vertebroplasty for painful acute osteoporotic vertebral fractures (VERTOS IV).* Trials, 2011. **12**: p. 93.

141. Carli, D., W.J. Rooij, and P. Lohle. *A Trial of Vertebroplasty for Painful Chronic Osteoporotic Vertebral Fractures (Vertos V), NCT01963039.* [cited 2016 May 8]; Available from: https://clinicaltrials.gov/ct2/show/NCT01963039.

142. ClinicalTrials.gov. *A Trial of Vertebroplasty for Painful Chronic Osteoporotic Vertebral Fractures (Vertos V)*. 2016 [cited July 3, 2016; Available from: https://clinicaltrials.gov/ct2/show/record/NCT01963039.

143. ClinicalTrials.gov. *A trial of Vertebroplasty for Painful Acute Osteoporotic Vertebral Fractures (Vertos IV)*. 2014 [cited 2016 July 3]; Available from: https://clinicaltrials.gov/ct2/show/record/NCT01200277.

144. Boonen, S., et al., *Balloon kyphoplasty for the treatment of acute vertebral compression fractures: 2-year results from a randomized trial.* J Bone Miner Res, 2011. **26**(7): p. 1627-37.

145. Borgstrom, F., et al., *The impact of different health dimensions on overall quality of life related to kyphoplasty and non-surgical management.* Osteoporos Int, 2013. **24**(7): p. 1991-9.

146. Goz, V., et al., *Vertebroplasty and kyphoplasty: national outcomes and trends in utilization from 2005 through 2010.* Spine J, 2015. **15**(5): p. 959-65.

147. Mehio, A.K., et al., *Comparative hospital economics and patient presentation: vertebroplasty and kyphoplasty for the treatment of vertebral compression fracture.* AJNR Am J Neuroradiol, 2011. **32**(7): p. 1290-4.

148. Kondo, K.L., *Osteoporotic vertebral compression fractures and vertebral augmentation.* Semin Intervent Radiol, 2008. **25**(4): p. 413-24.

149. Barr, J.D., et al., *Position statement on percutaneous vertebral augmentation: a consensus statement developed by the Society of Interventional Radiology (SIR), American Association of Neurological Surgeons (AANS) and the Congress of Neurological Surgeons (CNS), American College of Radiology (ACR), American Society of Neuroradiology (ASNR), American Society of Spine Radiology (ASSR), Canadian Interventional Radiology Association (CIRA), and the Society of NeuroInterventional Surgery (SNIS).* J Vasc Interv Radiol, 2014. **25**(2): p. 171-81.

150. Zhao, G., X. Liu, and F. Li, *Balloon kyphoplasty versus percutaneous vertebroplasty for treatment of osteoporotic vertebral compression fractures (OVCFs).* Osteoporos Int, 2016.

151. Teng, M.M., et al., *Intraspinal leakage of bone cement after vertebroplasty: a report of 3 cases.* AJNR. American journal of neuroradiology, 2006. **27**(1): p. 224-9.

152. Matouk, C.C., et al., *Cement embolization of a segmental artery after percutaneous vertebroplasty: a potentially catastrophic vascular complication.* Interv Neuroradiol, 2012. **18**(3): p. 358-62.

153. Rothermich, M.A., et al., *Pulmonary cement embolization after vertebroplasty requiring pulmonary wedge resection.* Clin Orthop Relat Res, 2014. **472**(5): p. 1652-7.

154. Baroud, G., et al., *Load shift of the intervertebral disc after a vertebroplasty: a finite-element study.* Eur Spine J, 2003. **12**(4): p. 421-6.

155. Sebaaly, A., et al., *Vertebral Augmentation: State of the Art.* Asian Spine J, 2016. **10**(2): p. 370-6.

156. Lieberman, I.H., D. Togawa, and M.M. Kayanja, *Vertebroplasty and kyphoplasty: filler materials.* The spine journal : official journal of the North American Spine Society, 2005. **5**(6 Suppl): p. 305S-316S.

157. Camlioglu, E., A. Kelekis, and M. Radvany, *Personal Communication*. 2015: Society for Interventional Radiology Annual Scientific Meeting.

158. *Personal Communication: Dr. Jai Shiva Shankar, Neuro Radiologist, and Dr. Matthias Schmidt, Intervenational Radiologist, Nova Scotia Health Authority*. February 4, 2015.

159. Heini, P.F. and U. Berlemann, *Bone substitutes in vertebroplasty.* European spine journal : official publication of the European Spine Society, the European Spinal Deformity Society, and the European Section of the Cervical Spine Research Society, 2001. **10 Suppl 2**: p. S205-13.

160. Clarkin, O.M., et al., *Comparison of an experimental bone cement with a commercial control, Hydroset.* Journal of materials science. Materials in medicine, 2009. **20**(7): p. 1563-70.

161. Boyd, D., et al., *Comparison of an experimental bone cement with surgical Simplex P, Spineplex and Cortoss.* Journal of materials science. Materials in medicine, 2008. **19**(4): p. 1745-52.

162. Mosekilde, L. and L. Mosekilde, *Normal Vertebral Body Size and Compressive Strength - Relations to Age and to Vertebral and Iliac Trabecular Bone Compressive Strength.* Bone, 1986. **7**(3): p. 207-212.

163. O'Hara, R.M., et al., *Optimisation of the mechanical and handling properties of an injectable calcium phosphate cement.* Journal of materials science. Materials in medicine, 2010. **21**(8): p. 2299-305.

164. Lewis, G., *Properties of acrylic bone cement: State of the art review.* Journal of biomedical materials research, 1997. **38**(2): p. 155-182.

165. DiMaio, F.R., *The science of bone cement: A historical review.* Orthopedics, 2002. **25**(12): p. 1399-1407.

166. Lewis, G., *Percutaneous vertebroplasty and kyphoplasty for the stand-alone augmentation of osteoporosis-induced vertebral compression fractures: Present status and future directions.* Journal of Biomedical Materials Research Part B-Applied Biomaterials, 2007. **81B**(2): p. 371-386.

167. Meyer, P.R., Lautensc.Ep, and B.K. Moore, *Setting Properties of Acrylic Bone Cement.* Journal of Bone and Joint Surgery-American Volume, 1973. **A 55**(1): p. 149-156.

168. Leggat, P.A., D.R. Smith, and U. Kedjarune, *Surgical applications of methyl methacrylate: a review of toxicity.* Arch Environ Occup Health, 2009. **64**(3): p. 207-12.

169. Basko-Plluska, J.L., J.P. Thyssen, and P.C. Schalock, *Cutaneous and systemic hypersensitivity reactions to metallic implants.* Dermatitis, 2011. **22**(2): p. 65-79.

170. Ratner, B.D., *Biomaterials science : an introduction to materials in medicine*. 2nd ed. 2004, Amsterdam ; Boston: Elsevier Academic Press. xii, 851 p.

171. Huang, K.Y., J.J. Yan, and R.M. Lin, *Histopathologic findings of retrieved specimens of vertebroplasty with polymethylmethacrylate cement: case control study.* Spine (Phila Pa 1976), 2005. **30**(19): p. E585-8.

172. Tsai, T.T., et al., *Polymethylmethacrylate cement dislodgment following percutaneous vertebroplasty: a case report.* Spine, 2003. **28**(22): p. E457-60.

173. Erbe, E.M., T.D. Clineff, and G. Gualtieri, *Comparison of a new bisphenol-a-glycidyl dimethacrylate-based cortical bone void filler with polymethyl methacrylate.* European spine journal : official publication of the European Spine Society, the European Spinal Deformity Society, and the European Section of the Cervical Spine Research Society, 2001. **10 Suppl 2**: p. S147-52.

174. Hench, L., *The story of Bioglass¬Æ.* Journal of Materials Science: Materials in Medicine, 2006. **17**(11): p. 967-978.

175. Palussiere, J., et al., *Clinical results of an open prospective study of a bis-GMA composite in percutaneous vertebral augmentation.* European spine journal : official publication of the European Spine Society, the European Spinal Deformity Society, and the European Section of the Cervical Spine Research Society, 2005. **14**(10): p. 982-91.

176. Bae, H., et al., *Clinical Experience Using Cortoss for Treating Vertebral Compression Fractures With Vertebroplasty and Kyphoplasty Twenty Four-Month Follow-up.* Spine, 2010. **35**(20): p. E1030-E1036.

177. Middleton, E.T., et al., *The safety and efficacy of vertebroplasty using Cortoss cement in a newly established vertebroplasty service.* British journal of neurosurgery, 2008. **22**(2): p. 252-6.

178. Bae, H., et al., *A Prospective Randomized FDA-IDE Trial Comparing Cortoss With PMMA for Vertebroplasty A Comparative Effectiveness Research Study With 24-Month Follow-up.* Spine, 2012. **37**(7): p. 544-550.

179. Stryker. *Cortoss Bone Augmentation Material: Surgical Technique Guide*. 2012 [cited 2016 May 17]; Available from: http://rontis.gr/wp-content/uploads/2013/12/Cortoss-Bone-Augmentation-Material.pdf.

180. Palussiere, J., et al., *Clinical results of an open prospective study of a bis-GMA composite in percutaneous vertebral augmentation.* Eur Spine J, 2005. **14**(10): p. 982-91.

181. Geurtsen, W., *Biocompatibility of resin-modified filling materials.* Critical Reviews in Oral Biology & Medicine, 2000. **11**(3): p. 333-355.

182. Arcos, D., et al., *The relevance of biomaterials to the prevention and treatment of osteoporosis.* Acta Biomater, 2014. **10**(5): p. 1793-805.

183. Larsson, S. and G. Hannink, *Injectable bone-graft substitutes: current products, their characteristics and indications, and new developments.* Injury, 2011. **42 Suppl 2**: p. S30-4.

184. O'Hara, R.M., et al., *Optimisation of the mechanical and handling properties of an injectable calcium phosphate cement.* J Mater Sci Mater Med, 2010. **21**(8): p. 2299-305.

185. Zhang, J., et al., *Calcium phosphate cements for bone substitution: chemistry, handling and mechanical properties.* Acta Biomater, 2014. **10**(3): p. 1035-49.

186. Berlemann, U., et al., *Kyphoplasty for treatment of osteoporotic vertebral fractures: a prospective non-randomized study.* Eur Spine J, 2004. **13**(6): p. 496-501.

187. Schmelzer-Schmied, N., et al., *Comparison of kyphoplasty with use of a calcium phosphate cement and non-operative therapy in patients with traumatic non-osteoporotic vertebral fractures.* Eur Spine J, 2009. **18**(5): p. 624-9.

188. Reinhold, M., et al., *AO spine injury classification system: a revision proposal for the thoracic and lumbar spine.* Eur Spine J, 2013. **22**(10): p. 2184-201.

189. Blattert, T.R., L. Jestaedt, and A. Weckbach, *Suitability of a Calcium Phosphate Cement in Osteoporotic Vertebral Body Fracture Augmentation A Controlled, Randomized, Clinical Trial of Balloon Kyphoplasty Comparing Calcium Phosphate Versus Polymethylmethacrylate.* Spine, 2009. **34**(2): p. 108-114.

190. Perry, A., et al., *Biomechanical evaluation of kyphoplasty with calcium sulfate cement in a cadaveric osteoporotic vertebral compression fracture model.* The spine journal : official journal of the North American Spine Society, 2005. **5**(5): p. 489-93.

191. Thomas, M.V. and D.A. Puleo, *Calcium Sulfate: Properties and Clinical Applications.* Journal of Biomedical Materials Research Part B-Applied Biomaterials, 2009. **88B**(2): p. 597-610.

192. Marcia, S., et al., *Effectiveness of a bone substitute (CERAMENT) as an alternative to PMMA in percutaneous vertebroplasty: 1-year follow-up on clinical outcome.* Eur Spine J, 2012. **21 Suppl 1**: p. S112-8.

193. Hatten, H., *Abstract No. 262: Bone healing in vertebroplasty.* Journal of Vascular and Interventional Radiology, 2010. **21**(2, Supplement): p. S100.

194. Masala, S., et al., *Osteoporotic vertebral compression fracture augmentation by injectable partly resorbable ceramic bone substitute (Cerament (TM)|SPINESUPPORT): a prospective nonrandomized study.* Neuroradiology, 2012. **54**(11): p. 1245-1251.

195. Rauschmann, M., et al., *Bioceramic vertebral augmentation with a calcium sulphate/hydroxyapatite composite (Cerament,Ñ¢ SpineSupport) in vertebral compression fractures due to osteoporosis.* European Spine Journal, 2010. **19**(6): p. 887-892.

196. Nilsson, M., et al., *Factors influencing the compressive strength of an injectable calcium sulfate-hydroxyapatite cement.* J Mater Sci Mater Med, 2003. **14**(5): p. 399-404.

197. Wilson, A.D. and B.E. Kent, *New Translucent Cement for Dentistry - Glass Ionomer Cement.* British Dental Journal, 1972. **132**(4): p. 133-&.

198. Nicholson, J.W., *Chemistry of glass-ionomer cements: a review.* Biomaterials, 1998. **19**(6): p. 485-94.

199. Moshaverinia, A., et al., *A review of powder modifications in conventional glass-ionomer dental cements.* Journal of Materials Chemistry, 2011. **21**(5): p. 1319.

200. Frencken, J.E., et al., *Atraumatic restorative treatment (ART): rationale, technique, and development.* Journal of public health dentistry, 1996. **56**(3 Spec No): p. 135-40; discussion 161-3.

201. Berg, J.H. and T.P. Croll, *Glass ionomer restorative cement systems: an update.* Pediatric Dentistry, 2015. **37**(2): p. 116-24.

202. De Barra, E. and R.G. Hill, *Influence of alkali metal ions on the fracture properties of glass polyalkenoate (ionomer) cements.* Biomaterials, 1998. **19**(6): p. 495-502.

203. Varshneya, A.K., *Fundamentals of inorganic glasses / Arun K. Varshneya*. 1994, Boston: Academic Press. xvii, 570 p.

204. Zachariasen, W.H., *The atomic arrangement in glass.* Journal of the American Chemical Society, 1932. **54**: p. 3841-3851.

205. Henderson, G.S., *THE STRUCTURE OF SILICATE MELTS: A GLASS PERSPECTIVE.* The Canadian Mineralogist, 2005. **43**(6): p. 1921-1958.

206. Sun, K.H., *Fundamental Condition of Glass Formation.* Journal of the American Ceramic Society, 1947. **30**(9): p. 277-281.

207. Dietzel, A., *Relation between surface tension and structure of glass fusions.* Kolloid-Zeitschrift, 1942. **100**(3): p. 368-380.

208. Shelby, J.E., *Introduction to glass science and technology*. 2nd ed. 2005, Cambridge: Royal Society of Chemistry. xvi, 291 p.

209. Wren, A.W., et al., *Comparison of a SiO2-CaO-ZnO-SrO glass polyalkenoate cement to commercial dental materials: glass structure and physical properties.* Journal of Materials Science-Materials in Medicine, 2013. **24**(2): p. 271-280.

210. Wren, A.W., et al., *Gallium containing glass polyalkenoate anti-cancerous bone cements: glass characterization and physical properties.* Journal of materials science. Materials in medicine, 2012.

211. Boyd, D., et al., *The role of Sr2+ on the structure and reactivity of SrO-CaO-ZnO-SiO2 ionomer glasses.* Journal of materials science. Materials in medicine, 2008. **19**(2): p. 953-7.

212. Boyd, D., et al., *An investigation into the structure and reactivity of calcium-zinc-silicate ionomer glasses using MAS-NMR spectroscopy.* J Mater Sci Mater Med, 2006. **17**(5): p. 397-402.

213. Smith, D.C., *Development of glass-ionomer cement systems.* Biomaterials, 1998. **19**(6): p. 467-78.

214. Ngo, H. and S. Opsahl-Vital, *Minimal intervention dentistry II: part 7. Minimal intervention in cariology: the role of glass-ionomer cements in the preservation of tooth structures against caries.* British Dental Journal, 2014. **216**(10): p. 561-5.

215. Dowling, A.H. and G.J.P. Fleming, *Can poly(acrylic) acid molecular weight mixtures improve the compressive fracture strength and elastic modulus of a glass-ionomer restorative?* Dental Materials, 2011. **27**(11): p. 1170-1179.

216. Hallab, N.J. and J.J. Jacobs, *Chapter II.5.6 - Orthopedic Applications*, in *Biomaterials Science (Third Edition)*, B.D. Ratner, et al., Editors. 2013, Academic Press. p. 841-882.

217. Loewenstein, W., *The Distribution of Aluminum in the Tetrahedra of Silicates and Aluminates.* American Mineralogist, 1954. **39**(1-2): p. 92-96.

218. Hill, R.G. and A.D. Wilson, *Some Structural Aspects of Glasses Used in Ionomer Cements.* Glass Technology, 1988. **29**(4): p. 150-158.

219. Forsten, L., *Fluoride release and uptake by glass-ionomers and related materials and its clinical effect.* Biomaterials, 1998. **19**(6): p. 503-8.

220. Matsuya, S., et al., *Structural characterization of ionomer glasses by multinuclear solid state MAS-NMR spectroscopy.* Journal of Non-Crystalline Solids, 2007. **353**(3): p. 237-243.

221. Stamboulis, A., R.G. Hill, and R.V. Law, *Characterization of the structure of calcium alumino-silicate and calcium fluoro-alumino-silicate glasses by magic angle spinning nuclear magnetic resonance (MAS-NMR).* Journal of Non-Crystalline Solids, 2004. **333**(1): p. 101-107.

222. De Barra, E. and R.G. Hill, *Influence of glass composition on the properties of glass polyalkenoate cements. Part III: influence of fluorite content.* Biomaterials, 2000. **21**(6): p. 563-569.

223. Griffin, S.G. and R.G. Hill, *Influence of glass composition on the properties of glass polyalkenoate cements. Part II: influence of phosphate content.* Biomaterials, 2000. **21**(4): p. 399-403.

224. Moshaverinia, A., et al., *A review of polyelectrolyte modifications in conventional glass-ionomer dental cements.* Journal of Materials Chemistry, 2012. **22**(7): p. 2824.

225. Alhalawani, A.M.F., et al., *The role of poly(acrylic acid) in conventional glass polyalkenoate cements.* Journal of Polymer Engineering, 2016. **36**(3): p. 221-237.

226. Lohbauer, U., *Dental Glass Ionomer Cements as Permanent Filling Materials? - Properties, Limitations and Future Trends.* Materials, 2010. **3**(1): p. 76-96.

227. Culbertson, B.M., *Glass-ionomer dental restoratives.* Progress in Polymer Science, 2001. **26**(4): p. 577-604.

228. Hill, R.G., *The Fracture Properties of Glass Polyalkenoate Cements as a Function of Cement Age.* Journal of Materials Science, 1993. **28**(14): p. 3851-3858.

229. Khoroushi, M. and F. Keshani, *A review of glass-ionomers: From conventional glass-ionomer to bioactive glass-ionomer.* Dental research journal, 2013. **10**(4): p. 411-420.

230. Wilson, A.D., S. Crisp, and G. Abel, *Characterization of Glass-Ionomer Cements .4. Effect of Molecular-Weight on Physical-Properties.* Journal of dentistry, 1977. **5**(2): p. 117-120.

231. Crisp, S., B.G. Lewis, and A.D. Wilson, *Characterization of Glass-Ionomer Cements .3. Effect of Polyacid Concentration on Physical-Properties.* Journal of dentistry, 1977. **5**(1): p. 51-56.

232. De Barra, E. and R. Hill, *Influence of poly(acrylic acid) content on the fracture behaviour of glass polyalkenoate cements.* Journal of Materials Science, 1998. **33**(23): p. 5487-5497.

233. Fennell, B. and R.G. Hill, *The influence of poly(acrylic acid) molar mass and concentration on the properties of polyalkenoate cements Part I - Compressive strength.* Journal of Materials Science, 2001. **36**(21): p. 5193-5202.

234. Fennell, B. and R.G. Hill, *The influence of poly(acrylic acid) molar mass and concentration on the properties of polyalkenoate cements - Part II Young's modulus and flexural strength.* Journal of Materials Science, 2001. **36**(21): p. 5177-5183.

235. Fennell, B. and R.G. Hill, *The influence of poly(acrylic acid) molar mass and concentration on the properties of polyalkenoate cements - Part III - Fracture toughness and toughness.* Journal of Materials Science, 2001. **36**(21): p. 5185-5192.

236. Wilson, A.D., et al., *The Influence of Polyacid Molecular-Weight on Some Properties of Glass-Ionomer Cements.* Journal of Dental Research, 1989. **68**(2): p. 89-94.

237. Hill, R.G., A.D. Wilson, and C.P. Warrens, *The Influence of Poly(Acrylic Acid) Molecular-Weight on the Fracture-Toughness of Glass Ionomer Cements.* Journal of Materials Science, 1989. **24**(1): p. 363-371.

238. Dowling, A.H. and G.J.P. Fleming, *The influence of poly(acrylic) acid number average molecular weight and concentration in solution on the compressive fracture strength and modulus of a glass-ionomer restorative.* Dental Materials, 2011. **27**(6): p. 535-543.

239. Akinmade, A.O. and J.W. Nicholson, *Glass-Ionomer Cements as Adhesives .2. Testing of Adhesive Joints.* Journal of Materials Science-Materials in Medicine, 1993. **4**(3): p. 219-224.

240. Wilson, A.D., H.J. Prosser, and D.M. Powis, *Mechanism of Adhesion of Poly-Electrolyte Cements to Hydroxyapatite.* Journal of Dental Research, 1983. **62**(5): p. 590-592.

241. Griffin, S. and R. Hill, *Influence of poly(acrylic acid) molar mass on the fracture properties of glass polyalkenoate cements.* Journal of Materials Science, 1998. **33**(22): p. 5383-5396.

242. Wilson, A.D., et al., *The Influence of Polyacid Molecular Weight on Some Properties of Glass-ionomer Cements.* Journal of Dental Research, 1989. **68**(2): p. 89-94.

243. Prentice, P., *The Influence of Molecular-Weight on the Fracture of Thermoplastic Glassy-Polymers.* Journal of Materials Science, 1985. **20**(4): p. 1445-1454.

244. Dowling, A.H. and G.J. Fleming, *The influence of poly(acrylic) acid number average molecular weight and concentration in solution on the compressive fracture strength and modulus of a glass-ionomer restorative.* Dent Mater, 2011. **27**(6): p. 535-43.

245. Cattani-Lorente, M.A., C. Godin, and J.M. Meyer, *Mechanical behavior of glass ionomer cements affected by long-term storage in water.* Dent Mater, 1994. **10**(1): p. 37-44.

246. Williams, J.A. and R.W. Billington, *Changes in Compressive Strength of Glass Ionomer Restorative Materials with Respect to Time Periods of 24 H to 4 Months.* Journal of Oral Rehabilitation, 1991. **18**(2): p. 163-168.

247. Pearson, G.J. and A.S. Atkinson, *Long-Term Flexural Strength of Glass Ionomer Cements.* Biomaterials, 1991. **12**(7): p. 658-660.

248. Nicholson, J.W., *Glass-ionomer cements: A review of their engineering properties.* Biodental Engineering, 2010: p. 113-116.

249. Baig, M.S., C.H. Lloyd, and G.J.P. Fleming, *Fracture toughness testing: A discriminatory mechanical testing performance indicator for glass-ionomer restoratives?* Dental Materials, 2015. **31**(8): p. 877-886.

250. Lloyd, C.H. and L. Mitchell, *The Fracture-Toughness of Tooth Colored Restorative Materials.* Journal of Oral Rehabilitation, 1984. **11**(3): p. 257-272.

251. Goldman, M., *Fracture Properties of Composite and Glass Ionomer Dental Restorative Materials.* Journal of Biomedical Materials Research, 1985. **19**(7): p. 771-783.

252. Griffin, S.G. and R.G. Hill, *Influence of glass composition on the properties of glass polyalkenoate cements. Part I: influence of aluminium to silicon ratio.* Biomaterials, 1999. **20**(17): p. 1579-1586.

253. Billington, R.W., J.A. Williams, and G.J. Pearson, *Ion processes in glass ionomer cements.* J Dent, 2006. **34**(8): p. 544-55.

254. Hatton, P.V. and I.M. Brook, *Characterization of the Ultrastructure of Glass-Ionomer (Poly-Alkenoate) Cement.* British Dental Journal, 1992. **173**(8): p. 275-277.

255. Wilson, A.D., *Acidobasicity of oxide glasses used in glass ionomer cements.* Dental Materials, 1996. **12**(1): p. 25-29.

256. Nicholson, J.W., et al., *A Study of the Nature and Formation of Zinc Polyacrylate Cement Using Fourier-Transform Infrared-Spectroscopy.* Journal of Biomedical Materials Research, 1988. **22**(7): p. 623-631.

257. Brauer, D.S., et al., *Bactericidal strontium-releasing injectable bone cements based on bioactive glasses.* J R Soc Interface, 2012.

258. Wilson, A.D., J.M. Paddon, and S. Crisp, *Hydration of Dental Cements.* Journal of Dental Research, 1979. **58**(3): p. 1065-1071.

259. Jonck, L.M. and C.J. Grobbelaar, *Ionos bone cement (glass-ionomer): an experimental and clinical evaluation in joint replacement.* Clin Mater, 1990. **6**(4): p. 323-59.

260. Ramsden, R.T., R.C.D. Herdman, and R.H. Lye, *Ionomeric Bone-Cement in Neuro-Otologic Surgery.* Journal of Laryngology and Otology, 1992. **106**(11): p. 949-953.

261. Jonck, L.M. and C.J. Grobbelaar, *A glass ionomer for reconstructive surgery. Ionogran--an ionomeric micro implant. A biological evaluation.* Clin Mater, 1992. **9**(2): p. 85-103.

262. Jonck, L., C. Grobbelaar, and H. Strating, *The biocompatibility of glass-ionomer cement in joint replacement: bulk testing.* Clinical Materials, 1989. **4**(2): p. 85-107.

263. Jonck, L., C. Grobbelaar, and H. Strating, *Biological evaluation of glass-ionomer cement (Ketac-0) as an interface material in total joint replacement. A screening test.* Clinical Materials, 1989. **4**(3): p. 201-224.

264. Learmonth, I.D., C. Young, and C. Rorabeck, *The operation of the century: total hip replacement.* Lancet, 2007. **370**(9597): p. 1508-19.

265. Geyer, G. and J. Helms, *Reconstructive Measures in the Middle-Ear and Mastoid Using a Biocompatible Cement - Preliminary Clinical-Experience.* Clinical Implant Materials, 1990. **9**: p. 529-535.

266. Babighian, G., *Use of a Glass Ionomer Cement in Otologic Surgery - a Preliminary-Report.* Journal of Laryngology and Otology, 1992. **106**(11): p. 954-959.

267. Helms, J. and G. Geyer, *Closure of the petrous apex of the temporal bone with ionomeric cement following translabyrinthine removal of an acoustic neuroma.* J Laryngol Otol, 1994. **108**(3): p. 202-5.

268. Kempf, H.G., P.R. Issing, and T. Lenarz, *[Ionomer cement in cochlear implant surgery--applications and long-term outcome]*. Laryngorhinootologie, 1996. **75**(7): p. 388-91.

269. Geyer, G. and J. Helms, *[Ionomer cement prostheses in reconstructive middle ear surgery]*. HNO, 1997. **45**(6): p. 442-7.

270. Maassen, M.M. and H.P. Zenner, *Tympanoplasty type II with ionomeric cement and titanium-gold-angle prostheses.* Am J Otol, 1998. **19**(6): p. 693-9.

271. Kjeldsen, A.D. and A.M. Grontved, *Tympanoplasty with ionomeric cement.* Acta Otolaryngol Suppl, 2000. **543**: p. 130-1.

272. Wisniewski, H.M. and G.Y. Wen, *Aluminium and Alzheimer's disease.* Ciba Foundation Symposium, 1992. **169**: p. 142-154.

273. Kopeloff, L.M., S.E. Barrera, and N. Kopeloff, *Recurrent convulsion seizures in animals produced by immunological and chemical means.* Am J Psychiatry, 1942. **98**: p. 881-901.

274. Alfrey, A.C., G.R. Legendre, and W.D. Kaehny, *Dialysis Encephalopathy Syndrome - Possible Aluminum Intoxication.* New England Journal of Medicine, 1976. **294**(4): p. 184-188.

275. Renard, J.L., D. Felten, and D. Bequet, *Post-otoneurosurgery aluminium encephalopathy.* Lancet, 1994. **344**(8914): p. 63-4.

276. Hantson, P., et al., *Encephalopathy with seizures after use of aluminium-containing bone cement.* Lancet, 1994. **344**(8937): p. 1647.

277. Boyce, B.F., et al., *Hypercalcaemic osteomalacia due to aluminium toxicity.* Lancet, 1982. **2**(8306): p. 1009-13.

278. Blades, M.C., et al., *In vivo skeletal response and biomechanical assessment of two novel polyalkenoate cements following femoral implantation in the female New Zealand White rabbit.* J Mater Sci Mater Med, 1998. **9**(12): p. 701-6.

279. Winship, K.A., *Toxicity of Aluminum - a Historical Review .1.* Adverse Drug Reactions and Toxicological Reviews, 1992. **11**(2): p. 123-141.

280. Cournotwitmer, G., et al., *Aluminum Localization in Bone from Hemodialyzed Patients - Relationship to Matrix Mineralization.* Kidney International, 1981. **20**(3): p. 375-385.

281. Mjoberg, B., et al., *Aluminum, Alzheimer's disease and bone fragility.* Acta Orthopaedica Scandinavica, 1997. **68**(6): p. 511-514.

282. *<Z. Kristallogra. 2000 MimakiThe bond character of rutile type SiO2 GeO2 and SnO2 investigated by molecular orbital calculation.pdf>*.

283. Yamaguchi, M. and T. Matsui, *Stimulatory effect of zinc-chelating dipeptide on deoxyribonucleic acid synthesis in osteoblastic MC3T3-E1 cells.* Peptides, 1996. **17**(7): p. 1207-11.

284. Ovesen, J., et al., *The positive effects of zinc on skeletal strength in growing rats.* Bone, 2001. **29**(6): p. 565-70.

285. Towler, M.R., et al., *A preliminary study of an aluminum-free glass polyalkenoate cement.* Journal of Materials Science Letters, 2002. **21**(14): p. 1123-1126.

286. Boyd, D., et al., *The antibacterial effects of zinc ion migration from zinc-based glass polyalkenoate cements.* J Mater Sci Mater Med, 2006. **17**(6): p. 489-94.

287. ISO9917, *Dentistry - Water based cements*, in *Part 1: Powder/liquid acid-base cements*. 2007.

288. ISO5833, *Implants for surgery*, in *Acrylic resin cements*. 2002.

289. Fuchs, M., et al., *Therapeutic ion-releasing bioactive glass ionomer cements with improved mechanical strength and radiopacity.* Frontiers in Materials, 2015. **2**: p. 63.

290. Hurrell-Gillingham, K., et al., *In vitro biocompatibility of a novel Fe2O3 based glass ionomer cement.* J Dent, 2006. **34**(8): p. 533-8.

291. Hurrell-Gillingham, K., et al., *Devitrification of ionomer glass and its effect on the in vitro biocompatibility of glass-ionomer cements.* Biomaterials, 2003. **24**(18): p. 3153-3160.

292. Coughlan, A., et al., *Does elevating silver content in zinc-based glass polyalkenoate cements increase their antibacterial efficacy against two common bacteria using the agar gel diffusion method?* J Biomater Appl, 2013. **27**(7): p. 840-7.

293. Coughlan, A., et al., *Antibacterial coatings for medical devices based on glass polyalkenoate cement chemistry.* Journal of Materials Science-Materials in Medicine, 2008. **19**(12): p. 3555-3560.

294. Alhalawani, A.M., et al., *A Novel Glass Polyalkenoate Cement for Fixation and Stabilisation of the Ribcage, Post Sternotomy Surgery: An ex-Vivo Study.* J Funct Biomater, 2013. **4**(4): p. 329-57.

295. Khader, B., et al., *Glass Polyalkenoate Cements Designed for Cranioplasty Applications: An Evaluation of Their Physical and Mechanical Properties.* Journal of Functional Biomaterials, 2016. **7**(2): p. 8.

296. Wren, A., D. Boyd, and M.R. Towler, *The processing, mechanical properties and bioactivity of strontium based glass polyalkenoate cements.* J Mater Sci Mater Med, 2008. **19**(4): p. 1737-43.

297. Clarkin, O., D. Boyd, and M.R. Towler, *Comparison of failure mechanisms for cements used in skeletal luting applications.* J Mater Sci Mater Med, 2009. **20**(8): p. 1585-94.

298. Boyd, D., et al., *The role of Sr2+ on the structure and reactivity of SrO-CaO-ZnO-SiO2 ionomer glasses.* J Mater Sci Mater Med, 2008. **19**(2): p. 953-7.

299. Wren, A.W., et al., *The structural role of titanium in Ca–Sr–Zn–Si/Ti glasses for medical applications.* Journal of Non-Crystalline Solids, 2011. **357**(3): p. 1021-1026.

300. Kim, D.A., et al., *Development of a novel aluminum-free glass ionomer cement based on magnesium/strontium-silicate glasses.* Mater Sci Eng C Mater Biol Appl, 2014. **42**: p. 665-71.

301. Coughlan, A., et al., *Does elevating silver content in zinc-based glass polyalkenoate cements increase their antibacterial efficacy against two common bacteria using the agar gel diffusion method?* Journal of Biomaterials Applications, 2013. **27**(7): p. 840-847.

302. Micoulaut, M., L. Cormier, and G.S. Henderson, *The structure of amorphous, crystalline and liquid GeO2.* Journal of Physics: Condensed Matter, 2006. **18**(45): p. R753-R784.

303. Hannon, A.C., et al., *A model for the Ge–O coordination in germanate glasses.* Journal of Non-Crystalline Solids, 2007. **353**(18-21): p. 1688-1694.

304. Catauro, M. and A. Marotta, *The non-isothermal devitrification of glasses in the CaO center dot 4GeO(2)-SrO center dot 4GeO2 composition range.* Thermochimica Acta, 2001. **371**(1-2): p. 121-126.

305. Mansour, E., et al., *Structure-properties changes in ZnO-PbO-GeO2 glasses.* The European Physical Journal B, 2011. **83**(2): p. 133-141.

306. Bergeron, B., et al., *First investigations of the influence of IVB elements (Ti, Zr, and Hf) on the chemical durability of soda-lime borosilicate glasses.* Journal of Non-Crystalline Solids, 2010. **356**(44-49): p. 2315-2322.

307. Li, S., et al., *Structure and properties of zinc aluminophosphate glasses and those doped with zirconium dioxide.* Journal of Non-Crystalline Solids, 2015. **419**: p. 45-50.

308. Galoisy, L., *Structure-property relationships in industrial and natural glasses.* Elements, 2006. **2**(5): p. 293-297.

309. Connelly, A.J., et al., *The structural role of Zr within alkali borosilicate glasses for nuclear waste immobilisation.* Journal of Non-Crystalline Solids, 2011. **357**(7): p. 1647-1656.

310. Angeli, F., et al., *Influence of zirconium on the structure of pristine and leached soda-lime borosilicate glasses: Towards a quantitative approach by 17O MQMAS NMR.* Journal of Non-Crystalline Solids, 2008. **354**(31): p. 3713-3722.

311. Simhan, R.G., *Chemical Durability of Zro2 Containing Glasses.* Journal of Non-Crystalline Solids, 1983. **54**(3): p. 335-343.

312. Arab, M., et al., *Aqueous alteration of five-oxide silicate glasses: Experimental approach and Monte Carlo modeling.* Journal of Non-Crystalline Solids, 2008. **354**(2-9): p. 155-161.

313. Duée, C., et al., *Predicting bioactive properties of phosphosilicate glasses using mixture designs.* Journal of Non-Crystalline Solids, 2013. **362**: p. 47-55.

314. Duée, C., et al., *Mixture designs applied to glass bioactivity evaluation in the Si–Ca–Na system.* Journal of Non-Crystalline Solids, 2009. **355**(16-17): p. 943-950.

315. Duée, C., et al., *Predicting glass transition and crystallization temperatures of silicate bioglasses using mixture designs.* Journal of Non-Crystalline Solids, 2012. **358**(8): p. 1083-1090.

316. Kehoe, S., X.F. Zhang, and D. Boyd, *Composition-property relationships for an experimental composite nerve guidance conduit: evaluating cytotoxicity and initial tensile strength.* J Mater Sci Mater Med, 2011. **22**(4): p. 945-59.

317. Kehoe, S., et al., *Predicting the thermal responses and radiopacity of multicomponent zinc–silicate bioglasses: A focus on ZnO, La2O3, SiO2 and TiO2.* Journal of Non-Crystalline Solids, 2012. **358**(23): p. 3388-3395.

318. Kehoe, S., et al., *Mixture designs to assess composition-structure-property relationships in SiO(2)-CaO-ZnO-La(2)O(3)-TiO(2)-MgO-SrO-Na(2)O glasses: potential materials for embolization.* J Biomater Appl, 2013. **28**(3): p. 416-33.

319. Kehoe, S., N. Kilcup, and D. Boyd, *Evaluation of cytotoxicity for novel composite embolic microspheres: Material optimization by response surface methodology.* Materials Letters, 2012. **86**: p. 13-17.

320. McGirt, M.J., et al., *Vertebroplasty and kyphoplasty for the treatment of vertebral compression fractures: an evidenced-based review of the literature.* The spine journal : official journal of the North American Spine Society, 2009. **9**(6): p. 501-8.

321. Boyd, D., et al., *Zinc-based glass polyalkenoate cements with improved setting times and mechanical properties.* Acta biomaterialia, 2008. **4**(2): p. 425-31.

322. Engelbrecht, E., G. von Foerster, and G. Delling, *Ionogran in revision arthroplasty.* Journal of Bone and Joint Surgery-British Volume, 2000. **82B**(2): p. 192-199.

323. Hantson, P., et al., *Encephalopathy with seizures after use of aluminium-containing bone cement.* The Lancet, 1994. **344**(8937): p. 1647.

324. Hoang-Xuan, K., et al., *Myoclonic encephalopaty after exposure to aluminium.* The Lancet, 1996. **347**(9005): p. 910-911.

325. Reusche, E., et al., *Ionomeric cement and aluminium encephalopathy.* The Lancet, 1995. **345**(8965): p. 1633-1634.

326. Reusche, E., et al., *Subacute fatal aluminum encephalopathy after reconstructive otoneurosurgery: a case report.* Human pathology, 2001. **32**(10): p. 1136-40.

327. Nicholson, J.W. and B. Czarnecka, *Review paper: Role of aluminum in glass-ionomer dental cements and its biological effects.* Journal of biomaterials applications, 2009. **24**(4): p. 293-308.

328. Hurrell-Gillingham, K., et al., *In vitro biocompatibility of a novel Fe2O3 based glass ionomer cement.* Journal of dentistry, 2006. **34**(8): p. 533-538.

329. Towler, M.R., et al., *Zinc ion release from novel hard tissue biomaterials.* Bio-Medical Materials and Engineering, 2004. **14**(4): p. 565-572.

330. Boyd, D., et al., *The antibacterial effects of zinc ion migration from zinc-based glass polyalkenoate cements.* Journal of Materials Science-Materials in Medicine, 2006. **17**(6): p. 489-494.

331. Wren, A., D. Boyd, and M.R. Towler, *The processing, mechanical properties and bioactivity of strontium based glass polyalkenoate cements.* Journal of Materials Science-Materials in Medicine, 2008. **19**(4): p. 1737-1743.

332. Clarkin, O., D. Boyd, and M.R. Towler, *Strontium-based glass polyalkenoate cements for luting applications in the skeleton.* Journal of biomaterials applications, 2010. **24**(6): p. 483-502.

333. Wren, A.W., et al., *A spectroscopic investigation into the setting and mechanical properties of titanium containing glass polyalkenoate cements.* Journal of Materials Science-Materials in Medicine, 2010. **21**(8): p. 2355-2364.

334. Paul, A., *Chemistry of glasses*. 1982, London ; New York: Chapman and Hall. ix, 293 p.

335. Ginebra, M.P., et al., *Mechanical performance of acrylic bone cements containing different radiopacifying agents.* Biomaterials, 2002. **23**(8): p. 1873-1882.

336. Ramaswamy, Y., et al., *The responses of osteoblasts, osteoclasts and endothelial cells to zirconium modified calcium-silicate-based ceramic.* Biomaterials, 2008. **29**(33): p. 4392-402.

337. Angeli, F., et al., *Boron Speciation in Soda-Lime Borosilicate Glasses Containing Zirconium.* Journal of the American Ceramic Society, 2010. **93**(9): p. 2693-2704.

338. Lin, M.H., et al., *Comparison of organic and inorganic germanium compounds in cellular radiosensitivity and preparation of germanium nanoparticles as a radiosensitizer.* International Journal of Radiation Biology, 2009. **85**(3): p. 214-226.

339. Gerber, G.B. and A. LÈonard, *Mutagenicity, carcinogenicity and teratogenicity of germanium compounds.* Mutation Research/Reviews in Mutation Research, 1997. **387**(3): p. 141-146.

340. ISO9917, *Dentistry - Water-based cements*. 2007.

341. Smith, W.F., *Experimental design for formulation*. ASA-SIAM series on statistics and applied probability. 2005, Philadelphia
Alexandria, Va.: Society for Industrial and Applied Mathematics ;
American Statistical Association. xix, 367 p.

342. Kehoe, S., et al., *Mixture designs to assess composition-structure-property relationships in SiO2-CaO-ZnO-La2O3-TiO2-MgO-SrO-Na2O glasses: Potential materials for embolization.* Journal of biomaterials applications, 2012.

343. Mirkhani, S.A., et al., *Determination of the glass transition temperature of ionic liquids: A molecular approach.* Thermochimica Acta, 2012. **543**: p. 88-95.

344. Williams, J.A., R.W. Billington, and G.J. Pearson, *The effect of the disc support system on biaxial tensile strength of a glass ionomer cement.* Dent Mater, 2002. **18**(5): p. 376-9.

345. Higgs, W.A.J., et al., *A simple method of determining the modulus of orthopedic bone cement.* Journal of biomedical materials research, 2001. **58**(2): p. 188-195.

346. Boyd, D., et al., *An investigation into the structure and reactivity of calcium-zinc-silicate ionomer glasses using MAS-NMR spectroscopy.* Journal of materials science. Materials in medicine, 2006. **17**(5): p. 397-402.

347. Henderson, G.S., *The Germanate Anomaly: What do we know?* Journal of Non-Crystalline Solids, 2007. **353**(18-21): p. 1695-1704.

348. Henderson, G.S., et al., *The structure of GeO2–SiO2 glasses and melts: A Raman spectroscopy study.* Journal of Non-Crystalline Solids, 2009. **355**(8): p. 468-474.

349. Salmon, P.S., et al., *Structure of glassy GeO2.* Journal of Physics-Condensed Matter, 2007. **19**(41).

350. Hill, R., *An alternative view of the degradation of bioglass.* Journal of Materials Science Letters, 1996. **15**(13): p. 1122-1125.

351. Wren, A.W., et al., *Comparison of a SiO2-CaO-ZnO-SrO glass polyalkenoate cement to commercial dental materials: glass structure and physical properties.* Journal of Materials Science: Materials in Medicine, 2012: p. 1-10.

352. Azillah, M.A., H.M. Anstice, and G.J. Pearson, *Long-term flexural strength of three direct aesthetic restorative materials.* Journal of Dentistry, 1998. **26**(2): p. 177-182.

353. Bridger, R.S., *Introduction to ergonomics*. 3rd ed. 2009, Boca Raton: CRC Press. xxix, 776 p.

354. Tang, H.M., et al., *Glass polyalkenoate cements based on simple CaO-Al2O3-SiO2 glasses.* Materials Science and Technology, 2015. **31**(2): p. 197-202.

355. Matsuya, S., T. Maeda, and M. Ohta, *IR and NMR Analyses of Hardening and Maturation of Glass-ionomer Cement.* Journal of Dental Research, 1996. **75**(12): p. 1920-1927.

356. Fleming, G., *Influence of powder/liquid mixing ratio on the performance of a restorative glass-ionomer dental cement.* Biomaterials, 2003. **24**(23): p. 4173-4179.

357. Dickey, B., et al., *The effect of composition and annealing on the properties of aluminum free GPCs: A preliminary evaluation.* Materials Letters, 2014. **129**: p. 191-194.

358. Kiri, L. and D. Boyd, *Predicting composition-property relationships for glass ionomer cements: A multifactor central composite approach to material optimization.* J Mech Behav Biomed Mater, 2015. **46**: p. 285-291.

359. Wasson, E.A. and J.W. Nicholson, *A Study of the Relationship between Setting Chemistry and Properties of Modified Glass Poly(Alkenoate) Cements.* British Polymer Journal, 1990. **23**(1-2): p. 179-183.

360. Wasson, E.A. and J.W. Nicholson, *Change in Ph during Setting of Polyelectrolyte Dental Cements.* Journal of Dentistry, 1993. **21**(2): p. 122-126.

361. Shyam, A. and E. Lara-Curzio, *The double-torsion testing technique for determination of fracture toughness and slow crack growth behavior of materials: A review.* Journal of Materials Science, 2006. **41**(13): p. 4093-4104.

362. Young, A., *FTIR investigation of monomer polymerisation and polyacid neutralisation kinetics and mechanisms in various aesthetic dental restorative materials.* Biomaterials, 2004. **25**(5): p. 823-833.

363. Tomlinson, S.K., et al., *Investigation of the dual setting mechanism of a novel dental cement using infrared spectroscopy.* Vibrational Spectroscopy, 2007. **45**(1): p. 10-17.

364. Fantinel, F., et al., *Complexation of polyacrylates by Ca2+ ions. Time-resolved studies using attenuated total reflectance Fourier transform infrared dialysis spectroscopy.* Langmuir, 2004. **20**(7): p. 2539-42.

365. Cook, W.D., *Dental Poly-Electrolyte Cements .1. Chemistry of the Early Stages of the Setting Reaction.* Biomaterials, 1982. **3**(4): p. 232-236.

366. Talal, A., et al., *Effect of ultrasound on the setting characteristics of glass ionomer cements studied by Fourier transform infrared spectroscopy.* J Mater Sci Mater Med, 2009. **20**(1): p. 405-11.

367. De Maeyer, E.A.P., R.M.H. Verbeeck, and C.W.J. Vercruysse, *Infrared Spectrometric Study of Acid-degradable Glasses.* Journal of Dental Research, 2002. **81**(8): p. 552-555.

368. Madon, M., et al., *A Vibrational Study of Phase-Transitions among the GeO2 Polymorphs.* Physics and Chemistry of Minerals, 1991. **18**(1): p. 7-18.

369. Munhoz, T., et al., *Setting of commercial glass ionomer cement Fuji IX by (27)Al and (19)F MAS-NMR.* J Dent, 2010. **38**(4): p. 325-30.

370. Michaelis, V.K., et al., *Germanium-73 NMR of amorphous and crystalline GeO2.* Chemical Communications, 2009(31): p. 4660-4662.

371. Sutrisno, A., et al., *Characterization of Zn-Containing Metal-Organic Frameworks by Solid-State 67Zn NMR Spectroscopy and Computational Modeling.* Chemistry-a European Journal, 2012. **18**(39): p. 12251-12259.

372. Frencken, J.E. and C.J. Holmgren, *Caries management through the Atraumatic Restorative Treatment (ART) approach and glass-ionomers: update 2013.* Braz Oral Res, 2014. **28**(1): p. 5-8.

373. Frencken, J.E., *The state-of-the-art of ART sealants.* Dent Update, 2014. **41**(2): p. 119-20, 122-4.

374. Frencken, J.E., *The state-of-the-art of ART restorations.* Dent Update, 2014. **41**(3): p. 218-20, 222-4.

375. Frencken, J.E. and C.J. Holmgren, *ART: a minimal intervention approach to manage dental caries.* Dent Update, 2004. **31**(5): p. 295-8, 301.

376. van 't Hof, M.A., et al., *The atraumatic restorative treatment (ART) approach for managing dental caries: a meta-analysis.* Int Dent J, 2006. **56**(6): p. 345-51.

377. Valliant, E.M., et al., *Calcium polyphosphate as an additive to zinc-silicate glass ionomer cements.* J Biomater Appl, 2015. **30**(1): p. 61-70.

378. Dowling, A.H., et al., *Improving the standard of the standard for glass ionomers: an alternative to the compressive fracture strength test for consideration?* J Dent, 2012. **40**(3): p. 189-201.

379. Fleming, G.J., A.H. Dowling, and O. Addison, *The crushing truth about glass ionomer restoratives: exposing the standard of the standard.* J Dent, 2012. **40**(3): p. 181-8.

380. Towler, M.R., et al., *Modelling of the glass phase in fly ashes using network connectivity theory.* Journal of Chemical Technology & Biotechnology, 2002. **77**(3): p. 240-245.

381. Wren, A.W., et al., *Comparison of a SiO(2)-CaO-ZnO-SrO glass polyalkenoate cement to commercial dental materials: glass structure and physical properties.* J Mater Sci Mater Med, 2013. **24**(2): p. 271-80.

382. Tomlinson, S.K., et al., *Investigation of the dual setting mechanism of a novel dental cement using infrared spectroscopy.* Vibrational Spectroscopy, 2007. **45**(1): p. 10-17.

383. Nicholson, J.W., et al., *Fourier Transform Infrared Spectroscopic Study of the Role of Tartaric Acid in Glass-ionomer Dental Cements.* Journal of Dental Research, 1988. **67**(12): p. 1451-1454.

384. Alvarado-Rivera, J., et al., *Effect of CeO2 on the Glass Structure of Sodium Germanate Glasses.* Journal of the American Ceramic Society, 2014. **97**(11): p. 3494-3500.

385. Moharram, M.A., S.M. Rabie, and H.M. El-Gendy, *Infrared spectra of gamma-irradiated poly(acrylic acid)-polyacrylamide complex.* Journal of Applied Polymer Science, 2002. **85**(8): p. 1619-1623.

386. Kalampounias, A.G., *IR and Raman spectroscopic studies of sol-gel derived alkaline-earth silicate glasses.* Bulletin of Materials Science, 2011. **34**(2): p. 299-303.

387. Younas, B., et al., *In situ reaction kinetic analysis of dental restorative materials.* The European Physical Journal Applied Physics, 2013. **64**(3): p. 30701.

388. Wang, R.F., et al., *Structure and luminescent property of Er3+-doped germanate glasses.* Journal of Non-Crystalline Solids, 2014. **383**: p. 200-204.

389. Kamitsos, E.I., et al., *Structure-property correlation in glasses by infrared reflectance spectroscopy.* Journal of Non-Crystalline Solids, 1997. **222**: p. 59-68.

390. Chelcea, R., et al., *Structural study of ternary iron-lead-germanate glass ceramics.* Spectrochimica Acta Part a-Molecular and Biomolecular Spectroscopy, 2011. **79**(3): p. 481-485.

391. Pascuta, P., et al., *The local structure of bismuth germanate glasses and glass ceramics doped with europium ions evidenced by FT-IR spectroscopy.* Vibrational Spectroscopy, 2008. **48**(2): p. 281-284.

392. Pernice, P., et al., *Glass transition temperature and devitrification study of barium germanate glasses.* Journal of Non-Crystalline Solids, 1997. **210**(1): p. 23-31.

393. Dickey, B., et al., *Development and evaluation of an inherently radiopaque, adhesive bone cement for vertebroplasty.* Journal of Vascular and Interventional Radiology, 2013. **24**(4): p. S33.

394. Deb, S., et al., *A novel acrylic copolymer for a poly(alkenoate) glass-ionomer cement.* Journal of Materials Science-Materials in Medicine, 2003. **14**(7): p. 575-581.

395. Fleming, G.J.P., A.A. Farooq, and J.E. Barralet, *Influence of powder/liquid mixing ratio on the performance of a restorative glass-ionomer dental cement.* Biomaterials, 2003. **24**(23): p. 4173-4179.

396. Nomoto, R., et al., *Effect of mixing method on the porosity of encapsulated glass ionomer cement.* Dental Materials, 2004. **20**(10): p. 972-978.

397. Wilson, A.D., J.M. Paddon, and S. Crisp, *The Hydration of Dental Cements.* Journal of Dental Research, 1979. **58**(3): p. 1065-1071.

398. Kiri, L., M. Filiaggi, and D. Boyd, *Methotrexate-loaded glass ionomer cements for drug release in the skeleton: An examination of composition-property relationships.* J Biomater Appl, 2016. **30**(6): p. 732-739.

399. Prentice, L.H., M.J. Tyas, and M.F. Burrow, *The effect of particle size distribution on an experimental glass-ionomer cement.* Dental Materials, 2005. **21**(6): p. 505-510.

400. Baig, M.S. and G.J.P. Fleming, *Conventional glass-ionomer materials: A review of the developments in glass powder, polyacid liquid and the strategies of reinforcement.* Journal of Dentistry, 2015. **43**(8): p. 897-912.

401. Galoisy, L., et al., *Evidence for 6-coordinated zirconium in inactive nuclear waste glasses.* Journal of the American Ceramic Society, 1999. **82**(8): p. 2219-2224.

402. Holl, R., M. Kling, and E. Schroll, *Metallogenesis of germanium - A review.* Ore Geology Reviews, 2007. **30**(3-4): p. 145-180.

403. Liu, J., et al., *In situ synthesis of Zn2GeO4 hollow spheres and their enhanced photocatalytic activity for the degradation of antibiotic metronidazole.* Dalton Transactions, 2013. **42**(14): p. 5092-5099.

404. Tsai, M.Y., et al., *Water-driven formation of luminescent Zn2GeO4 nanorods from Zn-containing Ge nanoparticles.* Crystal Growth & Design, 2008. **8**(7): p. 2264-2269.

405. Su, Y., et al., *Bulk-quantity synthesis and photoluminescence properties of chain-like GeO2/ZnGeO3 crystal structures.* Materials Letters, 2005. **59**(24-25): p. 2990-2993.

406. Ngo, H.C., et al., *Chemical exchange between glass-ionomer restorations and residual carious dentine in permanent molars: An in vivo study.* Journal of Dentistry, 2006. **34**(8): p. 608-613.

407. Benelli, E.M., et al., *In-Situ Anticariogenic Potential of Glass-Ionomer Cement.* Caries Research, 1993. **27**(4): p. 280-284.

408. Seaborn, C.D. and F.H. Nielsen, *Effects of germanium and silicon on bone mineralization.* Biol Trace Elem Res, 1994. **42**(2): p. 151-64.

409. Dermience, M., et al., *Effects of thirty elements on bone metabolism.* J Trace Elem Med Biol, 2015. **32**: p. 86-106.

410. Schauss, A.G., *Nephrotoxicity in humans by the ultratrace element germanium.* Ren Fail, 1991. **13**(1): p. 1-4.

411. Schauss, A.G., *Nephrotoxicity and neurotoxicity in humans from organogermanium compounds and germanium dioxide.* Biol Trace Elem Res, 1991. **29**(3): p. 267-80.

412. Dickinson, V., *Composition-property relationships in multi-component germanium-based polyalkenoate cements*, in *School of Biomedical Engineering*. 2014, Dalhousie University: Halifax, Canada.

413. Pierlot, C.M., L. Kiri, and D. Boyd, *Effect of Ge/Si ratio on genotoxicity of germanium-containing glass ionomer cements.* Materials Letters, 2016. **168**: p. 151-154.

414. Pierlot, C.M., et al., *A Pilot Evaluation of an Aluminum Free Glass Polyalkenoate Cement using A Sub-Chronic Osseous Defect Model in New Zealand White Rabbits.* Materials Letters, 2016. **Under Review, May 19, 2016**.

415. Henderson, G.S., L.G. Soltay, and H.M. Wang, *Q speciation in alkali germanate glasses.* Journal of Non-Crystalline Solids, 2010. **356**(44-49): p. 2480-2485.

416. Lapeyre, C., et al., *Local Order around Germanium in Glasses of the System Sio2-Geo2-B2o3-Na2o - a X-Ray Absorption-Spectroscopy Study.* Bulletin De Mineralogie, 1983. **106**(1-2): p. 77-85.

417. Sakka, S. and K. Kamiya, *Structure of Alkali Germanate Glasses Studied by Spectroscopic Techniques.* Journal of Non-Crystalline Solids, 1982. **49**(1-3): p. 103-116.

418. Sayers, D.E., E.A. Stern, and F.W. Lytle, *New Determination of Amorphous Germanium Structure Using X-Ray Absorption Spectroscopy.* Bulletin of the American Physical Society, 1971. **16**(3): p. 302-&.

419. Vaccari, M., et al., *A new EXAFS investigation of local structural changes in amorphous and crystalline GeO2 at high pressure.* Journal of Physics-Condensed Matter, 2009. **21**(14).

420. Boppana, V.B.R., N.D. Hould, and R.F. Lobo, *Synthesis, characterization and photocatalytic properties of novel zinc germanate nano-materials.* Journal of Solid State Chemistry, 2011. **184**(5): p. 1054-1062.

421. Anderson, M.J. and P.J. Whitcomb, *DOE simplified : practical tools for effective experimentation*. 2nd ed. 2007, New York, N.Y.: Productivity Press. xiii, 241 p.

422. Micoulaut, M., L. Cormier, and G.S. Henderson, *The structure of amorphous, crystalline and liquid GeO2.* Journal of Physics-Condensed Matter, 2006. **18**(45): p. R753-R784.

423. Neuville, D.R., D. de Ligny, and G.S. Henderson, *Advances in Raman Spectroscopy Applied to Earth and Material Sciences.* Spectroscopic Methods in Mineralology and Materials Sciences, 2014. **78**: p. 509-541.

424. Henderson, G.S. and M.E. Fleet, *The Structure of Glasses Along the Na2o-Geo2 Join.* Journal of Non-Crystalline Solids, 1991. **134**(3): p. 259-269.